

PERIPHERAL NERVE IMAGING

EDITED BY: Felix Tobias Kurz, Olivier Scheidegger and Matthew Craig Evans
PUBLISHED IN: Frontiers in Neuroscience



frontiers

Frontiers eBook Copyright Statement

The copyright in the text of individual articles in this eBook is the property of their respective authors or their respective institutions or funders. The copyright in graphics and images within each article may be subject to copyright of other parties. In both cases this is subject to a license granted to Frontiers.

The compilation of articles constituting this eBook is the property of Frontiers.

Each article within this eBook, and the eBook itself, are published under the most recent version of the Creative Commons CC-BY licence.

The version current at the date of publication of this eBook is CC-BY 4.0. If the CC-BY licence is updated, the licence granted by Frontiers is automatically updated to the new version.

When exercising any right under the CC-BY licence, Frontiers must be attributed as the original publisher of the article or eBook, as applicable.

Authors have the responsibility of ensuring that any graphics or other materials which are the property of others may be included in the CC-BY licence, but this should be checked before relying on the CC-BY licence to reproduce those materials. Any copyright notices relating to those materials must be complied with.

Copyright and source acknowledgement notices may not be removed and must be displayed in any copy, derivative work or partial copy which includes the elements in question.

All copyright, and all rights therein, are protected by national and international copyright laws. The above represents a summary only. For further information please read Frontiers' Conditions for Website Use and Copyright Statement, and the applicable CC-BY licence.

ISSN 1664-8714

ISBN 978-2-88976-574-4

DOI 10.3389/978-2-88976-574-4

About Frontiers

Frontiers is more than just an open-access publisher of scholarly articles: it is a pioneering approach to the world of academia, radically improving the way scholarly research is managed. The grand vision of Frontiers is a world where all people have an equal opportunity to seek, share and generate knowledge. Frontiers provides immediate and permanent online open access to all its publications, but this alone is not enough to realize our grand goals.

Frontiers Journal Series

The Frontiers Journal Series is a multi-tier and interdisciplinary set of open-access, online journals, promising a paradigm shift from the current review, selection and dissemination processes in academic publishing. All Frontiers journals are driven by researchers for researchers; therefore, they constitute a service to the scholarly community. At the same time, the Frontiers Journal Series operates on a revolutionary invention, the tiered publishing system, initially addressing specific communities of scholars, and gradually climbing up to broader public understanding, thus serving the interests of the lay society, too.

Dedication to Quality

Each Frontiers article is a landmark of the highest quality, thanks to genuinely collaborative interactions between authors and review editors, who include some of the world's best academicians. Research must be certified by peers before entering a stream of knowledge that may eventually reach the public - and shape society; therefore, Frontiers only applies the most rigorous and unbiased reviews. Frontiers revolutionizes research publishing by freely delivering the most outstanding research, evaluated with no bias from both the academic and social point of view. By applying the most advanced information technologies, Frontiers is catapulting scholarly publishing into a new generation.

What are Frontiers Research Topics?

Frontiers Research Topics are very popular trademarks of the Frontiers Journals Series: they are collections of at least ten articles, all centered on a particular subject. With their unique mix of varied contributions from Original Research to Review Articles, Frontiers Research Topics unify the most influential researchers, the latest key findings and historical advances in a hot research area! Find out more on how to host your own Frontiers Research Topic or contribute to one as an author by contacting the Frontiers Editorial Office: frontiersin.org/about/contact

PERIPHERAL NERVE IMAGING

Topic Editors:

Felix Tobias Kurz, Heidelberg University Hospital, Germany

Olivier Scheidegger, University Hospital Bern, Switzerland

Matthew Craig Evans, Imperial College London, United Kingdom

Citation: Kurz, F. T., Scheidegger, O., Evans, M. C., eds. (2022). Peripheral Nerve Imaging. Lausanne: Frontiers Media SA. doi: 10.3389/978-2-88976-574-4

Table of Contents

- 05** ***Diabetic Polyneuropathy Is Associated With Pathomorphological Changes in Human Dorsal Root Ganglia: A Study Using 3T MR Neurography***
Johann M. E. Jende, Zoltan Kender, Christian Rother, Lucia Alvarez-Ramos, Jan B. Groener, Mirko Pham, Jakob Morgenstern, Dimitrios Oikonomou, Artur Hahn, Alexander Juerchott, Jennifer Kollmer, Sabine Heiland, Stefan Kopf, Peter P. Nawroth, Martin Bendszus and Felix T. Kurz
- 14** ***Sural Nerve Perfusion in Mice***
Anete Dudele, Peter Mondrup Rasmussen and Leif Østergaard
- 26** ***Diffusion Tensor Imaging of the Sciatic Nerve as a Surrogate Marker for Nerve Functionality of the Upper and Lower Limb in Patients With Diabetes and Prediabetes***
Johann M. E. Jende, Zoltan Kender, Christoph Mooshage, Jan B. Groener, Lucia Alvarez-Ramos, Jennifer Kollmer, Alexander Juerchott, Artur Hahn, Sabine Heiland, Peter Nawroth, Martin Bendszus, Stefan Kopf and Felix T. Kurz
- 37** ***Multisequence Quantitative Magnetic Resonance Neurography of Brachial and Lumbosacral Plexus in Chronic Inflammatory Demyelinating Polyneuropathy***
Xiaoyun Su, Xiangquan Kong, Osamah Alwalid, Jing Wang, Huiting Zhang, Zuneng Lu and Chuansheng Zheng
- 47** ***MRI DTI and PDFF as Biomarkers for Lower Motor Neuron Degeneration in ALS***
Thorsten Lichtenstein, Alina Sprenger, Kilian Weiss, Nils Große Hokamp, David Maintz, Marc Schlamann, Gereon R. Fink, Helmar C. Lehmann and Tobias D. Henning
- 55** ***Magnetic Resonance Imaging as a Biomarker in Diabetic and HIV-Associated Peripheral Neuropathy: A Systematic Review-Based Narrative***
Matthew C. Evans, Charles Wade, David Hohenschurz-Schmidt, Pete Lally, Albert Ugwudike, Kamal Shah, Neal Bangerter, David J. Sharp and Andrew S. C. Rice
- 82** ***Fractional Anisotropy and Troponin T Parallel Structural Nerve Damage at the Upper Extremities in a Group of Patients With Prediabetes and Type 2 Diabetes – A Study Using 3T Magnetic Resonance Neurography***
Johann M. E. Jende, Zoltan Kender, Jakob Morgenstern, Pascal Renn, Christoph Mooshage, Alexander Juerchott, Stefan Kopf, Peter P. Nawroth, Martin Bendszus and Felix T. Kurz
- 90** ***High-Resolution Ultrasound and Magnetic Resonance Imaging of Abnormal Ligaments in Thoracic Outlet Syndrome in a Series of 16 Cases***
Suren Jengojan, Maria Bernathova, Thomas Moritz, Gerd Bodner, Philipp Sorgo and Gregor Kasprian

99 *Magnetic Resonance Neurography Reveals Smoking-Associated Decrease in Sciatic Nerve Structural Integrity in Type 2 Diabetes*

Johann M. E. Jende, Christoph Mooshage, Zoltan Kender, Stefan Kopf, Jan B. Groener, Sabine Heiland, Alexander Juerchott, Peter Nawroth, Martin Bendszus and Felix T. Kurz

110 *Quantitative MR-Neurography at 3.0T: Inter-Scanner Reproducibility*

Fabian Preisner, Rouven Behnisch, Véronique Schwehr, Tim Godel, Daniel Schwarz, Olivia Foesleitner, Philipp Bäumer, Sabine Heiland, Martin Bendszus and Moritz Kronlage

120 *Performance of Single-Shot Echo-Planar Imaging in Diffusion Tensor Imaging in Rat Sciatic Nerve Compared With Readout-Segmented Echo-Planar Imaging*

Yueyao Chen, Zhongxian Pan, Fanqi Meng, Zhujing Li, Yuanming Hu, Xuewen Yu, Jinyun Gao, Yihao Guo, Hanqing Lyu and Xiaofeng Lin



Diabetic Polyneuropathy Is Associated With Pathomorphological Changes in Human Dorsal Root Ganglia: A Study Using 3T MR Neurography

OPEN ACCESS

Edited by:

Nico Sollmann,
University Hospital rechts der Isar,
Technical University of Munich,
Germany

Reviewed by:

Dimitrios C. Karampinos,
Technical University of Munich,
Germany
Theodoros Soldatos,
Iasis Diagnostic Center, Greece
Houchun H. Hu,
Hyperfine Research, Inc., United
States

*Correspondence:

Felix T. Kurz
felix.kurz@med.uni-heidelberg.de

Specialty section:

This article was submitted to
Brain Imaging Methods,
a section of the journal
Frontiers in Neuroscience

Received: 08 June 2020

Accepted: 24 August 2020

Published: 25 September 2020

Citation:

Jende JME, Kender Z, Rother C,
Alvarez-Ramos L, Groener JB,
Pham M, Morgenstern J,
Oikonomou D, Hahn A, Juerchott A,
Kollmer J, Heiland S, Kopf S,
Nawroth PP, Bendszus M and Kurz FT
(2020) Diabetic Polyneuropathy Is
Associated With Pathomorphological
Changes in Human Dorsal Root
Ganglia: A Study Using 3T MR
Neurography.
Front. Neurosci. 14:570744.
doi: 10.3389/fnins.2020.570744

Johann M. E. Jende¹, Zoltan Kender², Christian Rother¹, Lucia Alvarez-Ramos², Jan B. Groener^{2,3,4}, Mirko Pham^{1,5}, Jakob Morgenstern², Dimitrios Oikonomou², Artur Hahn¹, Alexander Juerchott¹, Jennifer Kollmer¹, Sabine Heiland^{1,6}, Stefan Kopf^{2,3}, Peter P. Nawroth^{2,3,7}, Martin Bendszus¹ and Felix T. Kurz^{1*}

¹ Department of Neuroradiology, Heidelberg University Hospital, Heidelberg, Germany, ² Department of Endocrinology, Diabetology and Clinical Chemistry (Internal Medicine 1), Heidelberg University Hospital, Heidelberg, Germany, ³ German Center of Diabetes Research, München-Neuherberg, Germany, ⁴ Medicover Neuroendokrinologie, Munich, Germany, ⁵ Department of Neuroradiology, Würzburg University Hospital, Würzburg, Germany, ⁶ Division of Experimental Radiology, Department of Neuroradiology, Heidelberg University Hospital, Heidelberg, Germany, ⁷ Joint Institute for Diabetes and Cancer at Helmholtz-Zentrum Munich and Heidelberg University, Heidelberg, Germany

Diabetic neuropathy (DPN) is one of the most severe and yet most poorly understood complications of diabetes mellitus. *In vivo* imaging of dorsal root ganglia (DRG), a key structure for the understanding of DPN, has been restricted to animal studies. These have shown a correlation of decreased DRG volume with neuropathic symptom severity. Our objective was to investigate correlations of DRG morphology and signal characteristics at 3 Tesla (3T) magnetic resonance neurography (MRN) with clinical and serological data in diabetic patients with and without DPN. In this cross-sectional study, participants underwent 3T MRN of both L5 DRG using an isotropic 3D T2-weighted, fat-suppressed sequence with subsequent segmentation of DRG volume and analysis of normalized signal properties. Overall, 55 diabetes patients (66 ± 9 years; 32 men; 30 with DPN) took part in this study. DRG volume was smaller in patients with severe DPN when compared to patients with mild or moderate DPN (134.7 ± 21.86 vs 170.1 ± 49.22; $p = 0.040$). In DPN patients, DRG volume was negatively correlated with the neuropathy disability score ($r = -0.43$; 95%CI = -0.66 to -0.14 ; $p = 0.02$), a measure of neuropathy severity. DRG volume showed negative correlations with triglycerides ($r = -0.40$; 95%CI = -0.57 to -0.19 ; $p = 0.006$), and LDL cholesterol ($r = -0.33$; 95%CI = -0.51 to -0.11 ; $p = 0.04$). There was a strong positive correlation of normalized MR signal intensity (SI) with the neuropathy symptom score in the subgroup of patients with painful DPN ($r = 0.80$; 95%CI = 0.46 to 0.93 ; $p = 0.005$). DRG SI was positively correlated with HbA1c levels ($r = 0.30$; 95%CI = 0.09 to 0.50 ;

$p = 0.03$) and the triglyceride/HDL ratio ($r = 0.40$; 95%CI = 0.19 to 0.57; $p = 0.007$). In this first *in vivo* study, we found DRG morphological degeneration and signal increase in correlation with neuropathy severity. This elucidates the potential importance of MR-based DRG assessments in studying structural and functional changes in DPN.

Keywords: diabetic polyneuropathy, dorsal root ganglion, magnetic resonance neurography, neuropathic pain, peripheral nervous system

INTRODUCTION

Distal symmetric diabetic polyneuropathy (DPN) is one of the most frequent and most severe complications of diabetes mellitus (Papanas and Ziegler, 2015; Nawroth et al., 2017). Although several cellular mechanisms and clinical risk factors associated with DPN have been described, the underlying pathophysiology remains poorly understood (Feldman et al., 2017). One of the major challenges for the investigation of structural changes in the central and the peripheral nervous system in human DPN is that tissue biopsies are mostly restricted to distal nerves like the sural nerve or intradermal nerve fibers (Mohseni et al., 2017). Studies that combine histological analyses of proximal structures like the sciatic nerve or dorsal root ganglia with serological parameters or behavioral traits therefore remain restricted to animal models (Novak et al., 2015).

High resolution magnetic resonance neurography (MRN) at 3 Tesla (3T), however, is a non-invasive technique that allows the detection and quantification of structural nerve lesions in patients at a fascicular level (Jende et al., 2018b, 2019a; Kurz et al., 2018). Recent MRN studies have found that nerve damage in DPN predominates at a proximal level, that proximal nerve lesions are reliably correlated with clinical parameters and serological risk factors, and that structural remodeling of sciatic nerve fascicles differs between painful and painless DPN (Pham et al., 2011; Jende et al., 2018a, 2019a; Groener et al., 2019). The finding of a proximal predominance of nerve lesions in DPN raises the question whether dorsal root ganglia also show structural alterations in DPN (Kobayashi and Zochodne, 2018).

Previous histological studies on the dorsal root ganglion (DRG) of deceased diabetes patients have found morphological changes like thickening of the perineural cell basement membrane, indicating that structural changes in DPN are not restricted to the distal peripheral nerves but also affect the DRG (Johnson, 1983). In addition, it is known from animal studies in streptozotocin (STZ) induced DPN that several metabolic and immunologic processes in the DRG are of importance in painful DPN and that a decrease in DRG volume is associated with the severity of neuropathic symptoms (Sidenius and Jakobsen, 1980; Warzok et al., 1987; Novak et al., 2015; Sango et al., 2017; Kobayashi and Zochodne, 2018). The aim of this study was to investigate correlations between DRG size and normalized signal

intensity (SI) in 3T MRN with clinical and serological data in diabetes patients with and without DPN.

MATERIALS AND METHODS

Study Participants

This study was approved by the local ethics committee (HEIST-DiC, local ethics number S-383/2016, clinicaltrials.gov identifier NCT03022721). Participants with either type 1 diabetes or type 2 diabetes took part in this prospective, cross-sectional study between September 2016 and June 2018. 120 diabetes patients were approached, of whom 65 were excluded. The process of patient selection is illustrated in **Figure 1**. Study participants were recruited from the Outpatient Clinic of Internal Medicine of our hospital. Participation in the study was voluntary and all participants gave written informed consent. Overall exclusion criteria were age <18, pregnancy, any contraindications for MRI, any history of lumbar surgery or disc protrusion, any other risk factors for polyneuropathy such as alcoholism, malignant or infectious diseases, hypovitaminosis, monoclonal gammopathy, any previous or ongoing exposure to neurotoxic agents, any chronic neurological diseases such as Parkinson's disease, restless legs syndrome, or multiple sclerosis.

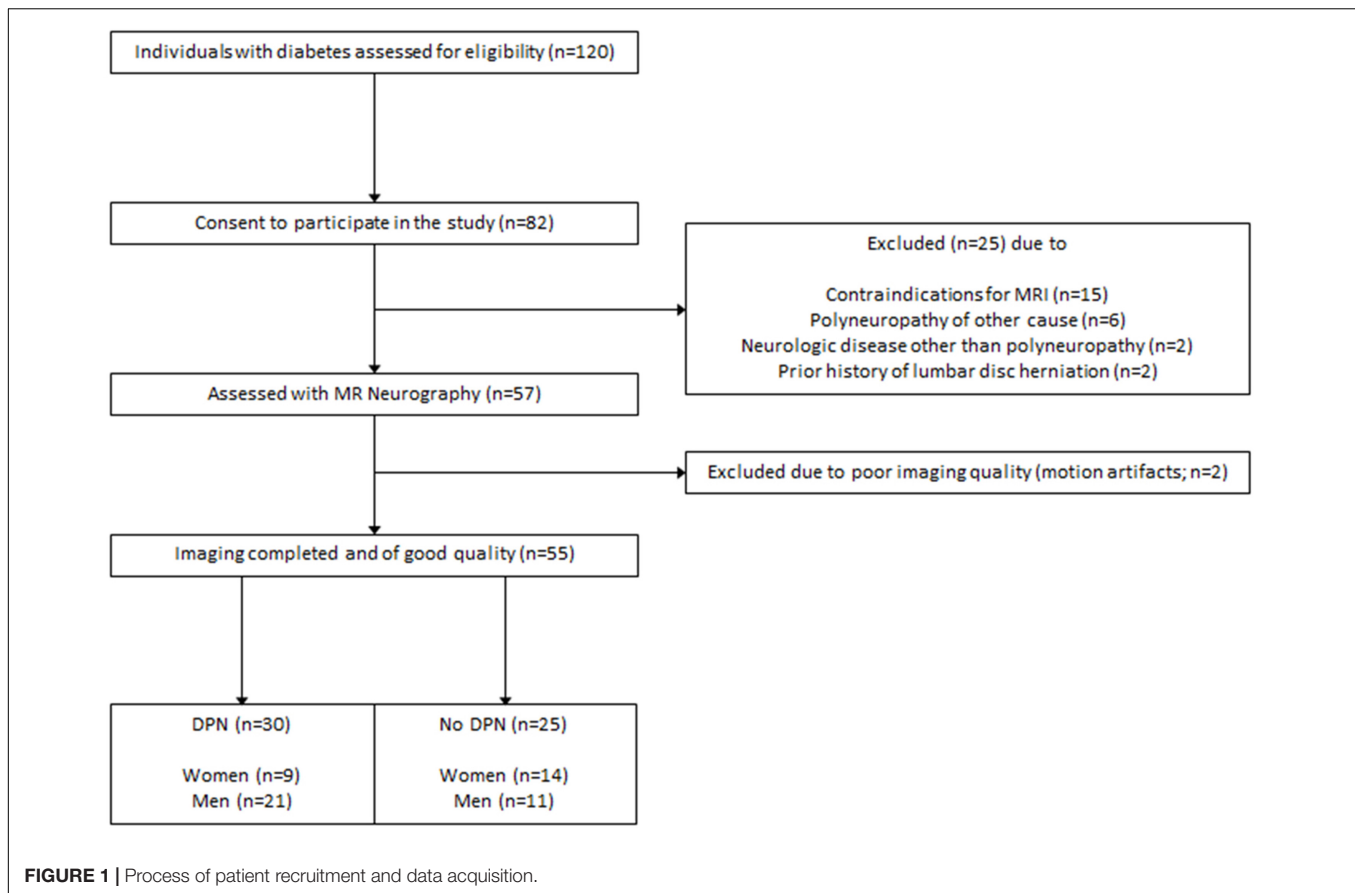
Clinical Examination

A detailed medical history was documented and an assessment of neuropathic symptoms was performed in every participant using the neuropathy disability score (NDS) and the neuropathy symptom score (NSS) (Young et al., 1993). In accordance with the guidelines issued by the German Society for Diabetology, the presence of DPN was determined by a score of ≥ 4 in NDS or NSS. Polyneuropathy was defined as mild to moderate with an NSS <7 or an NDS ≤ 8 and as severe with an NSS ≥ 7 and an NDS > 8. If a discrepancy between NDS and NSS was found, the higher score was chosen (Haslbeck et al., 2004).

Sensory symptoms were derived from the NSS questionnaire. While there are many numerical scales to score pain in DPN, (Shillo et al., 2019) we chose a binary definition for painful and painless DPN depending on whether participants with DPN either experienced painful symptoms for more than 3 months, or not. Painful symptoms were burning, lancinating, or any other painful sensations that could not be explained by other causes than DPN. If participants presented with a combination of painful and painless symptoms (e.g., burning and numbness), DPN was defined as painful.

Blood was drawn in fasting state and proceeded immediately under standardized conditions in the Central Laboratory of

Abbreviations: DPN, diabetic polyneuropathy; DRG, dorsal root ganglion; HDL, high-density lipoprotein; LDL, low-density lipoprotein; MRI, magnetic resonance imaging; MRN, magnetic resonance neurography; NDS, neuropathy disability score; NSS, neuropathy symptom score; SI, normalized signal intensity; T, Tesla.



our university hospital. The estimated glomerular filtration rate was calculated with the chronic kidney disease epidemiology collaboration formula (Levey et al., 2009).

MR Neurography Protocol

All participants underwent high-resolution MR neurography of the lumbosacral plexus in a 3T MRI scanner (TIM TRIO, SIEMENS, Erlangen, Germany). The following coils were used: a 32-channel spine coil (Spine 32 3T TIM Coil, SIEMENS Healthineers, Erlangen, Germany) and a 18-channel flex coil (Body 18 3T TIM Coil SIEMENS Healthineers, Erlangen, Germany). MR images were then acquired using a T2-weighted (T2w), three-dimensional inversion recovery sequence with sampling perfection with application-optimized contrasts using different flip angle evolution with the following parameters: field of view = 305 mm × 305 mm, voxel size = 0.95 mm × 0.95 mm × 0.95 mm, variable flip angle variation with (pseudo) steady-state flip angle = 120°, receiver bandwidth = 504 Hz/pixel, repetition time = 3000 ms, echo time = 202 ms, inversion time = 210 ms, echo train length = 209, echo spacing = 14.35 ms, number of signal averages = 2; no parallel imaging, matrix size = 320 × 320 × 104, native acquisition plane: coronal, and acquisition time 8:32 min. Since several studies on DPN in animal models have investigated the L5 DRG and since previous studies on DRG imaging in humans have come to show that L5 DRG are the largest of the lumbar DRG, the sequence was

centered to the intervertebral space of L5/S1 (Wattig et al., 1987; Silverstein et al., 2015).

Image Post-processing

With 55 participants examined and 104 slices per participant, a total number of 5720 images were acquired. All images were pseudonymized. Images were analyzed in a semi-automatic approach using ImageJ (Rha et al., 2015) and custom-written code in Matlab v7.14.0.0739 (R2012a, Mathworks, Natwick, United States). Anatomical segmentation of both left and right L5 dorsal root ganglion was performed manually for each participant on coronal reformatted images angulated to the intervertebral space between L5 and S1. All images that contained L5 DRG were used for segmentation for each participant. Segmentation was performed manually by two radiologists (JJ and FK) with 5 and 7 years of experience in neuroradiology, respectively, blinded to all clinical data. This produced stacks of binarized images with values 1 for voxels that contained DRG and values 0 for voxels that did not. We used coronal reformats for segmentation since DRG resemble ellipsoids whose main axes form a smaller angle with the normal vector on axial planes than with the normal vector on coronal planes, see e.g., (Hasegawa et al., 1996) that found an angulation of approximately 28 degrees versus the normal vector on axial planes for L5 DRG. DRG voxels at the periphery of each DRG cross-section on every considered plane only contain a part of

the respective DRG, thus producing a segmentation error that is proportional to the DRG circumference divided by the DRG area, and which is smaller for segmentation on coronal versus axial reformats due to the typical angulation of L5 DRG and the increased eccentricity of the ellipse-like cross-sections on coronal reformats. The resulting binarized image stacks of L5 DRG were analyzed in Matlab to obtain total DRG volume as the sum of all voxel volumes of both ganglia, respectively. DRG signal intensity values were first standardized to a distribution of signal intensity values of a representative artifact-free adjacent muscle tissue VOI with no discernible crossing vessels by subtracting each DRG signal intensity value with the mean value of the muscle VOI signal intensity distribution and dividing the result with the standard deviation of the muscle VOI signal intensity distribution. The resulting standardized signal intensity values were then normalized by dividing each value with the maximum of the standardized DRG signal intensity values among all participants to obtain units between 0 and 1. An illustration of DRG segmentation and three-dimensional reconstruction of nerve lesions is given in **Figure 2**.

Statistical Analysis

Statistical data analysis was performed with GraphPad Prism 6. All data were tested for Gaussian normal distribution using the D'Agostino-Pearson omnibus normality test. If a Gaussian normal distribution was given, *t*-tests were used for comparisons of two groups. If data were not Gaussian distributed, the Mann-Whitney rank sum test was used for comparisons of two groups. Non-parametric Spearman correlation was applied for correlation analysis. All correlations were controlled for age as a potential confounder using partial correlation analysis adjusted for age. For all tests, the level of significance was defined at $p < 0.05$. All results are presented as mean values \pm standard deviation (SD). The inter-rater agreement in DRG volume

segmentation was determined with the intra-class correlation coefficient (ICC) with the specific model ICC (A,1; McGraw and Wong, 1996). ICC scores below 0.4 are considered as poor agreement, 0.4–0.6 as reasonable agreement, 0.6–0.7 as good agreement, and 0.7–1 as excellent agreement (Bartko, 1991).

RESULTS

Demographic and Clinical Data

Overall, 55 participants (mean age 66 ± 9 years, 32 men) with either DPN ($n = 30$) or no DPN ($n = 25$) took part in this study. Six patients were active smokers, whereas 49 patients did not smoke. Of the 30 DPN patients, 19 had mild to moderate symptoms, whereas 11 suffered from severe DPN. Over all participants, NSS and NDS scores were both positively correlated with age ($r = 0.31$; 95%CI = 0.04 to 0.54; $p = 0.02$ and $r = 0.31$; 95%CI = 0.04 to 0.54; $p = 0.02$, respectively). All subsequent correlation analyses were therefore controlled for age as a potential confounder. Of all acquired serological parameters, triglycerides and the triglyceride/HDL index were the only parameters associated with the NDS ($r = 0.45$; 95%CI = 0.25 to 0.62; $p = 0.001$ and $r = 0.44$, 95%CI = 0.24 to 0.61; $p = 0.003$, respectively) and the NSS ($r = 0.30$; 95%CI = 0.08 to 0.49; $p = 0.04$ and $r = 0.34$; 95%CI = 0.12 to 0.52; $p = 0.03$). Triglycerides were higher in DPN patients compared to patients without DPN ($236.5 \text{ mg/dl} \pm 248$ vs $114.4 \text{ mg/dl} \pm 62.8$; $p = 0.02$), whereas the triglycerides/HDL ratio was not (4.95 ± 5.60 vs 2.41 ± 2.16 ; $p = 0.27$). An overview of clinical, demographic and serological data of study participants is given in **Table 1**.

MRN Imaging Data

L5 DRG Volume

The ICC for DRG volume segmentation was determined as 0.88. DRG volume was negatively associated with NDS ($r = -0.43$;

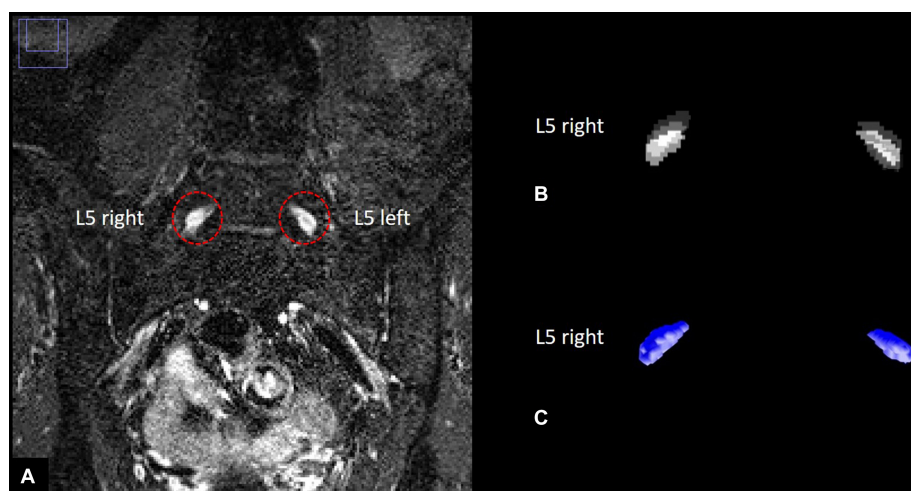


FIGURE 2 | Human dorsal root ganglia (DRG) segmentation. **(A)** Left and right L5 dorsal root ganglion on a T2-weighted, three-dimensional inversion recovery sequence with sampling perfection with application-optimized contrasts using different flip angle evolution. **(B)** Stacks of binarized masks of the left and right L5 dorsal root ganglion. **(C)** Three-dimensional reconstruction of DRG volume.

TABLE 1 | Demographic, MRN, and serologic data in patients with and without diabetic neuropathy.

Parameter	DPN (n = 30)	No DPN (n = 25)	P-Value
Women	9	14	n.a.
Men	21	11	n.a.
Type 1 diabetes	8	11	n.a.
Type 2 diabetes	22	14	n.a.
Mean Age (years)	68.38 ± 7.53 (n = 31)	59.24 ± 10.08 (n = 24)	0.02 ^M
Disease duration (years)	24.38 ± 13.56 (n = 31)	26.75 ± 13.98 (n = 24)	0.53 ^T
Body mass index (kg/m ²)	28.59 ± 4.81 (n = 31)	28.09 ± 4.66 (n = 24)	0.70 ^T
DRG volume (mm ³)	158.3 ± 44.99	150.2 ± 35.56	0.47 ^M
DRG normalized signal intensity	0.524 ± 0.066	0.519 ± 0.114	0.55 ^M
HbA1c (mmol/mol) (%)	59 ± 15	59 ± 10	0.54 ^M
Creatinine (mg/dl)	7.55 ± 1.38 (n = 31)	7.58 ± 0.98 (n = 24)	
Glomerular filtration rate (ml/min)	0.93 ± 0.24 (n = 31)	0.89 ± 0.36 (n = 23)	0.26 ^T
Total cholesterol (mg/dl)	80.69 ± 21.65 (n = 29)	80 ± 23.88 (n = 24)	0.91 ^T
LDL cholesterol (mg/dl)	177.60 ± 42.62 (n = 29)	176.8 ± 32.86 (n = 22)	0.94 ^T
HDL cholesterol (mg/dl)	89.51 ± 27.73 (n = 28)	96.14 ± 30.75 (n = 21)	0.46 ^T
HDL cholesterol (mg/dl)	54.65 ± 20.82 (n = 27)	57.71 ± 16.55 (n = 23)	0.59 ^T
Triglycerides (mg/dl)	236.50 ± 248.00 (n = 27)	114.4 ± 62.80; (n = 22)	0.02 ^M
Triglycerides/HDL ratio	4.95 ± 5.60	2.41 ± 2.16	0.27 ^M

All values are shown as mean ± standard deviation. ^M = p-value obtained from a Mann-Whitney test. ^T = p-value obtained from T-test. n.a., not applicable; HbA1c, glycated hemoglobin; LDL, low density lipoprotein; HDL, high density lipoprotein.

95%CI = -0.66 to -0.14; *p* = 0.02, **Figures 3A–C**) in patients with DPN, but not in patients without DPN (*r* = 0.17; 95%CI = -0.26 to 0.54; *p* = 0.43). No correlation was found between DRG volume and the NSS score. In patients without DPN, the only correlation found was between DRG volume and triglycerides (*r* = -0.49; 95%CI = -0.76 to -0.08; *p* = 0.020). No further correlations were found in this group. Although no difference was found between DRG volume in patients with and without DPN (158.3 ± 44.99 vs 150.2 ± 35.56; *p* = 0.47), DRG volume was smaller in patients with severe DPN when compared to mild or moderate DPN (134.7 mm³ ± 21.86 vs 170.1 mm³ ± 49.22; *p* = 0.04). Patients who were smoking showed smaller DRG volumes than non-smokers (114.0mm³ ± 14.36 vs 158.7 mm³ ± 40.41; *p* = 0.02). There was no difference in DRG size between painful and painless DPN (149.5 ± 30.02 vs 156.1 ± 43.54; *p* = 0.80). Over all participants, L5 DRG volume showed negative correlations with triglycerides (*r* = -0.40; 95%CI = -0.57 to -0.19; *p* = 0.006), and LDL cholesterol (*r* = -0.33; 95%CI = -0.51 to -0.11; *p* = 0.04). No such correlation was found for disease duration (*r* = -0.12; 95%CI = -0.34 to 0.10; *p* = 0.38), body mass index (*r* = 0.05; 95%CI = -0.17 to 0.27; *p* = 0.72), or HbA1c levels (*r* = -0.17; 95%CI = -0.38 to 0.06; *p* = 0.23).

L5 DRG T2-Weighted Normalized Signal Intensity

There was a strong positive correlation of the SI with NSS (*r* = 0.80; 95%CI = 0.46 to 0.93; *p* = 0.005, **Figures 3D–F**) and a moderate correlation between SI and NDS (*r* = 0.66; 95%CI = 0.21 to 0.88; *p* = 0.04) in patients with painful DPN. No such correlations were found in patients with non-painful DPN (*r* = -0.11; 95%CI = -0.49 to 0.28; *p* = 0.65) or no DPN (*r* = -0.14; 95%CI = -0.52 to 0.29; *p* = 0.50). Over all participants, L5 DRG T2w SI was positively correlated with HbA1c levels

(*r* = 0.30; 95%CI = 0.09 to 0.50; *p* = 0.03), triglycerides (*r* = 0.37; 95%CI = 0.16 to 0.55; *p* = 0.01), and the triglycerides/HDL ratio (*r* = 0.40; 95%CI = 0.19 to 0.57; *p* = 0.007). A negative correlation was found between SI and serum HDL (*r* = -0.35; 95%CI = -0.53 to -0.35; *p* = 0.02). No significant correlations were found between disease duration (*r* = -0.08; 95%CI = -0.30 to 0.15; *p* = 0.58), or body mass index (*r* = 0.23; 95%CI = -0.01 to 0.44; *p* = 0.10). No significant difference was found for SI between patients with and without DPN (0.52 ± 0.07 vs 0.52 ± 0.11; *p* = 0.55), between DPN patients with mild or moderate DPN and severe DPN (0.52 ± 0.06 vs 0.53 ± 0.08; *p* = 0.85), or between patients with painful and painless DPN (0.52 ± 0.10 vs 0.52 ± 0.05; *p* = 0.77). An overview of all correlations of DRG imaging parameters with demographic, clinical and serological data is given in in **Tables 1–3**.

DISCUSSION

To our knowledge, this MRN pilot study on the L5 DRG in DPN is the first to objectify *in vivo* signs of DRG morphological degeneration in DPN and to investigate whether MR signal alterations of the DRG are correlated with the severity of painful symptoms in DPN. We found that DRG volume was significantly smaller in patients with severe DPN when compared to patients with mild or moderate DPN and, accordingly, that there is a moderate negative correlation between DRG volume and NDS in DPN. We further found a strong positive correlation between DRG SI and NSS in painful DPN. In the context of previous histological studies on DRG in rodent models of DPN, our results indicate that a progression in functional loss in both sensory and motor qualities codified by higher NDS scores is associated with DRG atrophy (Kobayashi and Zochodne, 2018).

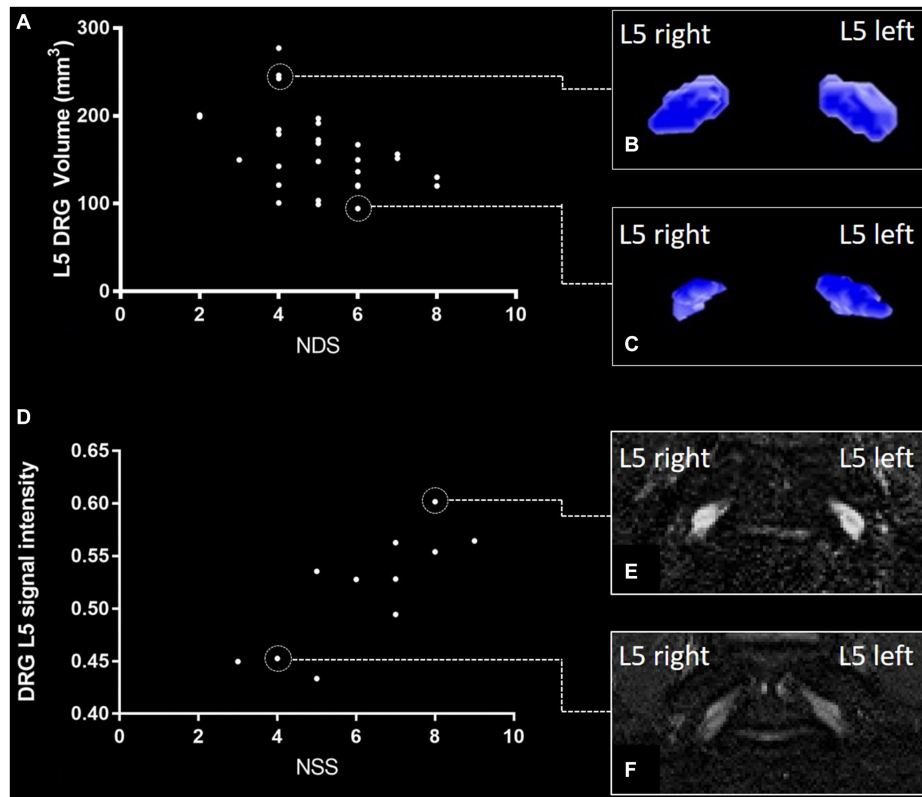


FIGURE 3 | L5 dorsal root ganglion (DRG) volume and normalized signal intensity (SI) versus neuropathy disability score (NDS) and neuropathy symptom score (NSS). **(A)** Correlation of NDS and L5 DRG volume in patients with diabetic polyneuropathy [DPN; ($r = -0.43$; 95%CI = -0.66 to -0.14 ; $p = 0.02$)]. **(B)** DRG volumetry of a patient with a total L5 DRG volume of 277 mm³. **(C)** DRG volumetry of a patient with a total L5 DRG volume of 94 mm³. **(D)** Correlation of L5 DRG SI and NSS in painful DPN ($r = 0.80$; 95%CI = 0.46 to 0.93 ; $p = 0.005$). **(E)** L5 DRG SI in a patient with severe painful DPN (SI = 0.61 ± 0.094). **(F)** L5 DRG SI in a patient with mild painful DPN (SI = 0.45 ± 0.054).

TABLE 2 | Correlation of dorsal root ganglia volume and normalized signal intensity with clinical parameters.

	L5 dorsal root ganglia volume in mm ³ (n = 55)			L5 dorsal root ganglia normalized signal intensity (n = 55)		
	r	95%CI	p	R	95%CI	p
L5 dorsal root ganglia volume (mm ³)	n.a.	n.a.	n.a.	0.12	-0.16 to 0.38	0.39
L5 dorsal root ganglia normalized signal intensity	0.12	-0.16 to 0.38	0.39	n.a.	n.a.	n.a.
NDS (n = 55)	<0.01	-0.22 to 0.22	0.99	0.13	-0.10 to 0.34	0.36
NDS DPN (n = 30)	-0.43	-0.66 to -0.14	0.02	0.03	-0.28 to 0.34	0.88
NSS (n = 55)	0.02	-0.20 to 0.25	0.87	0.10	-0.12 to 0.32	0.46
NSS DPN (n = 30)	-0.06	-0.37 to 0.25	0.74	0.22	-0.10 to 0.49	0.28
NSS painful DPN (n = 11)	0.33	-0.24 to 0.72	0.36	0.80	0.46 to 0.93	0.005
NSS painless DPN (n = 19)	-0.11	-0.49 to 0.28	0.65	-0.09	-0.47 to 0.30	0.71
NDS painful DPN (n = 11)	-0.05	-0.56 to 0.49	0.90	0.66	0.21 to 0.88	0.04
NDS painless DPN (n = 19)	-0.41	-0.69 to -0.01	0.11	-0.11	-0.49 to 0.28	0.64

All correlation coefficients are calculated as Spearman coefficients, corrected for age. 95%CI = 95% confidence interval; n.a. = not applicable. NSS = neuropathy symptom score; NDS = neuropathy disability score.

The structural equivalent for the DRG normalized signal intensity that increases with symptom severity in painful DPN remains to be determined.

The fact that no correlation was found between DRG volume and SI among study participants indicates that changes in DRG

SI are not necessarily accompanied by changes in DRG volume and vice versa. This suggests that both parameters are needed to adequately describe DRG changes in T2D DPN with respect to DRG function and clinical DPN severity, thus being two potential indicators for DPN progression.

TABLE 3 | Correlation of dorsal root ganglia volume and normalized signal intensity with demographic and serologic data.

	L5 dorsal root ganglia volume in mm ³ (n = 55)			L5 dorsal root ganglia normalized signal intensity (n = 55)		
	r	95%CI	p	R	95%CI	p
BMI (kg/m ² ; n = 55)	0.05	-0.17 to 0.27	0.72	0.23	0.01 to 0.44	0.10
Disease duration (years; n = 55)	-0.12	-0.34 to 0.10	0.38	-0.08	-0.30 to 0.15	0.58
Creatinine (mg/dl; n = 54)	0.06	-0.16 to 0.28	0.66	0.21	-0.01 to 0.42	0.14
Glomerular filtration rate (ml/min; n = 53)	0.13	-0.09 to 0.35	0.35	-0.05	-0.27 to 0.18	0.73
Total serum cholesterol (mg/dl; n = 51)	-0.25	-0.45 to -0.03	0.08	0.03	-0.19 to 0.25	0.83
LDL (mg/dl; n = 49)	-0.33	-0.51 to -0.11	0.04	0.02	-0.20 to 0.25	0.89
HDL (mg/dl; n = 50)	0.04	-0.19 to 0.26	0.81	-0.35	-0.53 to -0.35	0.02
Triglycerides (mg/dl; n = 49)	-0.40	-0.57 to -0.19	0.006	0.37	0.16 to 0.55	0.01
Triglycerides/HDL ratio	-0.26	-0.46 to -0.04	0.08	0.40	0.19 to 0.57	0.007
HbA1c (mmol/mol; n = 55)	-0.17	-0.38 to 0.06	0.23	0.30	0.09 to 0.50	0.03

All correlation coefficients are calculated as Spearman coefficients, corrected for age. 95%CI = 95% confidence interval; n.a. = not applicable. BMI = body mass index; LDL = low density lipoprotein; HDL = high density lipoprotein; HbA1c = glycated hemoglobin.

With regard to serologic parameters, in our cohort, triglycerides were higher in DPN patients when compared to non-DPN patients and showed moderate positive correlations with both NDS scores and DRG SI, while there was a moderate negative correlation with DRG volume. The latter finding may indicate that higher levels of triglycerides are associated with DRG atrophy represented by DRG volume reduction. As the DRG consists of an inner layer comprised of nerve fibers and an outer layer containing the cell bodies of pseudo-unipolar sensory neurons and an adjacent capillary network, it remains to be determined whether a reduction in DRG size in severe DPN is the consequence of damage to one of the two layers or both layers (Sasaki et al., 1997). Since DRG volume was smaller in smokers when compared to non-smokers, and since it is known that smoking causes microvascular damage, it seems likely that damage to the DRG microcirculation is a contributing factor to DRG atrophy in DPN (Tesfaye et al., 2005; Clair et al., 2015). This hypothesis is further supported by the finding of a positive correlation between L5 DRG SI and triglycerides/HDL ratio, since an increase in the latter has been reported to be associated with microvascular pathology (Ain et al., 2019). The correlation of serum triglycerides with both clinical symptom severity and reduced DRG volume is in line with data from clinical studies that have found elevated triglycerides to be a risk factor for nerve damage and increased severity of neuropathic symptoms in DPN. (Tesfaye et al., 2005; Jaiswal et al., 2017). The finding, that both triglycerides and HbA1c levels are associated with an increase in DRG SI, further is in line with findings from a previous MRN study on sciatic nerve lesions in DPN that found T2w-hyperintense nerve lesions to be associated with elevated triglycerides and HbA1c levels (Jende et al., 2019a).

The negative correlation of the DRG volume with triglycerides and the negative correlation of DRG SI with HDL levels are further in line with results from previous MRN studies on the impact of cholesterol levels on sciatic nerve damage in DPN (Andersen et al., 2018; Jende et al., 2019b). The negative correlation between LDL cholesterol and DRG volume, however, contradicts the previous finding that lower LDL cholesterol is

associated with sciatic nerve damage in DPN (Jende et al., 2019b). One possible explanation for this discrepancy might be that LDL is required to supply cholesterol to Schwann cells and neurite tips for remyelination after damage to peripheral nerves in DPN, while DRG neurons do not require an equal amount of cholesterol but, instead, as a well vascularized structure, are prone to damage caused by microangiopathy, for which elevated LDL is a risk factor (de Chaves et al., 1997; Vance et al., 2000; Saher et al., 2011; Toth et al., 2012). This assumption, however, remains hypothetical and needs to be investigated by larger longitudinal studies. With regard to the correlation of serum triglycerides with DPN severity and both DRG volume and SI one may argue that triglycerides are elevated in patients with reduced renal function or renal failure and that, accordingly, the correlations found could just be epiphenomena of a reduced renal function in our cohort (Zhang et al., 2019). One has to consider, however, that there was no correlation between GFR or creatinine and triglycerides in our cohort. Still, our data do not allow proving a causal relationship between triglycerides and DRG volume or SI.

Our study is limited by the fact that no electrophysiological recordings were performed on the participants in order to further elucidate the impact of the DRG volume and SI on peripheral nerve function. It is unlikely, however, that changes to an anatomical structure located so far proximally will contribute to detectable and directly attributable changes to peripheral nerves especially at early stages of the disease. Furthermore, nerve conduction studies are limited in localizing disturbances of conduction or sensory action potentials with high spatial accuracy so that point localization to the DRG structure itself remains problematic. Another limitation is that the acquired T2w signal intensity is a non-quantitative parameter that is prone to various potential confounders that can differ between different MRI scanners. One must consider, however, that all images used in this study were acquired at the same scanner and that DRG signal intensity was normalized to adjacent muscle tissue, which should make the results reproducible. In future studies, quantitative T2 imaging of DRG and the assessment of other quantitative MRN imaging parameters such as proton density

and fractional anisotropy, that have been shown to be accurate markers of structural peripheral nerve integrity for different neuropathies, should be investigated (Godel et al., 2016; Kollmer et al., 2018; Jende et al., 2019b, 2020; Sollmann et al., 2019; Sato et al., 2020).

The aim of this pilot study was to investigate whether there was a correlation between DRG volume and normalized MR signal intensity of a typical plexus MR sequence, DPN severity and serological risk factors for DPN. We therefore chose the validated scores of NSS and NDS for the assessment of DPN severity. Although all of the risk factors correlated with DRG volume or SI have been shown to be risk factors for the development of DPN in longitudinal clinical studies, (Jaiswal et al., 2017; Andersen et al., 2018) our study does not allow for definite conclusions on a causal relation between serological risk factors and DRG parameters, due to its cross-sectional nature. It should also be considered that the primary aim of this study was to elucidate the use and feasibility of DRG imaging in DPN with regards to DPN severity and serological parameters.

In summary, this study is the first study to image and quantify the DRG in patients with DPN and the first *in vivo* DRG imaging study that found correlations with both clinical parameters of DPN severity and serological data. The study's findings suggest that DRG volume reduction in DPN is associated with higher levels of triglycerides and that DRG SI, which is associated with symptom severity in painful DPN, is increased by hyperglycemia, and a higher triglyceride/HDL ratio. These results parallel those from peripheral nerve imaging in DPN. Further longitudinal studies are required to investigate the impact of DRG volume and SI on the course of neuropathic symptoms in DPN and to further elucidate the underlying pathophysiological processes.

DATA AVAILABILITY STATEMENT

The data supporting the conclusions of this article will be made available upon reasonable request by any qualified researcher.

ETHICS STATEMENT

The studies involving human participants were reviewed and approved by Heidelberg University Hospital Ethics Committee.

REFERENCES

- Ain, Q., Asif, N., Alam, A., Gilani, M., Shahzad, N., and Sheikh, W. (2019). Triglycerides-to-HDL ratio as a marker of cardiac disease and vascular risk factors in adults. *J. Coll. Phys.* 29, 1034–1037. doi: 10.29271/jcsp.2019.11.1034
- Andersen, S. T., Witte, D. R., Dalsgaard, E.-M., Andersen, H., Nawroth, P., Fleming, T., et al. (2018). Risk factors for incident diabetic polyneuropathy in a cohort with screen-detected type 2 diabetes followed for 13 years: addition-denmark. *Diabetes Care* 41, 1068–1075. doi: 10.2337/dc17-2062
- Bartko, J. J. (1991). Measurement and reliability: statistical thinking considerations. *Schizophr. Bull.* 17, 483–489. doi: 10.1093/schbul/17.3.483
- Clair, C., Cohen, M. J., Eichler, F., Selby, K. J., and Rigotti, N. A. (2015). The effect of cigarette smoking on diabetic peripheral neuropathy: a systematic review and meta-analysis. *J. Gen. Intern. Med.* 30, 1193–1203. doi: 10.1007/s11606-015-3354-y

The patients/participants provided their written informed consent to participate in this study.

AUTHOR CONTRIBUTIONS

JJ, MP, MB, SH, PN, and FK designed and coordinated the study. JJ, DO, JG, JK, AJ, and FK contributed to the organization of the participants. JJ, CR, MP, AJ, and FK collected the MR data. AH and FK developed image analysis tools. ZK, LA-R, JG, DO, and SK collected clinical, serological and electrophysiological the data. JJ and FK analyzed the data and wrote the manuscript with input from all co-authors. All authors contributed to the article and approved the submitted version.

FUNDING

MB received grants from the Dietmar Hopp foundation, the European Union and the German Research Council (DFG, SFB 1118, and 1158). The German research council (DFG, SFB 1158) provided financial support for personnel expenditure, MR imaging costs and costs for the technical equipment required for electrophysiological and serological analysis. The DFG had no influence on the study design, collection and analysis of data or on the writing of the article. FK was supported by the German Research Foundation (KU 3555/1-1) and the Hoffmann-Klose foundation of Heidelberg University Hospital. JJ was supported by the International Foundation for Research in Paraplegia which provided financial support for the development of image analysis tools.

ACKNOWLEDGMENTS

We thank Mrs. Johanna Kreck (Department of Neuroradiology, Heidelberg University Hospital) for her ongoing support and excellent technical performance of all MRN examinations. This study was supported by the German Research Council (SFB 1158 and 1118) and by the International Foundation for Research in Paraplegia (IRP).

- de Chaves, E. I., Rusiñol, A. E., Vance, D. E., Campenot, R. B., and Vance, J. E. (1997). Role of lipoproteins in the delivery of lipids to axons during axonal regeneration. *J. Biol. Chem.* 272, 30766–30773. doi: 10.1074/jbc.272.49.30766
- Feldman, E. L., Nave, K.-A., Jensen, T. S., and Bennett, D. L. H. (2017). New horizons in diabetic neuropathy: mechanisms, bioenergetics, and pain. *Neuron* 93, 1296–1313. doi: 10.1016/j.neuron.2017.02.005
- Godel, T., Pham, M., Heiland, S., Bendszus, M., and Bäumer, P. (2016). Human dorsal-root-ganglion perfusion measured in-vivo by MRI. *Neuroimage* 141, 81–87. doi: 10.1016/j.neuroimage.2016.07.030
- Groener, J. B., Jende, J. M. E. J., Kurz, F. T. F., Kender, Z., Treede, R. R.-D., Schuh-Hofer, S., et al. (2019). Understanding diabetic neuropathy: from subclinical nerve lesions to severe nerve fiber deficits. A cross-sectional study in patients with type 2 diabetes and healthy controls. *Diabetes* 69, 436–447. doi: 10.2337/db19-0197

- Hasegawa, T., Mikawa, Y., Watanabe, R., and An, H. S. (1996). Morphometric analysis of the lumbosacral nerve roots and dorsal root ganglia by magnetic resonance imaging. *Spine* 21, 1005–1009. doi: 10.1097/00007632-19960510-00001
- Haslbeck, M., Luft, D., Neundörfer, B., Stracke, H., Ziegler, D., and Stracke, H. (2004). *Diagnosis, Treatment and Follow-up of Diabetic Neuropathy Diagnosis, Therapy and Follow-up of Sensorimotor Diabetic Neuropathy*, 2nd Edn. Berlin: German Diabetes Association, 8–10.
- Jaiswal, M., Divers, J., Dabelea, D., Isom, S., Bell, R. A., Martin, C. L., et al. (2017). Prevalence of and risk factors for diabetic peripheral neuropathy in youth with type 1 and type 2 diabetes: search for diabetes in youth study. *Diabetes Care* 40, 1126–1132.
- Jende, J. M. E., Groener, J. B., Kender, Z., Rother, C., Hahn, A., Hilgenfeld, T., et al. (2019a). Structural nerve remodeling on 3-T MR Neurography differs between painful and painless diabetic polyneuropathy in either type 1 or type 2 diabetes. *Radiology* 294, 405–414. doi: 10.1148/radiol.2019191347
- Jende, J. M. E., Groener, J. B., Kender, Z., Hahn, A., Morgenstern, J., Heiland, S., et al. (2020). Troponin T parallels structural nerve damage in type 2 diabetes A cross sectional study using magnetic resonance neurography. *Diabetes* 69, 713–723. doi: 10.2337/db19-1094
- Jende, J. M. E., Groener, J. B., Oikonomou, D., Heiland, S., Kopf, S., Pham, M., et al. (2018a). Diabetic neuropathy differs between type 1 and type 2 diabetes: insights from magnetic resonance neurography. *Ann. Neurol.* 83, 588–598. doi: 10.1002/ana.25182
- Jende, J. M. E., Groener, J. B., Rother, C., Kender, Z., Hahn, A., Hilgenfeld, T., et al. (2019b). Association of serum cholesterol levels with peripheral nerve damage in patients with type 2 diabetes. *JAMA Netw. Open* 2:e194798. doi: 10.1001/jamanetworkopen.2019.4798
- Jende, J. M. E., Hauck, G. H., Diem, R., Weiler, M., Heiland, S., Wildemann, B., et al. (2018b). Peripheral nerve involvement in multiple sclerosis: demonstration by magnetic resonance neurography. *Ann. Neurol.* 82, 676–685. doi: 10.1002/ana.25068
- Johnson, P. C. (1983). Thickening of the human dorsal root ganglion perineurial cell basement membrane in diabetes mellitus. *Muscle Nerve* 6, 561–565. doi: 10.1002/mus.880060805
- Kobayashi, M., and Zochodne, D. W. (2018). Diabetic neuropathy and the sensory neuron: new aspects of pathogenesis and their treatment implications. *J. Diabetes Invest.* 9, 1239–1254. doi: 10.1111/jdi.12833
- Kollmer, J., Kästel, T., Jende, J. M. E., Bendszus, M., and Heiland, S. (2018). Magnetization transfer ratio in peripheral nerve tissue. *Invest. Radiol.* 53:1. doi: 10.1007/978-3-030-06217-0_5-1
- Kurz, F. T., Buschle, L. R., Hahn, A., Jende, J. M. E., Bendszus, M., Heiland, S., et al. (2018). Diffusion effects in myelin sheath free induction decay. *J. Magn. Reson.* 297, 61–75. doi: 10.1016/j.jmr.2018.10.001
- Levey, A. S., Stevens, L. A., Schmid, C. H., Zhang, Y. L., Castro, A. F., Feldman, H. I., et al. (2009). A new equation to estimate glomerular filtration rate. *Ann. Intern. Med.* 150, 604–612.
- McGraw, K. O., and Wong, S. P. (1996). Forming inferences about some intraclass correlation coefficients. *Psychol. Methods* 1, 30–46. doi: 10.1037/1082-989x.1.1.30
- Mohseni, S., Badii, M., Kylhammar, A., Thomsen, N. O. B., Eriksson, K.-F., Malik, R. A., et al. (2017). Longitudinal study of neuropathy, microangiopathy, and autophagy in sural nerve: implications for diabetic neuropathy. *Brain Behav.* 7:e00763. doi: 10.1002/brb3.763
- Nawroth, P. P., Bendszus, M., Pham, M., Jende, J., Heiland, S., Ries, S., et al. (2017). The quest for more research on painful diabetic neuropathy. *Neuroscience* 387, 28–37. doi: 10.1016/j.neuroscience.2017.09.023
- Novak, P., Pimentel, D. A., Sundar, B., Moonis, M., Qin, L., and Novak, V. (2015). Association of statins with sensory and autonomic ganglionopathy. *Front. Aging Neurosci.* 7:191. doi: 10.3389/fnagi.2015.00191
- Papanas, N., and Ziegler, D. (2015). Risk factors and comorbidities in diabetic neuropathy: an update 2015. *Rev. Diabet. Stud.* 12, 48–62. doi: 10.1900/rds.2015.12.48
- Pham, M., Oikonomou, D., Bäumer, P., Bierhaus, A., Heiland, S., Humpert, P. M., et al. (2011). Proximal neuropathic lesions in distal symmetric diabetic polyneuropathy. *Diabetes Care* 34, 721–723. doi: 10.2337/dc10-1491
- Rha, E. Y., Kim, J. M., and Yoo, G. (2015). Volume measurement of various tissues using the image J software. *J. Craniofac. Surg.* 26, e505–e506. doi: 10.1097/SCS.0000000000002022
- Saher, G., Quintes, S., and Nave, K.-A. (2011). Cholesterol: a novel regulatory role in myelin formation. *Neuroscience* 17, 79–93. doi: 10.1177/1073858410373835
- Sango, K., Mizukami, H., Horie, H., and Yagihashi, S. (2017). Impaired axonal regeneration in diabetes. perspective on the underlying mechanism from in vivo and in vitro experimental studies. *Front. Endocrinol.* 8:12. doi: 10.3389/fendo.2017.00012
- Sasaki, H., Schmelzer, J. D., Zollman, P. J., and Low, P. A. (1997). Neuropathology and blood flow of nerve, spinal roots and dorsal root ganglia in longstanding diabetic rats. *Acta Neuropathol.* 93, 118–128. doi: 10.1007/s004010050592
- Sato, T., Eguchi, Y., Norimoto, M., Inoue, M., Enomoto, K., Watanabe, A., et al. (2020). Diagnosis of lumbar radiculopathy using simultaneous MR neurography and apparent T2 mapping. *J. Clin. Neurosci.* 78, 339–346. doi: 10.1016/j.jocn.2020.04.072
- Shillo, P., Sloan, G., Greig, M., Hunt, L., Selvarajah, D., Elliott, J., et al. (2019). Painful and painless diabetic neuropathies: what is the difference? *Curr. Diab. Rep.* 19:32. doi: 10.1007/s11892-019-1150-5
- Sidenius, P., and Jakobsen, J. (1980). Reduced perikaryal volume of lower motor and primary sensory neurons in early experimental diabetes. *Diabetes* 29, 182–187. doi: 10.2337/diabetes.29.3.182
- Silverstein, M. P., Romrell, L. J., Benzel, E. C., Thompson, N., Griffith, S., and Lieberman, I. H. (2015). Lumbar dorsal root Ganglia location: an anatomic and MRI assessment. *Int. J. spine Surg.* 9:3. doi: 10.14444/2003
- Sollmann, N., Weidlich, D., Cervantes, B., Klupp, E., Ganter, C., Kooijman, H., et al. (2019). High isotropic resolution T2 mapping of the lumbosacral plexus with T2-prepared 3D turbo spin echo. *Clin. Neuroradiol.* 29, 223–230. doi: 10.1007/s00062-017-0658-9
- Tesfaye, S., Chaturvedi, N., Eaton, S. E. M., Ward, J. D., Manes, C., Ionescu-Tirgoviste, C., et al. (2005). Vascular risk factors and diabetic neuropathy. *New Engl. J. Med.* 352, 341–350. doi: 10.1056/NEJMoa032782
- Toth, P. P., Simko, R. J., Palli, S. R., Koselleck, D., Quimbo, R. A., and Cziraky, M. J. (2012). The impact of serum lipids on risk for microangiopathy in patients with type 2 diabetes mellitus. *Cardiovasc. Diabetol.* 11:109. doi: 10.1186/1475-2840-11-109
- Vance, J. E., Campenot, R. B., and Vance, D. E. (2000). The synthesis and transport of lipids for axonal growth and nerve regeneration. *Biochim. Biophys. Acta* 1486, 84–96. doi: 10.1016/s1388-1981(00)00050-0
- Warzok, R., Wattig, B., Rudel, J., Schwanengel, H., and Timmel, A. (1987). [Morphology of diabetic neuropathy]. *Zentralblatt fur Allg. Pathol. u. Pathol. Anat.* 133, 119–126.
- Wattig, B., Warzok, R., von Zglinicki, T., Röder, H., and Radzewitz, B. (1987). [Experimental diabetic neuropathy. Morphometric studies of spinal ganglia cells in short-term streptozotocin-induced diabetes]. *Zentralblatt fur Allg. Pathol. u. Pathol. Anat.* 133, 127–132.
- Young, M. J., Boulton, A. J. M., Macleod, A. F., Williams, D. R. R., and Onksen, P. H. S. (1993). A multicentre study of the prevalence of diabetic peripheral neuropathy in the United Kingdom hospital clinic population. *Diabetologia* 36, 150–154. doi: 10.1007/bf00400697
- Zhang, X., Wang, B., Yang, J., Wang, J., Yu, Y., Jiang, C., et al. (2019). Serum lipids and risk of rapid renal function decline in treated hypertensive adults with normal renal function. *Am. J. Hypertens.* 32, 393–401. doi:10.1093/ajh/hpz001

Conflict of Interest: MB received grants and personal fees from Codman, Guerbet, Bayer, and Novartis, personal fees from Roche, Teva, Springer, Boehringer, and grants from Siemens. JG was employed by company Medicover GmbH.

The remaining authors declare that the research was conducted in the absence of any commercial or financial relationships that could be construed as a potential conflict of interest.

Copyright © 2020 Jende, Kender, Rother, Alvarez-Ramos, Groener, Pham, Morgenstern, Oikonomou, Hahn, Juerchott, Kollmer, Heiland, Kopf, Nawroth, Bendszus and Kurz. This is an open-access article distributed under the terms of the Creative Commons Attribution License (CC BY). The use, distribution or reproduction in other forums is permitted, provided the original author(s) and the copyright owner(s) are credited and that the original publication in this journal is cited, in accordance with accepted academic practice. No use, distribution or reproduction is permitted which does not comply with these terms.



Sural Nerve Perfusion in Mice

Anete Dudele^{1,2*}, Peter Mondrup Rasmussen¹ and Leif Østergaard^{1,2,3}

¹ Center of Functionally Integrative Neuroscience (CFIN), Department of Clinical Medicine, Aarhus University, Aarhus, Denmark, ² The International Diabetic Neuropathy Consortium, Aarhus University Hospital, Aarhus, Denmark, ³ Department of Neuroradiology, Aarhus University Hospital, Aarhus, Denmark

Peripheral nerve function is metabolically demanding and nerve energy failure has been implicated in the onset and development of diabetic peripheral neuropathy and neuropathic pain conditions. Distal peripheral nerve oxygen supply relies on the distribution of red blood cells (RBCs) in just a few, nearby capillary-sized vessels and is therefore technically challenging to characterize. We developed an approach to characterize distal sural nerve hemodynamics in anesthetized, adult male mice using *in vivo* two-photon laser scanning microscopy. Our results show that RBC velocities in mouse sural nerve vessels are higher than those previously measured in mouse brain, and are sensitive to hindlimb temperatures. Nerve blood flow, measured as RBC flux, however, was similar to that of mouse brain and unaffected by local temperature. Power spectral density analysis of fluctuations in RBC velocities over short time intervals suggest that the technique is sufficiently sensitive and robust to detect subtle flow oscillations over time scales from 0.1 to tens of seconds. We conclude that *in vivo* two-photon laser scanning microscopy provides a suitable approach to study peripheral nerve hemodynamics in mice, and that local temperature control is important during such measurements.

OPEN ACCESS

Edited by:

Olivier Scheidegger,
University Hospital Bern, Switzerland

Reviewed by:

Alberto L. Vazquez,
University of Pittsburgh, United States
Patrick J. Drew,
Pennsylvania State University (PSU),
United States

*Correspondence:

Anete Dudele
anete.dudele@cfi.au.dk

Specialty section:

This article was submitted to
Brain Imaging Methods,
a section of the journal
Frontiers in Neuroscience

Received: 02 July 2020

Accepted: 09 November 2020

Published: 10 December 2020

Citation:

Dudele A, Rasmussen PM and
Østergaard L (2020) Sural Nerve
Perfusion in Mice.
Front. Neurosci. 14:579373.
doi: 10.3389/fnins.2020.579373

Keywords: mice, sural nerve, nerve blood flow, hindlimb temperature, red blood cell velocity, two-photon microscopy

INTRODUCTION

Nerve blood flow is important for peripheral nerve function and nerve blood flow deficits have been implicated in peripheral nerve pathologies, e.g., diabetic peripheral neuropathy (DPN) and neuropathic pain conditions (Cameron and Cotter, 1997; Lim et al., 2015). Metabolic demands of neural tissue are very high and this is reflected in the tissue blood flow. Peripheral nerve blood flow is comparable to blood flow measured in cortical and spinal cord gray matter, and is higher than in white matter of the spinal cord (Zochodne, 2018). However, unlike the brain, peripheral nervous tissue is not prone to ischemic injury, partly due to its redundant, segmental blood supply and high overall ischemic tolerance. It takes as long as 1–3 h of ischemia to induce permanent axonal damage in peripheral nerves (Zochodne, 2018). However, peripheral nerves affected by diabetes are more sensitive to ischemic damage and this has been attributed to chronic insufficient oxygenation due to capillary dysfunction (Østergaard et al., 2015).

The measurement of blood supply in peripheral nerves is challenging, particularly at the capillary level. Although chronic hypoxia has been implicated in the onset and progression of DPN, nerve blood supply has thus far mainly been measured in the larger, more proximal peripheral nerves (Tuck et al., 1984; Newrick et al., 1986; Østergaard et al., 2015). In the larger nerves, such

as the rat sciatic nerve, absolute nerve blood supply (in mL blood per 100 g tissue per minute) can be measured by radiotracer and hydrogen clearance methods, while relative nerve blood flow can be estimated over time using laser Doppler flow (LDF) probes. LDF measurements, however, have limited spatial specificity as they are based on laser light reflected by moving red blood cells (RBC) down to depth of 250 μm , making this method prone to signal contributions from surrounding tissue, particularly in small nerves (Zochodne, 2018).

Accurate measurements of blood flow in small distal, peripheral nerves in the 50–200 μm diameter range are important, not only to understand how their metabolic demands are met, but also to understand whether limited oxygenation and microvascular changes play a role in the pathophysiology of diseases that first affect the most peripheral nerve fibers, such as DPN (Gonçalves et al., 2017). Such measurements are extremely challenging, however, as these nerves receive their blood supply from just a few microvessels, often on the nerve's surface, as nerve diameters approach the typical diffusion lengths for molecular oxygen.

The aim of this study was to develop an approach to characterize distal peripheral nerve hemodynamics in mice sural nerves located in the hindlimb using *in vivo* two-photon laser scanning microscopy (TPLSM), based on techniques previously used to study perfusion across individual capillaries in the cerebral cortex in rats (Kleinfeld et al., 1998). Because peripheral nerves are prone to temperature changes (Dines et al., 1997), which occur in relation to the surgical exposure necessary for *in vivo* microscopy (Roche et al., 2019), we first applied the method to characterize the effects of local hindlimb temperature on hemodynamic recordings in the sural nerves of mice.

MATERIALS AND METHODS

Animals

Male C57BL/6J Bom mice (Taconic, Lille Skensved, Denmark) were acclimated to our animal facility for a minimum of 1 week. Mice were housed in groups at 22–24°C and approximately 55% air humidity with a 12:12 h light:dark cycle starting at 7 AM. Mice had access to water and chow *ad libitum* (Altromin, 1324 Rodent Diet, Brogaarden, Gentofte, Denmark) at all times.

Ten mice underwent *in vivo* imaging at the age of 15–19 weeks, weighing 27–37 g (mean \pm SEM 31.1 \pm 0.8 g). Additional five mice at the age 18–19 weeks, weighing 28–35 g (mean \pm SEM, 30.2 \pm 1.2 g) were used for perfusion with gelatinized India Ink and the following histology analyses.

Histology

India Ink Perfusion

Mice were anesthetized with 5% isoflurane inhalation in atmospheric air followed by an intraperitoneal injection of sodium pentobarbital overdose. Immediately after cessation of spontaneous respiration, mice were placed under a heating lamp to keep the temperature at 37°C, the heart exposed by

an incision through the ribcage, and a needle connected to a perfusion pump inserted into the left ventricle. A small hole was cut in the right ventricle and the mouse was then perfused with warm (37°C) heparinized PBS for 10 min at a flow rate of 4 ml/min using a peristaltic perfusion pump (Minipuls 3, Gilson, Villiers, France). This was followed by 5 min of perfusion with a warm (37°C) solution of 10% India Ink in deionized water with 2% gelatin (Xue et al., 2014) at a flow rate of 4 ml/min. The carcass was then placed in a sealed plastic bag and immersed in ice water for 30 min to solidify the gelatin. The skin on the lower hindlimb was removed and the sural nerve with its over- and under-laying muscles was dissected and embedded in a mold in optimal cutting temperature compound (QPath, VWR Inc., West Chester, PA, United States) and frozen on dry ice.

Ten μm thick transversal sections of the lower limb muscles and nerve were cut using a cryostat (Cryostar NX70, Thermo Scientific, Waltham MA; United States) and immediately visualized under light microscope (Leica DM5000 B, Wetzlar, Germany). Images were captured and then analyzed using Fiji (Schindelin et al., 2012; Rueden et al., 2017). One section was analyzed for each mouse to determine the cross-sectional area of each nerve fiber, and the number of vessels within (endoneurial vessels) and directly adjacent to (epineurial vessels) the nerve fiber. Epineurial vessels were subdivided into “large” and “small” adjacent vessels, as illustrated in **Figures 1A,B**, where “vein” is a “large” adjacent vessel, and the capillaries labeled “c” are small epineurial vessels. Then, the total number of vessels per nerve fiber area were calculated, including the large and small vessels.

In vivo Imaging Surgical Preparation

On the day of *in vivo* imaging, each mouse was weighed and anesthetized by 5% isoflurane mixed with medical air supplemented with oxygen to a FiO_2 of approximately 25%. Immediately following induction, the mouse was placed on a heating pad and its core body temperature maintained at 37°C with a thermostat connected to the mouse rectal probe (HB 101/2, Harvard Apparatus, Holliston, MA, United States). Isoflurane was maintained at 1.75–2% during surgery, and reduced to 1–1.25% during *in vivo* imaging protocol.

Following local hair removal and disinfection with 70% (v/v) alcohol, the trachea was exposed by a midline skin incision and blunt dissection through connective tissue and muscle. Following a small incision in the trachea just below the larynx, a 2.5 cm long, 0.86 mm inner diameter (ID) and 1.27 mm outer diameter (OD) PE-90 polyethylene tube (BD Intramedic, Clay Adams Brand, Sparks, MD, United States) was inserted into the trachea and secured by sutures. After the skin was sutured, the tube was connected to a mechanical ventilator (SAR-830/AP ventilator, CWE Inc., Ardmore, PA, United States) with ventilation flow set at 60 cc/min, individually adjusted ventilation rate, and 1:1 inspiration/expiration ratio. End-tidal CO_2 levels in expired air were monitored using a micro-capnograph (Microcapstar, CWE Inc., Ardmore, PA, United States), which was calibrated

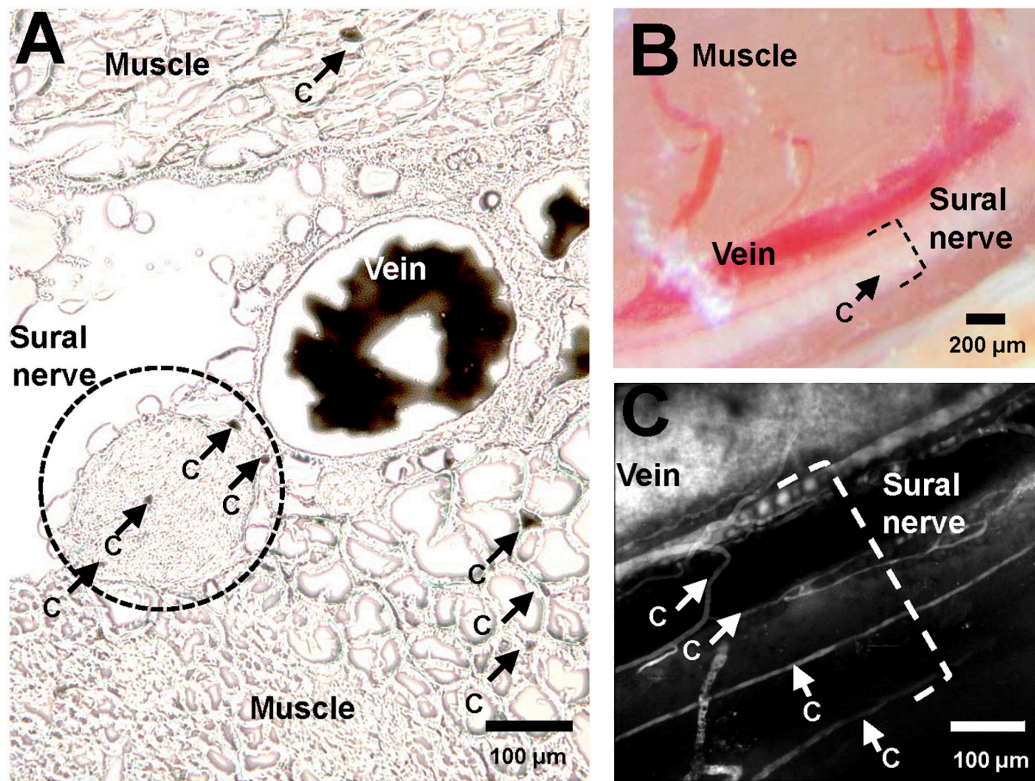


FIGURE 1 | Vasculature of murine sural nerve. **(A)** Cross section of murine sural nerve and surrounding tissue at the approximate location of *in vivo* imaging. Vasculature visualized using perfusion with gelatinized India Ink. Frozen, unfixed 10 μm thick sections visualized under light microscope. Sural nerve highlighted by a dashed black circle. Some tissue capillaries in nerve and muscle are indicated by black arrows and letter “c”. **(B)** Murine sural nerve preparation visualized through surgical microscope after preparation of sural nerve window. Sural nerve highlighted by black dashed bracket. One small vessel, indicated by a black arrow and letter “c” can be seen crossing the nerve. **(C)** Maximum intensity projection image of a volumetric two-photon *in vivo* scan of murine sural nerve and its vasculature. Only vasculature is labeled with fluorescent dye, therefore it appears in white. The nerve is not labeled, therefore it is not visible, but its location is highlighted with a white dashed bracket. Sural nerve vessels where single file RBC passage has been observed indicated with white arrows and letter “c”.

prior to surgery using two point calibration using medical air and 5% CO_2 .

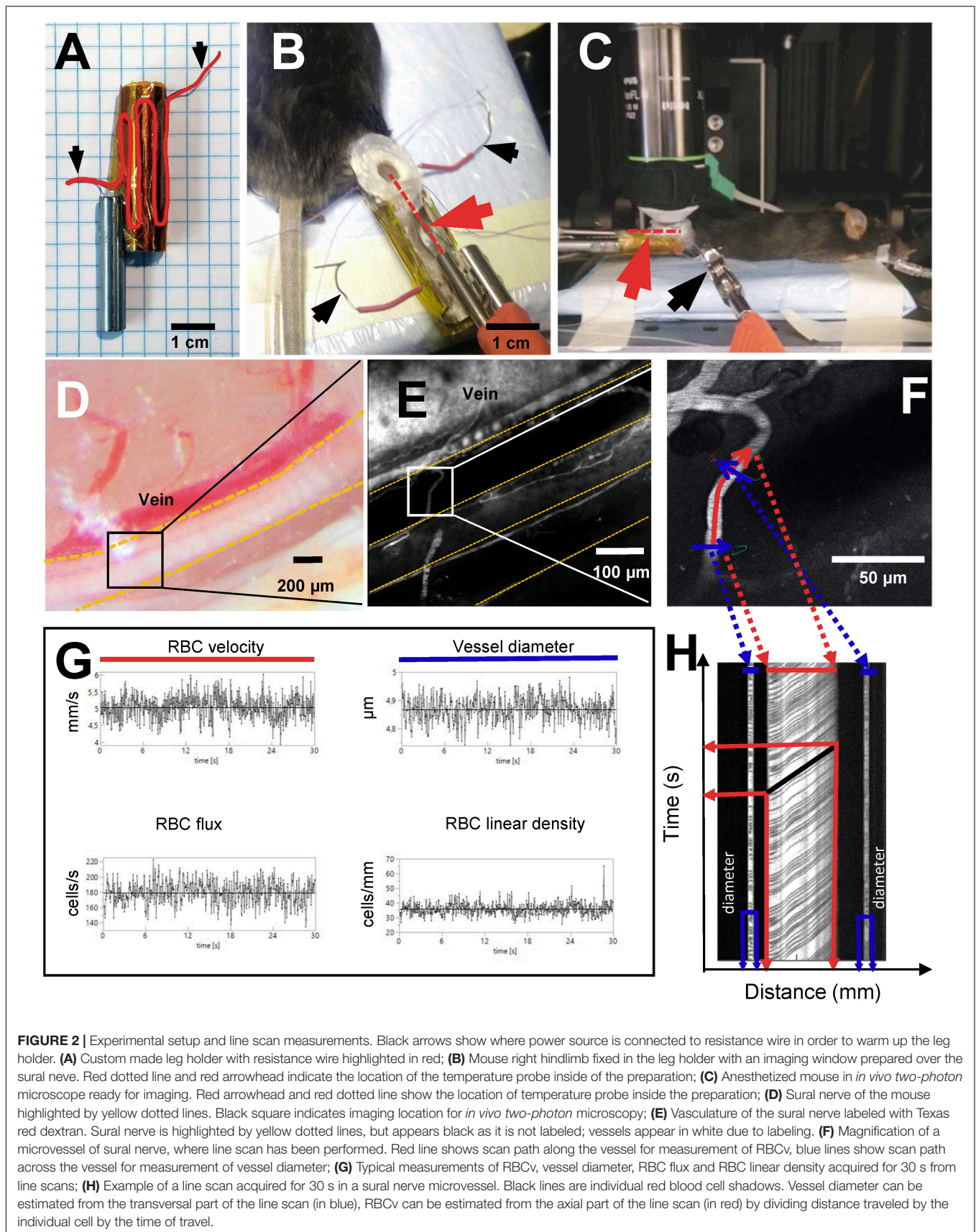
An inguinal skin incision was performed in the left hindlimb to cannulate the femoral artery and vein using 0.28 mm ID and 0.61 mm OD PE-10 polyethylene catheters (BD Intramedic, Clay Adams Brand, Sparks, MD, United States). The venous catheter was used for fluorescent dextran dye injection, and the arterial catheter for continuous blood pressure and heart rate monitoring (BP-1 system, WPI Inc., Sarasota, FL, United States). Arterial pressure, ventilation rate, and end-tidal CO_2 were recorded and stored using 16/35 PowerLab data acquisition system (ADInstruments, Oxford, United Kingdom). Mean arterial pressure (MAP) and heart rate (HR) were calculated from the continuous blood pressure curves.

Nerve Window

Following intubation and catheterization, the mouse was placed in a prone position and the right hindlimb was fixed in a custom leg holder. The holder was made from a 3.5 cm long hollow (8 mm ID, 10 mm OD) stainless steel tube with the top section removed (Figures 2A,B). The outside of the holder (Figure 2A) was covered with kapton tape and a 17.5 cm long piece of

resistance wire (0.4 mm diameter, 3.9 ohm/m) was folded around it and secured using a second layer of kapton tape to ensure electrical insulation. The exposed ends of the resistance wire were connected to an adjustable linear power supply (GPS-2302, GW Instek, Taiwan) which was used to warm the fixed hindlimb to a desired temperature.

The right hindlimb was fixed in the holder using luting dental cement (GC Fuji PLUS, Leuven, Belgium). Following a popliteal incision, the semitendinous and posterior femoral biceps muscles were isolated by blunt dissection and retracted with sutures to expose the sural nerve without causing bleeding (Figures 2B,D). If any muscle bleeding occurred, hemostasis was secured by extra fine cauterizing forceps. The nerve was covered with a drop of low viscosity silicone (KWIK-SIL, World Precision Instruments, Sarasota, FL, United States) and a round 5 mm diameter coverslip. Dental cement was applied around the edge of the coverslip, fixing it to the leg holder and thus creating a stable sural nerve window (Figure 2B). Following these procedures, a 3 cm long, 0.33 mm hypodermic needle microprobe with a thermocouple (time constant 0.025 s, MT-29/3, Physitemp Instruments Inc, Clifton NJ, United States) was inserted into the leg, proximad and parallel to the nerve, and



advanced into the nerve window beneath the imaging plane (Red dotted line in **Figure 2B**). The probe was connected to the BAT-12 microprobe thermometer (Physitemp Instruments Inc., Clifton NJ, United States) and temperature was recorded using Power Lab data acquisition system.

After the completion of surgical preparation, the mouse was positioned under the objective of the two-photon laser microscope (**Figure 2C**).

Nerve perfusion was studied at peripheral temperatures of 37, 32, and 28°C, as recorded in the hindlimb of the anesthetized mice using the temperature needle microprobe. These temperatures were chosen, as they typically occur in the hindlimb before surgical exposure, after surgical exposure and window preparation, or after positioning for imaging using water immersion objective, respectively.

In vivo Imaging Protocol

Nerve perfusion measurements were conducted using a Prairie Ultima-IV *In vivo* Laser Scanning Microscope (Brucker Corporation, Billerica, MA, United States) equipped with an Olympus water immersion 20X objective with 1.0 numerical aperture and 2.0 mm working distance, with an x - y resolution of 0.21 μm and depth resolution of 0.81 μm . To image nerve vasculature, plasma was labeled by injecting 150 μL of 0.5% Texas-red dextran solution in sterile 0.9% saline (70,000 MW, 5 mg/mL, Thermo Fisher Scientific) through the femoral vein catheter. The dye was excited using a laser light wavelength of 900 nm, and fluorescence detected by a GaAsP photomultiplier (Hamamatsu, H7422-40) using a 660/40 nm-emission filter. Using this approach, the blood plasma fraction appears bright in the acquired images (**Figure 2E**), while unlabeled RBC appear as dark shadows (**Figures 2F,H**).

Throughout imaging, mouse core body temperature was maintained at 37°C, while hindlimb temperature was adjusted to 28, 32, and 37°C in a randomized order for nerve perfusion measurements. Accordingly, at the start of the *in vivo* imaging protocol, the temperature was set to one of the three temperatures, and nerve perfusion was measured within 3 min after the temperature had stabilized at the desired level. The time needed for limb temperature to stabilize never exceeded 12 min.

Red blood cell velocity (RBCv, mm/s), flux (RBC/s), linear density (LD, RBC/mm), and vessel diameter (μm) were measured in sural nerve microvessels where single file RBC passages were observed, avoiding vessels with stalled or no flow at the initial selection. Accordingly, in each animal, the selected vessels were scanned at all three temperatures when possible. In some instances, microscopic shifts in tissue position or technical issues related to TPLSM, prevented data acquisition during all three conditions. RBC dynamics were measured as previously described (Gutierrez-Jimenez et al., 2016). Briefly, line scans were planned using the “freehand line” function of the microscope. The line scan path was prescribed both along and across the axis of each vessel. **Figure 2F** shows a typical example of such a line for the line scan. The scan data acquired along the midline of the vessel, indicated by the red line in **Figure 2F**, was used to estimate RBCv, flux, and LD. The scan data acquired along the

line perpendicular to the vessel, indicated by the blue lines in **Figure 2F**, was used to estimate vessel diameter, and to provide an additional estimate of RBC flux and LD. The signal along each line scan was continuously recorded for 30 s at each of the temperatures.

Once the line scans had been performed at all temperatures, an angiogram of the nerve’s vasculature was acquired by recording a stack of two dimensional images in the z -direction, as deep as the preparation allowed.

Immediately after imaging, the mice were euthanized by sodium pentobarbital overdose (Exagon vet., Richter Pharma, Wels, Austria).

Image Processing

Vessel diameter, RBCv, flux and linear density were estimated from the line scans using software developed in-house for Matlab (R2016b, Mathworks Inc.) as previously described (Drew et al., 2010; Gutierrez-Jimenez et al., 2016).

The line scans acquired during the 30 s were stacked to create a two dimensional raw image with time on Y -axis and distance on X -axis (**Figure 2H**). In these images dark, angled streaks appear on the axial portion of the line scan (indicated in red in **Figures 2F,H**). The angle of each streak shows displacement of the individual RBC on both time and distance axes thus resulting in RBCv. These angles were determined automatically using Radon transform algorithm. Velocity estimates with signal to noise ratio below three were excluded from the analyses (Drew et al., 2010).

Vessel diameter was estimated from the cross sectional part of the line scan (indicated in blue in **Figures 2F,H**) as a full width at half maximum, assuming that the cross section represents the full diameter of the vessel. This was only done in the “light” portions of the cross sectional scan where no RBCs were present. RBC flux was determined utilizing temporal intensity changes in the signal, indicating presence or absence of RBC both from axial and cross sectional parts of the line scans. The intensity variation was analyzed using cluster analysis to determine presence of RBC in the vessel at the given time and RBC flux (cells per second) was calculated. RBC linear density was calculated as a ratio between RBCv and flux.

All estimates were derived using a sliding window approach. Accordingly, starting from time zero of each 30 s line scanning data set, each parameter (RBCv, Flux, LD, and capillary diameter) was estimated from data within a smaller time window with a specified duration. By gradually moving this time window by specified time-shifts (“sliding”) for the length of the 30 s scan, the dynamics of each parameter could be characterized by their time-course, as determined within time windows with a certain duration and overlap (**Supplementary Figure 1**). We tested a number of window durations and time shifts (overlap) prior to the data analysis (**Supplementary Figure 1**) to determine the most appropriate time resolution. Time windows of 100 ms duration and 50 ms time shift proved to provide the most reliable estimates, and sufficiently high temporal resolution to allow further power spectral density analyses (**Supplementary Figure 1**). Time series of all estimates were filtered for outliers, which were defined as data points more than

five median absolute deviations away from the median. Identified outlier points were excluded and interpolated with the nearest within-range values.

For temperature effects, we report averaged parameter values over the entire 30 s periods.

Blood Flow Oscillations

To determine whether our RBCv measurements were sufficiently sensitive to detect subtle oscillations in blood flow across different timescales (Stefanovska et al., 1999; Smirni et al., 2019), we subjected RBCv time series to power spectrum analysis using Matlab's Welch's power spectral density estimation function. Such oscillations are observed in peripheral vessels in mice and humans and they have been ascribed to specific cellular and physiological sources according to their characteristic frequency ranges (Stefanovska et al., 1999; Smirni et al., 2019). Based on the literature, we pre-defined frequency bands to include oscillations characteristic to their sources: 0–0.02 Hz (endothelial), 0.02–0.05 Hz (neurogenic), 0.05–0.15 Hz (myogenic), 0.15–3 Hz (respiration), and 3–10 Hz (heart rate). Of these, the latter two were expected to include the respiration and heart rates characteristic of our experiments.

Statistical Analyses

Data was analyzed by fitting a restricted maximum likelihood model with temperature and MAP as fixed effects, and individual vessels as a random effects using JMP 14.0 (SAS Institute Inc., Cary, NC, United States). MAP was included in the model as a covariate, therefore, when it did not have a significant effect on the parameter in question, it was removed from the model, and the reduced model fitted again. If temperature had a statistically significant effect we used the least squared means differences Tukey test as a *post hoc* test.

For outcomes that were estimated in duplicate (diameter) or triplicate (flux and linear density) per vessel, all measurements were included in the statistical analyses, by nesting them within each individual vessel. For flux and linear density estimates we also included the “estimation segment” (axial or transversal) as a covariate in the statistical model.

To evaluate whether vessel diameter had an effect on RBC velocity, flux or linear density a standard least squares model was fitted using JMP 14.0 with vessel diameter and temperature as model effects.

Data was visualized using Prism 8.3 (GraphPad Software Inc., San Diego, CA, United States).

All data presented as means \pm standard error of mean (SEM), unless otherwise indicated.

RESULTS

Nerve Vasculature

Figure 1A shows a typical example of a sural nerve cross section following perfusion with gelatinized India Ink. The sural nerve, located between muscle tissue, is highlighted by the black dotted line. Few endoneurial capillaries and several small epineurial vessels (marked with “c”) can be observed both in nerve sections

stained with gelatinized India Ink (**Figure 1A**) and in angiograms recorded *in vivo* using TPLSM (**Figure 1C**), but are barely discernible using the surgical microscope (**Figure 1B**). Across the five samples analyzed, there were between 0 and 3 endoneurial capillaries, and between 0 and 5 epineurial small vessels per sample. Typically, the sural nerve was comprised of one to three nerve bundles, with a mean diameter of 167 μm (SEM \pm 34 μm) and cross section area of 0.026 \pm 0.009 mm^2 . The nerve always traveled in parallel with a large vessel of similar caliber with a mean diameter of 114 μm (SEM \pm 27 μm). On average, the total number of vessels associated with the nerve (including the large vessels) resulted in 330 \pm 97 vessels per mm^2 of the nerve. Omitting the large vessels from the estimate to obtain only microvascular vessel density resulted in 237 \pm 80 vessels per mm^2 , while including only the endoneurial vessels resulted in 52 \pm 25 vessels per mm^2 .

The average sural nerve vessel diameter, measured during *in vivo* microscopy was 6 μm , ranging from 3.14 to 10.96 μm (**Figure 3B**). Note that only vessels with single file RBC passage were imaged, therefore larger vessels of the sural nerves were not included in this estimate. Hindlimb temperature or MAP did not affect vessel diameter (**Figure 3B**).

Nerve Perfusion

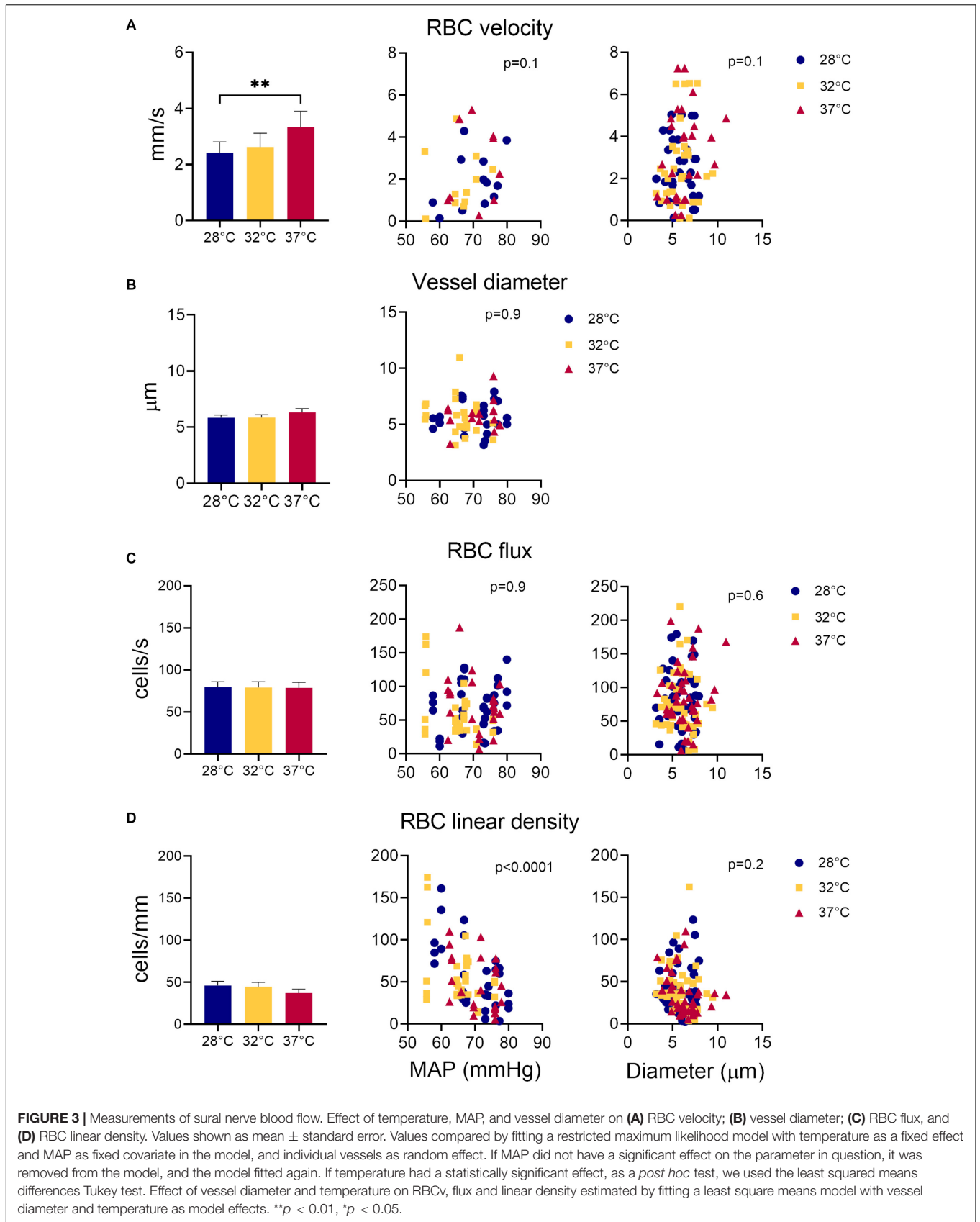
Overall, RBCv in sural nerve vessels ranged broadly from 0.12 – 7.25 mm/s with a mean velocity of 2.77 mm/s . **Figure 3A** shows an increase in RBCv with increasing hindlimb temperatures ($p = 0.002$). Compared to 28°C, RBCv was 14% higher at 32°C and 33% higher at 37°C. However, the difference was only statistically significant comparing RBCv at 28°C and 37°C where the difference (Δ) was 0.88 with confidence interval (CI) [0.33; 1.44] ($p = 0.0015$), but not between 28°C and 32°C ($\Delta = 0.48$, CI [−0.02; 0.98], $p = 0.06$) or between 32°C and 37°C ($\Delta = 0.40$, CI [−0.16; 0.96] $p = 0.19$). RBCv was not affected by MAP.

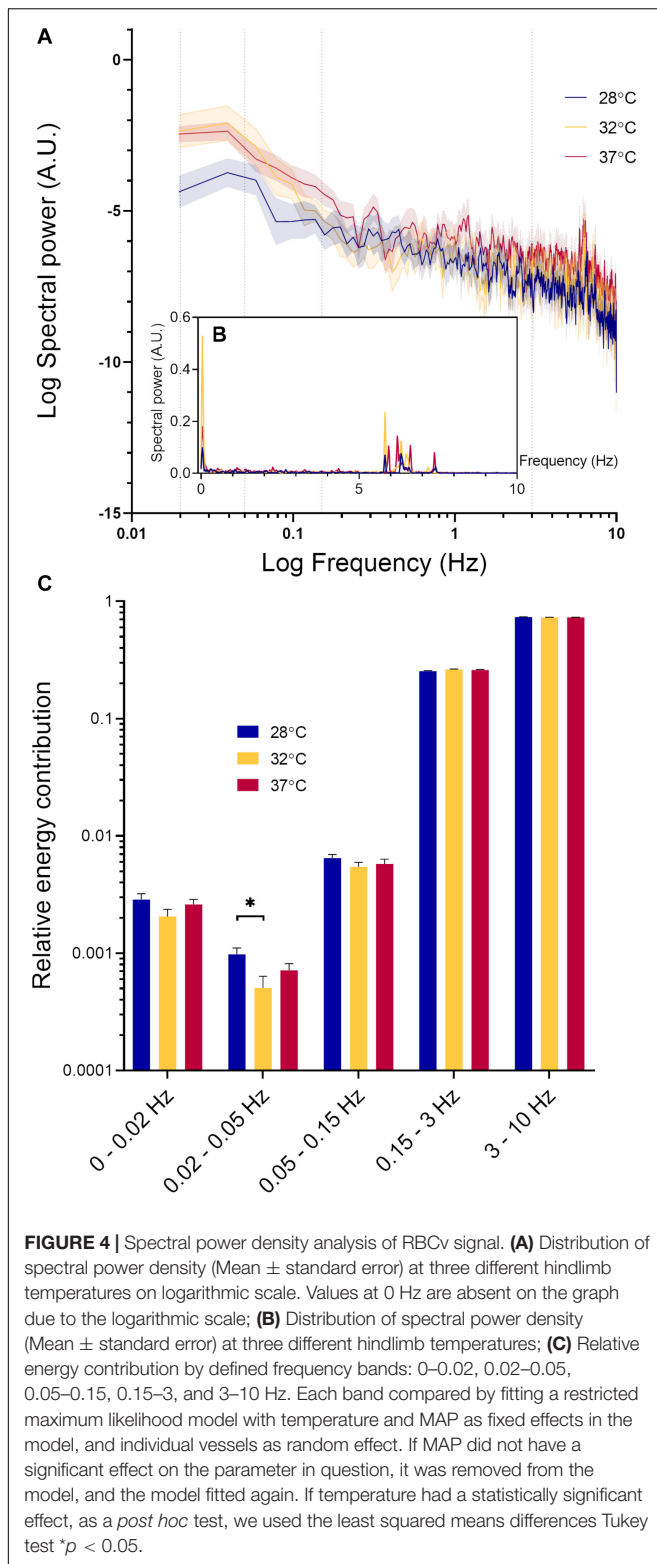
Neither RBC flux (**Figure 3C**) nor LD (**Figure 3D**) were affected by hindlimb temperature. Increased MAP lead to a decrease in RBC LD (**Figure 3D**, estimate = −2.66, $p < 0.0001$) but had no effect on RBC flux (**Figure 3C**). Estimates of both RBC flux and LD were significantly higher when derived from the transversal part of the line scan, compared to those derived from the axial part of the line scan (Flux: $p < 0.0001$, Estimate = 15.4; LD: $p < 0.002$, Estimate = 6.16).

Vessel diameters did not have a significant effect on RBCv, flux or LD.

RBCv Oscillations

Figure 2G shows a typical example of RBCv signal acquired for 30 s. From this recording, it is possible to observe both rapid fluctuations in RBCv, as well as slower oscillations around the mean, as indicated by the black horizontal line. To characterize this variability in RBCv, we performed a power spectral density analysis on each of the acquired time series and compared the outcomes at different temperatures. **Figure 4A** shows how the power of RBCv oscillations is distributed by frequencies. Pronounced peaks in spectral power appear at frequencies between 5.5–8.8 Hz (**Figure 4** and **Supplementary Figure 2**). These peaks correspond well to the heart rate measured by





arterial catheterization, which averaged at 6.7 ± 0.4 Hz. During imaging, mice were mechanically ventilated at an average frequency of 1.6 ± 0.05 Hz, however, no clear peaks appear at this frequency after power spectral density analysis (**Figure 4**

and **Supplementary Figure 2**). Another pronounced peak appears at low frequencies (0–0.15 Hz) at all three hindlimb temperatures (**Figure 4**).

In **Figure 4C**, the spectral power density of RBCv oscillations was normalized and grouped according to the five predefined frequency bands. The high frequency oscillations (3–10 Hz) had the highest relative power contribution, followed by oscillations at the lower frequencies (0.15–3 Hz). Spectral power within these intervals was not significantly affected by MAP or temperature. The relative power contribution from the low frequency oscillations (0–0.15 Hz) was much lower than that by the high frequency oscillations (0.15–10 Hz) at all temperatures. The oscillations within frequency range 0.02–0.05 Hz were significantly affected by temperature ($p = 0.03$). Pairwise comparison revealed a statistically significant difference between 28°C and 32°C ($\Delta = 0.00046$, CI [0.000058; 0.00087], $p = 0.02$), but not between other pairs. RBCv oscillations within the lowest frequency band 0–0.02 Hz increased significantly with increasing MAP (Estimate = 0.00007, $p < 0.05$), but not by temperature. Finally, oscillations in RBCv between 0.05–0.15 Hz were not affected by MAP or temperature.

DISCUSSION

This study presents a nerve window technique, whereby the hindlimb of a mouse is fixed and the sural nerve exposed to allow for *in vivo* TPLSM studies and careful hindlimb temperature control. This preparation is sufficiently stable to allow *in vivo* observations of the nerve's microcirculation, including line-scanning to detect the passage of individual RBCs through capillary-sized nerve microvessels. The RBCv measurements were sufficiently sensitive and robust to detect subtle flow oscillations over time scales from 0.1 to tens of seconds. Our measurements show that RBCv in murine distal sural nerves increases with temperature, underscoring the importance of maintaining hindlimb temperature constant at the physiologically relevant level of 37°C. Using TPLSM, we observed that the sural nerve receives its blood supply through a few small vessels, located on the surface of the nerve as well as within the nerve. Using sural nerve sections labeled with gelatinized India Ink, we were able to verify that *in vivo* measurements were comprehensive and representative of the whole vasculature of the nerve, as the number and size of sural nerve vessels observed in sections corresponded well with those we observed during *in vivo* scans.

The diameter of vessels within which we recorded RBC dynamics using TPLSM is similar to that described in brain tissue of mice and rats (Kleinfeld et al., 1998; Stefanovic et al., 2008; Gutierrez-Jimenez et al., 2016; Dorr et al., 2017; Anzabi et al., 2019) and in rat tibial nerves (Sakita et al., 2014, 2016). This is in contrast to a detailed morphological study of the more proximal, sciatic nerve vasculature in rats and mice, where the smallest nerve vessel sizes were between 8 and 9 μm in diameter, larger than muscle tissue microvessels (ca. 5 μm in diameter) (Bell and Weddell, 1984). These differences might be due to the different methods used to measure vessel diameters. *In vivo*

microscopy, used in our study and in the five studies of the brain (Kleinfeld et al., 1998; Stefanovic et al., 2008; Gutierrez-Jimenez et al., 2016; Dorr et al., 2017; Anzabi et al., 2019), reveals vessel diameters without artifacts induced by tissue fixation, but also selects vessels with single file RBC passage, possibly underestimating mean tissue microvessel diameter. In the study of the rat tibial nerve, whole vasculature was perfused with gelatinized contrast and sections were studied (Sakita et al., 2014, 2016). In this way, the inclusion of vessels of all diameters (i.e., also those larger than the vessels with single file RBC passage) may lead to higher vessel diameter estimates. How the fixation artifact may change diameter estimates compared to vessel diameters *in vivo* is uncertain due to the finite thickness of the vessel wall and its constituents (basal membrane, endothelial cells, glycocalyx layer) and possible varying effects of fixation on them. Hence, the difference between our findings and those reported by Bell and Weddell (1984) might be explained by tissue fixation. Additionally, species used, location of the nerve, and even the age of the animal can affect vessel diameter, as shown by (Sakita et al., 2014, 2016) where tibial nerve capillary diameter was reduced with age in rats.

When only the endoneurial vessels are included in the estimation of sural nerve vessel density in mice our results show a density of 52 vessels per mm^2 . This is comparable to studies in human sural nerves (Mohseni et al., 2017; Kan et al., 2018) and in rat sciatic nerves where endoneurial vessel density ranges between 49 and 98 vessels per mm^2 , respectively. Yet these values are well below those reported for brain and muscle tissue, where vessel density can be as high as 375 vessels/ mm^2 in the mouse (Li et al., 2008) and 244 vessels/ mm^2 in rat brain and up to 500 vessels/ mm^2 in mouse muscle tissue (Bell and Weddell, 1984). When we included all the vessels associated with the sural nerve in the vessel density calculation (small endoneurial vessels, small vessels on the nerve's surface and the large adjacent vessels), vessel density approached that observed in brain and muscle tissue at ca. 330 vessels/ mm^2 . As arterioles have previously been reported to play a role in oxygen diffusion in the muscle (Ellsworth and Pittman, 1990) and in the brain (Sakadžić et al., 2014), it is reasonable to include them in sural nerve vascular density estimates, as they are likely to contribute to oxygenation of the sural nerve. In addition, in such small nerve fibers as murine sural nerve, the small "epineurial" vessels are likely to act as nutritive vessels, due to absence of thick diffusive barriers, such as epineurial connective tissue.

RBCv in sural nerves in mice was several fold higher than that previously reported in mice and rat brain capillaries using TPLSM where RBCv values ranged between 0.4 mm/s to 1.4 mm/s in mice (Gutierrez-Jimenez et al., 2016; Gutiérrez-Jiménez et al., 2017) and 0.77 mm/s in rats (Kleinfeld et al., 1998) under varying anesthetic protocols. In fact, RBCv in sural nerve was more similar to cortical arteriolar RBCv of 2.4 mm/s measured in mice under a matching anesthetic protocol (Dorr et al., 2017). Cortical arterioles, however, had much larger vessel diameters (ca. 12 μm) compared to the vessels of the sural nerve (6 μm). RBCv in cortical arterioles was measured using a water immersion objective, without additional control of surface temperature of the brain, and, as has been shown by

(Roche et al., 2019), this not only significantly reduces cortical temperature, but also RBCv and flux both in awake and anesthetized mice. Maintaining cortical temperature at 37°C in awake mice or at 35–36°C in anesthetized mice using either a dry air objective, or a warmed water immersion objective leads to significantly higher RBCv and flux measurements in cortical capillaries (Roche et al., 2019). This corresponds well with our findings of increased RBCv in sural nerve vessels with increasing hindlimb temperatures (**Figure 3A**), as we found a non-significant 15% increase in RBCv from 32°C to 37°C and a greater, statistically significant 33% increase in RBCv from 28°C to 37°C. Alongside the study by (Roche et al., 2019), our results highlight the importance of careful control of experimental variables on primary experimental outcomes, such as changes in tissue temperature due to imaging with a water immersion objective. As cortical arteriolar RBCv of 2.4 mm/s was measured using a water immersion objective, without specifically controlling brain's surface temperature (Dorr et al., 2017), it is likely that the surface of the brain during these measurements was similar to that measured by (Roche et al., 2019) under similar conditions and was ca. 32°C. Also in the sural nerve vessels at 32°C and 28°C RBCv was 2.6 and 2.4 mm/s, respectively. Therefore, RBCv in sural nerves is more similar to RBCv in cortical arterioles and not capillaries, in spite of diameter differences.

It is well established that blood flow increases in response to local heating in skin, muscle and brain (Heinonen et al., 2011; Wang et al., 2014). In cerebral circulation blood flow acts as a heat sink, removing excess heat from the brain parenchyma (Wang et al., 2014). In the skin, which acts to dissipate the heat from the body, increase in the blood flow has been ascribed to a combination of neural regulation and local nitric oxide release (Minson et al., 2001). In the muscle, both nitric oxide release and elevation of tissue oxygen consumption at increased temperatures (Q_{10} effect) are thought to have an effect on local blood flow increase (Heinonen et al., 2011). RBC flux in sural nerves (79 cells/s) was comparable to that previously reported in murine brain capillaries under isoflurane anesthesia [62 cells/s (Gutierrez-Jimenez et al., 2016)]. However, unlike in the brain where increasing surface temperature elevated RBC flux (Roche et al., 2019), warming of the hindlimb did not increase RBC flux in the sural nerve (**Figure 3C**). The absence of temperature effect on RBC flux in our study is also in contrast to previous measurements of sciatic nerve blood flow in rats measured using LDF, where nerve blood flow was *lower* at higher hindlimb temperatures (Dines et al., 1997, 1999). In these studies the decrease in nerve blood flow was paralleled by an increase in blood flow to the muscle (Dines et al., 1997, 1999). The absence of RBC flux changes in response to warming in sural nerve in our study points to a tight local regulation of blood flow at the microvascular level. In peripheral nerves microvascular innervation and local endothelial signaling play an important role in maintaining the vascular tone (Zochodne, 2018) and power spectral density analysis of RBCv signal indicates that both mechanisms might be at play in the microvasculature of the sural nerve (**Figure 4**). Power spectral density analysis showed that RBCv oscillations between 0.02 and 0.05 Hz, potentially

corresponding to neurogenic regulation (Smirni et al., 2019), were reduced at 32°C compared to 28°C. Oscillations at the very low frequencies (0–0.02 Hz), potentially corresponding to the endothelial involvement and nitric oxide release (Stefanovska et al., 1999; Smirni et al., 2019), appeared more pronounced at 32°C and 37°C than at 28°C but were not statistically different, however, were significantly increased by increasing MAP. Even though the relatively short recoding lengths of 30 s limit the strength of conclusions that can be derived from the changes in oscillations in RBCv signal, the analysis shows that local blood flow control in the nerve is affected by changing temperatures and by MAP. Further studies designed to target endothelial, neurogenic and myogenic regulatory mechanisms in sural nerve vasculature are necessary to elucidate their role in local nerve blood flow regulation at capillary level. In previous studies MAP increased sciatic nerve blood flow in rats (Low and Tuck, 1984), however, we did not observe a statistically significant effect of MAP on RBCv or RBC flux. There was, however, a significant effect of MAP on RBC linear density (Figure 3D) with linear density decreasing with increasing MAP. The absence of effect of MAP on RBCv and RBC flux in our study is also likely due to the small vessels examined in our study.

Limitations to the Study

Anesthesia inadvertently and inevitably affects animal physiology, thus making studies of blood flow under any anesthetic regime inherently challenging. Without consideration for the local temperature, a wide range of RBCv values has been measured in brain capillaries of mice under different anesthetics. Highest values in C57 male mice are reported under isoflurane anesthesia (1.4 mm/s) (Gutiérrez-Jiménez et al., 2016), with much lower values under α -chloralose anesthesia (0.4 mm/s) (Gutiérrez-Jiménez et al., 2017). These values differ from those recorded in brains of awake mice first by Drew et al. (2010) where values ranged between 0.1–2 mm/s and by Roche et al. (2019) with RBCv at 0.75 mm/s. But all are lower than RBCv measured in the vessels of the sural nerve (from 2.4 mm/s at 28°C to 3.3 mm/s at 37°C) under isoflurane anesthesia. It is possible that isoflurane anesthesia in this experiment caused sural nerve RBCv to increase, such as it has been observed in the brain (1.4 mm/s on isoflurane vs 0.75 mm/s awake), where it is attributed to vasodilatory effects of isoflurane (Matta et al., 1999). The vasodilatory effect might have also lead to an overestimation of vessel diameters. However, even in that case, capillary RBCv in mouse sural nerves is higher than in the brain, while diameters of vessels with single file RBC passages are comparable to those in the brain (Dorr et al., 2017; Anzabi et al., 2019). Although hemodynamic measurements in the brain tissue of awake mice are becoming more common (Roche et al., 2019), preparation and fixation of the hindlimb in awake mice is currently not done.

Another challenge is the terminal nature of the current study protocol. It is not possible to study how blood flow changes over the course of time in the same mouse through e.g., disease progression. Potentially, this might be amended by optimizing the surgical preparation of the sural nerve window, and enabling the mouse to be recovered after imaging to allow

for repeated imaging over time. However, this might be faced with the challenge of the repeated surgery, which might lead to surrounding tissue damage, and thereby affect study results.

CONCLUSION

The novel peripheral nerve window technique presented here is suitable for detailed investigation of sural nerve hemodynamics in mice. Moreover, our results show that *in vivo* TPLSM is a fitting approach for hemodynamic studies in sural nerves. In such small and distal peripheral nerve fibers, counting individual RBC passages and measuring RBC velocity in individual small vessels provides a comprehensive assessment of local hemodynamics. In future studies combination of this method with calcium imaging (Fontaine et al., 2018) or use of oxygen sensitive dyes (Sakadžić et al., 2014) will enable us to study how nerve's activity and metabolism are supported by perfusion in health and disease. Furthermore, this method will also enable us to study how pharmacological or physiological challenges affect local hemodynamics in the nerve. Our results have also shown that during these studies it is important to control and report the exact temperature of the exposed hindlimb of the mouse, due to its effects on estimates of RBCv.

DATA AVAILABILITY STATEMENT

The raw data supporting the conclusions of this article will be made available by the authors, without undue reservation.

ETHICS STATEMENT

The study was reviewed and approved by the Danish Animal Experiments Inspectorate, animal experimentation permit #2016-15-0201-00966.

AUTHOR CONTRIBUTIONS

AD and LØ conceived the study. AD performed the experiments, drafted the manuscript, and designed the figures. AD and PR processed and analyzed the data. PR developed methods for the data processing and analysis. All authors interpreted the results and read, made critical revisions to, and approved the final version of the manuscript.

FUNDING

The study was supported by a Novo Nordisk Foundation Challenge Programme grant (NNF14OC0011633).

ACKNOWLEDGMENTS

We would like to thank Susanne Smith Christensen for her technical assistance, Eugenio Gutiérrez-Jiménez for his support with optical systems, Nina K. Iversen for her

support with microsurgical techniques and overall lab management, and Sebastian Frische for advice on histological techniques. We are very grateful to Troels Staehelin Jensen for his support to this project as a part of the IDNC research effort.

SUPPLEMENTARY MATERIAL

The Supplementary Material for this article can be found online at: <https://www.frontiersin.org/articles/10.3389/fnins.2020.579373/full#supplementary-material>

Supplementary Figure 1 | RBCv image analyses and windowing. Vessel diameter, RBCv, flux and linear density were estimated from the line scans using a sliding window approach to provide time series of these estimates (Drew et al., 2010). Overlapping temporal windows are positioned over the 2D line scan images, and diameter, velocity, flux, and linear density are estimated from line scan

data within each window. The temporal resolution and noise of the resulting time series depend on window size and window shift. Smaller window sizes increase the temporal resolution of the estimate, but also increase standard deviation of the estimate for the whole period of estimation. We tested several combinations of sizes and temporal shifts of the windows to establish how that affects the signal of interest (averages across the temporal sequence) (A–E). Average RBCv (F) is not changed by the size and shift of the estimation window, until the window size becomes too small (in this case (E): 10 ms window with 5 ms overlap). All estimates acquired from imaging were filtered for outliers defined as more than five median absolute deviations away from the median. Identified outlier points were replaced by interpolated values estimated from the nearest within-range values. The mean \pm SD of the raw or unfiltered values are plotted in (F) as black symbols, and filtered values as open symbols.

Supplementary Figure 2 | Example of spectral power density analysis of single velocity time series, estimated using a temporal window of 100 ms and a window shift of 50 ms (Supplementary Figure 1). A distinct density peak is observed at the measured hear rate. Frequency of measured ventilation is also indicated, but not easily discernible from the trace.

REFERENCES

- Anzabi, M., Angleys, H., Aamand, R., Ardalan, M., Mouridsen, K., Rasmussen, P. M., et al. (2019). Capillary flow disturbances after experimental subarachnoid hemorrhage: a contributor to delayed cerebral ischemia? *Microcirculation* 26, 1–11. doi: 10.1111/micc.12516
- Bell, M. A., and Weddell, A. G. M. (1984). A morphometric study of intrafascicular vessels of mammalian sciatic nerve. *Muscle Nerve* 7, 524–534. doi: 10.1002/mus.880070703
- Cameron, N. E., and Cotter, M. A. (1997). Metabolic and vascular factors in the pathogenesis of diabetic neuropathy. *Diabetes* 46, S31–S37.
- Dines, K. C., Calcutt, N. A., Nunag, K. D., Mizisin, A. P., and Kalichman, M. W. (1999). Effects of hindlimb temperature on sciatic nerve laser Doppler vascular conductance in control and streptozotocin-diabetic rats. *J. Neurol. Sci.* 163, 17–24. doi: 10.1016/S0022-510X(99)00013-1
- Dines, K. C., Mizisin, A. P., Jorge, M. C., Nunag, K. D., and Kalichman, M. W. (1997). Effects of body and hindlimb temperature on laser Doppler blood flow and vascular conductance in rat sciatic nerve and skeletal muscle. *J. Neurol. Sci.* 148, 7–13. doi: 10.1016/s0022-510x(96)05347-6
- Dorr, A., Thomason, L. A., Koletar, M. M., Joo, I. L., Steinman, J., Cahill, L. S., et al. (2017). Effects of voluntary exercise on structure and function of cortical microvasculature. *J. Cereb. Blood Flow Metab.* 37, 1046–1059. doi: 10.1177/0271678X16669514
- Drew, P. J., Blinder, P., Cauwenberghs, G., Shih, A. Y., and Kleinfeld, D. (2010). Rapid determination of particle velocity from space-time images using the Radon transform. *J. Comput. Neurosci.* 29, 5–11. doi: 10.1007/s10827-009-0159-1
- Ellsworth, M. L., and Pittman, R. N. (1990). Arterioles supply oxygen to capillaries by diffusion as well as by convection. *Am. J. Physiol. Hear. Circ. Physiol.* 258, 78–81. doi: 10.1152/ajpheart.1990.258.4.h1240
- Fontaine, A. K., Anderson, H. E., Caldwell, J. H., and Weir, R. F. (2018). Optical read-out and modulation of peripheral nerve activity. *Neural Regen. Res.* 13, 58–61. doi: 10.4103/1673-5374.224364
- Gonçalves, N. P., Vægter, C. B., Andersen, H., Østergaard, L., Calcutt, N. A., and Jensen, T. S. (2017). Schwann cell interactions with axons and microvessels in diabetic neuropathy. *Nat. Rev. Neurol.* 13, 135–147. doi: 10.1038/nrneurol.2016.201
- Gutiérrez-Jiménez, E., Angleys, H., Rasmussen, P. M., Mikkelsen, I. K., Mouridsen, K., and Østergaard, L. (2017). The effects of hypercapnia on cortical capillary transit time heterogeneity (CTH) in anesthetized mice. *J. Cereb. Blood Flow Metab.* 38, 290–303. doi: 10.1177/0271678X17692598
- Gutiérrez-Jimenez, E., Cai, C., Mikkelsen, I. K., Rasmussen, P. M., Angleys, H., Merrild, M., et al. (2016). Effect of electrical forepaw stimulation on capillary transit-time heterogeneity (CTH). *J. Cereb. Blood Flow Metab.* 1, 1–8. doi: 10.1177/0271678X16631560
- Heinonen, I., Brothers, R. M., Kempainen, J., Knuuti, J., Kalliokoski, K. K., and Crandall, C. G. (2011). Local heating, but not indirect whole body heating, increases human skeletal muscle blood flow. *J. Appl. Physiol.* 111, 818–824. doi: 10.1152/jappphysiol.00269.2011
- Kan, H.-W., Hsieh, J.-H., Chien, H.-F., Lin, Y.-H., Yeh, T.-Y., Chao, C.-C., et al. (2018). CD40-mediated HIF-1 α expression underlying microangiopathy in diabetic nerve pathology. *Dis. Model. Mech.* 11:dmm033647. doi: 10.1242/dmm.033647
- Kleinfeld, D., Mitra, P. P., Helmchen, F., and Denk, W. (1998). Fluctuations and stimulus-induced changes in blood flow observed in individual capillaries in layers 2 through 4 of rat neocortex. *Proc. Natl. Acad. Sci. U.S.A.* 95, 15741–15746. doi: 10.1073/PNAS.95.26.15741
- Li, J. M., Mogi, M., Iwanami, J., Min, L. J., Tsukuda, K., Sakata, A., et al. (2008). Temporary pretreatment with the angiotensin II type 1 receptor blocker, valsartan, prevents ischemic brain damage through an increase in capillary density. *Stroke* 39, 2029–2036. doi: 10.1161/STROKEAHA.107.503458
- Lim, T. K., Shi, X. Q., Johnson, J. M., Rone, M. B., Antel, J. P., David, S., et al. (2015). Peripheral nerve injury induces persistent vascular dysfunction and endoneurial hypoxia, contributing to the genesis of neuropathic pain. *J. Neurosci.* 35, 3346–3359. doi: 10.1523/JNEUROSCI.4040-14.2015
- Low, P. A., and Tuck, R. R. (1984). Effects of changes of blood pressure, respiratory acidosis and hypoxia on blood flow in the sciatic nerve of the rat. *J. Physiol.* 347, 513–524. doi: 10.1113/jphysiol.1984.sp015079
- Matta, B. F., Heath, K. J., Tipping, K., and Summors, A. C. (1999). Direct cerebral vasodilatory effects of sevoflurane and isoflurane. *Anesthesiology* 91, 677–680. doi: 10.1097/0000542-199909000-00019
- Minson, C. T., Berry, L. T., and Joyner, M. J. (2001). Nitric oxide and neurally mediated regulation of skin blood flow during local heating. *J. Appl. Physiol.* 91, 1619–1626. doi: 10.1152/jappl.2001.91.4.1619
- Mohseni, S., Badii, M., Kylhammar, A., Thomsen, N. O. B., Eriksson, K. F., Malik, R. A., et al. (2017). Longitudinal study of neuropathy, microangiopathy, and autophagy in sural nerve: implications for diabetic neuropathy. *Brain Behav.* 7, 1–9. doi: 10.1002/brb3.763
- Newrick, P. G., Wilson, A. J., Jakubowski, J., Boulton, A. J. M., and Ward, J. D. (1986). Sural nerve oxygen tension in diabetes. *Br. Med. J.* 293, 1053–1054. doi: 10.1136/bmj.293.6554.1053
- Østergaard, L., Finnerup, N. B., Terkelsen, A. J., Olesen, R. A., Drasbek, K. R., Knudsen, L., et al. (2015). The effects of capillary dysfunction on oxygen and glucose extraction in diabetic neuropathy. *Diabetologia* 58, 666–677. doi: 10.1007/s00125-014-3461-z
- Roche, M., Chaigneau, E., Rungta, R. L., Boido, D., Weber, B., and Charpak, S. (2019). In vivo imaging with a water immersion objective affects brain temperature, blood flow and oxygenation. *eLife* 8:e47324. doi: 10.7554/elife.47324
- Rueden, C. T., Schindelin, J., Hiner, M. C., DeZonia, B. E., Walter, A. E., Arena, E. T., et al. (2017). ImageJ2: imageJ for the next generation of scientific image data. *BMC Bioinformatics* 18:529. doi: 10.1186/s12859-017-1934-z
- Sakadžić, S., Mandeville, E. T., Gagnon, L., Musacchia, J. J., Yaseen, M. A., Yucel, M. A., et al. (2014). Large arteriolar component of oxygen delivery implies

- a safe margin of oxygen supply to cerebral tissue. *Nat. Commun.* 5:5734. doi: 10.1038/ncomms6734
- Sakita, M., Murakami, S., and Fujino, H. (2014). The morphological changes in the capillary architecture of the tibial nerve associated with spontaneous aging and aerobic exercise intervention during aging in rats. *J. Phys. Ther. Sci.* 26, 263–267. doi: 10.1589/jpts.26.263
- Sakita, M., Murakami, S., and Fujino, H. (2016). Age-related morphological regression of myelinated fibers and capillary architecture of distal peripheral nerves in rats. *BMC Neurosci.* 17:39. doi: 10.1186/s12868-016-0277-4
- Schindelin, J., Arganda-Carreras, I., Frise, E., Kaynig, V., Longair, M., Pietzsch, T., et al. (2012). Fiji: an open-source platform for biological-image analysis. *Nat. Methods* 9, 676–682. doi: 10.1038/nmeth.2019
- Smirni, S., McNeilly, A. D., MacDonald, M. P., McCrimmon, R. J., and Khan, F. (2019). In-vivo correlations between skin metabolic oscillations and vasomotion in wild-type mice and in a model of oxidative stress. *Sci. Rep.* 9, 1–15. doi: 10.1038/s41598-018-36970-4
- Stefanovic, B., Hutchinson, E., Yakovleva, V., Schram, V., Russell, J. T., Belluscio, L., et al. (2008). Functional reactivity of cerebral capillaries. *J. Cereb. Blood Flow Metab.* 28, 961–972. doi: 10.1038/sj.jcbfm.9600590
- Stefanovska, A., Bracic, M., and Kvernmo, H. D. (1999). Wavelet analysis of oscillations in the peripheral blood circulation measured by laser Doppler technique. *IEEE Trans. Biomed. Eng.* 46, 1230–1239. doi: 10.1109/10.790500
- Tuck, R. R., Schmelzer, J. D., and Low, P. A. (1984). Endoneurial blood flow and oxygen tension in the sciatic nerves of rats with experimental diabetic neuropathy. *Brain* 107(Pt 3), 935–950. doi: 10.1093/brain/107.3.935
- Wang, H., Wang, B., Normoyle, K. P., Jackson, K., Spitzer, K., Sharrock, M., et al. (2014). Brain temperature and its fundamental properties: a review for clinical neuroscientists. *Front. Neurosci.* 8:307. doi: 10.3389/fnins.2014.00307
- Xue, S., Gong, H., Jiang, T., Luo, W., Meng, Y., Liu, Q., et al. (2014). Indian-ink perfusion based method for reconstructing continuous vascular networks in whole mouse brain. *PLoS One* 9:e88067. doi: 10.1371/journal.pone.0088067
- Zochodne, D. W. (2018). Local blood flow in peripheral nerves and their ganglia: resurrecting key ideas around its measurement and significance. *Muscle Nerve* 57, 884–895. doi: 10.1002/mus.26031 doi: 10.1002/mus.26031

Conflict of Interest: The authors declare that the research was conducted in the absence of any commercial or financial relationships that could be construed as a potential conflict of interest.

Copyright © 2020 Dudele, Rasmussen and Østergaard. This is an open-access article distributed under the terms of the Creative Commons Attribution License (CC BY). The use, distribution or reproduction in other forums is permitted, provided the original author(s) and the copyright owner(s) are credited and that the original publication in this journal is cited, in accordance with accepted academic practice. No use, distribution or reproduction is permitted which does not comply with these terms.



Diffusion Tensor Imaging of the Sciatic Nerve as a Surrogate Marker for Nerve Functionality of the Upper and Lower Limb in Patients With Diabetes and Prediabetes

OPEN ACCESS

Edited by:

Itamar Ronen,
Leiden University Medical Center,
Netherlands

Reviewed by:

Donnie Cameron,
University of East Anglia,
United Kingdom
Artur Krzyżak,
AGH University of Science
and Technology, Poland

*Correspondence:

Felix T. Kurz
felix.kurz@med.uni-heidelberg.de;
felix.kurz@gmx.net

Specialty section:

This article was submitted to
Brain Imaging Methods,
a section of the journal
Frontiers in Neuroscience

Received: 16 December 2020

Accepted: 10 February 2021

Published: 03 March 2021

Citation:

Jende JME, Kender Z,
Mooshage C, Groener JB,
Alvarez-Ramos L, Kollmer J,
Juerchott A, Hahn A, Heiland S,
Nawroth P, Bendszus M, Kopf S and
Kurz FT (2021) Diffusion Tensor
Imaging of the Sciatic Nerve as
a Surrogate Marker for Nerve
Functionality of the Upper and Lower
Limb in Patients With Diabetes
and Prediabetes.
Front. Neurosci. 15:642589.
doi: 10.3389/fnins.2021.642589

Johann M. E. Jende¹, Zoltan Kender², Christoph Mooshage¹, Jan B. Groener^{2,3,4}, Lucia Alvarez-Ramos², Jennifer Kollmer¹, Alexander Juerchott¹, Artur Hahn¹, Sabine Heiland^{1,5}, Peter Nawroth^{2,4,6}, Martin Bendszus¹, Stefan Kopf^{2,4} and Felix T. Kurz^{1*}

¹ Department of Neuroradiology, Heidelberg University Hospital, Heidelberg, Germany, ² Department of Endocrinology, Diabetology and Clinical Chemistry, Heidelberg University Hospital, Heidelberg, Germany, ³ Medicover Neuroendocrinology, Munich, Germany, ⁴ German Center of Diabetes Research (DZD), Associated Partner in the DZD, München-Neuherberg, Germany, ⁵ Division of Experimental Radiology, Department of Neuroradiology, Heidelberg, Germany, ⁶ Joint Institute for Diabetes and Cancer at Helmholtz-Zentrum Munich and Heidelberg University, Heidelberg, Germany

Background: Nerve damage in diabetic neuropathy (DN) is assumed to begin in the distal legs with a subsequent progression to hands and arms at later stages. In contrast, recent studies have found that lower limb nerve lesions in DN predominate at the proximal sciatic nerve and that, in the upper limb, nerve functions can be impaired at early stages of DN.

Materials and Methods: In this prospective, single-center cross-sectional study, participants underwent diffusion-weighted 3 Tesla magnetic resonance neurography in order to calculate the sciatic nerve's fractional anisotropy (FA), a surrogate parameter for structural nerve integrity. Results were correlated with clinical and electrophysiological assessments of the lower limb and an examination of hand function derived from the Purdue Pegboard Test.

Results: Overall, 71 patients with diabetes, 11 patients with prediabetes and 25 age-matched control subjects took part in this study. In patients with diabetes, the sciatic nerve's FA showed positive correlations with tibial and peroneal nerve conduction velocities ($r = 0.62$; $p < 0.001$ and $r = 0.56$; $p < 0.001$, respectively), and tibial and peroneal nerve compound motor action potentials ($r = 0.62$; $p < 0.001$ and $r = 0.63$; $p < 0.001$, respectively). Moreover, the sciatic nerve's FA was correlated with the Pegboard Test results in patients with diabetes ($r = 0.52$; $p < 0.001$), prediabetes ($r = 0.76$; $p < 0.001$) and in controls ($r = 0.79$; $p = 0.007$).

Conclusion: This study is the first to show that the sciatic nerve's FA is a surrogate marker for functional and electrophysiological parameters of both upper and lower limbs in patients with diabetes and prediabetes, suggesting that nerve damage in these patients is not restricted to the level of the symptomatic limbs but rather affects the entire peripheral nervous system.

Keywords: magnetic resonance imaging, diabetic polyneuropathy, magnetic resonance neurography, diffusion tensor imaging, fractional anisotropy, diabetes, prediabetes

INTRODUCTION

Distal symmetric diabetic polyneuropathy (DN) is one of the most severe complications of diabetes mellitus (Tefaye et al., 2005; Feldman et al., 2017). DN is generally acknowledged to be a late complication of diabetes that starts at the level of the feet and then progresses further upwards until, at later stages, the upper limbs become involved as well, starting at the level of the hands (Nawroth et al., 2018). In contrast to the progression of clinical symptoms, recent studies applying high-resolution magnetic resonance neurography (MRN) at three Tesla (3T) have come to show that nerve lesions predominate proximally at the level of the sciatic nerve and that the sciatic nerve's fractional anisotropy (FA), a dimensionless quantity for directed diffusion in nerve tissue, is a highly sensitive parameter for structural nerve damage in patients with diabetic neuropathy in previous clinical studies (Vaeggemose et al., 2017b; Jende et al., 2019, 2020a). Despite the assumption that length-dependent nerve damage in DN starts at the level of the feet and progresses to further proximally with an involvement of the upper limbs at later stages, recent studies revealed that sensory and motor functions of the upper limb are frequently affected already at early stages of DN but often remain undiagnosed until a certain degree of functional impairment becomes apparent, indicating that the progression of nerve fiber damage at the level of the hands and arms may parallel the progression of nerve fiber damage at the level of the feet and legs (Kopf et al., 2018a; Yang et al., 2018).

The aim of this study was to elucidate correlations of the sciatic nerve's FA with clinical and electrophysiological parameters of the upper and lower limbs in patients with prediabetes and diabetes, and in an age-matched control group. Therefore, we chose an MRN protocol that combined T2-weighted and diffusion-weighted sequences with a subsequent automated approach for the calculation of the sciatic nerve's FA.

MATERIALS AND METHODS

Study Design and Participants

The local ethics committee approved this study (HEIST-DiC, local ethics number S-383/2016¹, identifier NCT03022721), and

Abbreviations: CI, confidence interval; CMAP, compound motor action potential; DN, diabetic neuropathy; mV, microvolt; NCV, nerve conduction velocity; NDS, neuropathy disability score; NSS, neuropathy severity score; SNAP, sensory nerve action potential.

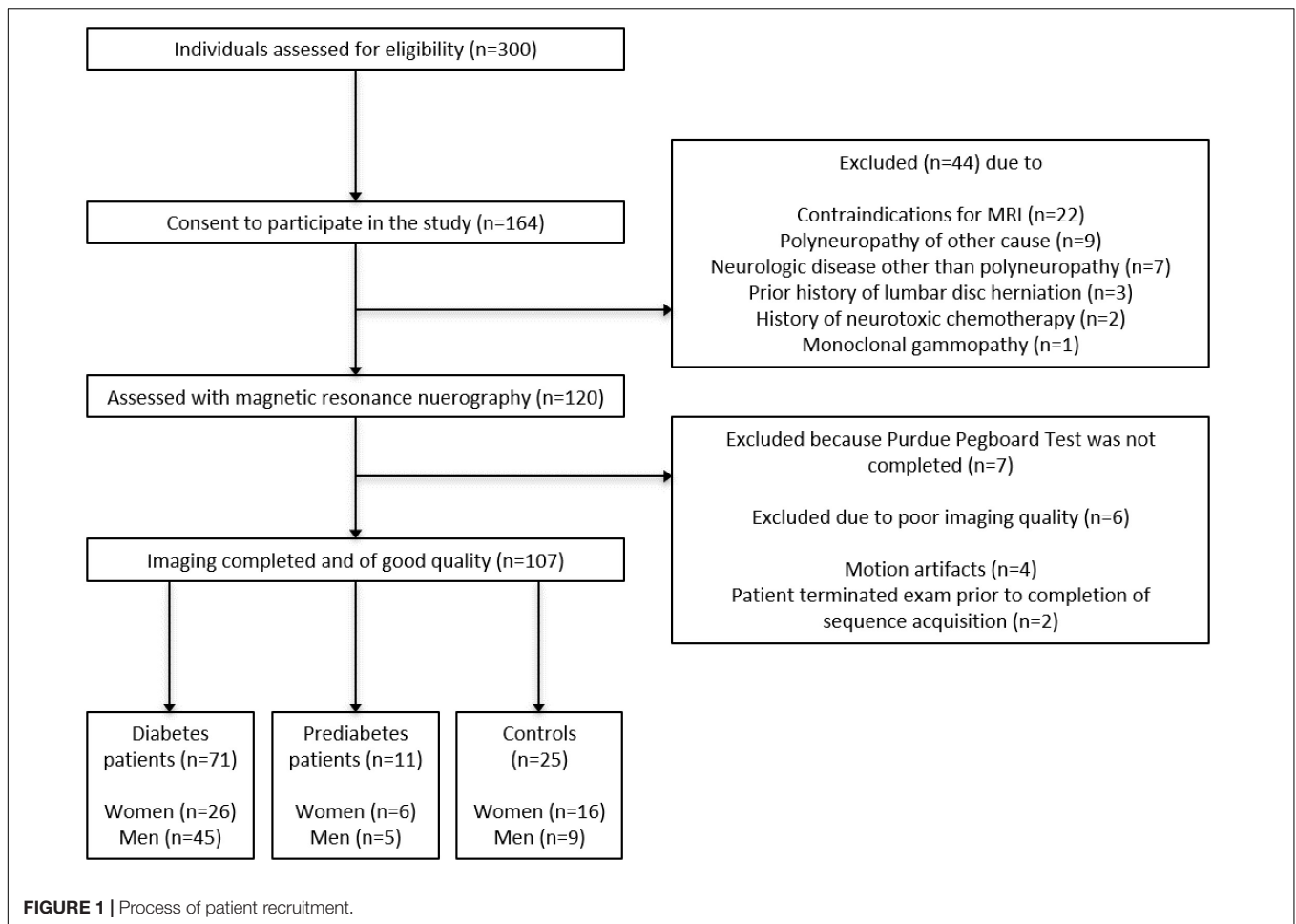
¹clinicaltrials.gov

all study participants gave informed, written consent. Prediabetes was defined as fasting glucose levels of 100–125 mg/dL or a 2-h glucose level of 140–199 mg/dL after 75 g glucose intake. Participants with glucose levels below these limits were defined as normal (healthy controls). Participants with glucose levels above the limit and absence of GAD or IA2 antibodies were defined as newly diagnosed type 2 diabetes (Kopf et al., 2018b). Overall, 71 patients with diabetes (12 with type 1 diabetes, 59 with type 2 diabetes; 26 female, 45 male; mean age 61.07 ± 1.57 ; age range 21–84 years), 11 patients with prediabetes (6 female, 5 male, 61.82 ± 2.85 , age range 47–78) and 25 age-matched control subjects (16 female, 9 male, mean age 56.24 ± 2.17 , age range 30–77) took part in this study between June 2016 and May 2020. Study participants were recruited from the Outpatient Clinic of Internal Medicine at Heidelberg University Hospital (Z.K., J.B.G., L.A., and S.K.). Participants formed a random series, meaning that they were not recruited and examined groupwise but in a randomized order. All participants were right-handed. Overall exclusion criteria were age <18, pregnancy, any history of lumbar surgery or disk extrusion, any contraindications for MR imaging, any other neuropathy-associated risk factors such as alcohol abuse, hypovitaminosis, malignant or infectious diseases, any previous or ongoing exposure to neurotoxic agents, monoclonal gammopathy, and any chronic neurological diseases such as Parkinson's disease, multiple sclerosis, or restless legs syndrome. The process of patient recruitment is illustrated in **Figure 1**.

Clinical and Electrophysiologic Examination

A detailed medical history was documented for every participant. The examination of neuropathic symptoms was performed according to the guidelines of the German Society for Diabetology comprising the neuropathy symptom score (NSS), the Neuropathy Disability Score (NDS) and electrophysiological examinations as outlined below (Young et al., 1993).

The electrophysiological examination (Viasys Healthcare VikingQuest®, Viasys Healthcare GmbH, Höchberg) of the right leg included: distal motor latencies of the right tibial and peroneal nerve, motor and sensory amplitudes (CMAPs and SNAPs, respectively) of the tibial, peroneal and sural nerves and nerve conduction velocities (NCVs) of the tibial, peroneal and sural nerves. It was assured that skin temperature was at least 32°C throughout the examination. Blood was drawn in fasting state and processed immediately under standardized conditions in the central laboratory of Heidelberg University



Hospital. All examinations were performed by clinicians with expertise in diabetology and more than 8 years of clinical experience (Z.K., J.B.G., and S.K.) and were surveyed by a clinician with expertise in internal medicine, diabetology, and laboratory medicine (P.N.) with more than 30 years of experience.

Measurement of Hand Dexterity and Fine Motoric Skills by Using the Purdue Pegboard Test

The Purdue Pegboard Test (Model 32020; Lafayette Instrument Co., Lafayette, IN, United States), an established and commonly used test for the assessment of both gross and fine motor skills of the arms and hands, was used to assess motoric skills and manual dexterity (Symonds et al., 2017). The test employs a board with two parallel rows of 25 cavities into which cylindrical metal pegs are to be placed and comprises a total of four trials. The test includes four subtests: testing of the dominant hand, testing of the non-dominant hand, testing of both hands, and an assembly test allowing use of both hands as described before. In the subsets for preferred, non-preferred, and both hands the examinee is required to place the pins as fast as possible, the score being the number of pins placed after 30 s (O'Donnell et al., 2017).

MRN Imaging Protocol

We performed high-resolution MRN of the right thigh in a 3.0 Tesla MR-scanner (Magnetom TIM-TRIO, Siemens Healthineers, Erlangen, Germany) for all study participants, using a 15-channel transmit-receive extremity coil. Participants were put in a supine position on the MRI transport table with the legs facing the scanner opening; the leg imaging coil, a 15-channel transmit-receive extremity coil, was placed around the right mid thigh and mid lower leg. The following sequences were used:

- (1) Axial high resolution T2-weighted turbo spin echo (TSE) 2D sequence with spectral fat saturation (mode: strong) without water suppression or magnetization preparation. The following parameters were used: relaxation time (TR) = 5,970 ms, echo time (TE) = 55 ms, field of view (FOV) = 160 mm² × 160 mm², matrix size = 512 × 512, slice thickness = 4 mm, interslice gap = 0.8 mm, voxel size = 0.3 mm³ × 0.3 mm³ × 4.0 mm³, 24 slices, 24 acquired images, receiver bandwidth = 181 Hz/pixel, echo spacing = 11.1 ms, turbo factor = 13, 15 echo trains per slice, parallel imaging factor = 2, averages = 3, acquisition time = 4:42 min.

(2) Axial diffusion-weighted 2-dimensional echo-planar sequence images were recorded with spectral attenuated inversion recovery fat suppression (saturation mode: skewed). The following parameters were used: TR = 5,100 ms; TE = 92.8 ms; b = 0 and 1,000 s/mm²; directions = 20; field of view 160 mm² × 160 mm²; matrix size 128 × 128; axial fat-suppressed, diffusion-weighted 2-dimensional echo-planar sequence with the following parameters: TR = 5,100 ms; TE = 92.8 ms; b = 0 and 1,000 s/mm²; directions = 20; field of view = 160 mm² × 160 mm²; matrix size = 128 × 128; slice thickness = 4 mm; voxel size = 1.3 mm³ × 1.3 mm³ × 4 mm³; no interslice gap, 24 slices, 1,512 acquired images, receiver bandwidth = 1,396 Hz/pixel, EPI factor = 128, parallel imaging factor = 3, averages = 3, acquisition time = 5:47 min.

MRN sequences were centered on the sciatic nerve's bifurcation to ascertain that the anatomical region mapped by MRN was comparable in all participants. All MRN Studies were performed by radiologists with more than 5 years of clinical experiences in MRN studies (J.M.E.J., J.K., A.J., and F.T.K.).

Image Post-processing and Analysis

The MRN analysis followed an established analysis pipeline for diffusion tensor imaging (DTI) images (Christidi et al., 2016). All images were pseudonymized and analyzed in an automated approach (J.M.E.J., C.M., F.T.K.) using Nordic BRAINEX, a Food and Drug Administration (FDA) approved processing software designed for automated calculation and reconstruction of fiber tracts in diffusion weighted imaging. Nordic BrainEx uses a variant of the Fiber Assignment by Continuous Tracking (FACT) algorithm to obtain fiber tracking within a volume-of-interest (VOI) (Mori et al., 1999; NordicNeuroLab AS, 2019). We closely followed the DTI module instructions for Nordic BRAINEX (NordicNeuroLab AS, 2019). DTI setting configurations were extracted from the headers of the uploaded DTI image data (e.g., number of gradient directions, averages, etc.). First, we co-registered DTI images to the T2w images. For subsequent pre-processing, we chose the options “motion correction” and “Eddy current correction” and adjusted a noise threshold to include all voxels within the sciatic nerve. We further chose a FA cutoff >0.1 as in previous studies on DTI analyses in peripheral nerves (Kwon et al., 2015; Oudeman et al., 2020) to reduce the impact of intra- and perineural fat on the calculated FA of fascicular structures (Kwon et al., 2015; Oudeman et al., 2020). The tract turning angle was chosen as 41.4 degrees, the minimum fiber length at 20 mm, and the number of seeds per voxel as 1, see also (NordicNeuroLab AS, 2019). We then manually focused a cube shaped VOI on the sciatic nerve.

The tensor eigenvalues λ_1 , λ_2 , and λ_3 and the average FA of the segmented nerve fibers were automatically determined in Nordic BRAINEX (NordicNeuroLab AS, 2019). Axial diffusivity (AD), radial diffusivity (RD) and mean diffusivity (MD) were calculated based on the obtained tensor eigenvalues as AD = λ_1 , RD = $(\lambda_2 + \lambda_3)/2$, and MD = $(\lambda_1 + \lambda_2 + \lambda_3)/3$ ¹⁶. A graphic

overview of the process of image co-registration and nerve segmentation is given in **Figure 2**.

Statistical Analysis

Statistical data analysis was performed with GraphPad Prism 7 and Matlab v7.14.0.0739, R2012a (J.M.E.J., A.H., and F.T.K.). We tested for Gaussian normal distribution with the D'Agostino-Pearson omnibus normality test. Depending on Gaussian distribution, ANOVAs, or Kruskal-Wallis tests were performed for comparisons of three groups and Bonferoni-corrected Spearman or Pearson correlation coefficients for correlation analysis.

For all tests, the level of significance was defined at $p < 0.05$. All results are presented as mean values ± standard deviation.

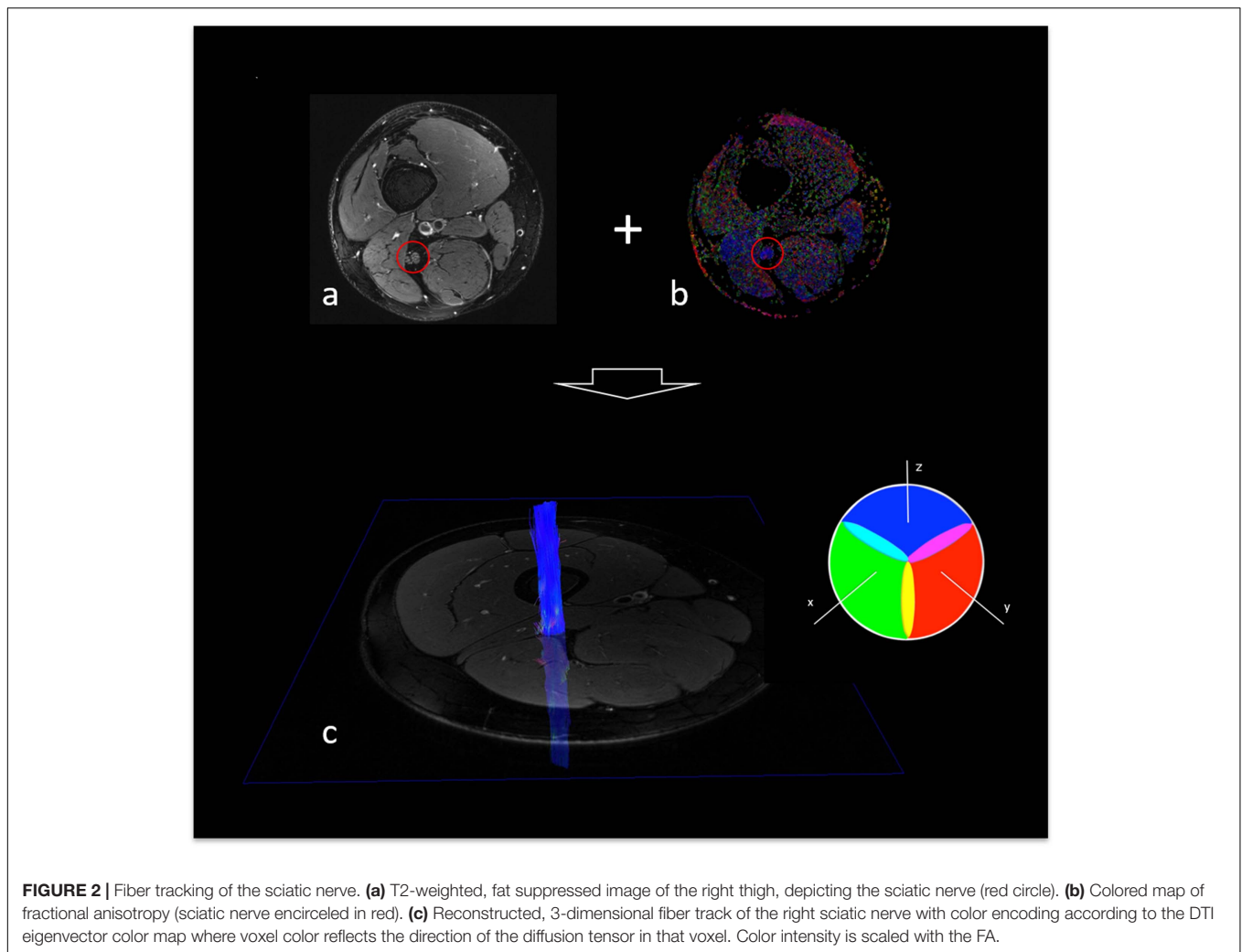
RESULTS

MRN Imaging, Demographic, Clinical and Serological Data

There was no difference between the three groups for participants' age ($p = 0.231$). HbA1c levels and triglyceride levels were higher in patients with diabetes when compared to patients with prediabetes or controls ($p < 0.001$ and $p = 0.002$, respectively). The total Pegboard score and the sciatic nerve's FA were lower in patients with diabetes when compared to controls ($p = 0.006$). No such difference could be found for AD ($p = 0.147$), RD ($p = 0.179$), or MD ($p = 0.810$). In controls, patients with prediabetes and patients with diabetes, the total pegboard score was negatively correlated with age ($r = -0.64$; $p = 0.001$, $r = 0.82$; $p = 0.002$, and $r = 0.60$; $p < 0.001$, respectively). The NDS and the NSS score were higher in patients with diabetes when compared to controls ($p < 0.001$). The mean FA for controls (0.48 ± 0.06) and prediabetic patients (0.48 ± 0.08) was well within the reference range of a healthy group of volunteers [0.507 ± 0.05 ; (Kronlage et al., 2018)], whereas the mean FA for patients with diabetes was not (0.43 ± 0.08). An overview of participants' characteristics is given in **Table 1**. Representative sciatic nerve fiber tracts from individuals of the three groups of participants (diabetes, prediabetes, controls) can be found in **Figure 3**. It can be seen that fiber tracts in the control patient are dense and contiguous (**Figure 3a**), which decreases for the prediabetes and diabetes patients (**Figures 3b,c**).

A negative association was found between the sciatic nerves' FA and patients' age in patients with diabetes ($r = -0.48$; $p < 0.001$) and controls ($r = -0.63$; $p = 0.001$) but not in patients with prediabetes ($r = 0.44$; $p = 0.202$). FA was negatively correlated with the NDS score in patients with diabetes, ($r = -0.53$; $p < 0.001$) and controls ($r = -0.47$; $p = 0.017$). A similar, yet not significant trend was seen in patients with prediabetes ($r = -0.58$; $p = 0.082$). In patients with diabetes, further negative associations of the FA were found with cystatin C ($r = -0.45$; $p < 0.001$). A detailed survey of correlations between the sciatic nerve's FA and demographic, clinical, and serological parameters is given in **Table 2**.

Similarly, as in previous studies, (Vaeggemose et al., 2017a, 2020; Kronlage et al., 2018). RD and MD (or apparent diffusion



coefficient ADC) showed correlations with clinical parameters that are in line with the correlations obtained for the fractional anisotropy FA. For instance, the mean diffusivity in the diabetes cohort is highly correlated with tibial NCV ($r = -0.31$, $p = 0.004$), and the Pegboard of the dominant and non-dominant hand ($r = -0.26$, $p = 0.026$, and $r = -0.31$, $p = 0.008$, respectively), as is the FA ($r = 0.47$, $p < 0.001$, and $r = 0.61$, $p < 0.001$, and $r = 0.43$, $p < 0.001$, respectively). Correlations of FA values with clinical, epidemiological, and serological data were generally better than those of RD and MD, which is why we focused on FA values; however, correlations of AD, RD, MD, and DTI tensor eigenvalues λ_2 and λ_3 with all relevant parameters are given in the **Supplementary Tables 1-5**, respectively.

MRN Results and Electrophysiological Data of the Lower Limb

In patients with diabetes, the sciatic nerves' FA showed positive correlations with tibial and peroneal NCVs ($r = 0.47$; $p < 0.001$, $r = 0.52$; $p < 0.001$, respectively), with tibial and peroneal nerve compound muscle action potential (CMAP) amplitudes and

sural nerve sensory nerve action potential (SNAP) amplitudes ($r = 0.62$; $p < 0.001$, $r = 0.62$; $p < 0.001$, and $r = 0.47$; $p = 0.006$, respectively). A similar, yet not significant trend was found for tibial nerve NCV and CMAP amplitudes in patients with prediabetes ($r = 0.61$; $p = 0.081$ and $r = 0.61$; $p = 0.081$, respectively). A summary of all correlations between the FA and electrophysiological data of the lower limb is given in **Table 2**.

MRN Results and Hand Function

The sciatic nerves' FA correlated positively with the total score of the pegboard-test in patients with diabetes, patients with prediabetes and controls ($r = 0.52$; $p < 0.001$, $r = 0.79$; $p = 0.007$, and $r = 0.76$; $p < 0.001$, respectively, **Figures 4A-C**). In all 4 subtests that comprise the Pegboard test, this finding could be reproduced: for patients with diabetes, patients with prediabetes and controls, significant correlations were found between FA and Pegboard scores of the dominant hand (**Figures 4D-F**) non-dominant hand (**Figures 4G-I**), testing of both hands (**Figures 4J-L**), and the assembly test (**Figures 4M-O**). A summary of the correlations between the sciatic nerves' FA and results of the Purdue Pegboard test is given in **Table 2**.

TABLE 1 | Demographic, clinical, serological, and electrophysiological data of patients with diabetes, patients with prediabetes, and controls.

	Diabetes patients	Prediabetes patients	Controls	p
Age (years)	61.1 ± 13.5	61.8 ± 9.5	56.2 ± 10.9	0.231
Number of women	26	6	16	n.a.
Number of men	45	5	9	n.a.
Body mass index (kg/m ²)	28.8 ± 4.1	28.5 ± 5.8	26.7 ± 6.4	0.131
NDS	3.0 ± 2.9	1.1 ± 1.7	0.9 ± 1.3	<0.001
NSS	3.5 ± 3.3	1.9 ± 2.9	0.1 ± 0.6	<0.001
Sciatic nerve's FA	0.43 ± 0.08	0.48 ± 0.08	0.48 ± 0.06	0.006
Total purdue pegboard score	60.8 ± 11.8	65.3 ± 11.7	71.6 ± 11.2	<0.001
HbA1c [% (mmol/mol)]	7.2 ± 1.28 (55 ± 14)	5.7 ± 0.48 (39 ± 5)	5.3 ± 0.36 (34 ± 4)	<0.001
Cystatin C (mg/dl)	0.96 ± 0.25	0.98 ± 0.19	0.89 ± 0.14	0.451
GFR (ml/min)	88.6 ± 18.6	84.7 ± 17.3	89.9 ± 15.9	0.660
Triglycerides (mg/dl)	175.1 ± 187.0	145.4 ± 96.8	101.6 ± 44.0	0.002
Total Cholesterol (mg/dl)	188.7 ± 43.4	197.3 ± 41.8	209.0 ± 40.0	0.056
HDL Cholesterol	53.9 ± 19.1	54.4 ± 14.7	62.5 ± 19.0	0.033
LDL Cholesterol	104.2 ± 34.5	113.8 ± 41.2	126.2 ± 36.7	0.007
Sural NCV (m/s)	44.0 ± 11.5	45.0 ± 5.5	45.6 ± 8.6	0.882
Sural SNAP (μV)	6.3 ± 4.2	6.2 ± 3.5	8.4 ± 5.8	0.236
Peroneal NCV (m/s)	40.1 ± 8.2	42.6 ± 3.3	45.4 ± 3.9	0.002
Peroneal CMAP (μV)	6.1 ± 3.9	5.8 ± 3.2	8.6 ± 4.9	0.033
Tibial NCV (m/s)	40.3 ± 8.0	44.4 ± 2.2	46.5 ± 5.1	<0.001
Tibial CMAP (μV)	11.3 ± 8.8	13.2 ± 6.2	15.4 ± 6.5	0.033

p values are displayed as results from comparisons of the three groups either by ANOVA or Kruskal Wallis test, depending on the Gaussian or non-Gaussian distribution of data. All values are shown as mean ± standard deviation. n.a., not applicable; NDS, Neuropathy Disability Score; NSS, Neuropathy Severity Score; FA, fractional anisotropy; HbA1c, glycated hemoglobin; GFR, glomerular filtration rate; HDL, high density lipoprotein; LDL, low density lipoprotein; NCV, nerve conduction velocity; m/s, meters per second; SNAP, sensory nerve action potential; CMAP, compound motor action potential; μV, microvolt.

Corresponding correlations for the subgroups of men and women are clearly visible, especially for the subgroup of women. We also tabularized the results from correlation analyses in both subgroups in **Supplementary Table 6**. Except for the Pegboard test of both hands in the men subgroup, all Pegboard parameters were significantly correlated with FA in the diabetes group. There was also a mild correlation of the Pegboard test of the dominant hand in the women subgroup and the control subgroup, as well as some further significant correlations between Pegboard parameters and FA in the control subgroups. Missing correlations in the prediabetes subgroups may be due to the small number of patients.

DISCUSSION

To our knowledge, this study is the first to show that the sciatic nerve's FA as a surrogate marker for nerve integrity correlates both with electrophysiological parameters of nerves in the distal lower limb and parameters of hand function in patients with diabetes. Also, this study is the first to show correlations between the sciatic nerve's FA and parameters of hand function in patients with prediabetes. Both results are of importance with regards to understanding the course of nerve damage in diabetic neuropathy: despite the assumption that nerve damage in DN parallels clinical symptoms and progresses from distally to proximally starting at the level of the feet and progressing further

onward to the level of the hands at later stages, our results indicate that neuropathic changes at the level of the upper limbs parallel those at the level of the lower limbs.

The finding that an association between the sciatic nerve's FA and functional parameters of the hands and the lower leg can already be displayed in patients with prediabetes suggests that functional impairment of the upper extremities occurs during the development of pathological glucose tolerance that later progresses into type 2 diabetes (American Diabetes Association, 2017). This is of importance for the understanding of the progression of neuropathic changes leading to diabetic neuropathy, since these findings suggest that structural nerve damage related to functional impairment occurs prior to or at very early stages of type 2 diabetes and is not, as mostly assumed, a late complication of this disease (Jende et al., 2018, 2020c). The finding that the proximally located sciatic nerve's FA correlates with functional parameters of the distal upper and lower limbs further indicates that the deterioration of nerve microstructure does not progress from distally to further proximally but rather suggests that the entire peripheral nervous system is already affected at the very beginning of DN. This is in line with results from previous studies on MRN in patients with and without DN that have found a proximal predominance of nerve lesions in DN in T2-weighted imaging (Jende et al., 2018, 2020b).

Since studies on MRN have come to show that nerve damage predominates at a proximal level in various neuropathies, the finding that the sciatic nerve's FA codifies functional parameters

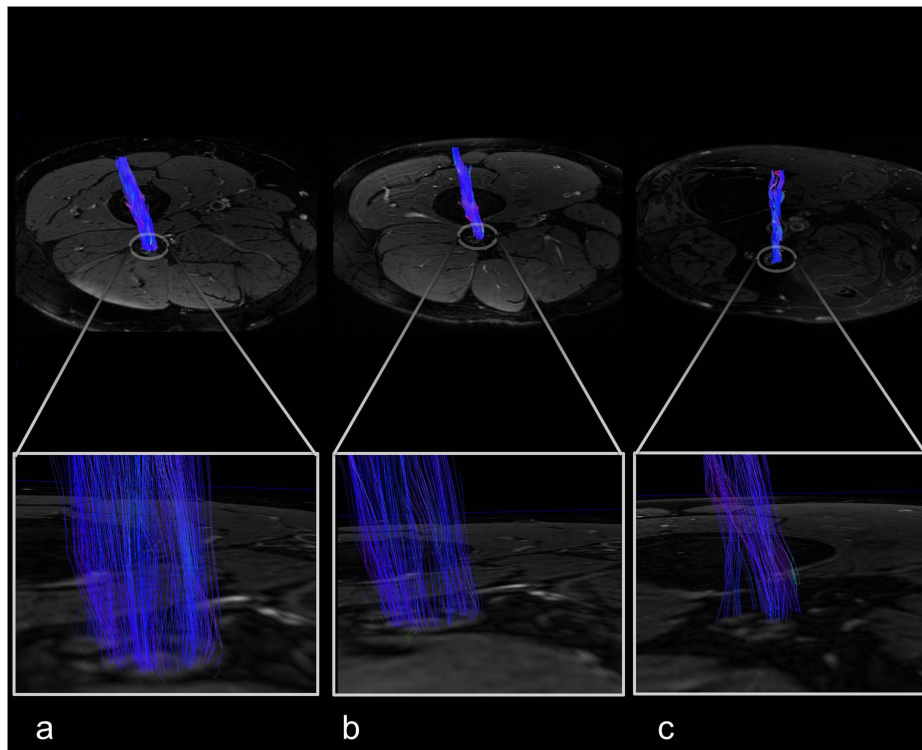


FIGURE 3 | Sciatric nerve fiber tracts with magnified views. **(a)** Female control, 67 years, neuropathy disability score (NDS) = 0. **(b)** Female prediabetes patient, 57 years, NDS = 3. **(c)** Male type 2 diabetes patient, 58 years, NDS = 7.

of the upper limb not just in patients with prediabetes and diabetes but also in controls without impaired glucose tolerance, may be of relevance not just for the course of nerve damage in DN but also other diseases of the central and peripheral nervous system (Jende et al., 2017). Additionally, our findings suggest that FA values represent an objective parameter for assessing the structural integrity of the entire peripheral nervous system in longitudinal clinical studies or interventional studies in patients with DN. One may of course argue that, since there was a correlation between participants' age and the sciatic nerve's FA in controls and patients with diabetes, the results of this study only display the well-established effect of aging on the structural and functional integrity of the peripheral nervous system (Kronlage et al., 2018). It should be considered, however, that in patients with prediabetes there was no correlation between age and FA whereas correlations between FA and parameters of hand function were significant.

The finding that there is no correlation between FA and patients' age in prediabetes patients but a positive correlation between FA and the scores of the Pegboard test can be explained by the fact that the performance in the Purdue Pegboard test is not just a matter of peripheral nerve function but also depends on cognitive and coordinative skills, which are known to decline with age (Geffe et al., 2016). The finding that there is a correlation of the Pegboard test's results with structural nerve integrity represented by the sciatic nerve's FA indicates that a reduction of the latter is associated with a reduced performance in the

Pegboard test and that, therefore, the structural integrity of peripheral nerves is of critical relevance for the performance in coordinative tasks. The finding that a reduction in FA is not correlated with age in the prediabetes group indicates that, other than cognitive and motor skills at the level of the central nervous system, diabetes-related structural damage to peripheral nerves occurs at very early stages of this disorder. This hypothesis is further supported by the finding that, while participant groups were matched for age, FA was significantly lower in diabetes patients when compared to controls. This indicates that, in addition to the process of aging, metabolic changes associated with prediabetes and diabetes cause auxiliary structural damage to peripheral nerves (Groener et al., 2020). However, it should be noted further that correlations between FA and Pegboard test parameters were significantly weaker for patients in the prediabetes group than for diabetes patients or the control group. Similarly, there are no significant correlations in the prediabetes group between FA and sural SNAP parameters or age, while there are in the diabetes and control group. In order to determine the exact impact of age and metabolic factors on nerve damage in prediabetes more closely, longitudinal studies with larger cohorts of prediabetes patients are required.

One may also argue that this study did not differentiate between type 1 diabetes and type 2 diabetes patients, although previous studies have shown that structural nerve damage differs between diabetes types for T2-weighted imaging (Jende et al., 2018). For DTI imaging, however, FA was found as a reliable

TABLE 2 | Correlations of the sciatic nerve's FA with clinical, epidemiological, and serological data of diabetes patients, prediabetes patients, and controls.

	FA diabetes patients		FA prediabetes patients		FA controls	
	<i>r</i>	<i>p</i>	<i>r</i>	<i>p</i>	<i>r</i>	<i>p</i>
Age (years)	-0.48	<0.001	0.44	0.202	-0.63	0.001
Body mass index (kg/m ²)	-0.18	0.140	-0.08	0.832	0.03	0.881
NDS	-0.53	<0.001	-0.58	0.082	-0.47	0.017
NSS	-0.20	0.106	-0.57	0.107	-0.36	0.107
HbA1c (%)	0.15	0.211	-0.07	0.844	-0.42	0.039
Cystatin C (mg/l)	-0.45	<0.001	-0.27	0.489	-0.22	0.320
Glomerular filtration rate (ml/min)	0.46	<0.001	0.21	0.571	0.23	0.291
Triglycerides (mg/dl)	0.05	0.694	0.06	0.876	-0.04	0.867
Total serum cholesterol (mg/dl)	0.17	0.151	-0.10	0.776	-0.15	0.462
HDL cholesterol (mg/dl)	0.17	0.157	-0.11	0.762	0.07	0.728
LDL cholesterol (mg/dl)	0.10	0.414	0.05	0.770	-0.18	0.396
Sural NCV(m/s)	0.24	0.128	-0.28	0.505	-0.12	0.568
Sural SNAP (μV)	0.47	0.006	0.30	0.471	0.58	0.003
Tibial NCV (m/s)	0.47	<0.001	0.61	0.081	0.35	0.099
Tibial CMAP (μV)	0.62	<0.001	0.61	0.081	0.30	0.150
Peroneal NCV (m/s)	0.52	<0.001	0.43	0.246	0.31	0.142
Peroneal CMAP (μV)	0.62	<0.001	0.51	0.160	0.18	0.411
Total Pegboard Test score	0.52	<0.001	0.79	0.007	0.76	<0.001
Pegboard Test of dominant hand	0.61	<0.001	0.65	0.044	0.64	0.001
Pegboard Test of non-dominant hand	0.43	<0.001	0.71	0.022	0.55	0.005
Pegboard Test of both hands	0.38	0.002	0.70	0.024	0.59	0.002
Pegboard Assembly Test	0.46	<0.001	0.71	0.022	0.61	0.001

NDS, Neuropathy Disability Score; NSS, Neuropathy Severity Score; HbA1c, glycated hemoglobin; GFR, glomerular filtration rate; HDL, high density lipoprotein; LDL, low density lipoprotein; NCV, nerve conduction velocity; m/s, meters per second; SNAP, sensory nerve action potential; CMAP, compound motor action potential; μV, microvolt.

marker for structural nerve integrity at the level of the lower limbs in both type 1 and type 2 diabetes (Vaeggemose et al., 2017a, 2020).

Our study is limited by the fact that only cross-sectional data were used, which does not allow for conclusions on the predictive value of the sciatic nerve's FA. Also, the group of prediabetes patients was too small to allow for exact conclusions of the interaction between aging and metabolic factors. Another limitation is that we were only testing motor function and coordination of the upper limbs but did not test for sensory gain or loss.

While, usually, improved tractography methods to select multi fiber tracts in cerebral imaging can be challenging due to the difficulty of selecting adequate regions of interest for tract seeding (Wilkins et al., 2015; Christidi et al., 2016), the VOI selection in sciatic nerve processing is straight-forward due to the nature of peripheral nerves that can be easily identified on T2w images. Nordic BrainEx was shown to agree in major fiber bundle reconstruction with other major software vendors such as DSI Studio or Philips FiberTrak, while there were differences for smaller fiber bundles (Christidi et al., 2016). It should therefore be noted that systematic errors during the automated reconstruction process may impact the DTI parameter results, however, the FACT algorithm used in Nordic BRAINEX is a commonly used DTI reconstruction algorithm, and seeding errors are supposedly low in lieu of the above considerations (Mukherjee et al., 2008).

Further potential sources of error are the FA cutoff, which we chose in agreement with previous publications on peripheral nerve DTI analyses (Kwon et al., 2015; Oudeman et al., 2020), partial volume effects, and, naturally, experimental parameters such as resolution and signal-to-noise ratios (Okamoto et al., 2010; Barrio-Arranz et al., 2015). We chose a comparatively high DTI in-plane resolution, see e.g. (van Steenkiste et al., 2016), to reduce DTI processing errors, as well as multiple averages to reduce signal-to-noise ratio. Considering that sciatic nerve fat fractions are elevated in patients with increased BMI, a missing correlation of sciatic nerve FA with BMI (Table 2) indicates that there is no significant impact of intra- or perineural fat on FA calculation.

One further limitation may be the spatial heterogeneity of the gradients (Krzyżak and Olejniczak, 2015; Borkowski and Krzyżak, 2019). Taken together, these types of errors are likely averaged for a larger number of patients, as in the diabetes and control group.

In summary, this study is the first to show that the sciatic nerve's FA is a surrogate marker for nerve function of the distal upper and lower limbs in patients with diabetes and prediabetes. Our findings suggest that proximal nerve damage in diabetes parallels distal nerve function even before patients start to experience clinical symptoms, which may also be relevant with regard to PNS damage in other neuropathies. Further longitudinal studies on the predictive value of the sciatic nerve's

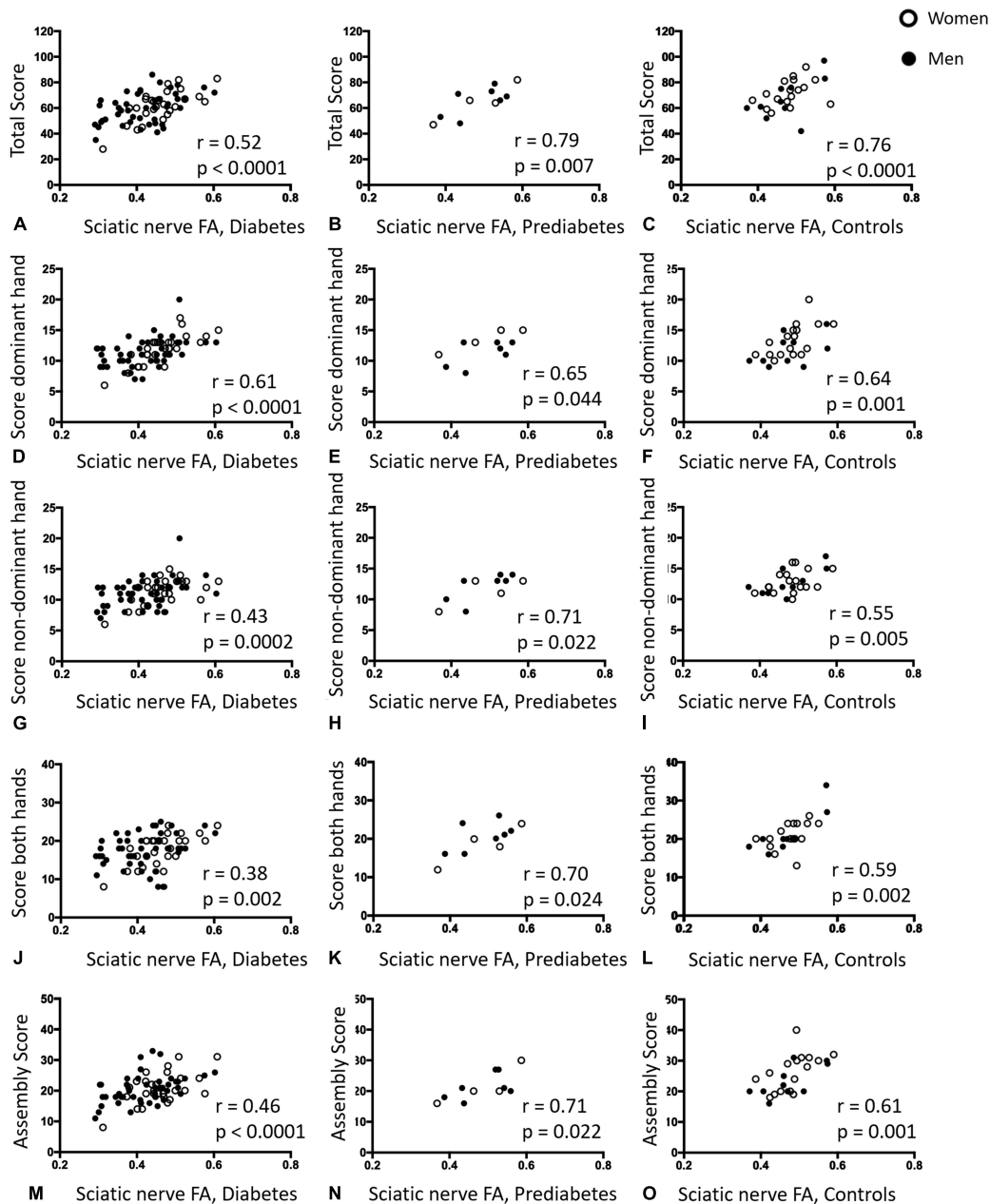


FIGURE 4 | Correlative statistics of Purdue Pegboard Test scores and sciatic nerve fractional anisotropy. **(A)** Correlation of the sciatic nerve's fractional anisotropy (FA) in patients with diabetes with the total Purdue Pegboard Test score ($r = 0.52$; $p < 0.001$; 95% confidence interval (CI) = 0.31 to 0.67). **(B)** Correlation of the sciatic nerve's FA in patients with prediabetes with the total Purdue Pegboard Test score ($r = 0.79$; $p = 0.007$; 95% CI = 0.31 to 0.95). **(C)** Correlation of the sciatic nerve's FA in controls with the total Purdue Pegboard Test score ($r = 0.76$; $p < 0.001$; 95%CI = 0.52 to 0.89). **(D)** Correlation of the sciatic nerve's FA in patients with diabetes with the Purdue Pegboard Test score of the dominant hand ($r = 0.61$; $p < 0.001$; 95%CI = 0.43 to 0.74). **(E)** Correlation of the sciatic nerve's FA in patients with prediabetes with the Purdue Pegboard Test score of the dominant hand ($r = 0.65$; $p = 0.044$; 95%CI = 0.52 to 0.90). **(F)** Correlation of the sciatic nerve's FA in controls with the Purdue Pegboard Test score of the dominant hand ($r = 0.64$; $p = 0.001$; 95%CI = 0.22 to 0.77). **(G)** Correlation of the sciatic nerve's FA in patients with diabetes with the Purdue Pegboard Test score of the non-dominant hand ($r = 0.43$; $p = 0.0002$; 95%CI = 0.22 to 0.60). **(H)** Correlation of the sciatic nerve's FA in patients with prediabetes with the Purdue Pegboard Test score of the non-dominant hand ($r = 0.71$; $p = 0.022$; 95%CI = 0.21 to 0.92). **(I)** Correlation of the sciatic nerve's FA in controls with the Purdue Pegboard Test score of the non-dominant hand ($r = 0.55$; $p = 0.005$; 95%CI = 0.19 to 0.76). **(J)** Correlation of the sciatic nerve's FA in patients with diabetes with the Purdue Pegboard Test score of both hands ($r = 0.38$; $p = 0.002$; 95%CI = 0.14 to 0.54). **(K)** Correlation of the sciatic nerve's FA in patients with prediabetes with the Purdue Pegboard Test score of both hands ($r = 0.70$; $p = 0.024$; 95%CI = 0.16 to 0.91). **(L)** Correlation of the sciatic nerve's FA in controls with the Purdue Pegboard Test score of both hands ($r = 0.59$; $p = 0.002$; 95%CI = 0.37 to 0.84). **(M)** Correlation of the sciatic nerve's FA in patients with diabetes with the Purdue Pegboard Test assembly score ($r = 0.46$; $p < 0.001$; 95%CI = 0.26 to 0.63). **(N)** Correlation of the sciatic nerve's FA in patients with prediabetes with the Purdue Pegboard Test assembly score ($r = 0.71$; $p = 0.022$; 95%CI = 0.20 to 0.92). **(O)** Correlation of the sciatic nerve's FA in controls with the Purdue Pegboard Test assembly score ($r = 0.61$; $p = 0.001$; 95%CI = 0.26 to 0.79).

FA for disease progression in DN and other neuropathies are warranted.

DATA AVAILABILITY STATEMENT

The datasets presented in this article are not readily available because they contain sensitive patient information. The data supporting the conclusions of this article will be made available upon reasonable request by any qualified researcher. Requests to access the datasets should be directed to FK, felix.kurz@med.uni-heidelberg.de.

ETHICS STATEMENT

The studies involving human participants were reviewed and approved by the Ethics Committee of the Medical Faculty of the University of Heidelberg. The patients/participants provided their written informed consent to participate in this study.

AUTHOR CONTRIBUTIONS

JJ, MB, SH, PN, and FK designed and coordinated the study. JJ, CM, JG, JK, AJ, and FK contributed to the organization of participants. JJ, AJ, and FK collected MR data. AH and FK developed image analysis tools. ZK, LA-R, JG, and SK collected clinical, serological, and electrophysiological data. JJ and FK analyzed the data, wrote the manuscript with input from all co-authors.

FUNDING

The German research council (DFG, SFB 1158) and the international Foundation for Research in paraplegia (IRP) provided financial support for personnel expenditure, MR imaging costs and costs for the technical equipment required for electrophysiological and serological analysis. The DFG and the IRP had no influence on the study design, collection and

analysis of data or on the writing of the article. JJ received grants from the German Research Foundation (SFB 1158) and from the International Foundation for Research in Paraplegia. ZK received grants from the Deutsches Zentrum für Diabetesforschung (DZD) e.V. CM reports no disclosures. JG received grants from the Deutsches Zentrum für Diabetesforschung (DZD) e.V. LA-R reports no disclosures. JK received research grants, personal fees, and lecture honoraria from Alnylam Pharmaceutical (MA, United States), the Olympia Morata stipend grant from the Medical Faculty of the University of Heidelberg, lecture honoraria and financial support for conference attendance from Pfizer, and advises for Akcea Therapeutics. AJ received a grant from the Dietmar Hopp foundation (grant No. 23011228). AH received grants from the German Research Foundation (DFG grant KU 3555/1-1). SH received a grant from the Dietmar Hopp foundation (grant No. 23011228) and the German Research Council (DFG, SFB 1118). PN received grants from the German research Council (DFG, SFB 1118 and 1158) and from Novo Nordisk. MB received grants and personal fees from Codman, Guerbet, Bayer and Novartis, personal fees from Roche, Teva, Springer, Boehringer, Grifols, Braun and grants from the European Union, Siemens, the Dietmar Hopp foundation, Stryker and the German Research Council (DFG, SFB 1118 and 1158). SK reports no disclosures. FK was supported by the German Research Foundation (KU 3555/1-1) and the Hoffmann-Klose foundation of Heidelberg University Hospital.

ACKNOWLEDGMENTS

We thank Mrs. Dorothea Willich (Department of Neuroradiology, Heidelberg University Hospital) for her ongoing support and excellent technical performance of all MRN examinations.

SUPPLEMENTARY MATERIAL

The Supplementary Material for this article can be found online at: <https://www.frontiersin.org/articles/10.3389/fnins.2021.642589/full#supplementary-material>

REFERENCES

- American Diabetes Association (2017). 2. Classification and diagnosis of diabetes. *Diabetes Care* 40(Suppl. 1), S11–S24. doi: 10.2337/dc17-S005
- Barrio-Arranz, G., de Luis-García, R., Tristán-Vega, A., Martín-Fernández, M., and Aja-Fernández, S. (2015). Impact of MR acquisition parameters on DTI scalar indexes: a tractography based approach. *PLoS One* 10:e0137905. doi: 10.1371/journal.pone.0137905
- Borkowski, K., and Krzyżak, A. T. (2019). Assessment of the systematic errors caused by diffusion gradient inhomogeneity in DTI-computer simulations. *NMR Biomed.* 32:e4130. doi: 10.1002/nbm.4130
- Christidi, F., Karavasili, E., Samiotis, K., Bisdas, S., and Papanikolaou, N. (2016). Fiber tracking: a qualitative and quantitative comparison between four different software tools on the reconstruction of major white matter tracts. *Eur. J. Radiol. Open* 3, 153–161. doi: 10.1016/J.EJRO.2016.06.002
- Feldman, E. L., Nave, K.-A., Jensen, T. S., and Bennett, D. L. H. (2017). New horizons in diabetic neuropathy: mechanisms, bioenergetics, and pain. *Neuron* 93, 1296–1313.
- Geffé, S., Schindlbeck, K. A., Mehl, A., Jende, J., Klostermann, F., and Marzinzik, F. (2016). The single intake of levodopa modulates implicit learning in drug naïve, de novo patients with idiopathic Parkinson's disease. *J. Neural Transm.* 123, 601–610. doi: 10.1007/s00702-016-1557-y
- Groener, J. B., Jende, J. M. E., Kurz, F. T., Kender, Z., Treede, R.-D., Schuh-Hofer, S., et al. (2020). Understanding diabetic neuropathy—from subclinical nerve lesions to severe nerve fiber deficits: a cross-sectional study in patients with type 2 diabetes and healthy control subjects. *Diabetes* 69, 436–447. doi: 10.2337/db19-0197
- Jende, J. M. E., Groener, J. B., Kender, Z., Hahn, A., Morgenstern, J., Heiland, S., et al. (2020a). Troponin T parallels structural nerve damage in type 2 diabetes: a cross-sectional study using magnetic resonance neurography. *Diabetes* 69, 713–723. doi: 10.2337/db19-1094

- Jende, J. M. E., Groener, J. B., Kender, Z., Rother, C., Hahn, A., Hilgenfeld, T., et al. (2020b). Structural nerve remodeling at 3-T MR neurography differs between painful and painless diabetic polyneuropathy in type 1 or 2 diabetes. *Radiology* 294, 405–414. doi: 10.1148/radiol.2019191347
- Jende, J. M. E., Groener, J. B., Oikonomou, D., Heiland, S., Kopf, S., Pham, M., et al. (2018). Diabetic neuropathy differs between type 1 and type 2 diabetes: insights from magnetic resonance neurography. *Ann. Neurol.* 83, 588–598.
- Jende, J. M. E., Groener, J. B., Rother, C., Kender, Z., Hahn, A., Hilgenfeld, T., et al. (2019). Association of serum cholesterol levels with peripheral nerve damage in patients with type 2 diabetes. *JAMA Netw. Open* 2:e194798.
- Jende, J. M. E., Hauck, G. H., Diem, R., Weiler, M., Heiland, S., Wildemann, B., et al. (2017). Peripheral nerve involvement in multiple sclerosis: demonstration by magnetic resonance neurography. *Ann. Neurol.* 82, 676–685.
- Jende, J. M. E., Kender, Z., Rother, C., Alvarez-Ramos, L., Groener, J. B., Pham, M., et al. (2020c). Diabetic polyneuropathy is associated with pathomorphological changes in human dorsal root ganglia: a study using 3T MR neurography. *Front. Neurosci.* 14:570744. doi: 10.3389/fnins.2020.570744
- Kopf, S., Groener, J. B., Kender, Z., Fleming, T., Bischoff, S., Jende, J., et al. (2018a). Deep phenotyping neuropathy: an underestimated complication in patients with pre-diabetes and type 2 diabetes associated with albuminuria. *Diabetes Res. Clin. Pract.* 146, 191–201. doi: 10.1016/j.diabres.2018.10.020
- Kopf, S., Groener, J. B., Kender, Z., Fleming, T., Brune, M., Riedinger, C., et al. (2018b). Breathlessness and restrictive lung disease: an important diabetes-related feature in patients with type 2 diabetes. *Respiration* 96, 29–40. doi: 10.1159/000488909
- Kronlage, M., Schwehr, V., Schwarz, D., Godel, T., Uhlmann, L., Heiland, S., et al. (2018). Peripheral nerve diffusion tensor imaging (DTI): normal values and demographic determinants in a cohort of 60 healthy individuals. *Eur. Radiol.* 28, 1801–1808. doi: 10.1007/s00330-017-5134-z
- Krzyżak, A. T., and Olejniczak, Z. (2015). Improving the accuracy of PGSE DTI experiments using the spatial distribution of b matrix. *Magn. Reson. Imaging* 33, 286–295. doi: 10.1016/j.mri.2014.10.007
- Kwon, B. C., Koh, S. H., and Hwang, S. Y. (2015). Optimal parameters and location for diffusion-tensor imaging in the diagnosis of carpal tunnel syndrome: a prospective matched case-control study. *AJR Am. J. Roentgenol.* 204, 1248–1254. doi: 10.2214/AJR.14.13371
- Mori, S., Crain, B. J., Chacko, V. P., and van Zijl, P. C. (1999). Three-dimensional tracking of axonal projections in the brain by magnetic resonance imaging. *Ann. Neurol.* 45, 265–269. doi: 10.1002/1531-8249(199902)45:2<265::aid-ana21<3.0.co;2-3
- Mukherjee, P., Berman, J. I., Chung, S. W., Hess, C. P., and Henry, R. G. (2008). Diffusion tensor MR imaging and fiber tractography: theoretic underpinnings. *Am. J. Neuroradiol.* 29, 632–641. doi: 10.3174/ajnr.A1051
- Nawroth, P. P., Bendszus, M., Pham, M., Jende, J., Heiland, S., Ries, S., et al. (2018). The quest for more research on painful diabetic neuropathy. *Neuroscience* 387, 28–37. doi: 10.1016/j.neuroscience.2017.09.023
- NordicNeuroLab AS (2019). *nordic BrainEX Tutorial - DTI Module*. Available online at: <http://downloads.nordicneurolab.com/SW/nBX/Tutorials/Tutorial%20-%20DTI.pdf> (accessed January 31, 2021).
- O'Donnell, L. J., Suter, Y., Rigolo, L., Kahali, P., Zhang, F., Norton, I., et al. (2017). Automated white matter fiber tract identification in patients with brain tumors. *Neuroimage Clin.* 13, 138–153. doi: 10.1016/j.nicl.2016.11.023
- Okamoto, Y., Kunimatsu, A., Kono, T., Nasu, K., Sonobe, J., and Minami, M. (2010). Changes in MR diffusion properties during active muscle contraction in the calf. *Magn. Reson. Med. Sci.* 9, 1–8. doi: 10.2463/mrms.9.1
- Oudeman, J., Eftimov, F., Strijkers, G. J., Schneiders, J. J., Roosendaal, S. D., Engbersen, M. P., et al. (2020). Diagnostic accuracy of MRI and ultrasound in chronic immune-mediated neuropathies. *Neurology* 94, e62–e74. doi: 10.1212/WNL.0000000000008697
- Symonds, T., Campbell, P., and Randall, J. A. (2017). A review of muscle- and performance-based assessment instruments in DM1. *Muscle Nerve* 56, 78–85. doi: 10.1002/mus.25468
- Tesfaye, S., Chaturvedi, N., Eaton, S. E. M., Ward, J. D., Manes, C., Ionescu-Tirgoviste, C., et al. (2005). Vascular risk factors and diabetic neuropathy. *N. Engl. J. Med.* 352, 341–350. doi: 10.1056/NEJMoa032782
- Vaeggemose, M., Haakma, W., Pham, M., Ringgaard, S., Tankisi, H., Ejksjaer, N., et al. (2020). Diffusion tensor imaging MR neurography detects polyneuropathy in type 2 diabetes. *J. Diabetes Complications* 34:107439. doi: 10.1016/j.jdiacomp.2019.107439
- Vaeggemose, M., Pham, M., Ringgaard, S., Tankisi, H., Ejksjaer, N., Heiland, S., et al. (2017a). Diffusion tensor imaging MR neurography for the detection of polyneuropathy in type 1 diabetes. *J. Magn. Reson. Imaging* 45, 1125–1134. doi: 10.1002/jmri.25415
- Vaeggemose, M., Pham, M., Ringgaard, S., Tankisi, H., Ejksjaer, N., Heiland, S., et al. (2017b). Magnetic resonance neurography visualizes abnormalities in sciatic and tibial nerves in patients with type 1 diabetes and neuropathy. *Diabetes* 66, 1779–1788. doi: 10.2337/db16-1049
- van Steenkiste, G., Jeurissen, B., Baete, S., den Dekker, A. J., Poot, D. H. J., Boada, F., et al. (2016). *High Resolution Diffusion Tensor Reconstruction from Simultaneous Multi-Slice Acquisitions in a Clinically Feasible Scan time*. *Proceedings of the International Society for Magnetic Resonance in Medicine* 0002. Available online at: <http://ismrm.gitlab.io/2016/0002.html> (Accessed February 3, 2021).
- Wilkins, B., Lee, N., Gajawelli, N., Law, M., and Laporé, N. (2015). Fiber estimation and tractography in diffusion MRI: development of simulated brain images and comparison of multi-fiber analysis methods at clinical b-values. *Neuroimage* 109, 341–356. doi: 10.1016/j.neuroimage.2014.12.060
- Yang, C.-J., Hsu, H.-Y., Lu, C.-H., Chao, Y.-L., Chiu, H.-Y., and Kuo, L.-C. (2018). Do we underestimate influences of diabetic mononeuropathy or polyneuropathy on hand functional performance and life quality? *J. Diabetes Investig.* 9, 179–185. doi: 10.1111/jdi.12649
- Young, M. J., Boulton, A. J., MacLeod, A. F., Williams, D. R., and Sonksen, P. H. (1993). A multicentre study of the prevalence of diabetic peripheral neuropathy in the United Kingdom hospital clinic population. *Diabetologia* 36, 150–154. doi: 10.1007/BF00400697

Conflict of Interest: The authors declare that the research was conducted in the absence of any commercial or financial relationships that could be construed as a potential conflict of interest.

Copyright © 2021 Jende, Kender, Mooshage, Groener, Alvarez-Ramos, Kollmer, Juerchott, Hahn, Heiland, Nawroth, Bendszus, Kopf and Kurz. This is an open-access article distributed under the terms of the Creative Commons Attribution License (CC BY). The use, distribution or reproduction in other forums is permitted, provided the original author(s) and the copyright owner(s) are credited and that the original publication in this journal is cited, in accordance with accepted academic practice. No use, distribution or reproduction is permitted which does not comply with these terms.



Multisequence Quantitative Magnetic Resonance Neurography of Brachial and Lumbosacral Plexus in Chronic Inflammatory Demyelinating Polyneuropathy

OPEN ACCESS

Edited by:

Felix Tobias Kurz,
Heidelberg University Hospital,
Germany

Reviewed by:

Yongsheng Chen,
Wayne State University, United States
Sabine Heiland,
Heidelberg University Hospital,
Germany

*Correspondence:

Chuansheng Zheng
whxhchuansheng@126.com

† These authors have contributed
equally to this work

Specialty section:

This article was submitted to
Brain Imaging Methods,
a section of the journal
Frontiers in Neuroscience

Received: 03 January 2021

Accepted: 25 June 2021

Published: 23 July 2021

Citation:

Su X, Kong X, Alwalid O, Wang J,
Zhang H, Lu Z and Zheng C (2021)
Multisequence Quantitative Magnetic
Resonance Neurography of Brachial
and Lumbosacral Plexus in Chronic
Inflammatory Demyelinating
Polyneuropathy.
Front. Neurosci. 15:649071.
doi: 10.3389/fnins.2021.649071

Xiaoyun Su¹, Xiangquan Kong¹, Osamah Alwalid¹, Jing Wang¹, Huiting Zhang²,
Zuneng Lu^{3†} and Chuansheng Zheng^{1*†}

¹ Department of Radiology, Union Hospital, Tongji Medical College, Huazhong University of Science and Technology, Wuhan, China, ² Siemens Healthineers, Shanghai, China, ³ Department of Neurology, Renmin Hospital of Wuhan University, Wuhan, China

Background and Purpose: Chronic inflammatory demyelinating polyneuropathy (CIDP) is an uncommon demyelinating disorder. Although treatable, it is difficult to diagnose. The purpose of this study was to evaluate the diagnostic performance and abnormalities of plexus via quantitative multisequence magnetic resonance neurography (MRN) for CIDP.

Methods: Brachial and lumbosacral (LS) plexus of 37 CIDP patients and 37 age- and gender-matched controls were examined by using multisequence MRN. Nerve diameter, nerve-to-muscle T2 signal intensity ratio (nT2), contrast-enhanced ratio (CR), fractional anisotropy (FA), and apparent diffusion coefficient (ADC) were determined in both plexus, and tractographies were performed. The disease histories and the Inflammatory Rasch-built Overall Disability Scale (I-RODS) questionnaire scores were documented before MRI scans.

Results: The sizes of nerve roots were larger in CIDP ($p < 0.01$). CR, nT2, and ADC were significantly higher, while FA was lower in CIDP than in controls ($p < 0.01$). FA had the highest sensitivity (0.809) and area under the curve (AUC) (0.925), while the highest specificity was 0.961 for CR in single parameters. The combination of FA and CR has the highest sensitivity, specificity, accuracy, and AUC in the LS plexus. CR only had a weak correlation with nT2 ($p < 0.05$). ADC and diameter had a positive correlation with nT2, and the diameter and nT2 had a negative correlation with FA in CIDP ($p < 0.05$). FA had a negative correlation with the duration in the CIDP ($r's = -0.404, p < 0.05$). There

was no significant correlation between the I-RODS scores and MR multiparameters ($p < 0.05$).

Conclusion: Multisequence MRN possesses a high diagnostic performance in the LS plexus. Sampling perfection with application-optimized contrasts using different flip angle evolutions (SPACE) combined with DTI and contrast enhancement serves as a recommended composite protocol for CIDP.

Keywords: magnetic resonance neurography, diffusion tensor imaging, Polyradiculoneuropathy, chronic inflammatory demyelinating, plexus, contrast

INTRODUCTION

Chronic inflammatory demyelinating polyneuropathy (CIDP) is an acquired immune-mediated and treatable demyelinating disorder of the peripheral nervous system (Rotta et al., 2000; Vallat et al., 2010; Latov, 2014). CIDP is most frequently observed in adult men and has an annual incidence of 0.48 per 100,000 individuals in the population (Iijima et al., 2008). The diagnosis and management of CIDP can be difficult and are mainly based on clinical features and nerve conduction studies (Latov, 2014; Querol et al., 2017; Rajabally et al., 2017). However, CIDP is characterized clinically by heterogeneous, sensory, and motor impairment with a chronic progressive or relapsing–remitting course (Rotta et al., 2000; Alabdali et al., 2017). Therefore, patients frequently undergo electrophysiology, lumbar puncture examinations, and at times even nerve biopsy for establishing the diagnosis. However, a major limitation of neuroelectrophysiology is the inability to assess nerves at all sites, especially the proximal nerve roots of the deep plexus that are often involved (Lichtenstein et al., 2018).

Hypertrophy with T2 signal alterations or gadolinium enhancement of peripheral nerves has been described on MRI in patients with CIDP, but it is only a supportive criterion (level C recommendation) according to the 2010 guidelines of the European Federation of Neurological Societies/Peripheral Nerve Society (Van den Bergh et al., 2010). Conventional MR neurography provides only a view of the limited region of nerve trunks, or a description of the morphological and signal abnormalities. More commonly, MR neurography, based on heavily T2-weighted imaging with fat suppression combined with T1-weighted sequences, is used to assess peripheral neuropathy (Takahara et al., 2008; Yoshida et al., 2015). However, this may not enough identify the condition of complicated diseases, especially when hypertrophy has not yet appeared in the peripheral nerves at the early stage. CIDP is considered to be an autoimmune disease involving the cellular and humoral immune responses. Gadolinium enhancement on MRI may also work by indicating the presence of an inflammatory process, as occurs in CIDP (Duggins et al., 1999). However, quantitative studies on the enhancement of the nerves are rarely done.

In this study, we have implemented a quantitative multisequence protocol for brachial and lumbosacral (LS) plexus neurography to gain a multifaceted biological characterization of peripheral nerve tissues. Concurrently, the potential correlation

between parameters and their diagnostic efficiency were investigated to come up with optimal combined sequences.

MATERIALS AND METHODS

Subjects

The study was performed with the approved by the ethics review committee (No. IORG0003571) and was registered on ClinicalTrials.gov (ChiCTR1800016450).

All subjects signed a written informed consent prior to enrolment. The study was conducted from March 2016 to September 2019. Thirty-seven newly diagnosed patients (newly diagnosed and re-diagnosed cases, who were previously misdiagnosed) with typical CIDP were recruited from the Neuromuscular Center of our hospital. The inclusion criteria for CIDP are follows: typical CIDP; a neurologist verified that their conditions met the European Federation of Neurological Societies/Peripheral Nerve Society diagnostic criteria; spectrum of typical CIDP; and definite chronic progressive and relapsing courses only. The disease histories and the Inflammatory Rasch-built Overall Disability Scale (I-RODS) questionnaire scores, which have proved as an outcome measurement for assessing activity limitations, were documented before MRI scans individually in patients. Additionally, 37 healthy controls who matched patients with CIDP in age (± 2 years) and gender were recruited from our institution. Exclusion criteria included any contraindication to MRI and the presence of renal insufficiency.

Magnetic Resonance Neurography

MR neurography was performed on a 3-T whole-body MR system (MAGNETOM Trio, Siemens Healthcare, Erlangen, Germany). A four-channel neck and contiguous three-multichannel body matrix coils linked to the spine element coils were employed from the skull base to the upper thigh.

The MRI protocol of the brachial and LS plexus included volumetric interpolated breath-hold examination (VIBE), turbo inversion recovery magnitude (TIRM), and three-dimensional (3D) sampling perfection with application-optimized contrasts using different flip angle evolutions (SPACE) sequences on the coronal plane and the single-shot echo-planar-imaging (EPI)-based DTI sequence on the axial plane. The multi-sequences of the brachial and LS plexus were scanned separately. First, TIRM,

VIBE, and DTI sequences were performed. Then, a macrocyclic gadolinium-based contrast agent (Gadovist, Bayer Healthcare, Leverkusen, Germany) was injected intravenously at a dose of 0.1 ml/kg with a flow rate of 1.5 ml/s. Finally, contrast-enhanced (ce)-VIBE was scanned immediately after the injection of a contrast agent, then 3D SPACE was applied. The center k-space line of ce-VIBE was located at 80 s. Specific sequence parameters are shown in **Supplementary Table 1**. The duration of each scan session was 50 min.

Image Post-processing and Analysis

Post-processing of raw MRI data and DTI analysis were performed with software provided by the MR system manufacturer (Syngo MR Workspace, Siemens Healthcare). Qualitative and quantitative assessments were performed independently by two experienced radiologists (J.W., > 10 years of neuroimaging experience; X.S., > 3 years of neuroimaging experience), who were blinded to the clinical information. The final averaged values were obtained by three repeated measurements in each parameter. Furthermore, one of the radiologists (X.S.) carried out a second-time quantitative assessment after 12 weeks. Two radiologists qualitatively assessed for abnormal findings (hypertrophy or/and hyperintensity/contrast enhancement) of the brachial and LS plexus with blind, separately. Abnormal MR findings of diffusion tensor tractography were recorded. For any disagreements between the two radiologists in the qualitative assessments, the final conclusion was taken by consensus.

Quantitative Analysis

Nerve Diameters

The diameters of the nerve roots at C5-C8 and L4-S1 levels were measured perpendicular to their long axes, at 1.0 cm away from the dorsal root ganglion (DRG) on both sides on the maximum intensity projection (MIP, 15 slices and thickness was 15.0 mm) images from the 3D SPACE image. The diameters of the bilateral sciatic and femoral nerves were determined at the upper edges of the femoral heads in the coronal and sagittal planes, respectively.

Contrast-Enhanced Ratios

The contrast-enhanced ratios (CR) of bilateral C5-C8 and L4-S1 nerve roots were determined at the same location by copying the ROI between the ce VIBE and non-ce VIBE sequences, at 1.0 cm away from the DRG. The background noise was measured outside of the body region. The ce nerve signal-to-noise ratio (ce nSNR) = nerve signal intensity_{ceVIBE}/background noise_{ceVIBE}. The non-ce nSNR = nerve signal intensity_{non-ceVIBE}/background noise_{non-ceVIBE}. The CR was defined as CR = ce nSNR/non-ce nSNR.

Nerve-to-Muscle T2 Signal Intensity Ratios

The nerve-to-muscle T2 signal intensity ratios (nT2) were obtained by placing the ROI on bilateral C5-C8 and L4-S1 nerve roots and calculated in relation to the adjacent deep cervical and iliopsoas muscles on the TIRM sequence. The nT2 was defined as the following: nT2 = nerve root T2 signal intensity/adjacent muscle T2 signal intensity.

DTI Parameters

The average apparent diffusion coefficient (ADC) and fractional anisotropy (FA) values were calculated on the DTI by hand-operated circular ROI in an anatomical b0 field image that was drawn beyond 1.0 cm of the DRG at the bilateral C5-C8 and L4-S1 nerve roots. For diffusion tensor tractography, a turning angle of 30° and an FA threshold of 0.10 were employed. The step size of the deterministic tractography algorithm was 1.0 mm.

Nerve diameters were reported separately for the C5-C8 and L4-S1 nerve roots. Also, the CR, nT2 values, and DTI parameters were represented by a value for the brachial plexus and LS plexus, respectively, as a whole.

Quality Analysis

The image quality was evaluated based on the degree and uniformity of fat suppression and the presence of motion artifacts affecting the nerve visualization. It was scored on a scale from 1 to 3 (1: excellent, 2: moderate, 3: poor) on morphological sequences, including VIBE, TIRM, and SPACE. The DTI quality was assessed depending on the presence of motion artifacts and distortion, (1) excellent, artifact-free or a little; (2) moderate, some artifacts or distortion not affecting measurement; and (3) poor, severe artifacts and image distortions. Images with “poor” classification were excluded.

Statistical Analysis

Statistical analysis was performed by IBM SPSS statistical software version 25 (IBM Corp., Armonk, NY, United States) and GraphPad Prism 7.0 (GraphPad software, San Diego, CA, United States). Categorical variables were summarized as frequencies and proportions. The median (M) and interquartile range (IQR) were expressed in non-normal distributed continuous data. The Wilcoxon signed-rank test was used to assess the differences in each parameter between the patients and controls. ROC curve analysis was used to determine the diagnostic efficiency. The joint analysis of the MR parameters was conducted using a binary logistical regression, and the generated variable probability was fitted to the joint curve of ROC. Correlation or partial correlation analyses after adjustment for gender and age were performed using Spearman’s correlation coefficients. Intraclass correlation coefficients (ICC) were calculated to the consistency of the inter- and intra-observer. Multiple-hypothesis testing was addressed with Bonferroni correction. Two-tailed $p < 0.05$ was considered statistically significant.

RESULTS

A total of 74 subjects (37 patients with CIDP, 37 age- and gender-matched controls) were studied. The clinical characteristics are provided in **Table 1**.

Quality Assessments

The quality assessment of the brachial and LS plexus achieved the rating of “excellent” in over half of the images (**Supplementary Table 2**). One of the patients with CIDP only performed the

brachial plexus imaging and did not complete the LS plexus imaging due to the involuntary movements of the feet. Therefore, the LS plexus images of this patient and the paired control were excluded. One brachial VIBE image and DTI images of brachial and LS plexus were rated as “poor” qualities and were excluded with the corresponding control images (**Supplementary Table 2**).

Images and Qualitative Analysis

Abnormal findings (nerve hypertrophy or/and hyperintensity/contrast enhancement) were noticed in the brachial plexus of 22/37 (59.5%) and in the LS plexus of 27/36 (75.0%) of the patients with CIDP, and in none of the healthy controls (**Supplementary Figure 1**). The coherence rate of the two radiologists was 96% (72/75) in the qualitative assessments.

Hypertrophy and enhancement were illustrated as seen in the brachial and LS plexus MR neurography of the patients with CIDP (**Figures 1, 2**). The thickening, irregularity, and partial discontinuity of the brachial and LS plexus were found on diffusion tensor tractography in patients with CIDP (**Figure 3**). The reconstructed fiber bundles of the plexus in controls are also shown in **Figure 3**. Representative *B*-value = 0 image, ADC, and FA maps of nerve roots in patients with CIDP are exhibited in **Supplementary Figure 2**.

Quantitative Analysis

The diameters of the C5–C8 and L4–S1 nerve roots and sciatic and femoral nerves were significantly larger in patients with CIDP than in healthy controls (all $p < 0.001$, **Supplementary Table 3** and **Supplementary Figure 3**). The CR, nT2, and ADC of the brachial and LS nerve roots were significantly higher in patients with CIDP than in controls, while FA was lower in CIDP ($p < 0.01$, **Figure 4** and **Table 2**).

Analysis of Diagnostic Accuracy

In a single-parameter model, FA had the largest area under the curve (AUC) (0.925) using a cutoff value of 0.361, with the highest sensitivity (80.9%) and accuracy (0.73) in the LS plexus (**Table 3** and **Figure 5**), while the highest specificity was 96.1%

given by CR in the LS plexus (**Table 3**). The AUC, sensitivity, specificity, and accuracy of the combined two-parameter analysis are provided in **Supplementary Table 3**. The combined analysis of FA and CR demonstrated the highest AUC (0.973), sensitivity (92.2%), specificity (96.3%), and accuracy (0.885) in the LS plexus, which have significant differences among each pair, respectively (**Figure 5** and **Supplementary Tables 4, 5**).

Correlations With MR Parameters

Both the diameter and nT2 had moderate negative correlations with FA in patients with CIDP ($|r_s| = 0.41–0.52$; $p < 0.05$) and corresponding weak or no correlations in controls (**Table 4**). Both the ADC and diameter had moderate positive correlations with nT2 in patients with CIDP ($|r_s| = 0.51–0.61$; $p < 0.05$) and corresponding weak positive or no correlations in controls (**Table 4**). There was a moderate negative correlation between FA and ADC ($|r_s| = 0.40–0.50$; $p < 0.01$) and a weak positive correlation between diameter and ADC both in patients with CIDP and controls ($|r_s| = 0.35–0.38$; $p < 0.01$). CR had a weak correlation with nT2 and no significant correlation with other parameters in patients with CIDP and controls (**Table 4**).

Correlations Between Clinical and MR Parameters

There was a moderate negative correlation between FA value with the course duration in the CIDP patients ($r_s = -0.404$, $p < 0.05$; **Table 5**). There was, however, no significant correlation between the I-RODS scores and MR multiparameters.

Inter- and Intra-Observer Performance

There were good inter- and intra-observer consistencies for each parameter assessed in the individual nerve roots. The ranges of the intraclass correlation coefficients (inter- and intra-observer) were 0.823–0.934 for the diameter in C5–C8, L4–S1, sciatic, and femoral nerve roots and 0.781–0.873 for CR, 0.792–0.853 for nT2, 0.732–0.859 for FA, and 0.729–0.823 for ADC in C5–C8 and L4–S1 nerve roots, respectively.

DISCUSSION

We here present a novel multiparametric MR imaging paradigm that allows the simultaneous quantifications of the architectural configuration and microstructural properties in the brachial and LS plexus. Our data not only confirmed the findings that the diameter, nT2, and ADC of nerve roots are increased while FA is reduced in CIDP patients but also helped to analyze the diagnostic performance separately and in combination. FA of the LS plexus possessed the highest sensitivity and accuracy, while CR had the highest specificity in the single-parameter model. Furthermore, the combination of FA and CR had the best diagnostic efficiency. Nonetheless, our results do not considerably differ to those by Breckwoldt et al. (2015) who suggested that FA combined with nT2 had the highest diagnostic efficiency in peripheral polyneuropathy. This discrepancy may be due to the fact that contrast enhancement has not been incorporated, and

TABLE 1 | Clinical characteristics¹.

	CIDP	Control	<i>p</i> value
Total number	37	37	<i>n/a</i>
Age (years)	51 (19–71)	50 (20–69)	0.832
Weight (kg)	62.4 (16.5)	65.3 (12.3)	0.478
Height (cm)	168.1 (16.9)	165.4 (15.4)	0.380
Gender (male/female)	26/11	26/11	<i>n/a</i>
The period ^a (Months)	18 (7, 36)	<i>n/a</i>	<i>n/a</i>
Dominant involved extremities (L/U/L&U)	16/7/14	<i>n/a</i>	<i>n/a</i>
Treatment (S/IVIG)	8/5	<i>n/a</i>	<i>n/a</i>
Treatment duration	7 (8), <i>n</i> = 10	<i>n/a</i>	<i>n/a</i>
I-RODS score	35.5 (13.5)	<i>n/a</i>	<i>n/a</i>

¹CIDP, chronic inflammatory demyelinating polyneuropathy; I-RODS, Rasch-built Overall Disability Scale; U, upper limbs; L, lower limbs; S, steroids; *n/a*, not available. The numbers in parentheses indicate the interquartile range. ^aThe period between the onset of initial symptoms and the confirmed diagnosis (*M*).

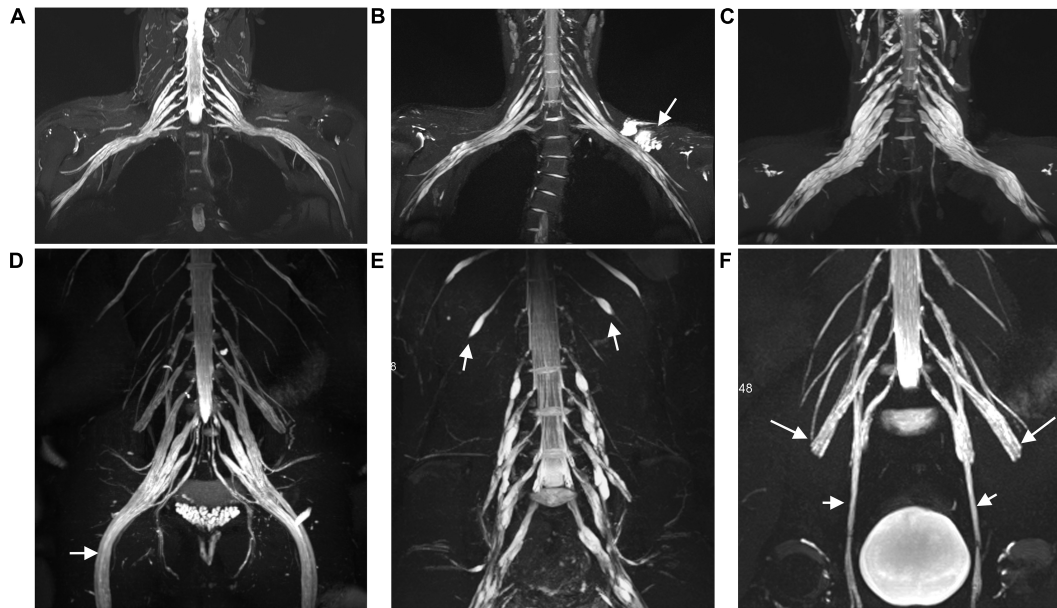


FIGURE 1 | Representative coronal MIP images (SPACE) show diffuse uniform and multifocal fusiform hypertrophy of the brachial (**A–C**) and lumbosacral (**D–F**) plexus in patients with CIDP. The sciatic (arrow in **D**), intercostal (arrow in **E**), femoral (long arrows in **F**), and obturator nerve (arrows in **F**) involvements present diffuse symmetrical hypertrophy. A patient with a 7-year disease course showing uniform thickening in the brachial plexus (**B**), but multifocal fusiform hypertrophy in the lumbosacral plexus (**E**). The lesion with a long T2 signal on the left side represents a subcutaneous hemangioma (arrow in **B**). Image (**C**) shows multifocal fusiform hypertrophy with striking increased T2 signal intensity in the brachial plexus.

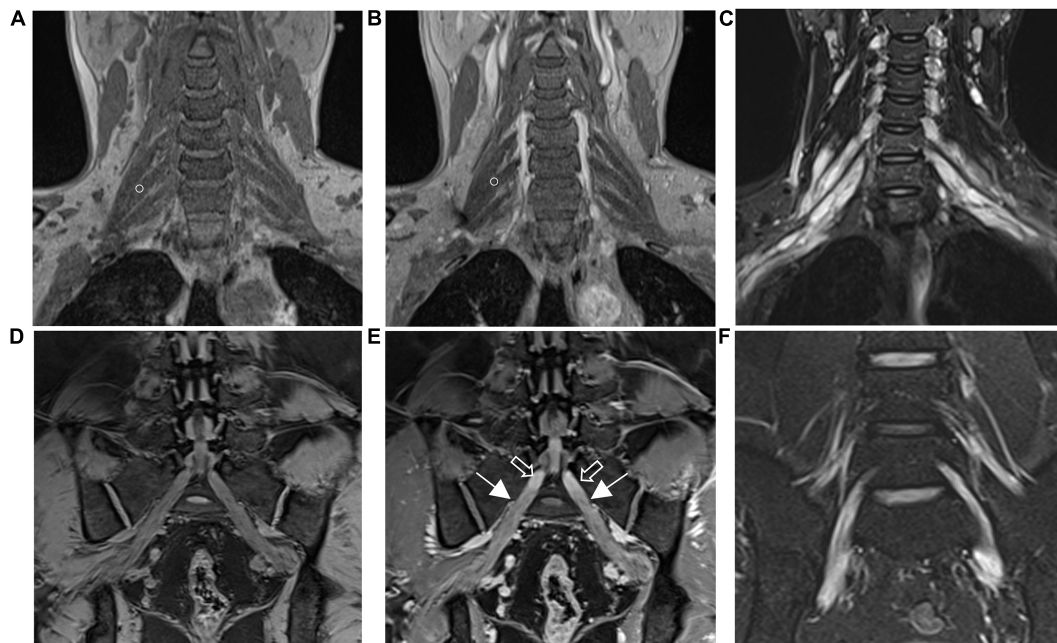


FIGURE 2 | The brachial (**A,B**) and lumbosacral (**D,E**) plexus on non-contrast-enhanced volumetric interpolated breath-hold examination (VIBE) (**A,D**) and contrast-enhanced VIBE sequences (**B,E**), respectively. Images show the right C7 nerve root with absence of enhancement (circles in **A,B**). Bilateral S1 nerve roots demonstrate obviously enhanced (arrows in **E**) and vividly enhancing ganglia (hollow arrows in **E**). Images on turbo inversion recovery magnitude (TIRM) show a striking increased T2 signal intensity in the brachial (**C**) and lumbosacral (**F**) plexus. The CR, ce nSNR/non-ce nSNR; SNR, nerve signal intensity/background noise; ce, contrast-enhanced; nT2, nerve root T2 signal intensity/adjacent muscle T2 signal intensity.

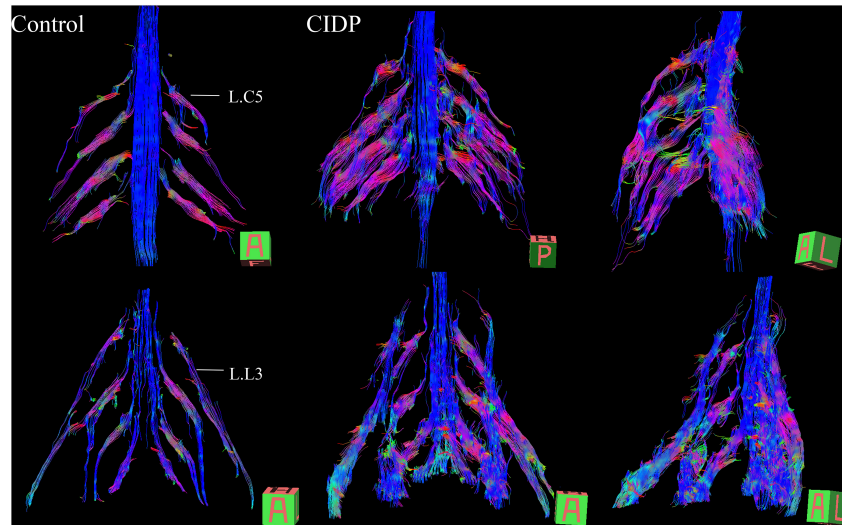


FIGURE 3 | Diffusion tensor tractography (DTT) of healthy control and CIDP patients shows the bundles of plexus nerve fiber and their branches in three-dimensional views. Tractography shows thickened, partially discontinuous, and distorted fiber tracts of the brachial and lumbosacral plexus and their branches in patients with CIDP. A, anterior view; P, posterior view; A–L, left-frontal oblique view. The main dominant direction of diffusion is color-coded (blue: z-axis = nerve course; red: x-axis (left/right); green: y-axis (up/down)).

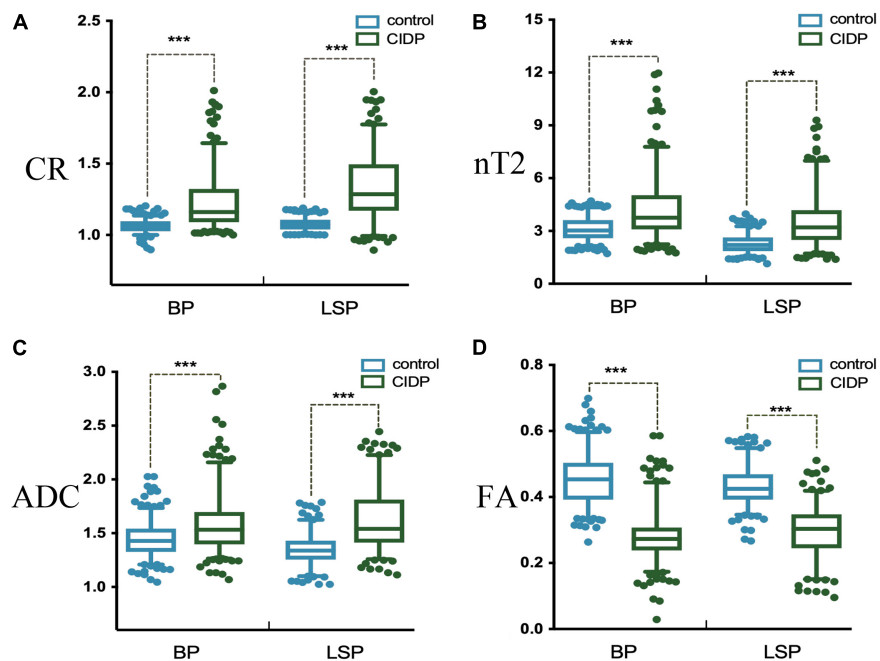


FIGURE 4 | Contrast-enhanced ratio (A), nerve-to-muscle T2 signal intensity ratio (B), and apparent diffusion coefficient (C) of the brachial and lumbosacral nerve roots were significantly higher in patients with CIDP than in controls. Fractional anisotropy (D) of the brachial and lumbosacral nerve roots was significantly lower in patients with CIDP than in controls. * $p < 0.05$; *** $p < 0.001$; BP, brachial plexus; LSP, lumbosacral plexus.

the enrolment of patients with various etiologies probably was not the representative of CIDP entity.

Several previous studies have described the diffuse swelling and high signal intensity on T2-weighted images in nerve trunks and plexus (Goedee et al., 2017; Hiwatashi et al., 2017; Jomier et al., 2020). We observed that brachial, LS

plexus, and their branches showed uniform symmetrical or multifocal fusiform thickening in patients with CIDP. Our findings confirmed that quantitative analysis performs better compared to qualitative description. Hypertrophy of the nerves can be attributed to the inflammatory infiltrate and onion-bulb formation due to repeated demyelination and remyelination

TABLE 2 | Multiparameters for brachial and LS plexi².

		CR	nT2	FA	ADC
BP	CIDP	1.16 (0.23)	3.75 (1.94)	0.273 (0.09)	1.533 (0.302)
	Control	1.06 (0.07)	3.06 (1.03)	0.454 (0.112)	1.339 (0.289)
LSP	CIDP	1.29 (0.32)	3.21 (1.68)	0.303 (0.103)	1.541 (0.400)
	Control	1.07 (0.07)	2.20 (0.78)	0.425 (0.044)	1.339 (0.177)

²BP, brachial plexus; LSP, lumbosacral plexus; CIDP, chronic inflammatory demyelinating polyneuropathy; CR, contrast-enhanced ratio; nT2, nerve-to muscle T2 signal intensity ratio; FA, fractional anisotropy. The numbers in parentheses indicate the interquartile range.

TABLE 3 | ROC curve analysis on single-parameter model³.

		D	nT2	CR	ADC	FA
AUC	BP	0.729	0.712	0.706	0.659	0.872
	LSP	0.854	0.797	0.841	0.801	0.925
Sensitivity (%)	BP	51.3	45.4	46.5	39.9	77.5
	LSP	71.6	66.7	72.5	68.6	80.9
Specificity (%)	BP	90.5	89.0	93.3	87.5	85.0
	LSP	87.7	81.4	96.1	77.9	92.2
Youden's index	BP	0.418	0.344	0.428	0.274	0.625
	LSP	0.593	0.481	0.686	0.465	0.731

³D, diameter; nT2, nerve-to muscle T2 signal intensity ratio; CR, contrast-enhanced ratio; FA, fractional anisotropy; BP, brachial plexus; LSP, lumbosacral plexus.

(Ginsberg et al., 2004). Our study provides proof for a moderate correlation of nerve diameters and nT2/DTI parameters in our cohort, which support this hypothesis. Once an onion-bulb hypertrophy has been formed, it is rarely resorbed by treatment.

The reported increased T2 signal in CIDP is plausible given the pathologic processes with the interstitial edema, increased myelin membranes, or macromolecules by remyelination (Piccione et al., 2016; Rajabally et al., 2017). It is suggested that nT2 may be helpful for the inflammatory neuropathy prognosis evaluation in longitudinal studies, as it is sensitive to the intra-neural water content (Kronlage et al., 2017a). By the use of a CIDP model, non-obese diabetic mice, it was demonstrated that nT2 could be used

as a marker for monitoring the response to treatment (Meyer Zu Horste et al., 2016), and that more clinical studies are needed.

It is generally acknowledged that the DTI is a non-invasive functional MR for peripheral nerve, which depicts the microstructural integrity of neural tissue (Kronlage et al., 2017b). Previous studies have exclusively reported DTI parameter alterations in the limb nerves in patients with CIDP (Kakuda et al., 2011; Lichtenstein et al., 2018); our study assesses the diagnostic accuracy of DTI with tractography in the brachial and LS plexus, which complements with the literature. A previous study found that abnormalities are present in both the proximal

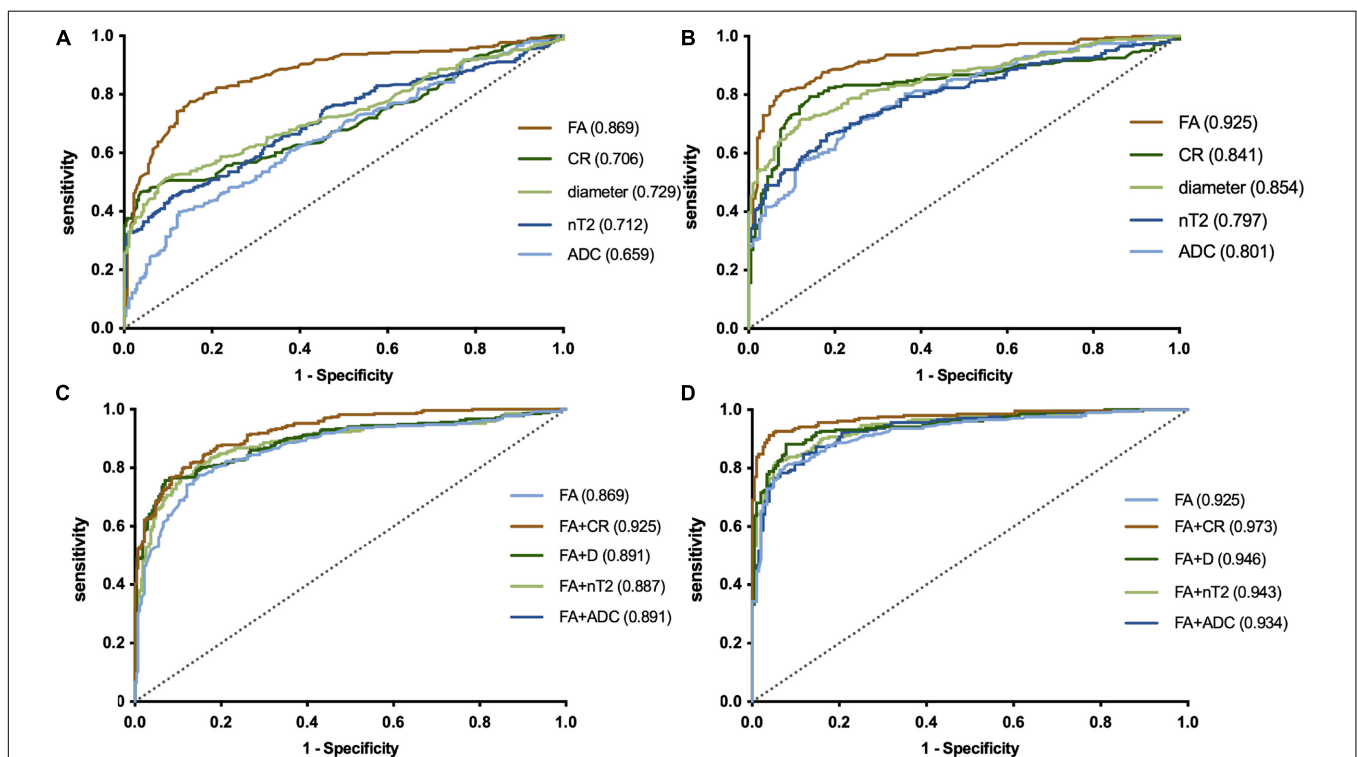


FIGURE 5 | ROC plots revealing the performance of a single-parameter model in the plexus (A, brachial plexus; B, LS plexus) and the combined model in the plexus (C, brachial plexus; D, LS plexus). The largest AUC was 0.925, using the cutoff value of 0.361 for the fractional anisotropy (FA) of the LS plexus in a single-parameter model (B). The combined analysis demonstrated that the combination of FA and the contrast-enhanced ratio has the largest AUC (0.973) in the LS plexus (B). LS, lumbosacral. The numbers in parentheses indicate the respective AUC values.

and distal nerves, and the demyelination is more pronounced proximally than distally (Markvardsen et al., 2016; Lehmann et al., 2019). Some researchers also suggested that the exploration of proximal nerve segments can be particularly useful in diseases with multifocal demyelinating lesions such as CIDP (Hughes et al., 2001; Vallat et al., 2010). Therefore, DTI has become important in the assessment of proximal nerve segments that cannot be evaluated by standard electrophysiological methods or ultrasound (Kakuda et al., 2011). Of note is that the FA threshold of the CIDP patients should be lower than that of healthy subjects in tractography. When below the threshold (we set the FA value to 0.1), fiber tracking will be interrupted.

Brachial EPI-based DTI is susceptible to respiratory motion artifacts. The optimal cutoff value in our cohort was 0.36 for an average FA of the nerve roots, which is lower than the one given by Markvardsen et al. (2016) who defined a cutoff value of 0.45 of the sciatic nerve to identify CIDP. This could be that the measurements are depending on not only the nerves but also the segments and the sequence parameters. Previous studies have reported that FA gradually decreased with increasing age (Guggenberger et al., 2012). To avoid this potential age-related confounder, we included age-matched controls.

The blood–nerve barrier (BNB) defines the intra-neural microenvironment of the peripheral nervous system. These tight junctions, especially the innermost casing connections, provide a barrier to the diffusion of various tracers with larger molecular weight, such as contrast agents (Olsson and Reese, 1971). In the peripheral nerves of CIDP patients, increased permeability of the BNB appears to be the cause of spinal roots and cauda equina enhancement. Early studies have indicated a decreased number of tight-junction proteins claudin 5 and ZO-1 in the sural nerve biopsy specimens of CIDP patients (Kanda et al., 2004; Vallat et al., 2010). These findings may suggest that BNB not only has increased permeability but also has been damaged. Gadolinium enhancement has been detected in some, but not all, cases in inflammatory demyelinating neuropathies (Duggins et al., 1999; Tsuchiya et al., 2007). We reported the utility of contrast enhancement to quantify the alteration of the BNB permeability in the plexus. Our results suggest that the CR has the advantage of high specificity, but with relatively poor sensitivity. At present, there is no consensus that the enhancement indicates disease activity in researches (Kuwabara et al., 1997; Albulaihe et al., 2016; Decard et al., 2018). CR is likely to be a potential non-invasive repeatable MR biomarker for detecting and monitoring disease activity, which needs to be further worked on.

In our result, the diameter and nT2 had a moderate negative correlation with FA, and the diameter and ADC had a moderate positive correlation with nT2 in CIDP but had a corresponding weak or no correlation in controls. These results can be attributed to the pathophysiological basis of inflammatory cell infiltration, interstitial edema, repeated demyelination, and remyelination, which are reflected by multiple parameters. The moderate positive correlation of ADC with nT2 could be due to the relatively high *b*-value chosen in this study (T2 shine-through effect due to low SNR in b 900). CR only had a weak correlation with nT2 and no correlation with other parameters, likely

suggesting a representation of specific pathophysiological changes that would serve as a complementary MR biomarker to DTI.

Duration of disease showed a significantly negative correlation with mean FA. This indicates that the FA reflects the severity of nerve injury with disease duration to some extent. A few studies have suggested a negative association between FA and clinical outcome, including Inflammatory Neuropathy Cause and Treatment (INCAT) and Neuropathy Impairment Score (NIS) (Mathys et al., 2013; Markvardsen et al., 2016). However, we found no clear correlation between I-RODS with any MR parameters, which may require more trials with larger samples.

Limitations

Our study has several limitations. First, we did not directly correlate CR with disease activity, because it is difficult to obtain histologic results in all patients in our hospital. Second, some of the patients in our cohort have received therapy (steroids or IVIG) which may underestimate the diagnostic efficiency of MR examination; however, our result was still

TABLE 4 | Spearman correlation coefficients among multiparameters⁴.

		FA&D	FA&nT2	FA&CR	FA&ADC	CR&nT2
<i>r</i> 's (BP)	CIDP	−0.435**	−0.412**	0.183	−0.454**	0.216**
	Control	−0.166**	−0.119*	−0.066	−0.403**	0.111*
<i>r</i> 's (LSP)	CIDP	−0.520**	−0.455***	0.085	−0.498***	0.156*
	Control	−0.002	−0.051	0.021	−0.412**	0.162*
		nT2&ADC	D&nT2	CR&ADC	CR&D	D&ADC
<i>r</i> 's (BP)	CIDP	0.511**	0.578**	−0.135	−0.176	0.377**
	Control	0.215**	0.119*	−0.089	−0.201	0.348**
<i>r</i> 's (LSP)	CIDP	0.605**	0.509**	−0.109	0.077	0.362***
	Control	0.099	0.040	0.010	−0.064	0.358**

⁴*r*'s, Spearman correlation coefficient; BP, brachial plexus; LSP, lumbosacral plexus; FA, fractional anisotropy; CR, contrast-enhanced ratio; nT2, nerve-to muscle T2 signal intensity ratio; D, diameter; CIDP, chronic inflammatory demyelinating polyneuropathy; **p* < 0.05; ***p* < 0.01; ****p* < 0.001.

TABLE 5 | Correlations between clinical and MR parameters⁵.

	Duration		I-RODS	
	<i>r</i> 's	<i>p</i> #	<i>r</i> 's	<i>p</i> #
D	0.214	0.233	0.019	0.912
nT2	0.049	0.785	0.169	0.347
CR	−0.020	0.910	−0.151	0.404
FA	−0.406	0.016*	−0.066	0.716
ADC	0.124	0.480	−0.173	0.339

⁵#, Age- and sex-adjusted. *r*'s, Spearman correlation coefficient; *p*, *p* value; I-RODS, inflammatory Rasch-built overall disability scale; D, diameter; nT2, nerve-to muscle T2 signal intensity ratio; CR, contrast-enhanced ratio; FA, fractional anisotropy. MR parameters defined as the mean of brachial (bilateral C5–C8), lumbosacral (bilateral L4–S1) nerve roots. **p* < 0.05.

satisfactory. Moreover, it is hard to know whether prior drug treatment yet has any influence on the current state of this rare disease, which is mostly characterized by chronic progressive and relapsing courses. Third, quantitative or semiquantitative parameters, such as CR and nT2, would be influenced to some extent by sequence/scanner type/field strength, etc., so this needs to be interpreted with caution. The fourth is the lack of disease controls and patients with mimics of CIDP such as other chronic demyelination peripheral neuropathies, which limits the diagnostic specificity. The need persists for a differential diagnosis that distinguishes patients with CIDP or some of the diseases also harbor a similar clinical presentation and/or morphologic abnormalities.

CONCLUSION

In conclusion, we present a novel multiparametric MRI protocol that allows non-invasive quantification of the brachial and LS plexus nerve abnormality in CIDP patients. 3D SPACE with high-resolution MR neurography, combined with DTI and contrast enhancement, is a recommended composite protocol in diagnosis and management of CIDP.

DATA AVAILABILITY STATEMENT

The raw data supporting the conclusions of this article will be made available by the authors, without undue reservation.

REFERENCES

- Alabdali, M., Abraham, A., Alsulaiman, A., Breiner, A., Barnett, C., Katzberg, H. D., et al. (2017). Clinical characteristics, and impairment and disability scale scores for different CIDP disease activity status classes. *J. Neurol. Sci.* 372, 223–227. doi: 10.1016/j.jns.2016.11.056
- Albulaihe, H., Alabdali, M., Alsulaiman, A., Abraham, A., Breiner, A., Barnett, C., et al. (2016). Disease activity in chronic inflammatory demyelinating polyneuropathy. *J. Neurol. Sci.* 369, 204–209.
- Breckwoldt, M. O., Stock, C., Xia, A., Heckel, A., Bendszus, M., Pham, M., et al. (2015). Diffusion tensor imaging adds diagnostic accuracy in magnetic resonance neurography. *Invest. Radiol.* 50, 498–504. doi: 10.1097/rli.0000000000000156
- Decard, B. F., Pham, M., and Grimm, A. (2018). Ultrasound and MRI of nerves for monitoring disease activity and treatment effects in chronic dysimmune neuropathies – Current concepts and future directions. *Clin. Neurophysiol.* 129, 155–167. doi: 10.1016/j.clinph.2017.10.028
- Duggins, A. J., Mcleod, J. G., Pollard, J. D., Davies, L., Yang, F., Thompson, E. O., et al. (1999). Spinal root and plexus hypertrophy in chronic inflammatory demyelinating polyneuropathy. *Brain* 122, 1383–1390. doi: 10.1093/brain/122.7.1383
- Ginsberg, L., Malik, O., Kenton, A. R., Sharp, D., Muddle, J. R., Davis, M. B., et al. (2004). Coexistent hereditary and inflammatory neuropathy. *Brain* 127, 193–202. doi: 10.1093/brain/awh017
- Goedee, H. S., Jongbloed, B. A., Van Asseldonk, J. H., Hendrikse, J., Vrancken, A., Franssen, H., et al. (2017). A comparative study of brachial plexus sonography and magnetic resonance imaging in chronic inflammatory demyelinating neuropathy and multifocal motor neuropathy. *Eur. J. Neurol.* 24, 1307–1313. doi: 10.1111/ene.13380

ETHICS STATEMENT

The studies involving human participants were reviewed and approved by the present prospective study was approved by the Ethics Committee of Tongji Medical College, Huazhong University of Science and Technology (No. IORG0003571). The patients/participants provided their written informed consent to participate in this study.

AUTHOR CONTRIBUTIONS

CZ, XS, and XK conceived and designed. XS and JW analyzed the data. XS, CZ, ZL, and OA manuscript preparation. HZ and XK contributed reagents, materials, and analysis tools. All authors contributed to the article and approved the submitted version.

FUNDING

This work was supported by the National Natural Science Foundation of China (Grant Nos. 81470076 and 81701653).

SUPPLEMENTARY MATERIAL

The Supplementary Material for this article can be found online at: <https://www.frontiersin.org/articles/10.3389/fnins.2021.649071/full#supplementary-material>

- Guggenberger, R., Markovic, D., Eppenberger, P., Chhabra, A., Schiller, A., Nanz, D., et al. (2012). Assessment of median nerve with MR neurography by using diffusion-tensor imaging: normative and pathologic diffusion values. *Radiology* 265, 194–203. doi: 10.1148/radiol.12111403
- Hiwatashi, A., Togao, O., Yamashita, K., Kikuchi, K., Ogata, H., Yamasaki, R., et al. (2017). Evaluation of chronic inflammatory demyelinating polyneuropathy: 3D nerve-sheath signal increased with inked rest-tissue rapid acquisition of relaxation enhancement imaging (3D SHINKEI). *Eur. Radiol.* 27, 447–453. doi: 10.1007/s00330-016-4406-3
- Hughes, R., Bensa, S., Willison, H., Van Den Bergh, P., Comi, G., Illa, I., et al. (2001). Randomized controlled trial of intravenous immunoglobulin versus oral prednisolone in chronic inflammatory demyelinating polyradiculoneuropathy. *Ann. Neurol.* 50, 195–201. doi: 10.1002/ana.1088
- Iijima, M., Koike, H., Hattori, N., Tamakoshi, A., Katsuno, M., Tanaka, F., et al. (2008). Prevalence and incidence rates of chronic inflammatory demyelinating polyneuropathy in the Japanese population. *J. Neurol. Neurosurg. Psychiatry* 79, 1040–1043. doi: 10.1136/jnnp.2007.128132
- Jomier, F., Bousson, V., Viala, K., Pereon, Y., Magot, A., Cauquil, C., et al. (2020). Prospective study of the additional benefit of plexus magnetic resonance imaging in the diagnosis of chronic inflammatory demyelinating polyneuropathy. *Eur. J. Neurol.* 27, 181–187. doi: 10.1111/ene.14053
- Kakuda, T., Fukuda, H., Tanitame, K., Takasu, M., Date, S., Ochi, K., et al. (2011). Diffusion tensor imaging of peripheral nerve in patients with chronic inflammatory demyelinating polyradiculoneuropathy: a feasibility study. *Neuroradiology* 53, 955–960. doi: 10.1007/s00234-010-0833-z
- Kanda, T., Numata, Y., and Mizusawa, H. (2004). Chronic inflammatory demyelinating polyneuropathy: decreased claudin-5 and relocated ZO-1. *J. Neurol. Neurosurg. Psychiatry* 75, 765–769. doi: 10.1136/jnnp.2003.025692

- Kronlage, M., Baumer, P., Pitarokoili, K., Schwarz, D., Schwehr, V., Godel, T., et al. (2017a). Large coverage MR neurography in CIDP: diagnostic accuracy and electrophysiological correlation. *J. Neurol.* 264, 1434–1443. doi: 10.1007/s00415-017-8543-7
- Kronlage, M., Pitarokoili, K., Schwarz, D., Godel, T., Heiland, S., Yoon, M. S., et al. (2017b). Diffusion tensor imaging in chronic inflammatory demyelinating polyneuropathy: diagnostic accuracy and correlation with electrophysiology. *Invest. Radiol.* 52, 701–707. doi: 10.1097/rli.0000000000000394
- Kuwabara, S., Nakajima, M., Matsuda, S., and Hattori, T. (1997). Magnetic resonance imaging at the demyelinating foci in chronic inflammatory demyelinating polyneuropathy. *Neurology* 48, 874–877. doi: 10.1212/wnl.48.4.874
- Latov, N. (2014). Diagnosis and treatment of chronic acquired demyelinating polyneuropathies. *Nat. Rev. Neurol.* 10, 435–446. doi: 10.1038/nrneurol.2014.117
- Lehmann, H. C., Burke, D., and Kuwabara, S. (2019). Chronic inflammatory demyelinating polyneuropathy: update on diagnosis, immunopathogenesis and treatment. *J. Neurol. Neurosurg. Psychiatry* 90, 981–987. doi: 10.1136/jnnp-2019-320314
- Lichtenstein, T., Sprenger, A., Weiss, K., Slobocki, K., Cervantes, B., Karampinos, D., et al. (2018). MRI biomarkers of proximal nerve injury in CIDP. *Ann. Clin. Transl. Neurol.* 5, 19–28. doi: 10.1002/acn3.502
- Markvardsen, L. H., Vaeggemose, M., Ringgaard, S., and Andersen, H. (2016). Diffusion tensor imaging can be used to detect lesions in peripheral nerves in patients with chronic inflammatory demyelinating polyneuropathy treated with subcutaneous immunoglobulin. *Neuroradiology* 58, 745–752. doi: 10.1007/s00234-016-1692-z
- Mathys, C., Aissa, J., Meyer Zu Horste, G., Reichelt, D. C., Antoch, G., Turowski, B., et al. (2013). Peripheral neuropathy: assessment of proximal nerve integrity by diffusion tensor imaging. *Muscle Nerve* 48, 889–896. doi: 10.1002/mus.23855
- Meyer Zu Horste, G., Cordes, S., Pfaff, J., Mathys, C., Mausberg, A. K., Bendszus, M., et al. (2016). Predicting the response to intravenous immunoglobulins in an animal model of chronic neuritis. *PLoS One* 11:e0164099. doi: 10.1371/journal.pone.0164099
- Olsson, Y., and Reese, T. S. (1971). Permeability of vasa nervorum and perineurium in mouse sciatic nerve studied by fluorescence and electron microscopy. *J. Neuropathol. Exp. Neurol.* 30, 105–119. doi: 10.1097/00005072-197101000-00011
- Piccione, E. A., Engelstad, J., Dyck, P. J., Mauermann, M. L., Dispenzieri, A., and Dyck, P. J. (2016). Nerve pathologic features differentiate POEMS syndrome from CIDP. *Acta Neuropathol. Commun.* 4:116.
- Querol, L., Devaux, J., Rojas-Garcia, R., and Illa, I. (2017). Autoantibodies in chronic inflammatory neuropathies: diagnostic and therapeutic implications. *Nat. Rev. Neurol.* 13, 533–547. doi: 10.1038/nrneurol.2017.84
- Rajabally, Y. A., Stettner, M., Kieseier, B. C., Hartung, H.-P., and Malik, R. A. (2017). CIDP and other inflammatory neuropathies in diabetes — diagnosis and management. *Nat. Rev. Neurol.* 13, 599–611. doi: 10.1038/nrneurol.2017.123
- Rotta, F. T., Sussman, A. T., Bradley, W. G., Ram Ayyar, D., Sharma, K. R., and Shebert, R. T. (2000). The spectrum of chronic inflammatory demyelinating polyneuropathy. *J. Neurol. Sci.* 173, 129–139.
- Takahara, T., Hendrikse, J., Yamashita, T., Mali, W. P., Kwee, T. C., Imai, Y., et al. (2008). Diffusion-weighted MR neurography of the brachial plexus: feasibility study. *Radiology* 249, 653–660. doi: 10.1148/radiol.2492071826
- Tsuchiya, K., Imai, M., Tateishi, H., Nitatori, T., Fujikawa, A., and Takemoto, S. (2007). Neurography of the spinal nerve roots by diffusion tensor scanning applying motion-probing gradients in six directions. *Magn. Reson. Med. Sci.* 6, 1–5. doi: 10.2463/mrms.6.1
- Vallat, J. M., Sommer, C., and Magy, L. (2010). Chronic inflammatory demyelinating polyradiculoneuropathy: diagnostic and therapeutic challenges for a treatable condition. *Lancet Neurol.* 9, 402–412. doi: 10.1016/s1474-4422(10)70041-7
- Van den Bergh, P. Y., Hadden, R. D., Bouche, P., Cornblath, D. R., Hahn, A., Illa, I., et al. (2010). European Federation of Neurological Societies/Peripheral Nerve Society guideline on management of chronic inflammatory demyelinating polyradiculoneuropathy: report of a joint task force of the European federation of neurological societies and the peripheral nerve society – first revision. *Eur. J. Neurol.* 17, 356–363. doi: 10.1111/j.1468-1331.2009.02930.x
- Yoshida, T., Sueyoshi, T., Suwazono, S., and Suehara, M. (2015). Three-tesla magnetic resonance neurography of the brachial plexus in cervical radiculopathy. *Muscle Nerve* 52, 392–396. doi: 10.1002/mus.24560

Conflict of Interest: HZ was employed by the company Siemens Healthineers, Shanghai, China.

The remaining authors declare that the research was conducted in the absence of any commercial or financial relationships that could be construed as a potential conflict of interest.

Publisher's Note: All claims expressed in this article are solely those of the authors and do not necessarily represent those of their affiliated organizations, or those of the publisher, the editors and the reviewers. Any product that may be evaluated in this article, or claim that may be made by its manufacturer, is not guaranteed or endorsed by the publisher.

Copyright © 2021 Su, Kong, Alwalid, Wang, Zhang, Lu and Zheng. This is an open-access article distributed under the terms of the Creative Commons Attribution License (CC BY). The use, distribution or reproduction in other forums is permitted, provided the original author(s) and the copyright owner(s) are credited and that the original publication in this journal is cited, in accordance with accepted academic practice. No use, distribution or reproduction is permitted which does not comply with these terms.



MRI DTI and PDFF as Biomarkers for Lower Motor Neuron Degeneration in ALS

Thorsten Lichtenstein^{1*}, Alina Sprenger², Kilian Weiss^{1,3}, Nils Große Hokamp¹, David Maintz¹, Marc Schlamann¹, Gereon R. Fink^{2,4}, Helmar C. Lehmann² and Tobias D. Henning⁵

¹ Institute for Diagnostic and Interventional Radiology, Faculty of Medicine and University Hospital Cologne, University of Cologne, Cologne, Germany, ² Department of Neurology, University Hospital of Cologne, University of Cologne, Cologne, Germany, ³ Philips Healthcare, Hamburg, Germany, ⁴ Cognitive Neuroscience, Institute of Neuroscience and Medicine (INM-3), Research Centre Jülich, Jülich, Germany, ⁵ Department of Neuroradiology, Center Hospital Luxembourg, Luxembourg City, Luxembourg

OPEN ACCESS

Edited by:

Felix Tobias Kurz,
Heidelberg University Hospital,
Germany

Reviewed by:

Johann M. E. Jende,
Heidelberg University Hospital,
Germany
Swati Rane,
University of Washington,
United States

*Correspondence:

Thorsten Lichtenstein
thorsten.lichtenstein@uk-koeln.de

Specialty section:

This article was submitted to
Brain Imaging Methods,
a section of the journal
Frontiers in Neuroscience

Received: 17 March 2021

Accepted: 26 July 2021

Published: 26 August 2021

Citation:

Lichtenstein T, Sprenger A, Weiss K, Große Hokamp N, Maintz D, Schlamann M, Fink GR, Lehmann HC and Henning TD (2021) MRI DTI and PDFF as Biomarkers for Lower Motor Neuron Degeneration in ALS. *Front. Neurosci.* 15:682126. doi: 10.3389/fnins.2021.682126

Objective: To evaluate the utility of nerve magnetic resonance imaging (MRI), diffusion tensor imaging (DTI), and muscle MRI multi-echo Dixon for assessing lower motor neuron (LMN) degeneration in amyotrophic lateral sclerosis (ALS).

Methods: In this prospective observational cohort study, 14 patients with ALS and 13 healthy controls underwent a multiparametric MRI protocol, including DTI of the sciatic nerve and assessment of muscle proton density fat fraction of the biceps femoris and the quadriceps femoris muscles by a multi-echo Dixon sequence.

Results: In ALS patients, mean fractional anisotropy values of the sciatic nerve were significantly lower than those of healthy controls. The quadriceps femoris, but not the biceps femoris muscle, showed significantly higher intramuscular fat fractions in ALS.

Interpretation: Our study provides evidence that multiparametric MRI protocols might help estimate structural nerve damage and neurogenic muscle changes in ALS.

Keywords: amyotrophic lateral sclerosis, diffusion tensor imaging, proton density fat fraction, neurodegeneration, motor neuron disease

INTRODUCTION

Amyotrophic lateral sclerosis (ALS) is a neurodegenerative disease with a variable phenotype that primarily affects the motor system. Differences in phenotype include deviating affection patterns of the upper motor neuron (UMN) or lower motor neuron (LMN) and disease progression differences. This variability causes difficulties in monitoring the course of the disease. Especially when conducting research (e.g., to evaluate new therapies), the lack of sensitive methods to detect short-term changes is one of the critical challenges (Turner et al., 2009; Berry and Cudkowicz, 2011; Simon et al., 2015). Since damage to LMN is decisive for disease progression in ALS (Simon, 2016), it seems particularly promising to detect its degeneration as precisely as possible. So far, disease progression has been monitored using electrophysiological and clinical tests [in particular motor nerve conduction studies (mNCS) and motor unit number estimation (MUNE)] (Carvalho and de Swash, 2016). However, these clinical tests suffer from several limitations. For example, they depend on UMN function and the patient's overall clinical condition (Simon et al., 2014).

Magnetic resonance imaging (MRI) has the potential to become a valuable, non-invasive biomarker for neurodegeneration in ALS. Previously, MRI applications to ALS mainly focused on structural alterations of the ALS patients' brain and spinal cord. Numerous studies using diffusion tensor imaging (DTI) demonstrated degeneration of the corticospinal tract and motor-associated brain regions. Most studies demonstrated a decrease of DTI-based fractional anisotropy (FA), a marker for axonal degeneration and demyelinating conditions (Jende et al., 2020, 2021), which indicates an involvement of the UMN (Ellis et al., 1999; Toosy et al., 2003; Iwata et al., 2008; Blain et al., 2009; Metwalli et al., 2010; Cirillo et al., 2012; Bede et al., 2015).

In contrast, data about the MRI's utility to detect LMN degeneration in ALS are sparse (Grolez et al., 2016; Verber et al., 2019). Simon and colleagues recently demonstrated in 19 ALS patients reduced FA in tibial and peroneal nerve segments with subsequent decline at 6-months. These changes correlated with the ALS revised functional rating scale (ALSFRS-R) (Simon et al., 2017).

There is also only limited information about the MRI utility to monitor neurogenic muscle atrophy in ALS. T2-weighted whole-body muscle MRI shows increased relative T2 signal in most limb muscles of ALS patients, as recently reported by Jenkins and colleagues (Jenkins et al., 2018). Clinical and experimental studies indicate that denervated muscles display a reversible high T2 signal as early as 48 h after nerve injury (West et al., 1994; Bendszus et al., 2002). However, these changes are only small and decline with prolonged denervation (Zhang et al., 2008). Human studies also demonstrated that T2 hyperintensity does not correlate well with MR-neurographic parameters (Schwarz et al., 2015).

Recently, Klickovic and colleagues demonstrated in a cohort of 20 ALS patients the feasibility of quantifying muscle fat fraction using the MRI 3-point Dixon technique. They found higher fat fractions in ALS patients' calf muscles compared to controls (3.34 vs. 1.92%), which correlated well with functional scales (Klickovic et al., 2019).

We have established a multiparametric MRI imaging paradigm that allows simultaneous quantification of nerve injury and intramuscular fat fraction in lower limbs (Lichtenstein et al., 2017). Based on DTI scans of nerves and multi-echo Dixon MRI of adjacent muscles, this protocol detects structural nerve damage and neurogenic intramuscular fat accumulation in different neuropathic conditions. We hypothesized that this protocol might also be suitable for monitoring LMN degeneration in ALS and, therefore, conducted this exploratory study in ALS patients.

MATERIALS AND METHODS

Patients and Healthy Controls

Fourteen patients (6 female, 8 male, mean age 62 ± 6 years) with ALS and 13 healthy controls (6 female, 7 male, mean age 56 ± 9 years) participated in this study. All patients were diagnosed at the Department of Neurology, University

Hospital of Cologne, Cologne, Germany, based on the El Escorial Criteria (Ludolph et al., 2015). Patients with neuropathies and contraindications against MRI were excluded. Healthy controls were defined as individuals without anamnestic and clinical signs of polyneuropathy. All patients were on antiepileptic therapy with riluzole (50 mg twice a day). The local Ethics Committee approved the study, and all subjects gave written informed consent before inclusion. All patients received a standard clinical and electrophysiological assessment. The clinical investigation included a complete neurological examination. Besides, the ALSFRS-R was collected for each patient. Briefly, the ALSFRS-R summarizes physical impairment in activities of daily living for a patient with ALS and is used for measuring the progression of the disease (Cedarbaum et al., 1999). It is a revision of the ALSFRS that includes additional questions related to respiratory symptoms. The score includes 12 questions concerning physical functions (e.g., speaking, swallowing, walking) ranging from 0 (severe impairment) to 4 (no impairment) with a maximum score of 40 and a minimum score of 0. For electrophysiological examinations, standard nerve conduction studies were performed. The right tibial and peroneal nerves were used to measure the motor nerve conduction velocity (mNCV), the proximal and distal compound muscle action potential (CMAP), and distal motor latencies (DML). The right sural nerve was used to measure the sensory nerve conduction velocity (sNCV) and the sensory nerve action potential (SNAP). Standard electromyography (EMG) of the tibialis anterior, quadriceps, and biceps femoris muscles was performed using conventional EMG equipment and concentric needle electrodes.

MRI Protocol

All subjects were examined using an MRI protocol already established in patients with chronic inflammatory polyneuropathy for examining the sciatic nerve and the thigh muscles (Lichtenstein et al., 2017; Schneider et al., 2019). The examinations were performed on a 3T whole-body MRI system (Ingenia, Philips Healthcare, Best, Netherlands). As in the other studies, the patients were positioned in a supine position with feet first. The subjects' right thigh was examined deep inside a knee coil (dStream T/R Knee 16ch Coil, Philips Healthcare, Best, Netherlands) so that the coil center was located approx. 5–10 cm above the upper pole of the patella.

Planning Sequence

To delineate the nerve, a special orientation of a SHINKEI-based three-dimensional T2-weighted turbo spin echo (3D T2 TSE) sequence with fat and vascular signal suppression was used (Cervantes et al., 2015; Kasper et al., 2015; Kollmer et al., 2015). The exact parameters were: TR = 2,000, TE = 273, matrix size $216 \times 143 \times 143$, resolution $1.25 \times 1.25 \times 0.7 \text{ mm}^3$, scan duration 2:30 min.

T2-Weighted, mDixon TSE Sequence

The anatomical assessment was performed in a transversal, perpendicular to the sciatic nerve, T2-weighted mDixon TSE (2D T2 TSE) sequence. The parameters were: TR = 2,500 ms, TE = 60 ms, matrix size 640×468 , 30 slices with 4 mm slice

thickness and no interslice gap, resolution $0.3 \times 0.4 \times 4 \text{ mm}^3$, scan duration 5 min.

DTI

A DTI sequence based on single-shot echo-planar imaging was planned in the same way as the 2D T2 TSE. Sequence parameters were: TR = 6500 ms, TE = 62 msec, matrix size 128×130 , 20 layers with 4 mm layer thickness and without kerf, resolution $1.5 \times 1.5 \times 4 \text{ mm}^3$, b -values of 0 s/mm^2 and 800 s/mm^2 , in 20 directions, SENSE factor of 2, scan duration 9:00 min.

PDFF

A third, transversely recorded sequence, i.e., a six-echo multi-echo gradient echo sequence (mDixon Quant, Philips Healthcare, Best, Netherlands) generating proton density fat fraction (PDFF) maps, was similarly used for intramuscular fat quantification of the quadriceps femoris (QFM) and biceps femoris muscles (BFM). The parameters were as follows: TR = 10 ms, 6 echoes (TE1 = 1.45 ms, $\Delta\text{TE} = 1.1 \text{ ms}$), matrix $108 \times 107 \times 4 \text{ mm}^3$, voxel size $1.8 \times 1.8 \times 4 \text{ mm}$, 20 slices, flip angle 3° (to minimize T1 bias effects), recording time 1:05 min.

Data Analysis

A senior radiologist (T.L.) evaluated the MR images. Measurements were validated by a second senior radiologist (N. G. H.) based on independent assessment of a subset of study participants. The post-processing of the DTI raw data and the complete MRI analysis was performed with IntelliSpace Portal (IntelliSpace Portal 10.0, Philips Healthcare, Best, Netherlands).

To analyze the sciatic nerve in the DTI sequence, six subtotal freehand ROIs were drawn in six adjacent layers of color-coded fractional anisotropy images in correlation with the anatomical information of the $b = 0$ and 2D T2 TSE images. The average FA values of the six slices were then remeasured to obtain each subject's final FA value. Fiber tracking of the nerve was performed for illustration.

In the PDFF maps, freehand subtotal ROIs were drawn on the three most proximal slices into each part of the quadriceps femoris muscle (vastus lateralis, intermedius, medialis, rectus femoris) and into the short and long heads of the biceps femoris muscle for determination of the average intramuscular fat fraction. The ROIs were drawn within 2 mm of the muscle boundaries. The differing area sizes (A_i) of the individual ROIs [ROI $_i$ with individual fat fractions (FF $_i$)] were taken into account using the formula $\text{FF_mean_over_ROIs} = \frac{\sum (A_i * \text{FF}_i)}{\sum (A_i)}$, where the sum is the summation over all ROIs.

Statistics

Group comparison and analysis of interrater agreement were performed. For group comparison, analysis was performed using the Mann-Whitney U test. Correlations were assessed by non-parametric Spearman correlation tests. Intraclass correlation coefficients (ICC) were considered indicative of interrater reliability. All tests were performed using dedicated software (Statistics Package for Social Sciences (SPSS), v26, IBM, Armonk, NY, United States and Graph Pad Prism, v7, GraphPad Software, San Diego, CA, United States). A p -value < 0.05 was considered

statistically significant. Statistical analysis of the Graphs depict mean \pm standard error of the mean.

RESULTS

Demographics

There were no significant differences between the two cohorts in terms of the demographic data evaluated [sex, age, weight, body mass index (BMI)]. For a detailed comparison, see **Table 1**.

Clinical Characteristics of ALS Patients

The onset of disease occurred in the upper limbs in 50% of patients, the lower limbs in 28.57%, and the bulbar region in 21.42%. On average, the disease duration at the time of the examination was 4.8 ± 1 months. Mean ALSFRS-R score was 27.1 ± 1.77 .

TSE and DTI MRI Scans

The sciatic nerve was identified in all patients and controls on 3D and 2D T2 TSE MRI scans. DTI scans of the sciatic nerve in ALS patients showed significantly lower mean FA values than healthy controls. Mean values in ALS were 0.40 ± 0.012 ($p = 0.025$) compared to controls (0.44 ± 0.012) (**Figure 1**). Interrater reliability for DTI was excellent (ICC 0.873).

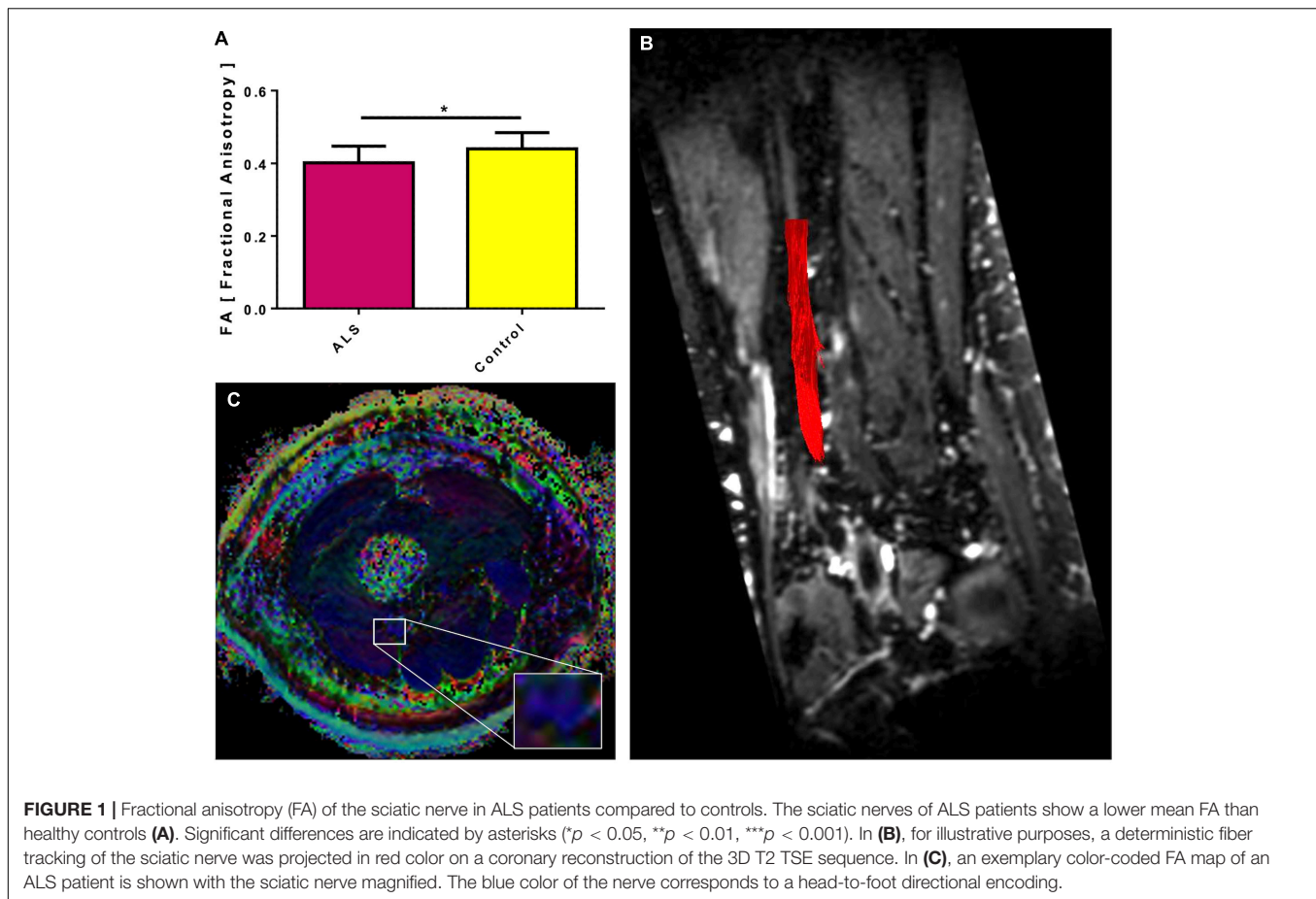
PDFF Mapping

The quadriceps femoris muscle of ALS patients showed significantly higher intramuscular fat fractions than in healthy controls (mean $5.35 \pm 1.2\%$ vs. 2.8 ± 1.67 , $p = 0.038$, **Figure 2A**). Intramuscular fat fractions in the biceps femoris muscle of ALS patients were also higher than in healthy controls, but this difference was not statistically different (mean 7.18 ± 1.24 vs. 5.03 ± 1.58 , $p = 0.155$, **Figure 2B**). ROI sizes were between 14 and 2,133 mm^2 . Even in rather severely affected patients, the increased intramuscular fat fraction of the examined muscles is often hardly recognizable visually compared to healthy controls (**Figure 2C**). Interrater reliability for PDFF mapping was excellent (QFM: ICC 0.983, BFM: ICC 0.984).

No significant correlations were observed between the FA values of the sciatic nerve and ALSFRS-R ($r = 0.12$ $p = 0.20$), the FA values of the sciatic nerve and CMAP amplitude of the tibial and peroneal nerves ($r = 0.2$ and 0.42 , $p = 0.493$ and

TABLE 1 | Clinical data.

	ALS	Controls	p value
Sex (female:male)	6:8	6:7	
Age (years)	62.6 (3.5)	56.9 (2.9)	0.06 (n.s.)
Height (cm)	172 (3.9)	179 (2.5)	0.28 (n.s.)
Weight (kg)	71.3 (4.0)	75.3 (4.68)	0.59 (n.s.)
BMI (cm/kg^2)	24.1 (1.4)	25.4 (2.6)	0.92 (n.s.)
Therapy (Riluzole)	14/14		
Disease duration (years)	0.5 (0.1)		



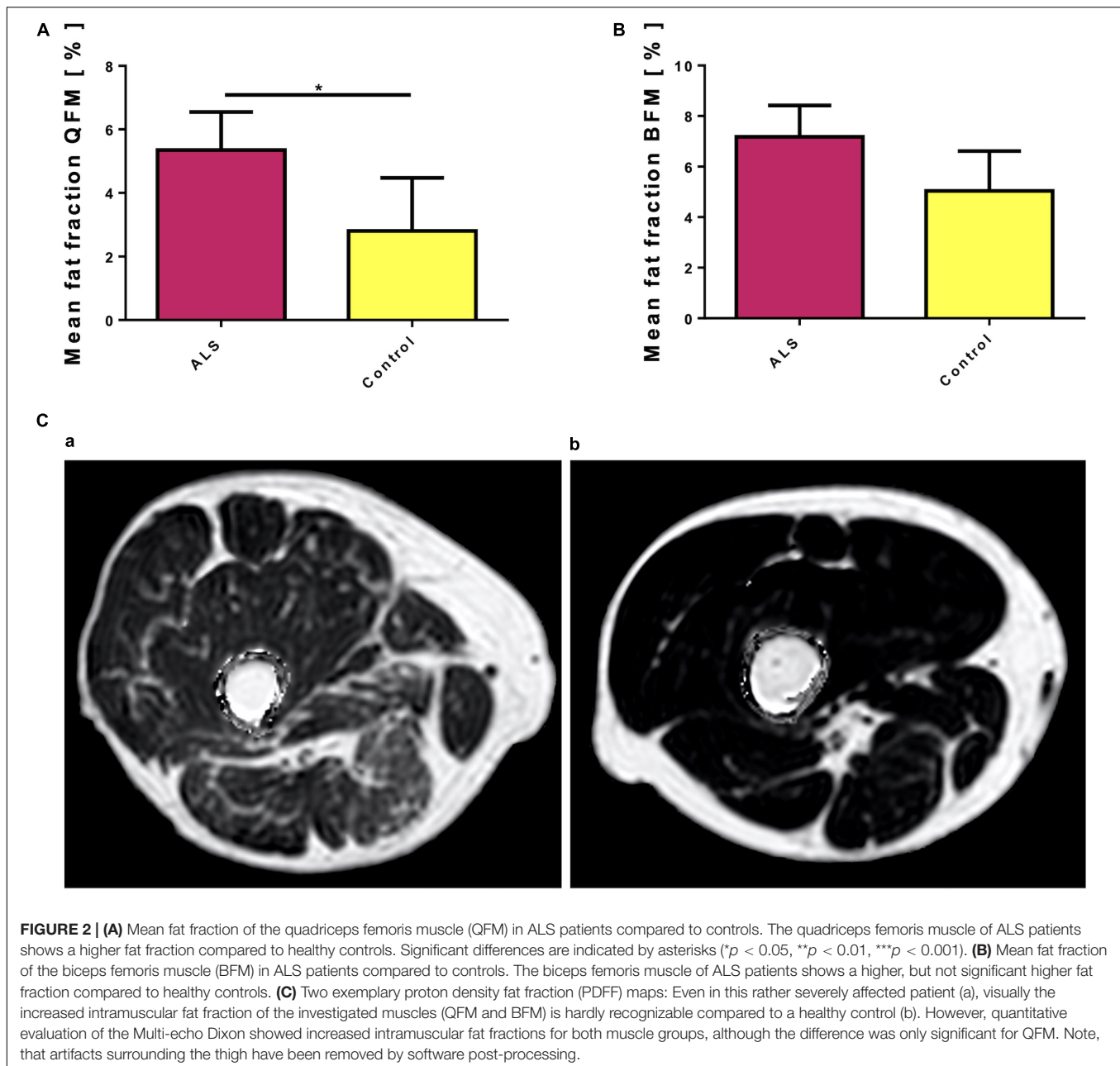
0.228), the FA values of the sciatic nerve and mean fat fraction of the BFM ($r = -0.495$, $p = 0.072$). A significant correlation was found between the FA values and mean fat fraction of the QFM in the ALS group ($r = -0.578$, $p = 0.03$). In the whole study population a significant correlation between FA and QFM as well as BFM could be established ($r = -0.533$, $p = 0.004$, $r = -0.468$, $p = 0.014$). Further correlations were found between QFM and BFM fat fraction all, HC and ALS and the whole study group ($r = 0.753$, $p = 0.003$, $r = 0.807$, $p < 0.001$, $r = 0.835$, $p < 0.001$). For a detailed list of electrophysiological data, see **Table 2**. Correlations between demographic and clinical data and the obtained imaging parameters are provided in **Table 3**.

DISCUSSION

Our exploratory study evaluated the utility of a previously established MRI protocol for monitoring structural nerve damage in the sciatic nerve and intramuscular fat fraction of mid-thigh muscles. Our main findings are that ALS patients' sciatic nerves demonstrate significantly lower FA values than healthy controls, and the thigh muscles in ALS patients accumulate more fat than thigh muscles from healthy controls. Although DTI derived FA in rodent (Takagi et al., 2009; Lehmann et al., 2010; Morisaki et al., 2011) and human peripheral nerves is

considered a valid measure for axonal integrity and can be used to monitor axonal loss and regeneration as well as for demyelinating conditions (Sheikh, 2010; Kakuda et al., 2011; Mathys et al., 2013; Jende et al., 2020, 2021), data about FA values in peripheral nerves of ALS patients are sparse. In line with our findings, Simon and colleagues reported 8–10% lower FA values in the tibial and peroneal nerves in ALS patients than controls. We focused our study on a more proximal nerve segment based on previous experience (Lichtenstein et al., 2017). The sciatic nerve's lower FA values indicate axon loss in our ALS patients, thereby clearly distinguish them from healthy subjects. This finding is remarkable since the clinical data and the ALSFRS-R scores indicate that most patients were primarily affected in their upper extremities and did not show significant lower limb weakness. Our study confirms previous electrophysiologic studies that determined latencies of M- and H-responses in the lower extremity and found (indirect) evidence for proximal sciatic nerve damage (Koutlidis et al., 1984).

Compared to our previous findings, the decrease in FA values in ALS was much less pronounced compared to CIDP. This finding can be explained by the fact that most sciatic nerve fibers are sensory (Schmalbruch, 1986). It is tempting to speculate that changes in the FA values in ALS might be even bigger in motor nerves (i.e., the femoral nerve). Further studies are warranted to pursue this issue.



Furthermore, we provide additional data about the utility of PDFF mapping to quantify fatty infiltration in thigh muscles in ALS. In contrast to the visual impression, which was often rather subtle, the PDFF mapping showed higher muscle fatty infiltration in the ALS patients. Thereby, fatty infiltration was much more obvious in the quadriceps femoris muscle, but not in the biceps femoris muscle. Remarkably, there was a significant correlation between the FA values and the QFM fat fractions. Similar results were recently reported by Klickovic and colleagues. Our absolute values were almost twofold higher than those reported by a recent study that quantified fat accumulation in motor neuron disease, including ALS (Klickovic et al., 2019). These differences can be

explained by different acquisition parameters, inter-MRI-vendor variability of PDFF mapping, and a difference in disease severity between the two examined cohorts. This issue emphasizes the importance of generating normal values and warrants caution regarding their interpretation when different acquisition software and hardware are used.

In this study, further correlations of minor relevance between the clinical or electrophysiological parameters and the measured image parameters or within the image parameters were also found. For example, significant correlations were found in parts between the intramuscular fat fractions of the examined muscles and the weight/BMI of the participants or in between the muscle groups.

TABLE 2 | Electrophysiological data.

Patient	Tibial nerve		Peroneal nerve		Sural nerve	
	NCV (m/s)	CMAP (mV)	NCV (m/s)	CMAP (mV)	NCV (m/s)	SNAP (μ V)
1	40	11.3	52	2.8	52	10
2	0	0	n.A.	n.A.	46	3
3	48	16.5	46	10.4	40	20
4	37	2.5	n.A.	n.A.	37	3
5	0	0	43	3.1	59	10
6	45	22.7	48	23.7	51	12
7	43	10.1	n.A.	n.A.	60	16
8	29	0.3	37	2.3	57	2
9	59	5.3	n.A.	n.A.	n.A.	n.A.
10	43	6.5	61	0.6	54	9
11	38.3	0.31	43.9	2.1	42	2.74
12	58.7	0.9	0	0	39.7	0.9
13	44	8.2	35	6.5	n.A.	n.A.
14	44	2.1	0	0	0	0

TABLE 3 | Correlations between the collected demographic and clinical data and the obtained imaging parameters.

	FA	QFM	BFM
Age HC	-0.115 ($p = 0.707$)	0.5220 ($p = 0.067$)	0.401 ($p = 0.174$)
Age patients	0.007 ($p = 0.982$)	-0.020 ($p = 0.946$)	0.055 ($p = 0.852$)
Age both	-0.269 ($p = 0.174$)	0.342 ($p = 0.080$)	0.278 ($p = 0.160$)
Height HC	-0.626 ($p = 0.022$)*	-0.094 ($p = 0.761$)	0.174 ($p = 0.570$)
Height patients (12/14)	0.028 ($p = 0.931$)	-0.413 ($p = 0.183$)	-0.147 ($p = 0.649$)
Height both	-0.134 ($p = 0.524$)	-0.376 ($p = 0.064$)	-0.076 ($p = 0.718$)
Weight HC	-0.635 ($p = 0.020$)*	0.215 ($p = 0.481$)	0.580 ($p = 0.038$)*
Weight patients (12/14)	-0.615 ($p = 0.033$)*	0.294 ($p = 0.354$)	0.559 ($p = 0.059$)
Weight both	-0.547 ($p = 0.005$)**	0.191 ($p = 0.359$)	0.531 ($p = 0.006$)**
BMI HC	-0.225 ($p = 0.459$)	0.187 ($p = 0.541$)	0.434 ($p = 0.138$)
BMI patients (12/14)	-0.643 ($p = 0.024$)*	0.587 ($p = 0.045$)*	0.678 ($p = 0.015$)*
BMI both	-0.445 ($p = 0.026$)*	0.325 ($p = 0.113$)	0.555 ($p = 0.004$)**
NCV tibial nerve	0.265 ($p = 0.361$)	-0.743 ($p = 0.002$)**	-0.606 ($p = 0.022$)*
CMAP tibial nerve	0.200 ($p = 0.493$)	-0.275 ($p = 0.341$)	-0.231 ($p = 0.427$)
NCV peroneal nerve (10/14)	-0.091 ($p = 0.802$)	0.559 ($p = 0.093$)	0.454 ($p = 0.089$)
CMAP peroneal nerve (10/14)	0.419 ($p = 0.228$)	-0.219 ($p = 0.544$)	-0.103 ($p = 0.776$)
NCV sural nerve (12/14)	-0.448 ($p = 0.145$)	0.056 ($p = 0.863$)	0.364 ($p = 0.245$)
SNAP sural nerve (12/14)	0.126 ($p = 0.696$)	0.119 ($p = 0.712$)	0.270 ($p = 0.396$)
Disease duration	0.002 ($p > 0.999$)	0.134 ($p = 0.649$)	0.165 ($p = 0.573$)

Significant differences are in bold and indicated by asterisks (* $p < 0.05$, ** $p < 0.01$, *** $p < 0.001$).

This study has several limitations. First, we only included a small number of patients. Second, our data lacks follow-up examinations. Due to the pseudonymization process, a true blinding to groups (healthy vs. patients) was not feasible; however, readers were blinded to demographics as well as to detailed clinical history. Furthermore, we did not do systematic follow-up examinations. The assessment of multiple nerves, as mentioned above, especially motor nerves (e.g., femoral nerve) could provide even more specific results. The healthy controls tended to be of slightly younger age compared to the patients without revealing significant relevance; however, this needs to be considered as some studies showed that FA of the sciatic nerve is negatively associated with age in

both healthy controls and patients with neuropathies (Kronlage et al., 2018; Jende et al., 2021). Of note, there was no significant correlation between age and FA values in our study cohort. Last, the use of further quantitative methods (e.g., T2 mapping) was omitted in favor of a time-optimized examination protocol.

In summary, we here present a multiparametric MRI protocol that allows non-invasive quantification of proximal structural nerve damage and muscle changes in ALS. We suggest that MR imaging of lower proximal limbs could be a valuable tool for quantifying the subclinical burden of axonal loss and neurogenic muscle changes in ALS. More extensive studies are justified to confirm its utility to serve as biomarkers in therapeutic trials.

DATA AVAILABILITY STATEMENT

The datasets presented in this article are not readily available due to data privacy reasons. Requests to access the datasets should be directed to TL, thorsten.lichtenstein@uk-koeln.de.

ETHICS STATEMENT

The studies involving human participants were reviewed and approved by the Ethics Commission of the Faculty of Medicine of Cologne University. The patients/participants provided their written informed consent to participate in this study.

AUTHOR CONTRIBUTIONS

TL: study concept, conducting the study, analysis of data, data interpretation, and drafting the manuscript. AS: study concept, conducting the study, analysis of data, drafting the manuscript for content, review, and editing. KW: study concept, technical assistance, review, and editing. NG: analysis of data, review,

and editing. DM, GF, and HL: study concept and drafting the manuscript for content. MS: data interpretation, drafting the manuscript for content, review, and editing. TH: study design and concept and drafting the manuscript. All authors contributed to the article and approved the submitted version.

FUNDING

TL received funding from the Faculty of Medicine of the University of Cologne (Koeln Fortune/Gerok 14/2015).

ACKNOWLEDGMENTS

We thank our patients for their participation in the study. We also thank Dimitrios Karampinos, Department of Diagnostic and Interventional Radiology, Technical University of Munich, Germany, for his assistance in MRI sequence optimization and his continuous advice. The technical support of Claudia Müller is also greatly appreciated.

REFERENCES

- Bede, P., Elamin, M., Byrne, S., McLaughlin, R. L., Kenna, K., Vajda, A., et al. (2015). Patterns of cerebral and cerebellar white matter degeneration in ALS. *J. Neurol. Neurosurg. Psychiatry* 86, 468–70. doi: 10.1136/jnnp-2014-308172
- Bendszus, M., Koltzenburg, M., Wessig, C., and Solymosi, L. (2002). Sequential MR imaging of denervated muscle: experimental study. *Ajnr. Am. J. Neuroradiol.* 23, 1427–1431.
- Berry, J. D., and Cudkovic, M. E. (2011). New considerations in the design of clinical trials for amyotrophic lateral sclerosis. *Clin. Investig.* 1, 1375–1389. doi: 10.4155/cli.11.127
- Blain, C. R., Williams, V. C., Johnston, C., Stanton, B. R., Ganesalingam, J., Jarosz, J. M., et al. (2009). A longitudinal study of diffusion tensor MRI in ALS. *Amyotroph. Lateral Scler.* 8, 348–355. doi: 10.1080/17482960701548139
- Carvalho, M., and de Swash, M. (2016). Lower motor neuron dysfunction in ALS. *Clin. Neurophysiol.* 127, 2670–2681. doi: 10.1016/j.clinph.2016.03.024
- Cedarbaum, J. M., Stambler, N., Malta, E., Fuller, C., Hilt, D., Thurmond, B., et al. (1999). The ALSFRS-R: a revised ALS functional rating scale that incorporates assessments of respiratory function. *J. Neurol. Sci.* 169, 13–21. doi: 10.1016/s0022-510x(99)00210-5
- Cervantes, B., Bauer, J. S., Zibold, F., Kooijman, H., Settles, M., Haase, A., et al. (2015). Imaging of the lumbar plexus: optimized refocusing flip angle train design for 3D TSE. *J. Magn. Reson. Imaging* 43, 789–99. doi: 10.1002/jmri.25076
- Cirillo, M., Esposito, F., Tedeschi, G., Caiazzo, G., Sagnelli, A., Piccirillo, G., et al. (2012). Widespread Microstructural White Matter Involvement in Amyotrophic Lateral Sclerosis: a Whole-Brain DTI Study. *Am J. Neuroradiol.* 33, 1102–1108. doi: 10.3174/ajnr.a2918
- Ellis, C. M., Simmons, A., Jones, D. K., Bland, J., Dawson, J. M., Horsfield, M. A., et al. (1999). Diffusion tensor MRI assesses corticospinal tract damage in ALS. *Neurology* 53, 1051–1058. doi: 10.1212/wnl.53.5.1051
- Grolez, G., Moreau, C., Danel-Brunaud, V., Delmaire, C., Lopes, R., Pradat, P. F., et al. (2016). The value of magnetic resonance imaging as a biomarker for amyotrophic lateral sclerosis: a systematic review. *BMC Neurol.* 16:155. doi: 10.1186/s12883-016-0672-6
- Iwata, N. K., Aoki, S., Okabe, S., Arai, N., Terao, Y., Kwak, S., et al. (2008). Evaluation of corticospinal tracts in ALS with diffusion tensor MRI and brainstem stimulation. *Neurology* 70, 528–532. doi: 10.1212/01.wnl.0000299186.72374.19
- Jende, J. M. E., Groener, J. B., Kender, Z., Hahn, A., Morgenstern, J., Heiland, S., et al. (2020). Troponin T Parallels Structural Nerve Damage in Type 2 Diabetes: a Cross-sectional Study Using Magnetic Resonance Neurography. *Diabetes* 69, 713–723. doi: 10.2337/db19-1094
- Jende, J. M. E., Kender, Z., Mooshage, C., Groener, J. B., Alvarez-Ramos, L., Kollmer, J., et al. (2021). Diffusion Tensor Imaging of the Sciatic Nerve as a Surrogate Marker for Nerve Functionality of the Upper and Lower Limb in Patients With Diabetes and Prediabetes. *Front Neurosci.* 15:642589. doi: 10.3389/fnins.2021.642589
- Jenkins, T. M., Alix, J. J. P., David, C., Pearson, E., Rao, D. G., Hoggard, N., et al. (2018). Imaging muscle as a potential biomarker of denervation in motor neuron disease. *J. Neurol. Neurosurg. Psychiatry* 89:248. doi: 10.1136/jnnp-2017-316744
- Kakuda, T., Fukuda, H., Tanitame, K., Takasu, M., Date, S., Ochi, K., et al. (2011). Diffusion tensor imaging of peripheral nerve in patients with chronic inflammatory demyelinating polyradiculoneuropathy: a feasibility study. *Neuroradiology* 53:960.
- Kasper, J. M., Wadhwa, V., Scott, K. M., Rozen, S., Xi, Y., and Chhabra, A. (2015). SHINKEI—a novel 3D isotropic MR neurography technique: technical advantages over 3DIRTSE-based imaging. *Eur. Radiol.* 25:1677.
- Klickovic, U., Zampedri, L., Sinclair, C. D. J., Wastling, S., Trimmel, K., Howard, R., et al. (2019). Skeletal muscle MRI differentiates SBMA and ALS and correlates with disease severity. *Neurology* 93, e895–e907. doi: 10.1212/WNL.0000000000008009
- Kollmer, J., Bendszus, M., and Pham, M. M. R. (2015). Neurography: diagnostic imaging in the PNS. *Clin. Neuroradiol.* 25:283289.
- Koutlidis, R. M., Recondo, J., and de Bathien, N. (1984). Conduction of the sciatic nerve in its proximal and distal segment in patients with ALS (amyotrophic lateral sclerosis). *J. Neurol. Sci.* 64, 183–191. doi: 10.1016/0022-510x(84)90036-4
- Kronlage, M., Schwehr, V., Schwarz, D., Godel, T., Uhlmann, L., Heiland, S., et al. (2018). Peripheral nerve diffusion tensor imaging (DTI): normal values and demographic determinants in a cohort of 60 healthy individuals. *Eur. Radiol.* 28, 1801–1808. doi: 10.1007/s00330-017-5134-z
- Lehmann, H. C., Zhang, J., Mori, S., and Sheikh, K. A. (2010). Diffusion tensor imaging to assess axonal regeneration in peripheral nerves. *Exp. Neurol.* 223:244.
- Lichtenstein, T., Sprenger, A., Weiss, K., Slebocki, K., Cervantes, B., Karampinos, D., et al. (2017). MRI biomarkers of proximal nerve injury in CIDP. *Ann. Clin. Transl. Neurol.* 5:28.
- Ludolph, A., Drory, V., Hardiman, O., Nakano, I., Ravits, J., Robberecht, W., et al. (2015). A revision of the El Escorial criteria - 20. *Amyotroph. Lateral*

- Scler. Frontotemporal Degener.* 16, 291–292. doi: 10.3109/21678421.2015.1049183
- Mathys, C., Aissa, J., Meyer Zu Hörste, G., Reichelt, D. C., Antoch, G., Turowski, B., et al. (2013). Peripheral Neuropathy: assessment of Proximal Nerve Integrity By Diffusion Tensor Imaging. *Muscle Nerve* 48:896.
- Metwalli, N. S., Benatar, M., Nair, G., Usher, S., Hu, X., Carew, J. D., et al. (2010). Utility of axial and radial diffusivity from diffusion tensor MRI as markers of neurodegeneration in amyotrophic lateral sclerosis. *Brain Res.* 1348, 156–164. doi: 10.1016/j.brainres.2010.05.067
- Morisaki, S., Kawai, Y., Umeda, M., Nishi, M., Oda, R., Fujiwara, H., et al. (2011). In vivo assessment of peripheral nerve regeneration by diffusion tensor imaging. *J. Magn. Reson. Imaging* 33, 535–542. doi: 10.1002/jmri.22442
- Schmalbruch, H. (1986). Fiber composition of the rat sciatic nerve. *Anatomical Rec.* 215, 71–81. doi: 10.1002/ar.1092150111
- Schneider, C., Sprenger, A., Weiss, K., Slebocki, K., Maintz, D., Fink, G. R., et al. (2019). MRI detects peripheral nerve and adjacent muscle pathology in non-systemic vasculitic neuropathy (NSVN). *J. Neurol.* 266, 975–981. doi: 10.1007/s00415-019-09224-0
- Schwarz, D., Weiler, M., Pham, M., Heiland, S., Bendszus, M., Bäumer, P., et al. (2015). Diagnostic Signs of Motor Neuropathy in MR Neurography: nerve Lesions and Muscle Denervation. *Eur. Radiol.* 25, 1497–1503. doi: 10.1007/s00330-014-3498-x
- Sheikh, K. A. (2010). Non-invasive imaging of nerve regeneration. *Exp. Neurol.* 223:76.
- Simon, N. G. (2016). Lower motor neurons – counting cogs in the ALS machine. *Clin. Neurophysiol.* 127, 2668–2669. doi: 10.1016/j.clinph.2016.03.023
- Simon, N. G., Huynh, W., Vucic, S., Talbot, K., and Kiernan, M. C. (2015). Motor neuron disease. *Intern. Med. J.* 45, 1005–1013.
- Simon, N. G., Lagopoulos, J., Paling, S., Pfluger, C., Park, S. B., Howells, J., et al. (2017). Peripheral nerve diffusion tensor imaging as a measure of disease progression in ALS. *J. Neurol.* 264:890.
- Simon, N. G., Turner, M. R., Vucic, S., Al-Chalabi, A., Shefner, J., Lomen-Hoerth, C., et al. (2014). Quantifying disease progression in amyotrophic lateral sclerosis. *Ann. Neurol.* 76, 643–657.
- Takagi, T., Nakamura, M., Yamada, M., Hikishima, K., Momoshima, S., Fujiyoshi, K., et al. (2009). Visualization of peripheral nerve degeneration and regeneration: monitoring with diffusion tensor tractography. *Neuroimage* 44:892.
- Toosy, A. T., Werring, D. J., Orrell, R. W., Howard, R. S., King, M. D., Barker, G. J., et al. (2003). Diffusion tensor imaging detects corticospinal tract involvement at multiple levels in amyotrophic lateral sclerosis. *J. Neurol. Neurosurg. Psychiatry* 74, 1250–1257. doi: 10.1136/jnnp.74.9.1250
- Turner, M. R., Kiernan, M. C., Leigh, P. N., and Talbot, K. (2009). Biomarkers in amyotrophic lateral sclerosis. *Lancet Neurol.* 8, 94–109.
- Verber, N. S., Shepherd, S. R., Sassani, M., McDonough, H. E., Moore, S. A., Alix, J. J. P., et al. (2019). Biomarkers in Motor Neuron Disease: a State of the Art Review. *Front. Neurol.* 10:291. doi: 10.3389/fneur.2019.00291
- West, G. A., Haynor, D. R., Goodkin, R., Tsuruda, J. S., Bronstein, A. D., Kraft, G., et al. (1994). Magnetic Resonance Imaging Signal Changes in Denervated Muscles after Peripheral Nerve Injury. *Neurosurgery* 35, 1077–85. doi: 10.1227/00006123-199412000-00010
- Zhang, J., Zhang, G., Morrison, B., Mori, S., and Sheikh, K. A. (2008). Magnetic resonance imaging of mouse skeletal muscle to measure denervation atrophy. *Exp. Neurol.* 212, 448–457. doi: 10.1016/j.expneurol.2008.04.033

Conflict of Interest: NG is an editorial board member of European Radiology and a speaker at the bureau of Philips Healthcare; received research support from Philips Healthcare; and is a consultant for Bristol-Myers Squibb. GF serves as an editorial board member of Cortex, Neurological Research and Practice, NeuroImage: Clinical, Zeitschrift für Neuropsychologie, and DGNeurologie; receives royalties from the publication of the books Funktionelle MRT in Psychiatrie und Neurologie, Neurologische Differentialdiagnose, and SOP Neurologie; receives royalties from the publication of the neuropsychological tests KAS and Köpfs; and received honoraria for speaking engagements from Bayer, Desitin, DGN, Ergo DKV, Forum für medizinische Fortbildung FomF GmbH, GSK, Medica Academy Messe Düsseldorf, Medicbrain Healthcare, Novartis, Pfizer, and Sportärztl. DM is a speaker at the bureau of Philips Healthcare. HL received honoraria for speaking and advisory board engagements or academic research support by Akcea, Alnylam, Biogen, Celgene, CSL Behring, Grifols, Gruenthal, LFB Pharma, Takeda, and UCB. MS received personal fees from Bayer and Biogen. KW was employed by company Philips Healthcare.

The remaining authors declare that the research was conducted in the absence of any commercial or financial relationships that could be construed as a potential conflict of interest.

Publisher's Note: All claims expressed in this article are solely those of the authors and do not necessarily represent those of their affiliated organizations, or those of the publisher, the editors and the reviewers. Any product that may be evaluated in this article, or claim that may be made by its manufacturer, is not guaranteed or endorsed by the publisher.

Copyright © 2021 Lichtenstein, Sprenger, Weiss, Große Hokamp, Maintz, Schlamann, Fink, Lehmann and Henning. This is an open-access article distributed under the terms of the Creative Commons Attribution License (CC BY). The use, distribution or reproduction in other forums is permitted, provided the original author(s) and the copyright owner(s) are credited and that the original publication in this journal is cited, in accordance with accepted academic practice. No use, distribution or reproduction is permitted which does not comply with these terms.



Magnetic Resonance Imaging as a Biomarker in Diabetic and HIV-Associated Peripheral Neuropathy: A Systematic Review-Based Narrative

Matthew C. Evans^{1,2*}, Charles Wade², David Hohenschurz-Schmidt¹, Pete Lally^{2,3}, Albert Ugwu-dike³, Kamal Shah³, Neal Bangarter³, David J. Sharp² and Andrew S. C. Rice¹

¹ Pain Research, Department of Surgery and Cancer, Faculty of Medicine, Imperial College London, London, United Kingdom, ² Department of Brain Sciences, Care Research and Technology Centre, UK Dementia Research Institute, London, United Kingdom, ³ Royal School of Mines, Imperial College London, London, United Kingdom

OPEN ACCESS

Edited by:

Nathalie Just,
INRA Centre Val de Loire, France

Reviewed by:

Eva-Maria Ratai,
Massachusetts General Hospital and
Harvard Medical School,
United States

Johann M. E. Jende,
Heidelberg University
Hospital, Germany

*Correspondence:

Matthew C. Evans
matthew.evans@imperial.ac.uk

Specialty section:

This article was submitted to
Brain Imaging Methods,
a section of the journal
Frontiers in Neuroscience

Received: 18 June 2021

Accepted: 17 August 2021

Published: 21 September 2021

Citation:

Evans MC, Wade C,
Hohenschurz-Schmidt D, Lally P,
Ugwu-dike A, Shah K, Bangarter N,
Sharp DJ and Rice ASC (2021)
Magnetic Resonance Imaging as a
Biomarker in Diabetic and
HIV-Associated Peripheral
Neuropathy: A Systematic
Review-Based Narrative.
Front. Neurosci. 15:727311.
doi: 10.3389/fnins.2021.727311

Background: Peripheral neuropathy can be caused by diabetes mellitus and HIV infection, and often leaves patients with treatment-resistant neuropathic pain. To better treat this condition, we need greater understanding of the pathogenesis, as well as objective biomarkers to predict treatment response. Magnetic resonance imaging (MRI) has a firm place as a biomarker for diseases of the central nervous system (CNS), but until recently has had little role for disease of the peripheral nervous system.

Objectives: To review the current state-of-the-art of peripheral nerve MRI in diabetic and HIV symmetrical polyneuropathy. We used systematic literature search methods to identify all studies currently published, using this as a basis for a narrative review to discuss major findings in the literature. We also assessed risk of bias, as well as technical aspects of MRI and statistical analysis.

Methods: Protocol was pre-registered on NIHR PROSPERO database. MEDLINE, Web of Science and EMBASE databases were searched from 1946 to 15th August 2020 for all studies investigating either diabetic or HIV neuropathy and MRI, focusing exclusively on studies investigating symmetrical polyneuropathy. The NIH quality assessment tool for observational and cross-sectional cohort studies was used for risk of bias assessment.

Results: The search resulted in 18 papers eligible for review, 18 for diabetic neuropathy and 0 for HIV neuropathy. Risk of bias assessment demonstrated that studies generally lacked explicit sample size justifications, and some may be underpowered. Whilst most studies made efforts to balance groups for confounding variables (age, gender, BMI, disease duration), there was lack of consistency between studies. Overall, the literature provides convincing evidence that DPN is associated with larger nerve cross sectional area, T2-weighted hyperintense and hypointense lesions, evidence of nerve oedema on Dixon imaging, decreased fractional anisotropy and increased apparent diffusion coefficient compared with controls. Analysis to date is largely restricted to the sciatic nerve or its branches.

Conclusions: There is emerging evidence that various structural MR metrics may be useful as biomarkers in diabetic polyneuropathy, and areas for future direction are discussed. Expanding this technique to other forms of peripheral neuropathy, including HIV neuropathy, would be of value.

Systematic Review Registration: (identifier: CRD 42020167322) https://www.crd.york.ac.uk/prospero/display_record.php?RecordID=167322.

Keywords: peripheral nerve, magnetic resonance imaging, diabetes, HIV, neuropathy

INTRODUCTION

Diabetic peripheral neuropathy (DPN) is a condition associated with both type 1 (T1DM) and type 2 diabetes mellitus (T2DM), presenting as a distal symmetrical, length-dependent degeneration, usually affecting sensory more than motor nerves. Diabetes mellitus is common, affecting around 8.8% of adults worldwide (International Diabetes Federation, 2015), and around half of these are estimated to develop DPN at some point in their lives (Tesfaye, 2011). Neuropathic pain is a common symptom, affecting around a quarter of those with DPN (Van Hecke et al., 2014), and is poorly responsive to analgesic medications (Finnerup et al., 2015).

The pathophysiology of DPN remains incompletely understood, and numerous mechanisms have been proposed, including hyperglycaemia (Won et al., 2012; Xu et al., 2014), increased activity of the polyol pathway (Brownlee, 2001) and dyslipidaemia (Tesfaye et al., 1996) [an excellent review of this topic can be found in Calcutt (2020)]. The polyol pathway received significant attention in the field for some time (Chung, 2003) providing hope that aldose reductase inhibitors (ARIs) could modify disease in DPN. However, meta-analyses of commercially available ARIs to date have not been successful, so these have largely been abandoned in clinical practise (Chalk et al., 2007; Calcutt and Fernyhough, 2016). DPN is classically described as a small fibre neuropathy, with a reduction in intra-epithelial nerve fibre density (IENFD) shown on skin biopsy (Lauria et al., 2010) reflecting a “die-back” pattern of loss of unmyelinated C fibres. However, pathological studies have also shown loss of larger, myelinated fibres, even early in the natural history of the disease (Behse et al., 1977), and autopsy studies of DPN have shown that fascicular damage begins in the proximal sciatic nerve and can be found along the length of the affected nerve (Dyck et al., 1986), which is supported by recent imaging studies showing proximal sciatic involvement in DPN (Groener et al., 2020). The pathological mechanism of the peripheral predominance of symptoms in DPN remains unclear, with likely roles for metabolic dysfunction (Freeman et al., 2016) and neuroinflammation (Leininger et al., 2004).

HIV infection also causes a symmetrical sensory-predominant polyneuropathy. HIV neuropathy is seen in 20–57% of patients infected with HIV, across low-, middle- and high-income countries (Cherry et al., 2016). The most common form of peripheral nerve lesion found in HIV is a length-dependent axonal degeneration of unmyelinated (C) and thinly myelinated (A δ) fibres, much like DPN (Cherry et al., 2012b). Two distinct

mechanisms appear to be involved in HIV neuropathy: (i) a direct toxic effect of anti-retroviral drugs (ARDs), particularly older di-deoxynucleotide agents (Cherry et al., 2012a; Kamerman et al., 2012), and (ii) an effect of the HIV virus itself, which seems to involve interaction of viral gp120 protein with macrophage CCR5/CXCR4, leading to an inflammatory cascade that results in axonal damage and degeneration (Lee et al., 2003; Moss et al., 2015). Other components of the HIV virus may also be involved in addition to gp120, including viral Transactivator of Transcription (Tat) (Wodarski et al., 2018). The biological mechanisms underlying pain in HIV neuropathy have been poorly elucidated, but various psychosocial factors have been identified (Scott et al., 2018; Scott, 2019).

Treatment of neuropathic pain (and other neuropathic symptoms) can be extremely difficult, with no true disease-modifying therapies for most underlying conditions, and meta-analyses demonstrating that existing therapies have modest efficacy, narrow therapeutic indices and that it is difficult to predict treatment responses at the individual patient level (Finnerup et al., 2015). Part of the challenge of drug development and clinical trial design is the lack of robust biomarkers for neuropathy and neuropathic pain.

Electrophysiological techniques allow probing of the electrical properties of nerves, which help identify axonal and demyelinating processes. However, nerve conduction studies only involve the largest myelinated fibres, so dysfunction of smaller A δ and C fibres will not be represented. Conversely, whilst skin biopsies can be used to assess epidermal nerve fibre density of the small, peripheral nerve fibres (Smith et al., 2005), this only provides information on structure but not function of nerves, and its application is anatomically limited in practise. The invasive nature of skin biopsy also precludes its use as a longitudinal biomarker. Therefore, we sorely need better, ideally non-invasive biomarkers of peripheral nerve damage, that are easily repeatable for longitudinal study.

Magnetic resonance imaging (MRI) would seem to be the ideal non-invasive biomarker and has found use with various diseases of the central nervous system. However, MRI has had limited application to the study of peripheral nerve disease. Until recently, technological challenges have impeded its use in this field, not of achieving sufficient resolution to provide useful information in structures with cross-sectional areas of 3–50 mm² (i.e., diameter of 2–8 mm). The increased availability of 3 Tesla (T) and 7T systems has changed the landscape in recent years. At higher field strength, MRI can offer fascicular

level resolution in larger peripheral nerves (Schmid et al., 2018), offering the possibility of a “virtual biopsy.” MR neurography uses structural T_1 -weighted, fat-suppressed T_2 -weighted and diffusion weighted sequences to image peripheral nerves. To date, this technology has found use mostly for compressive and traumatic neuropathies (Cudlip et al., 2002), immune mediated sensory and motor neuropathies (Kronlage et al., 2017), and degenerative diseases such as motor neurone disease (MND) (Gerevini et al., 2016).

In this systematic review we review the current state-of-the-art in applying MRI to understanding diabetic and HIV peripheral neuropathies, identifying the main findings in the field, assessing study quality, and suggesting areas for future research. We chose DPN as this is the most common cause of symmetrical polyneuropathy in the Western world. HIV neuropathy was chosen here because its clinical presentation is often indistinguishable from DPN, so would be an appropriate comparison. Also, given that it affects up to 57% of patients with HIV infection it is also not an uncommon condition in the west, but is of particular burden in areas of high HIV prevalence, such as Sub-Saharan Africa.

MATERIALS AND METHODS

Eligibility Criteria

We considered all original research studies relating to MRI in diabetic (T1DM or T2DM) or HIV polyneuropathy. Eligible imaging studies had to involve the peripheral nervous system, rather than the brain or spinal cord. We excluded studies restricted to the dorsal root ganglion, as whilst there is an emerging literature demonstrating pathological changes at this location (Jende et al., 2020c), it has its own unique anatomical and technical challenges for MRI compared with that of imaging of whole peripheral nerves, and therefore we felt warranted its own separate review as the field develops. There was no limit placed on sample size. The only inclusion criterion specific to study-design was that the studies must have had a group of patients with either diabetic neuropathy or HIV neuropathy, as well as a relevant control group (either a group of patients with diabetes or HIV without neuropathy, or healthy controls).

Conversely we excluded isolated case reports; studies with no disease control (i.e., diabetes without neuropathy) and/or healthy control group for comparison; studies investigating other patterns of nerve damage other than symmetrical polyneuropathy (e.g., isolated mononeuropathies, mono-neuritis multiplex, chronic immune demyelinating polyradiculoneuropathy, insulin neuritis, radiculopathy, plexopathy, ganglionopathy); studies involving neuropathies unrelated to the primary conditions of HIV or diabetes (e.g., HIV-related lymphoma, or secondary infections related to HIV or diabetes); and animal studies.

Information Search/Data Collection

We searched MEDLINE, Web of Science and EMBASE databases from 1946 to 15th August 2020. Search criteria were as follows:

Diabetic Neuropathy

(diabetes mellitus/ [MeSH term] OR “diabetes” OR “diabetic”)

AND

(diabetic neuropathies/ [MeSH term] OR polyneuropathies/ [MeSH term] OR small fibre neuropathy/ [MeSH term] OR “neuropathy” OR “neuropathic” OR “neuropathies” OR “polyneuropathy” OR “polyneuropathies”)

AND

(magnetic resonance imaging/ [MeSH term] OR “magnetic resonance imaging” OR “MRI” OR “nuclear magnetic resonance” OR “NMR”).

HIV Neuropathy

(HIV/ [MeSH term] OR HIV-1/ [MeSH term] OR HIV-2/ OR “HIV” OR “human immunodeficiency virus”)

AND

(polyneuropathies/ [MeSH term] OR small fibre neuropathy/ [MeSH term] OR “neuropathy” OR “neuropathic” OR “neuropathies” OR “polyneuropathy”)

AND

(magnetic resonance imaging/ [MeSH term] OR “magnetic resonance imaging” OR “MRI” OR “nuclear magnetic resonance” OR “NMR”)

Search results were extracted from each database as RIS files and subsequently imported to Covidence software (www.covidence.org) for analysis, and duplicates were automatically removed. Initial abstract and subsequent full text screening was carried out by two independent reviewers. Any conflicts were resolved by consensus discussion among the reviewers.

Risk of Bias Assessment

The NIH Quality Assessment Tool for Observational Cohort and Cross-Sectional Studies (<http://www.nhlbi.nih.gov/health-pro/guidelines/in-develop/cardiovascular-risk-reduction/tools/cohort>) was used. The assessment was performed in duplicate and conflicts were resolved by consensus discussion. The risk of bias tool comprises 14 questions; however 2 of the questions were removed because they were of relevance to prospective cohort studies only, rather than cross-sectional imaging studies forming this review (Question 3: Was the participation of eligible persons at least 50%; Question 13: Was loss to follow up <20%). For the remaining questions, “exposure,” or “independent variable” was treated as diabetes or clinical diabetic neuropathy, depending on the study in question. The one exception to this was studies investigating a link between MR changes and specific blood parameters (e.g., troponin T, cholesterol); these were additionally considered as “exposures” where relevant. “Outcome,” or “dependent variable(s)” corresponded to MRI outcomes. Finally, question 14 relates to the control of confounding variables. Based on an a-priori review of the literature for demographic effects on specific MR sequences, we identified 4 variables that should be considered confounds and controlled for accordingly: (i) age; (ii) gender; (iii) disease duration; (iv) BMI (Kollmer et al., 2018; Kronlage et al., 2018, 2019; Groener et al., 2020). This is discussed further in the Discussion section.

Other Outcome Measures

In addition to the above formal risk of bias assessment, given the relatively small number of studies meeting the inclusion criteria, we appraised each report in the discussion section according to pertinent quality outcomes for MRI studies specifically. These outcomes were: Sample size (whether power calculations have been performed); sample representativeness, and variables controlled for (age, gender, BMI, disease duration, medications, blood glucose and lipid measurements); any aspect of the MRI itself which limits interpretation of studies (field strength, spatial resolution, anatomy scanned); method of nerve segmentation (automated or manual: if automated, whether there is data presented in the paper or elsewhere demonstrating its accuracy; and if manual, whether data is provided on intra- and inter-rater reliability); statistical analysis. Study characteristics are shown in **Table 1**, and the main results summarised in **Table 2**.

RESULTS

Study Selection

Two thousand nine hundred seventy-five papers (duplicates excluded) were screened (by two independent reviewers) by reviewing titles and abstracts according to the inclusion/exclusion criteria itemised in the methods section above, of which 2,945 were deemed irrelevant, leaving 30 papers selected for full text screening. These papers were excluded largely because they involved conditions other than diabetic or HIV neuropathy (1635), or involved diabetic or HIV subjects but were either case reports, or on topics that fell outside of the review (e.g., imaging studies of Charcot arthropathy, or CNS imaging studies of HIV or infective complications of HIV). Twelve studies were excluded from full text screening, either because of study design not meeting inclusion criteria (letter to the editor, case reports, or studies not including any control group), patient population not being appropriate [investigating other forms of neuropathy such as chronic inflammatory demyelination polyneuropathy (CIDP) rather than HIV or diabetic neuropathy], or because the result was a conference proceeding with limited data and with no peer review. Finally, we were left with 18 studies which met eligibility for systematic review (see PRISMA flow chart in **Figure 1**). All 18 studies were focused on diabetic neuropathy, with no studies found to date investigating HIV neuropathy with MRI. The remainder of the results section will therefore be dedicated to discussing studies of diabetic neuropathy.

Risk of Bias Assessment

The risk of bias assessment is shown for each study in **Figure 2**. This demonstrates that most (if not all) studies failed to satisfy questions 5 and 14, which relate to sample size justification and confounding variables. For this question we chose the following variables as most pertinent confounds: (i) age; (ii) gender; (iii); BMI; (iv) diabetes duration (if more than one diabetes group in the study).

Question 2 asks whether the populations studied were clearly defined. Many of the earlier studies did not distinguish between type 1 and 2 diabetes, and often did not make clear from

the methods section the number of patients from each group, or which patients were on insulin treatment (Koechner et al., 1995; Shibata et al., 1998; Wu et al., 2017; Edward et al., 2020) (14/18 complied). Question 8 asks whether different “levels” of exposure were compared, which in this context relates to whether groups were stratified based on severity or duration of neuropathy or diabetes, to make a more convincing link between disease and MR biomarkers (9/18 complied). Question 10 relates to whether more than 1 time point was used (2/18 complied). Finally, question 12 asks whether outcomes were assessed in a blinded fashion; this was only clearly documented in 9/18 studies. However, of these 7/9 studies used (semi-)automated segmentation of MR images and DTI analysis pipelines which provide minimal opportunity to introduce bias (Pham et al., 2015; Vaeggemose et al., 2017a, 2020; Wu et al., 2017; Jende et al., 2019, 2020a; Edward et al., 2020).

The remaining questions demonstrated high compliance. However, it is worth noting that the three studies by Jende et al. (2018, 2019, 2020a) did not satisfy question 6, which pertains to whether the exposures were measured before the outcomes. In each of these studies, correlational relationships are made between specific MRI values and blood biomarkers (cholesterol and high sensitivity troponin T). As the authors themselves note in the discussion, the cross-sectional nature of the study limits causal relationships being made between variables.

NARRATIVE REVIEW

Dixon MRI

The earliest studies attempting to use MRI to non-invasively study peripheral nerves in DPN came from Eaton and Griffey in the late 1980s (Griffey et al., 1988; Koechner et al., 1995; Eaton et al., 1996). In a set of three papers, they used a proton-density-weighted Dixon sequence at 1.5 T as a measure of sural nerve water content. Dixon sequences capitalise on chemical shift, the phenomenon by which protons in fat and water have different resonant frequencies, and therefore over time their corresponding signal components alternate between being in- and opposed-phase. By acquiring two imaging (i.e., 2-point Dixon) or more and combining them mathematically, it is possible to derive water-only and fat-only images from these data. They used water-only Dixon images, normalised to a copper-sulphate (CuSO₄) control to derive an estimate of water content from proton density. They demonstrated higher nerve water content in patients with DPN compared with either diabetes without DPN, or healthy controls (Griffey et al., 1988; Koechner et al., 1995; Eaton et al., 1996). In their earlier study, they showed that sural nerve water content positively correlated with deficits on nerve conduction studies. Later, in a larger study using 79 patients with DPN, 75 patients with diabetes without DPN, and 72 non-diabetic healthy controls, Eaton et al. (1996) demonstrated that there was a subset of patients with diabetes without DPN who demonstrated nerve “hyperhydration” (>30% water content of nerve) with nerve conduction values approaching those in the DPN cohort, but when stratifying the DPN patients according to duration of neuropathy, there was a trend towards decreasing nerve water

TABLE 1 | Study characteristics.

References	Country conducted	Patient group	Control group	Variables controlled	Exclusion criteria
Griffey et al. (1988)	USA	<ul style="list-style-type: none"> Insulin-dependent diabetes with DPN (11) Insulin-dependent diabetes with DPN taking aldose reductase inhibitor (6) 	<ul style="list-style-type: none"> Insulin-dependent diabetes without DPN (11) Non-diabetic healthy control (11) 	Nil	<ul style="list-style-type: none"> Women Other causes polyneuropathy <ul style="list-style-type: none"> Renal failure Pernicious anaemia Alcoholism Heavy metal/toxin exposure Hypothyroidism
Koechner et al. (1995)	USA	<ul style="list-style-type: none"> Diabetes with DPN (13) 	<ul style="list-style-type: none"> Non-diabetic healthy control (5) 	Nil	Nil
Eaton et al. (1996)	USA	<ul style="list-style-type: none"> Diabetes with DPN (79) 	<ul style="list-style-type: none"> Diabetes without DPN (75) Non-diabetic healthy control (72) 	Statistically significant differences in age, gender, BMI., disease duration, and cardiovascular risk factors. No statistical control used.	<ul style="list-style-type: none"> Other neuropathy risk factors: <ul style="list-style-type: none"> Renal failure Hypothyroid Pernicious anaemia Alcoholism Neurosyphilis Heavy metal/toxin exposure Oedema in lower limbs
Shibata et al. (1998)	Japan	<ul style="list-style-type: none"> Non-insulin-dependent diabetes mellitus (92) 	<ul style="list-style-type: none"> Non-diabetic healthy control (19) 	Age, retinopathy, nephropathy	<ul style="list-style-type: none"> Oedema in lower limbs
Pham et al. (2011)	Germany	<ul style="list-style-type: none"> T2DM with DPN (10) T1DM with DPN (2) 	<ul style="list-style-type: none"> T2DM without DPN (10) T1DM without DPN (5) Non-diabetic healthy control (10) 	HbA1c, HTN, hyperlipidemia, CHD, myocardial infarction, smoking	Nil
Pham et al. (2015)	Germany	<ul style="list-style-type: none"> Diabetes with mild-moderate DPN (25) Diabetes with severe DPN (10) 	<ul style="list-style-type: none"> Diabetes without DPN (15) Non-diabetic healthy control (25) 	Age, sex, disease duration, Retinopathy, Nephropathy, CHD, HTN, Hypertension, Hyperlipidemia, Smoking, HbA1c, Cholesterol, Triglycerides, HDL, LDL, eGFR, BMI	<ul style="list-style-type: none"> Age < 18 or >75 Contraindication (CI) to MRI Symptomatic PAD or CVA Other neuropathy risk factors <ul style="list-style-type: none"> EtOH excess Autoimmune Systemic vasculitis ESRF
Vaeggemose et al. (2017a)	Denmark	<ul style="list-style-type: none"> T1DM with DPN (10) 	<ul style="list-style-type: none"> T1DM without DPN (10) Non-diabetic healthy control (10) 	Age, Disease duration, BMI, HbA1c	<ul style="list-style-type: none"> Severe cardiac/lung disease Acute or chronic MSK disorder Lower-limb asymmetric weakness CI to MRI Other neuropathy risk factors Acute metabolic dysregulation Chronic neurologic diseases Endocrine disorder

(Continued)

TABLE 1 | Continued

References	Country conducted	Patient group	Control group	Variables controlled	Exclusion criteria
Wu et al. (2017)	China	<ul style="list-style-type: none"> Diabetic patients – type not specified (10) 	<ul style="list-style-type: none"> Non-diabetic healthy control (12) 	Sex, age	<ul style="list-style-type: none"> Pregnancy CI to MRI Hx of leg or knee surgery Severe cardiac/lung disease Other neuropathy risk factors <ul style="list-style-type: none"> Metabolic disorder Endocrine disorder Exposure to neurotoxic agents Chronic neurologic diseases Neuromuscular/MSK disorder
Felisaz et al. (2017)	Italy	<ul style="list-style-type: none"> Diabetes with mild DPN (6) Diabetes with moderate/severe DPN (10) 	<ul style="list-style-type: none"> Non-diabetic healthy control (15) 	Sex, age	<ul style="list-style-type: none"> Unilateral neuropathy Compressive radiculopathy Posttraumatic radiculopathy Other neuropathy risk factors Severe cardiac/lung disease Acute or chronic MSK disorder Lower-limb asymmetric weakness Contra-indications to MRI Other neuropathy risk factors Acute metabolic dysregulation Chronic neurologic diseases Endocrine disorder
Vaeggemose et al. (2017b)	Denmark	<ul style="list-style-type: none"> Symptomatic mild T1DM Polyneuropathy (13) Symptomatic severe T1DM Polyneuropathy (11) 	<ul style="list-style-type: none"> T1DM without DPN (25) Non-diabetic healthy control (30) 	Age, gender, BMI, HbA1c	<ul style="list-style-type: none"> Severe cardiac/lung disease Acute or chronic MSK disorder Lower-limb asymmetric weakness Contra-indications to MRI Other neuropathy risk factors Acute metabolic dysregulation Chronic neurologic diseases Endocrine disorder
Wang et al. (2018)	China	<ul style="list-style-type: none"> Diabetes with DPN (22) – 16 T2DM, 6 T1DM 	<ul style="list-style-type: none"> Diabetes with DPN (20) – 17 T2DM, 3 T1DM Non-diabetic healthy control (20) 	Age, sex, BMI, HbA1c	<ul style="list-style-type: none"> Present or past foot osteomyelitis Present or past foot ulcer Known hx of foot fracture or surgery Skin swelling/lesions Other neuropathy risk factors <ul style="list-style-type: none"> EtOH excess Metabolic/toxic factors Inflammatory or hereditary
Jende et al. (2018)	Germany	<ul style="list-style-type: none"> T2DM with DPN (66) T1DM with DPN (18) 	<ul style="list-style-type: none"> T2DM without DPN (19) T1DM without DPN (17) 	Age, BMI, HbA1c, Cholesterol, eGFR, albumin/creatinine ratio	<ul style="list-style-type: none"> Age < 18 Pregnancy CI to MRI Hx of lumbar surgery Disc protrusion Other neuropathy risk factors <ul style="list-style-type: none"> EtOH excess Malignancy Infection Chronic bowel disease Hypovitaminosis Exposure to neurotoxic agents Chronic neurologic diseases Micro- or macrocytic anaemia Monoclonal gammopathy

(Continued)

TABLE 1 | Continued

References	Country conducted	Patient group	Control group	Variables controlled	Exclusion criteria
Jende et al. (2019)	Germany	<ul style="list-style-type: none"> T2DM with DPN (64) 	<ul style="list-style-type: none"> T2DM without DPN (36) 	Age, BMI, HbA1c, eGFR	<ul style="list-style-type: none"> Age < 18 Pregnancy CI to MRI Hx of lumbar surgery Disc protrusion Other neuropathy risk factors EtOH excess Malignancy Infection Hypovitaminosis Monoclonal gammopathy Exposure to neurotoxic agents Chronic neurologic diseases Renal insufficiency Microangiopathy
Jende et al. (2020a)	Germany	<ul style="list-style-type: none"> Painful DPN (64) – mixture T1DM and T2DM Non-painful DPN (37) - mixture T1DM and T2DM 	<ul style="list-style-type: none"> Diabetes without DPN (30) - mixture T1DM and T2DM 	Age, sex, HbA1c, diabetes duration, cholesterol, eGFR	<ul style="list-style-type: none"> Age < 18 Pregnancy CI to MRI Hx of lumbar surgery Disc protrusion Other neuropathy risk factors <ul style="list-style-type: none"> EtOH excess Malignancy Infection Hypovitaminosis Monoclonal gammopathy Exposure to neurotoxic agents Chronic neurologic diseases Pain disorder other than DPN
Groener et al. (2020)	Germany	<ul style="list-style-type: none"> T2DM with DPN (48) 	<ul style="list-style-type: none"> T2DM without DPN (13) Non-diabetic healthy control (12) 	Age, BMI, HbA1c, diabetes duration, protein:creatinine ratio, eGFR	<ul style="list-style-type: none"> Age < 18 Pregnancy CI to MRI Other neuropathy risk factors <ul style="list-style-type: none"> EtOH excess Malignancy Rheumatic autoimmune dx Spinal lesions Chronic neurologic diseases Renal insufficiency

(Continued)

TABLE 1 | Continued

References	Country conducted	Patient group	Control group	Variables controlled	Exclusion criteria
Edward et al. (2020)	Egypt	<ul style="list-style-type: none"> • T2DM with DPN (30) 	<ul style="list-style-type: none"> • Non-diabetic healthy controls (15) 	Age	<ul style="list-style-type: none"> • Evidence of nerve entrapment • Evidence of other neuropathies: <ul style="list-style-type: none"> ◦ Drug-induced/toxic ◦ Hereditary
Jende et al. (2020b)	Germany	<ul style="list-style-type: none"> • T2DM with DPN (28) 	<ul style="list-style-type: none"> • T1DM without DPN (23) • Non-diabetic healthy controls (10) 	Disease duration, HbA1c, BMI, eGFR	<ul style="list-style-type: none"> • Age < 18 • Pregnancy • CI to MRI • Other neuropathy risk factors • EtOH excess • Malignancy • Infectious diseases • Rheumatic autoimmune dx • Spinal lesions • Chronic neurologic diseases • Renal insufficiency
Vaeggemose et al. (2020)	Denmark	<ul style="list-style-type: none"> • T2DM with DPN (10) 	<ul style="list-style-type: none"> • T1DM without DPN (10) • Non-diabetic healthy controls (20) 	Age, diabetes duration, HbA1c	<ul style="list-style-type: none"> • Acute metabolic dysregulation • Severe cardiac or lung disease • Musculoskeletal disorders • Other endocrine/neurological disorders • Present or previous asymmetric weakness in the lower limbs • CI to MRI

TABLE 2 | Results summary.

References	Magnetic field strength (T)	Nerve/Segment	Results		
			Measurement (spatial resolution)	Mean \pm standard error (* indicates that values have been converted from the original standard deviation to standard error)	P-value
Griffey et al. (1988)	1.5	Sural nerve	Proton density Dixon sequence, water ratio with CuSO₄ phantom (0.312 x 0.615 x 3.0 mm³)		
			A: Diabetes with "Symptomatic" DPN B: Diabetes with "Treated Symptomatic" DPN C: "Neurologically Asymptomatic Diabetes" D: Non-diabetic healthy control	0.33 \pm 0.11 0.26 \pm 0.02 0.27 \pm 0.11 0.23 \pm 0.04	A vs. D: $p < 0.001$ B and C N.S. compared with D
Koechner et al. (1995)	1.5	Sural nerve	Proton density Dixon sequence, nerve hydration coefficient with CuSO₄ phantom (0.312 x 0.615 x 3.0 mm³)		
			A: Diabetes with "Symptomatic" DPN B: Non-diabetic healthy controls	31.4 \pm 2.4 24.6 \pm 1.2	No statistical comparison
Eaton et al. (1996)	1.5	Sural nerve	Proton density Dixon sequence, nerve hydration coefficient with CuSO₄ phantom (0.312 x 0.615 x 3.0 mm³)		
			A: Diabetes with "Symptomatic" DPN B: "Neurologically Asymptomatic Diabetes" C: Non-diabetic healthy control	30.4 \pm 5.8% 27.6 \pm 5.0% 24.8 \pm 3.5%	A vs. C: $p < 0.05$ A vs. B: $p < 0.05$ B vs. C: $p < 0.05$
Shibata et al. (1998)	1.5	Sural nerve	T₁ relaxometry, ms (resolution not specified)		
			A: Non-insulin-dependent diabetes mellitus B: Non-diabetic healthy controls	831 \pm 495 472 \pm 258	A vs. B: $p < 0.001$
			C: Non-insulin-dependent diabetes mellitus: pre-ARI treatment ($N = 12$) D: Non-insulin-dependent diabetes mellitus: post-ARI treatment ($N = 12$)	1,056 \pm 530 575 \pm 335	C vs. D: $p < 0.001$
			Nerve cross-sectional area, mm² Non-insulin-dependent diabetes mellitus Non-diabetic healthy controls	2.8 \pm 1.8 3.3 \pm 1.5	N.S.
Other correlations:					
T ₁ relaxometry and MNCV				$r = -0.426, p < 0.001$	
T ₁ relaxometry and CV _{R-R}				$r = -0.295, p < 0.001$	
T ₁ relaxometry and FPG				$r = 0.350, p < 0.001$	
T ₁ relaxometry and HbA1c				$r = 0.337, p < 0.001$	

(Continued)

TABLE 2 | Continued

References	Magnetic field strength (T)	Nerve/Segment	Results		
			Measurement (spatial resolution)	Mean ± standard error (* indicates that values have been converted from the original standard deviation to standard error)	P-value
Pham et al. (2011)	3	Sciatic nerve	T₂-weighted MRI (0.25 × 0.52 × 5.0 mm³)		
		Tibial nerve	Number of patients with observable lesions		
		Common peroneal nerve (above knee)	T2DM with DPN	3/10	No statistical comparison
			T1DM with DPN	1/2	
			T2DM without DPN	0/10	
			T1DM without DPN	0/10	
			Non-diabetic healthy controls	0/10	
			Mean contrast ratio between nerve and adjacent muscle	4.2 ± 0.9	
			A: Diabetic (T1DM/T2DM) with DPN and observable lesions as above (N = 4)	2.1 ± 0.3	A vs. C: p = 0.004
			B: Diabetic control subjects without DPN (N = 15)	1.9 ± 0.2	
			C: Non-diabetic healthy controls (N = 10)		
Pham et al. (2015)	3	Full length of sciatic/tibial/common peroneal (nerve root to ankle)	T₂-weighted MRI (0.4 × 0.3 × 3.5 mm³)		
			Number of proximal lesions		
			A: DM with severe DPN	57 ± 18.4	A vs. D: p < 0.0022 B vs. D: p < 0.0005 C vs. D: N.S E vs.
			B: DM with mild-moderate DPN	35 ± 4.0	
			C: DM without DPN	21 ± 5.5	
			D: Non-diabetic healthy controls	18 ± 3.6	
			Number of distal lesions		
			E: DM with severe DPN	22 ± 8.1	E: p < 0.0174
			F: DM with mild-moderate DPN	12 ± 1.8	F vs. H: N.S
			G: DM without DPN	8 ± 2.9	G vs. H: N.S.
			H: Non-diabetic healthy controls	8 ± 1.4	
			Average common peroneal vol per slice (mm³)[†]		
			I: DM with severe DPN	29.2 ± 3.0	F = 5.61 _(3,71) , p = 0.001 No pairwise comparisons given
			J: DM with mild-moderate DPN	24.6 ± 1.4	
			K: DM without DPN	23.6 ± 1.2	
			L: Non-diabetic healthy controls	23.5 ± 1.1	
			Average tibial vol per slice (mm³)[†]		
I: DM with severe DPN J: DM with mild-moderate DPN	74.4 ± 6.0	F = 5.61 _(3,71) , p = 0.001 No pairwise comparisons given			
K: DM without DPN	62.5 ± 2.7				
L: Non-diabetic healthy controls	60.4 ± 3.3				
	52.8 ± 1.4				

(Continued)

TABLE 2 | Continued

References	Magnetic field strength (T)	Nerve/Segment	Results			
			Measurement (spatial resolution)	Mean \pm standard error (* indicates that values have been converted from the original standard deviation to standard error)	P-value	
Vaeggemose et al. (2017a)	3	Sciatic nerve (thigh) Tibial nerve (calf)	Diffusion tensor imaging (1.36 x 1.36 x 3.0 mm³)			
			Fractional anisotropy (FA)			
			A: T1DM with DPN	0.37 \pm 0.02*	0.31 \pm 0.02*	Sciatic A vs. B: $p < 0.01$ A vs. C: $p < 0.01$ D vs. E: $p = 0.03$ D vs. F: $p < 0.01$ Others: N.S.
			B: T1DM without DPN	0.47 \pm 0.03*	0.41 \pm 0.02*	
			C: Non-diabetic healthy controls	0.49 \pm 0.01*	0.43 \pm 0.03*	
			Apparent diffusion coefficient (ADC; $\times 10^3 \text{mm}^2/\text{s}$)			
			D: T1DM with DPN	1.69 \pm 0.08*	1.87 \pm 0.14*	Tibial A vs. B: $p < 0.01$ A vs. C: $p < 0.01$ Others N.S.
			E: T1DM without DPN	1.50 \pm 0.02*	1.59 \pm 0.06*	
			F: Non-diabetic healthy controls	1.42 \pm 0.04*	1.57 \pm 0.08*	
			Multi-echo turbo spin echo sequence (0.3 x 0.3 x 3.0 mm)			
			T_2 relaxometry (ms)			
			G: T1DM with DPN	86 \pm 5.1*	65 \pm 4.7*	All comparisons N.S.
			H: T1DM without DPN	86 \pm 3.8*	63 \pm 3.2*	
			I: Non-diabetic healthy controls	79 \pm 3.2*	58 \pm 3.8*	
			Proton density			
			J: T1DM with DPN	314 \pm 24.3*	429 \pm 39.8*	All comparisons N.S.
			K: T1DM without DPN	346 \pm 18.0*	512 \pm 35.4*	
L: Non-diabetic healthy controls	302 \pm 16.8*	492 \pm 26.6*				
<u>Nerve cross-sectional area (m²)</u>						
M: T1DM with DPN	29 \pm 2.2*	8 \pm 0.9*	All comparisons N.S.			
N: T1DM without DPN	29 \pm 2.8*	6 \pm 0.6*				
O: Non-diabetic healthy controls	26 \pm 1.6*	7 \pm 0.6*				

(Continued)

TABLE 2 | Continued

References	Magnetic field strength (T)	Nerve/Segment	Results				
			Measurement (spatial resolution)	Mean ± standard error (* indicates that values have been converted from the original standard deviation to standard error)			P-value
Fellisaz et al. (2017)	3	Tibial nerve (ankle)	IDEAL (Dixon) sequence (0.117 × 0.143 × 2.0 mm³)	Mod-sev DPN (A)	Mild DPN (B)	Control (C)	<u>NV/FV/FNR</u>
			Nerve volumes (mm ³) -NV	383.0 ± 30.6	326.7 ± 48.4	286.8 ± 18.0	A vs. C: <i>p</i> < 0.03
			Fascicles volume (mm ³) -FV	251.4 ± 20.3	218.7 ± 29.7	198.4 ± 12.8	CSA
			Fascicles to nerve ratio -FNR	0.659 ± 0.014	0.677 ± 0.018	0.699 ± 0.11	A vs. C <i>p</i> < 0.01
			Cross-sectional areas (mm ²) -CSA	12.97 ± 0.91	12.62 ± 1.27	10.22 ± 0.45	B vs. C: <i>p</i> < 0.04
Vaeggemose et al. (2017b)	3	Sciatic nerve (thigh) Tibial (calf) 1	Diffusion tensor imaging (1.36 × 1.36 × 3.0 mm³)	Sciatic		Tibial	
			Fractional anisotropy (FA)				
			A: T1DM with severe DPN (11)	0.38 ± 0.01*	0.31 ± 0.02*		A vs. C and D: <i>p</i> < 0.01
			B: T1DM with mild-moderate DPN (13)	0.41 ± 0.02*	0.34 ± 0.02*		B vs. C and D: <i>p</i> < 0.01
			C: T1DM without DPN (25)	0.47 ± 0.01*	0.41 ± 0.01*		E vs. G and H: <i>p</i> < 0.05
			D: Non-diabetic healthy controls (30)	0.48 ± 0.01*	0.42 ± 0.01*		F vs. H: <i>p</i> < 0.05
			Apparent diffusion coefficient (ADC; × 10 ³ mm ² /s)				<u>Tibial</u>
			E: T1DM with severe DPN	1.62 ± 0.05*	1.78 ± 0.06*		A vs. C and D: <i>p</i> < 0.01
			F: T1DM with mild-moderate DPN	1.62 ± 0.07*	1.74 ± 0.12*		B vs. C and D: <i>p</i> < 0.01
			G: T1DM without DPN	1.52 ± 0.02*	1.59 ± 0.04*		E vs. G and H: <i>p</i> < 0.01
			H: Non-diabetic healthy controls	1.47 ± 0.03*	1.52 ± 0.03*		F vs. H: <i>p</i> < 0.05
			Multi-echo turbo spin echo sequence (0.3 × 0.3 × 3.0 mm³)				
			Proton density				
			I: T1DM with severe DPN	343 ± 23.2*	484 ± 26.2*		All comparisons N.S.
			J: T1DM with mild-moderate DPN	413 ± 34.4*	499 ± 41.3*		
			K: T1DM without DPN	403 ± 14.6*	570 ± 23.0*		
			L: Non-diabetic healthy controls	381 ± 14.6*	545 ± 20.4*		
			<i>T</i> ₂ relaxometry (ms)				
			M: T1DM with severe DPN	83 ± 2.1*	64 ± 1.8*		All comparisons N.S.
			N: T1DM with mild-moderate DPN	82 ± 4.4*	63 ± 3.6*		
O: T1DM without DPN	83 ± 1.8*	62 ± 1.8*					
P: Non-diabetic healthy controls	79 ± 1.5*	61 ± 1.8*					
Nerve cross-sectional area (mm ²)							
Q: T1DM with severe DPN	28 ± 2.4*	8 ± 0.9*		<u>Sciatic</u>			
R: T1DM with mild-moderate DPN	26 ± 1.4*	9 ± 1.1*		T vs. Q, R and S: <i>p</i> < 0.01			
S: T1DM without DPN	27 ± 1.6*	6 ± 1.4*		<u>Tibial</u>			
T: Non-diabetic healthy controls	21 ± 1.1*	7 ± 0.4*		S vs. R: <i>p</i> < 0.01			
				T vs. R: <i>p</i> < 0.05			

(Continued)

TABLE 2 | Continued

References	Magnetic field strength (T)	Nerve/Segment	Results			
			Measurement (spatial resolution)	Mean ± standard error (* indicates that values have been converted from the original standard deviation to standard error)	P-value	
Wang et al. (2018)	3	Tibial nerve (ankle)	T₂ relaxometry, ms (0.4 × 0.4 × 2.0 mm³) A: DM with DPN (22) B: DM without DPN (20) C: Non-diabetic healthy control Other Correlations: T ₂ relaxometry vs. HbA1c	55.1 ± 4.1 48.9 ± 3.1 45.6 ± 1.9	All comparisons $p < 0.001$ $r = 0.176$, N.S.	
Jende et al. (2018)	3	Sciatic nerve (thigh)	T₂-weighted imaging (0.5 × 0.3 × 4.0 mm³) A: All neuropathy (T1DM and T2DM) B: All no neuropathy (T1DM and T2DM) C: T1DM with neuropathy D: T2DM with neuropathy E: T1DM without neuropathy F: T2DM without neuropathy Other Correlations: T ₂ -weighted hyperintense lesions vs. tibial compound motor action potential T ₂ -weighted hyperintense lesions vs. peroneal nerve conduction T ₂ -weighted hyperintense lesions vs. NDS T ₂ -weighted hyperintense lesions vs. HbA1c T ₂ -weighted hypointense lesions vs. NDS T ₂ -weighted hypointense lesions vs. serum triglycerides T ₂ -weighted hypointense lesions vs. HDL	T₂-weighted hypointensities (mm³) 23.41 ± 2.69 11.43 ± 1.74 19.74 ± 5.57 27.54 ± 3.53 7.52 ± 0.97 16.83 ± 3.16	T₂-weighted hyperintensities (%) 13.93 ± 0.01 3.18 ± 0.004 19.67 ± 4.13 12.49 ± 1.23 2.80 ± 0.50 2.68 ± 0.43	<u>Hypointensities</u> A vs. B: $p = 0.002$ C vs. D: $p = 0.046$ E vs. F: $p = 0.027$ <u>Hyperintensities</u> A vs. B: $p < 0.0001$ C vs. D: $p = 0.027$ Others N.S. $r = -0.58$, $p < 0.0001$ $r = 0.51$, $p = 0.00002$ $r = 0.52$, $p < 0.0001$ $r = 0.23$, $p = 0.014$ $r = 0.28$, $p = 0.002$ $r = 0.34$, $p = 0.0003$ $r = -0.48$, $p < 0.0001$
Jende et al. (2019)	3	Tibial nerve (thigh)	T₂-weighted MRI (0.5 × 0.3 × 4.0 mm³) Hypointense lipid equivalent lesion (LEL) Maximum length of a lesion, mm Mean cross-sectional area of the tibial nerve (mm ³) [†] [†] Divide by slice thickness 4 mm to get average cross sectional area (mm ²) Other Correlations: Total serum cholesterol vs. lipid equivalent lesion (LEL) load LDL cholesterol vs. LEL load Total serum cholesterol vs. maximum lesion length (MLL) LDL cholesterol vs. MLL Total serum cholesterol vs. mean cross-sectional area (MCA) LDL cholesterol vs. MCA	T2DM with DPN 1.67 ± 2.03 63.47 ± 2.44 148.20 ± 5.24	T2DM without DPN 10.03 ± 0.87 50.07 ± 3.26 122.20 ± 3.82	$p < 0.001$ $p = 0.001$ $p < 0.001$ $r = -0.41$, $p < 0.001$ $r = -0.33$, $p = 0.003$ $r = -0.44$, $p < 0.001$ $r = 0.38$, $p = 0.001$ $r = -0.38$, $p < 0.001$ $r = 0.33$, $p = 0.002$

(Continued)

TABLE 2 | Continued

References	Magnetic field strength (T)	Nerve/Segment	Results				
			Measurement (spatial resolution)	Mean \pm standard error (* indicates that values have been converted from the original standard deviation to standard error)	P-value		
Jende et al. (2020a)	3	Tibial nerve (thigh)	T₂-weighted MRI (0.3 × 0.3 × 4.0 mm³)				
			<u>Lesions as % of nerve volume</u>	15.15 \pm 1.61	A vs. B: $p = 0.3$		
			A: Painful DPN	10.35 \pm 1.66	A vs. C: $p < 0.01$		
			B: Non-painful DPN	8.26 \pm 1.72	B vs. C: N.S.		
			C: Diabetes without DPN				
			<u>Maximum Length of a Lesion</u>				
			D: Painful DPN	63.62 mm \pm 3.01	D vs. E: $p = 0.0$		
			E: Non-painful DPN	51.35 mm \pm 4.58	3 D vs. F: $p < 0.01$		
			F: Diabetes without DPN	41.20 mm \pm 4.75	E vs. F: $p = 0.048$		
			<u>Cross-sectional area (mm²)[†]</u>				
			G: Painful DPN	136.4 mm ² \pm 4.58	All comparisons N.S.		
			H: Non-painful DPN	144.2 mm ² \pm 5.80			
			I: Diabetes without DPN	134.9 mm ² \pm 6.07			
[†] Divide by slice thickness 4 mm to get average cross sectional area (mm ²)							
Other Correlations:							
Hyperintense nerve lesion load vs. NDS				$r = 0.37, p < 0.05$			
Hyperintense nerve lesion load vs. NSS				$r = 0.41, p < 0.05$			
Hyperintense nerve lesion load vs. tibial nerve conduction velocity				$r = -0.23, p < 0.05$			
Mean nerve cross-sectional area vs. SC level				$r = -0.32, p < 0.05$			
Mean nerve cross-sectional area vs. LDL-C level				$r = -0.31, p < 0.05$			
Groener et al. (2020)	3	Sciatic nerve bifurcation	T₂-weighted MRI (0.5 × 0.3 × 4.0 mm³)				
			T ₂ -weighted hyperintense lesions/healthy nerve (%)	8.07 (1–49)	All comparisons N.S.		
			T2DM with DPN	6.13 (3–14)			
			T2DM without DPN	4.75 (2–12)			
			Non-diabetic healthy control				
			Other correlations/regressions:				
			T ₂ -weighted hyperintense lesions load vs. sex				$R^2 = 0.674, p = 0.31$
			T ₂ -weighted hyperintense lesions load vs. tibial conduction velocity				$r = -0.362, p = 0.005$
			hyperintense lesions load vs. tibial nerve amplitude				$r = -0.276, p = 0.035$
			T ₂ -weighted hyperintense lesions load vs. QST measure of mechanical detection				$r = -0.312, p = 0.007$
T ₂ -weighted hyperintense lesions load vs. QST measure of mechanical pain				$r = 0.246, p = 0.036$			
T ₂ -weighted hyperintense lesions load vs. QST measure of thermal detection / thermal pain				N.S.			

(Continued)

TABLE 2 | Continued

References	Magnetic field strength (T)	Nerve/Segment	Results			
			Measurement (spatial resolution)	Mean \pm standard error (* indicates that values have been converted from the original standard deviation to standard error)	P-value	
Edward et al. (2020)	1.5	Median nerve (forearm)	Diffusion tensor imaging (resolution not specified)			
			Fractional anisotropy (FA)			
			T2DM with DPN	0.49 \pm 0.05	0.42 \pm 0.04	Proximal: N.S Distal: $p = 0.016$
			Non-diabetic healthy controls	0.51 \pm 0.10	0.46 \pm 0.05	
			Apparent diffusion coefficient (ADC; $\times 10^3 \text{mm}^2/\text{s}$) T2DM with DPN			
			Non-diabetic healthy controls	1.196 \pm 0.199	1.379 \pm 0.209	Proximal: $p = 0.027$ Distal: $p < 0.001$
				1.070 \pm 0.112	1.149 \pm 0.064	
			Other correlations:			
			Distal median FA vs. distal radial conduction velocity			$r = 0.299, p = 0.02$
			Distal median FA vs. sensory amplitude			$r = 0.257, p = 0.048$
Median FA vs. proximal radial conduction velocity			$r = -0.267, p = 0.039$			
Distal median ADC vs. sensory amplitude			$r = -0.278, p = 0.032$			
Distal median FA vs. neuropathy disability score			$r = -0.518, p = 0.003$			
Distal median ADC vs. neuropathy disability score			$r = 0.482, p = 0.007$			
Jende et al. (2020b)	3	Tibial nerve (thigh)	Diffusion tensor imaging (1.3 \times 1.3 \times 4.0 mm³)			
			Fractional anisotropy (FA)			ANOVA $p < 0.001$ (no pairwise comparisons)
			T2DM with DPN	0.473 \pm 0.056		
			T2DM without DPN	0.531 \pm 0.038		
			Non-diabetic healthy controls	0.549 \pm 0.052		
			Other correlations:			
			Tibial FA vs. neuropathy symptoms score (NSS)			$r = -0.36, p = 0.009$
			Tibial FA vs. neuropathy disability score (NDS)			$r = -0.52, p < 0.001$
			Tibial FA vs. tibial nerve conduction velocity*			$r = 0.37, p = 0.011$
			Tibial FA vs. tibial amplitudes [†]			$r = 0.57, p < 0.001$
Tibial FA vs. tibial distal motor latencies*			$r = -0.32, p = 0.029$			
Tibial FA vs. high-sensitivity Troponin T (partial correlation accounting for age and cystatin C levels)						
o All T2DM subjects			$r = -0.31, p = 0.030$			
o T2DM with neuropathy [†]			$r = -0.61, p = 0.001$			
Similar data shown for Tibial FA vs. common peroneal electrophysiology (data not shown here)						

(Continued)

TABLE 2 | Continued

References	Magnetic field strength (T)	Nerve/Segment	Results			
			Measurement (spatial resolution)	Mean ± standard error (* indicates that values have been converted from the original standard deviation to standard error)	P-value	
Vaeggemose et al. (2020)	3	Sciatic nerve (thigh) Tibial nerve (calf)	Multi-echo turbo spin echo sequence (0.3 × 0.3 × 3.0 mm³)	Sciatic	Tibial	
			<u>T₂ relaxometry time (ms)</u>			
			A: T2DM with DPN	90 ± 5.7*	78 ± 7.6*	Tibial ANOVA <i>p</i> = 0.02 Sciatic ANOVA N.S.
			B: T2DM without DPN	84 ± 2.5*	62 ± 3.2	
			C: Non-diabetic healthy controls	81 ± 1.8*	61 ± 2.7*	
			<u>Proton density</u>			All comparisons N.S.
			D: T2DM with DPN	432 ± 25.9*	485 ± 37.3*	
			E: T2DM without DPN	380 ± 10.8*	548 ± 44.6*	
			F: Non-diabetic healthy controls	370 ± 18.3*	517 ± 24.8*	
			Diffusion tensor imaging (1.36 × 1.36 × 3.0 mm³)			
			<u>Fractional anisotropy (FA)</u>			
			G: T2DM with DPN	− 0.37 ± 0.02*	− 0.30 ± 0.02*	Sciatic and tibial: G vs. H <i>p</i> < 0.001
			H: T2DM without DPN	0.51 ± 0.02*	− 0.45 ± 0.02*	
			I: Non-diabetic healthy controls	− 0.48 ± 0.01*	− 0.42 ± 0.01*	H vs. I <i>p</i> < 0.01
			<u>Mean diffusivity (MD; × 10³ mm²/s)</u>			
			J: T2DM with DPN	− 1.75 ± 0.07	− 1.76 ± 0.08*	Sciatic and tibial: J vs. K <i>p</i> < 0.001
			K: T2DM without DPN	1.47 ± 0.03*	− 1.48 ± 0.06*	
			L: Non-diabetic healthy controls	− 1.58 ± 0.04*	− 1.56 ± 0.04*	J vs. L <i>p</i> < 0.05
			<u>Axial diffusivity (AD; × 10³ mm²/s)</u>			
			M: T2DM with DPN	− 2.42 ± 0.06*	− 2.32 ± 0.07*	Sciatic and tibial: M vs. O <i>p</i> < 0.01
N: T2DM without DPN	− 2.31 ± 0.04*	− 2.19 ± 0.06*				
O: Non-diabetic healthy controls	− 2.21 ± 0.04*	− 2.11 ± 0.03*				
<u>Radial diffusivity (RD; × 10³ mm²/s)</u>						
P: T2DM with DPN	1.41 ± 0.07*	− 1.48 ± 0.09*	Sciatic and tibial: P vs. Q <i>p</i> < 0.001			
Q: T2DM without DPN	1.05 ± 0.03*	− 1.13 ± 0.07*				
R: Non-diabetic healthy controls	1.27 ± 0.04*	− 1.29 ± 0.04*	Q vs. R <i>p</i> < 0.05			
			Tibial only P vs. R: <i>p</i> = 0.01			

For ease of comparison we have also converted any data expressed as standard deviation to standard error, by dividing the standard deviation by square root of *N*. These data are marked with an * so that readers can refer back to original data if required.

content, despite clearly worsening nerve conduction studies. This led the authors to hypothesise a bell-shaped distribution, with early diabetic neuropathy being associated with an oedematous phase, which “burns out” as the disease progresses.

These studies used a mixed population of T1DM and T2DM (most of which are insulin-dependent), but the proportion of T1DM and T2DM in each group is not clear, which limits interpretation given differences in MRI signature between T1DM and T2DM shown in some later studies. These early studies also did not control for pertinent confounding variables, and demonstrated statistically significant group differences in age, gender, disease duration and cardiovascular risk factors.

It should be noted that the increased water content demonstrated here was reversed with the use of an aldose reductase inhibitor (ARI) (Griffey et al., 1988). As discussed in the introduction, despite the biochemical rationale for why these agents might be effective in DPN, meta-analyses have failed to show any clinically meaningful benefit (Chalk et al., 2007). Therefore, whilst it is possible that use of these agents would have an effect on fluid compartments of nerve tissue, and therefore measures of water content on MRI, it does draw into question the clinical relevance of this imaging biomarker given the lack of clinical efficacy of ARIs.

More recently, however, Felisaz et al. (2017) have used a 3-point Dixon (IDEAL) sequence to obtain ultra-high resolution images of the tibial nerve at the ankle, with the fat-only images best visualising the interfascicular epineurium, and the water-only images (and T_1 -weighted turbo spin echo, TSE) giving the best contrast of nerve fascicles. This approach allowed imaging at a very high resolution ($0.11 \times 0.17 \times 2 \text{ mm}^3$), and segmentation of the nerve fascicles from the surrounding epineurium. The authors were able to demonstrate increased nerve volume and fascicle volume, but also a decreased nerve-to-fascicle ratio in DPN compared with healthy controls, suggestive of expansion of the epineurial connective tissue as well as fascicular enlargement in these patients.

T_1 Relaxometry

Shibata et al. (1998) studied 92 patients with non-insulin-dependent diabetes mellitus compared with 19 non-diabetic healthy controls using T_1 relaxometry (i.e., direct measurement of the longitudinal relaxation time T_1). They found higher T_1 in DPN ($831 \pm 495 \text{ ms}$) compared with healthy controls ($472 \pm 258 \text{ ms}$), which the authors proposed was due to nerve oedema. The authors also reported significant positive correlations for T_1 with glycaemic measures and heart rate variability (as a measure of autonomic function), and negative correlations with nerve conduction. Furthermore, they found that in a smaller group of 16 patients, T_1 was reduced by nearly 50% after treatment with Epalrestat, an aldose reductase inhibitor ($1,056 \pm 530 \text{ ms}$ pre-treatment; $573 \pm 335 \text{ ms}$ post-treatment), although the duration of treatment is not clear from the manuscript. Whilst measures of nerve conduction were carried out as part of this study, it is not clear from the methods how many of the patients with diabetes had a clinical diagnosis of DPN, and so it is not clear to what extent these changes represent neuropathic changes per se, or changes related to diabetes and confounding variables such as

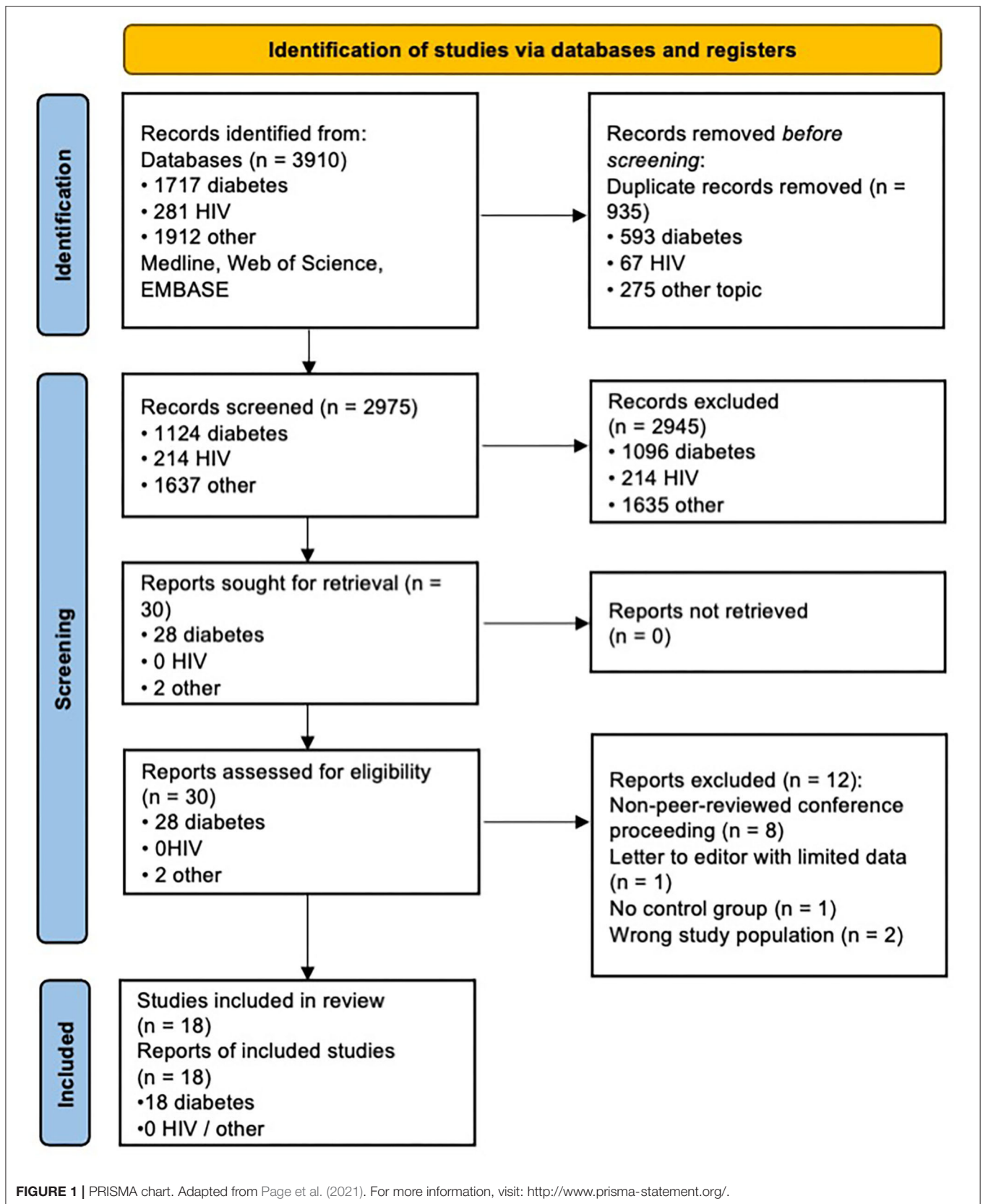
BMI. Also as was discussed above, the changes shown in this study were dramatically improved with ARI treatment, which is not thought to be effective for treating DPN.

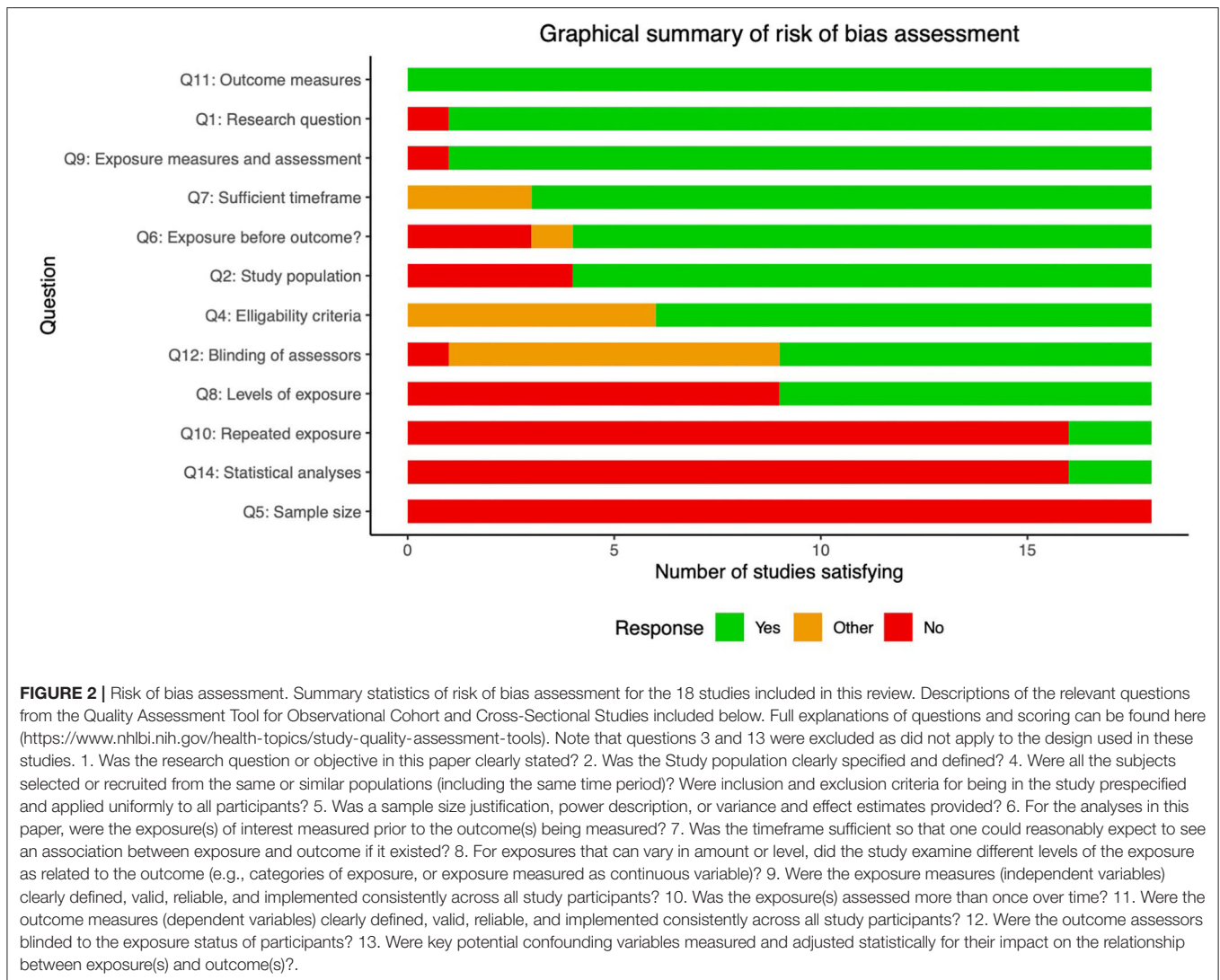
As described above, Felisaz et al. (2017) also used a T_1 -weighted TSE sequence in addition to Dixon imaging to provide ultra-high resolution at 3T of $0.11 \times 0.17 \text{ mm}^2$ in plane with 2 mm slice thickness, allowing separation of the nerve into fascicular and epineurial components, with findings discussed in the previous section.

T_2 -Weighted and Proton Density-Weighted MRI

T_2 -weighted imaging-based and T_2 relaxometry are the most commonly used methods for nerve imaging in the literature to date. This has been reported in a number of different ways, the most common using T_2 -weighted voxel intensities, with normalisation of signal intensity to some internal (adjacent muscle) or external (healthy control nerve signal intensity) control, and then using arbitrary cut offs to define “hyperintense” or “hypointense” lesions. Pham et al. (2011) was the earliest study to demonstrate proximal T_2 lesions in DPN, initially simply imaging patients with T1DM and T2DM with and without DPN, and had expert neuroradiologists review the T_2 -weighted images and code them as having visually apparent lesions or not. They reported that 3/10 of the patients with T2DM and DPN, and 1/2 of the patients with T1DM and DPN had observable lesions, but none of the diabetic patients without DPN (15) or healthy controls (25). They then calculated contrast ratios of T_2 -weighted signal intensity in nerve vs. adjacent muscle and showed increased signal intensity in those patients with visually observable lesions, compared with patients with diabetes but no DPN, or healthy controls. The latter is somewhat of an odd statistical comparison, as these subjects have by definition been chosen as having visually higher T_2 -weighted signal in segments of the nerve compared with their “control group” and it is not clear how this finding relates to the overall population of patients with DPN as assessed by clinical (rather than radiological) criteria. However, the same group subsequently published a paper with more objective metrics, where they normalised T_2 -weighted voxel intensity to age- and sex-matched healthy controls and used a cut off of $>1.5x$ above the average normalised signal intensity to define (hyperintense) lesions. They show both proximally and distally increasing lesion burden from diabetes with no DPN (proximal 21 ± 5.5 ; distal 8 ± 2.9), to mild-moderate DPN (proximal 35 ± 4.0 ; distal 12 ± 1.8), to severe DPN (proximal 57 ± 18.4 ; distal 22 ± 8.1), with significantly more lesions apparent proximally compared with distally. However, the latter statistic does not seem to have been adjusted for nerve cross-sectional area, which would be expected to decrease with more distal location.

These studies only consider hyperintense lesions, but lesions with low T_2 -weighted signal intensity are also possible. Jende et al. (2018) took a large cohort of T1DM and T2DM with (64) and without DPN (36). They manually segmented the sciatic nerve in the thigh and defined “hyperintense” lesions as those with signal intensity 25% above adjacent muscle tissue,





and “hypointense” as 25% below muscle tissue. Patients with DPN had significant more hyperintense and hypointense lesions compared with those without DPN, and when splitting the DPN group according to diabetes type, there were significant more hyperintense lesions in T1DM and more hypointense lesions in T2DM. Given that hyperintense lesion load correlated with HbA1c, whereas hypointense lesion load correlated with triglycerides and HDL cholesterol, the authors propose that hyperintense lesions are due to complications of hyperglycaemia (such as production of advanced glycation end products, AGEPs), whereas hypointense lesions reflect nerve lipid deposition. Note that the T_2 sequence employed here uses fat suppression, so areas of nerve with lipid deposition would be suppressed causing hypointensities. The fact that areas of low T_2 signal correspond to high T_1 signal is also supportive of the hypothesis that lipid deposition is the cause of T_2 hypointensities in this study. Increased hyperintense and hypointense lesions in DPN compared with diabetic controls have now been replicated in a number of follow up studies (Jende et al., 2019, 2020b; Groener

et al., 2020). These data also suggest that taking an average signal intensity as a measure of nerve pathology is fundamentally flawed if there are varying contributions of lesions with high or low signal, as a nerve with equal contributions of both may average to a normal range signal intensity.

Numerous associations have been made between lesions on T_2 -weighted imaging and other important outcomes in DPN, including electrophysiological measures (Jende et al., 2018, 2020b; Groener et al., 2020), NDS and NSS scores (Jende et al., 2018, 2020b), quantitative sensory testing (Groener et al., 2020) and glycaemic/lipid measures (Jende et al., 2018, 2019). Jende et al. (2020b) also show that maximum lesion length and lesion load is significantly higher for those with painful vs. painless DPN, and nerve cross-sectional area is correspondingly smaller, suggesting the possibility nerve MRI may be developed as a biomarker for neuropathic pain. Jende et al. (2019) also followed up their finding of an association of T_2 -weighted hypointense lesions with dyslipidaemia in a follow up study focusing on T2DM only. Somewhat in contrast to their previous findings in

a mixed sample of patients with diabetes, they demonstrated a negative correlation between hypointense lesion load and total ($r = -0.41$), HDL ($r = -0.30$) and LDL cholesterol ($r = -0.33$), suggesting that excessive lowering of cholesterol with statin use might actually promote DPN. This is in line with evidence that statins may limit the supply of cholesterol required for nerve repair (Gaist et al., 2002; Novak et al., 2015) and demonstrates the value of MRI biomarkers in informing pathogenesis. However, caution should be taken in interpreting this cross-sectional study, especially in light of the clear benefit of cholesterol lowering for macrovascular complications in diabetes (Hebert et al., 1997). Longitudinal and randomised control designs would be of benefit to better understand this relationship.

T_2 Relaxometry

Signal intensity in T_2 -weighted images is largely determined by the transverse relaxation time (T_2) of the tissue and its proton density, and some studies have calculated these more direct measures to study pathology in DPN. Vaeggemose et al. (2017a) calculated T_2 in patients with T1DM, and whilst they did not report significant group differences, there was a trend to longer T_2 for DPN in the sciatic nerve (DPN 86 ± 5.1 ms; control 79 ± 3.2 ms) and distal tibial nerve (DPN 65 ± 4.7 ms; control 58 ± 3.8 ms). The same group have reported this metric in two follow up papers (Vaeggemose et al., 2017b, 2020), and most recently Vaeggemose et al. (2017b) reported statistically longer T_2 in the distal tibial nerve for DPN (78 ± 7.6 ms) compared with diabetes without DPN (62 ± 3.2 ms) and healthy controls (61 ± 2.8 ms), with a non-significant trend in the same direction for the sciatic nerve. It should be noted that the sample sizes in the studies by Vaeggemose et al. are relatively modest with around 10 subjects per group. Wang et al. (2018) used a similar technique in a mixed group of T1DM and T2DM with a larger sample size and showed progressively longer T_2 in healthy controls (45.6 ± 1.9 ms) compared to diabetic patients without DPN (48.9 ± 3.1 ms) and those with DPN (55.1 ± 4.1 ms), with no relationship between T_2 and HbA1c. In contrast to these findings, Pham et al. (2015) used logistic regression to investigate whether there was a significant difference between patients with DPN of different severities and healthy controls and found a significant effect of proton density (severe DPN 360 ± 22.9 ; controls 288 ± 13.4), but no effect of T_2 relaxation. They also showed small but significant correlations between proton density and scores on the neuropathy disability score (NDS) and neuropathy symptom score (NSS). The authors propose that the findings discussed above relating to elevated signal in T_2 -weighted imaging actually relate to changes in proton density rather than T_2 itself, and that this suggests a change to the macromolecular environment through, for example, production of AGEs, rather than due to tissue oedema. However, this is not born out by other studies which have failed to show an effect of proton density (Vaeggemose et al., 2017a,b; Vaeggemose et al., 2020), although the smaller sample size of these studies should be taken into consideration.

Diffusion Tensor Imaging

Diffusion tensor imaging provides various metrics that can reflect aspects of nerve integrity, including fractional anisotropy

(FA), apparent diffusion coefficient/mean diffusivity (ADC/MD), radial diffusivity (RD) and axial diffusivity (AD). FA is a measure of the directionality of proton diffusion, with 0 representing isotropic diffusion and values closer to 1 indicating a strongly preferred direction of diffusion. Due to water diffusing preferentially along the axis of axons, nerves demonstrate higher FA values, and a reduction indicates loss of nerve structural integrity. Studies have consistently shown a reduction in FA in patients with DPN compared with both healthy controls and diabetic patients without DPN, for the sciatic nerve (Vaeggemose et al., 2017a,b; Vaeggemose et al., 2020), tibial nerve (Vaeggemose et al., 2017a,b; Wu et al., 2017; Vaeggemose et al., 2020; Jende et al., 2020a), and common peroneal nerve (Wu et al., 2017), which has been demonstrated at the thigh and ankle level. Edward et al. (2020) also demonstrated reduced FA in the distal median nerve in the wrist. ADC or MD is a measure of the average diffusivity of protons across all directions, with higher values in nerves suggesting some degree of axonal disruption (Tievsky et al., 1999). In line with the decreased FA values, the above studies also demonstrate increased MD values in each of the nerves (Vaeggemose et al., 2017a,b, 2020; Wu et al., 2017; Edward et al., 2020; Jende et al., 2020a). Importantly there seems to be clear evidence of increased MD and decreased FA in DPN compared with diabetes without DPN as well as healthy controls (Vaeggemose et al., 2017a,b; Jende et al., 2020a), and worsening of values in line with severity of DPN (Vaeggemose et al., 2017b). Therefore, these changes seem to reflect neuropathic changes per se, rather than changes related to diabetes.

Other important metrics can also be extracted from the diffusion tensor. AD represents the maximum diffusivity of protons along any axis (i.e., along the nerve axon), whereas RD is a measure of diffusivity perpendicular to this. Early work suggested that AD is sensitive to axonal loss and RD to demyelination, but it is now thought to be more complex than this, with RD also affected by demyelination, axon loss or reduced axonal density. One study to date has investigated these parameters in DPN, showing generally higher AD, RD and MD in DPN compared with diabetes without DPN, and higher for diabetes without DPN compared with healthy controls (Vaeggemose et al., 2020). However, the authors were less consistently able to show a significant difference between DPN and healthy controls, in part due to the increased variance in these measures in the DPN group and may be a reflection of the relatively small sample size in the diabetes groups (10 per group).

Nerve Cross-Sectional Area

Cross sectional area studied has most commonly been studied in the sciatic nerve and its branches at the level of the thigh. Note that some studies report true cross-sectional areas (Shibata et al., 1998; Vaeggemose et al., 2017a,b, 2020), whilst others report slice volume (cross-sectional area x slice thickness) (Pham et al., 2015; Jende et al., 2019, 2020b). The slice volumes discussed below have been converted to areas by dividing by slice thickness in order to allow for comparison between studies.

Two studies by Vaeggemose et al. (2017a,b) reported CSA for the sciatic nerve (encompassing both tibial and peroneal components) at the level of the distal thigh. In an earlier

study (Vaeggemose et al., 2017a) there was a higher CSA for T1DM with ($29 \pm 2.2 \text{ mm}^2$) and without DPN ($29 \pm 2.8 \text{ mm}^2$) compared with non-diabetic healthy controls ($26 \pm 1.6 \text{ mm}^2$), but this was not statistically significant. However, the sample size was only 10 per group in this study so may not have been powered for this comparison. The authors repeated this metric in a larger sample (Vaeggemose et al., 2017b) and showed statistically higher CSA in all diabetic patients ($28 \pm 2.4 \text{ mm}^2$ for severe DPN, $26 \pm 1.4 \text{ mm}^2$ in mild DPN, and $27 \pm 1.6 \text{ mm}^2$ in T1DM without DPN) compared with healthy controls ($21 \pm 1.1 \text{ mm}^2$). Jende et al. (2019) also scanned the sciatic nerve at the distal thigh, but restricted analysis to the tibial component. They did not include a healthy control group but showed an increased CSA for patients with T2DM with DPN ($37.1 \pm 1.3 \text{ mm}^2$) compared with those without DPN ($30.6 \pm 0.9 \text{ mm}^2$). In a follow up study, the same group compared a mixed population of T1DM and T2DM with painful neuropathy ($34.1 \pm 1.1 \text{ mm}^2$), painless neuropathy ($36.1 \pm 1.5 \text{ mm}^2$) and no neuropathy ($33.7 \pm 1.51 \text{ mm}^2$), demonstrating no statistically significant group differences (Jende et al., 2020b). However, the authors did demonstrate a negative correlation between CSA and conduction velocities of the tibial and common peroneal nerves, suggesting a relationship between CSA and nerve function, but not painful symptoms.

Pham et al. (2015) scanned the tibial and peroneal nerves of both the thigh and lower leg, and report average cross-sectional areas across the whole length of the nerve in DPN. They showed a significant group difference with ANOVA for both the tibial and common peroneal nerves. Whilst they did not report pairwise comparisons, for the tibial nerve there seems to be a stepwise increase in CSA compared to healthy controls ($15.1 \pm 0.4 \text{ mm}^2$) for diabetes without DPN ($17.3 \pm 0.9 \text{ mm}^2$), mild-moderate DPN ($17.9 \pm 0.8 \text{ mm}^2$) and most prominently, severe DPN ($21.3 \pm 1.7 \text{ mm}^2$). However, for the common peroneal nerve there only seems to be an increase from healthy controls ($6.7 \pm 0.3 \text{ mm}^2$) for the severe DPN group ($8.3 \pm 0.9 \text{ mm}^2$).

Finally, of studies investigating the tibial nerve CSA in the lower leg, Vaeggemose et al. (2017b) showed a higher CSA for patients with moderate DPN ($9 \pm 1.1 \text{ mm}^2$) compared with both T1DM without DPN ($6 \pm 1.4 \text{ mm}^2$) and healthy controls ($7 \pm 0.4 \text{ mm}^2$), but this was not replicated in another study by the same group (Vaeggemose et al., 2017a). Felisaz et al. (2017) investigated distal tibial nerve structure in diabetic neuropathy using ultra-high resolution MRMRI and showed higher CSA in mild DPN ($12.6 \pm 1.3 \text{ mm}^2$) and moderate-severe DPN ($13.0 \pm 0.9 \text{ mm}^2$) compared with non-diabetic healthy controls ($10.2 \pm 0.5 \text{ mm}^2$). Interestingly, this study obtained sufficient resolution to segment out the fascicles from surrounding epineurium and found a decreased fascicle-to-nerve ratio, most noticeable for severe DPN, suggestive of some expansion of the interfascicular epineurium as well as enlargement of the fascicles themselves. Only one study has reported sural nerve CSA in diabetes (Griffey et al., 1988), and there was no significant difference between groups noted. However, this study was published over 20 years ago using a 1.5 T system, so was likely limited by available signal-to-noise ratio.

Taken together, there seems to be reasonable evidence that diabetes (type 1 and type 2) increases the cross-sectional area of nerves (whether or not neuropathy is present), but there is insufficient evidence to suggest that nerve CSA is higher in patients with DPN compared with diabetic patients without DPN, or that it tracks with severity of DPN or painful neuropathy. The values reported here for CSA of the lower extremity nerves are largely in line with the ultrasound literature with regards to healthy controls (Lee and Dauphinée, 2005; Cartwright et al., 2008; Seok et al., 2014), save for the Vaeggemose study which seem much lower (26 mm^2) than values reported for the sciatic nerve at the thigh in healthy individuals ($42\text{--}52 \text{ mm}^2$). The data are also broadly in line with the ultrasound literature on DPN which shows that nerves are larger in diabetes compared with non-diabetic nerves and are larger in those with less well-controlled disease, including in those with DPN (Riazi et al., 2012; Breiner et al., 2017).

DISCUSSION

There is increasing interest in using MRI as a non-invasive biomarker in various neuropathies, including DPN. In this review we use systematic search tools to summarise this emerging field, with discussing biomarkers using T_1 -weighted, T_2 -weighted, proton density-weighted, relaxometry and diffusion tensor imaging. We also highlight the lack of research in HIV neuropathy. We will now discuss caveats and challenges in this field, and potential for future developments.

Confounding Variables and Control Groups

Choosing which confounding variables to control for with peripheral nerve imaging is difficult, as there is scarcity of evidence for how MRI metrics change with age and other demographic factors for peripheral nerve imaging compared with more commonly used imaging modalities like brain imaging. However, one study from Bendszus et al. used MR neuropathy in 60 healthy volunteers to examine the relationship with various demographic variables. For nerve CSA they found a trend towards increasing size with age, which was more pronounced at the sciatic nerve in the thigh (Kronlage et al., 2019). This finding is in agreement with some previous ultrasonographic studies showing increasing size with age (Cartwright et al., 2008). They also found a positive correlation between cross-sectional area and weight, height and BMI (Kronlage et al., 2019). T_2 was not found to be associated with any demographic variable in this study, and proton density was strongly negatively correlated with weight and BMI. Proton density also had a negative correlation with age in the sciatic nerve at the thigh, possibly secondary to fatty infiltration.

In this study, gender was only moderately associated with nerve CSA, but this relationship disappeared when accounting for bodyweight. In a second study, the same group investigated demographic influences in diffusion tensor parameters (Kronlage et al., 2018), showing an age-related decrease in FA, caused

by a reduction in axial, and an increase in radial diffusivity. FA was also negatively correlated with height, weight and BMI, and there was no association with gender for any metric after accounting for bodyweight. Whilst these studies on normal controls do not seem to show evidence for an effect of gender, one MR neurography study in DPN showed that male sex was associated with higher T_2 -weighted lesion volume in subjects with diabetic neuropathy (Groener et al., 2020). Age has also been associated with changes in other MR parameters including magnetisation transfer ratio (Kollmer et al., 2018).

Finally, in studies comparing multiple diabetes groups (e.g., with or without DPN), disease duration is an important variable to consider, as whilst various MRI measures become deranged in diabetic neuropathy per se, some studies show a difference between healthy controls and patients with diabetes without clinically apparent neuropathy (Eaton et al., 1996; Pham et al., 2011; Wang et al., 2018; Vaeggemose et al., 2020). At present it is unclear whether these changes represent subclinical neuropathic changes—and studies demonstrating an association between MR values and nerve conduction in patients with diabetes but no DPN would support this hypothesis—or incidental changes in nerve water content related to diabetes that have no effect on nerve function. Given this uncertainty, controlling for disease duration between DPN and non-DPN groups of diabetic patients would be prudent.

On a related point, the choice of control group differs between studies in the literature. Some studies compare patients with DPN to healthy controls (Shibata et al., 1998; Felisaz et al., 2017; Wu et al., 2017; Vaeggemose et al., 2020), others compare DPN to diabetes without neuropathy (Jende et al., 2018, 2019, 2020b) and other studies have both control groups (Griffey et al., 1988; Eaton et al., 1996; Pham et al., 2011, 2015; Vaeggemose et al., 2017a,b, 2020; Wang et al., 2018; Edward et al., 2020; Groener et al., 2020; Jende et al., 2020b). Including both control groups would be preferable, as this allows to distinguish changes related to diabetes and those directly related to neuropathy. However, MRI studies are expensive and resource-intensive, and sample sizes can be around 30–40 per group in well-powered studies. Therefore, of the two potential control groups, patients with diabetes without neuropathy may be the preferable choice, as these will control for confounds related to the underlying diabetic pathology including cardiovascular risk factors.

Accounting for confounding variables can be achieved in a number of ways. Firstly, groups can be “matched” for pertinent variables, most commonly done for age and gender. Alternatively, a variable can be controlled for statistically by using multiple regression or partial correlation methods. It is worth remembering for the latter approach that adding additional independent variables into a model risks compromising statistical power. Therefore, improved accounting for confounding variables by group-matching will preserve power and require smaller sample sizes.

Sample Size and Power Calculations

Our risk of bias assessment has shown that sample size estimations and power calculations are consistently absent from studies in this field. This is likely linked to the small number of studies having been published on this subject, with only 18 studies meeting the criteria of this review to date, most of which have been published in the past 5 years. Therefore, much of the work thus far has been relatively exploratory, and it would have been difficult until recently to estimate effect sizes. Also, analysis approaches differ substantially between studies which may impact differentially on sample size requirements and experimental power. However, there are probably sufficient data now using T_2 -weighted MRI, DTI, and measures of nerve cross sectional area to be able to make more informed decisions regarding expected effect sizes in the future. For example, with the approach taken by Jende et al. in analysis T_2 -weighted hyperintense and hypointense lesions, group sizes of around 40 seem to be required (Cohen's $d = 0.62$). Effect size for nerve CSA calculated from Jende et al. (2019) is slightly higher (Cohen's $d = 0.71$), suggesting a minimum sample size of 30 per group. However, it is noteworthy that results are inconsistent between different studies for nerve CSA, with some finding no significant difference (Jende et al., 2020b). DTI studies to date have used around 10 participants per group, which is around the minimal sample size given the effect sizes in these studies (Cohen's $d = 1.24$). Given that there seems to be trends for some metrics which did not consistently meet statistical significance (axial, radial and mean diffusivity), it may be that these studies were underpowered. Aiming for larger samples of 20–30 subjects per group in future studies may be beneficial.

Anatomy Scanned, Magnetic Field Strength, and Image Resolution

Whilst early studies in this field scanned the sural nerve at the level of the ankle (Griffey et al., 1988; Koechner et al., 1995; Eaton et al., 1996; Shibata et al., 1998), most of the studies published since 2011 have focused on the sciatic nerve and the proximal extent of one of its branches (tibial nerve, common peroneal nerve) (Pham et al., 2011; Wu et al., 2017; Jende et al., 2018, 2019, 2020b; Groener et al., 2020). The sciatic nerve at the level of the thigh is significantly larger compared with more distal nerves, making it more feasible to get sufficient resolution for analysis within the limits of current magnets and pulse sequences. Also, some studies have shown a proximal–distal gradient, with a greater number of lesions at the level of the thigh than in the calf, both for lesion-load on T_2 -weighted imaging (Pham et al., 2015), and fractional anisotropy measures (Vaeggemose et al., 2017a,b). This gradient seems at odds to symptoms in DPN, which seem to have a more distal predominance. However, respective authors note that the multifocal involvement of the fascicles of the thigh would correspond to histopathological findings seen at this location (Dyck et al., 1986). Some studies have also investigated more distal nerves such as distal tibial and common peroneal nerves (Pham et al., 2015; Felisaz et al., 2017;

Vaeggemose et al., 2017a,b, 2020; Wu et al., 2017), the sural nerve (Griffey et al., 1988; Koechner et al., 1995; Eaton et al., 1996; Shibata et al., 1998), and the median nerve in the arm (Edward et al., 2020).

In terms of magnetic field strength, all included studies used a 3 T MRI system, except for the earliest studies in the 1980's and early '90s (Griffey et al., 1988; Koechner et al., 1995; Eaton et al., 1996; Shibata et al., 1998) and one more recent diffusion tensor imaging study (Edward et al., 2020). This has allowed excellent spatial resolution and anatomic detail to be obtained for the relatively small structures imaged, with resolutions of around $0.3 \times 0.3 \text{ mm}^2$ to $0.3 \times 0.5 \text{ mm}^2$ in-plane, using 3–4 mm slice thickness for T_2 -weighted imaging (Pham et al., 2011, 2015; Vaeggemose et al., 2017a,b, 2020; Wu et al., 2017; Jende et al., 2018, 2019, 2020b). Studies using DTI have typically obtained a resolution of $1.25 \times 1.25 \text{ mm}^2$ to $1.36 \times 1.36 \text{ mm}^2$ in-plane resolution using slice thicknesses of 3–4 mm (Vaeggemose et al., 2017a,b, 2020; Wu et al., 2017; Jende et al., 2020a). One exception to the above is a study by Felisaz et al. (2017), who performed Dixon imaging in the distal tibial nerve at 3 T, using a spoiled gradient sequence with IDEAL, and by using a very restricted field of view they were able to push to a resolution of $0.117 \times 0.143 \times 2 \text{ mm}^3$. This impressive resolution is at the limit of what is currently achievable with 3 T systems. The authors were able to segment the nerve into fascicles and epineurium, demonstrating compartment-specific changes in DPN. However, it is worth noting that all of the studies in the field so far have sacrificed resolution in the slice direction (by having greater slice thickness) to provide optimal in-plane resolution. Whilst improving SNR, this will also create partial volume effects in the slice direction, leading to some small lesions potentially being missed.

Methods of Image Segmentation and Analysis

Analysing the MR indices described above generally requires a segmentation of nerve tissue from non-nerve tissue, so that the given index (e.g., signal intensity, T_2 , measures of diffusivity) can be calculated. While some of these techniques, such as DTI, use pre-existing software (generally adapted from brain imaging), which use in-built (semi)-automated segmentation, all studies focusing on T_2 -weighted MRI use an initial fully manual segmentation (Felisaz et al., 2017; Vaeggemose et al., 2017a,b, 2020; Jende et al., 2018, 2019, 2020b; Groener et al., 2020), generally performed by trained neuroradiologists with experience of nerve imaging. Manual segmentation is extremely time consuming and will become more so with the availability of higher resolution imaging. When multiple researchers are performing segmentation, it is also important to show intra- and inter-rater reliability, which is generally not discussed in papers to date. If the expectation is that segmenters should have substantial clinical training in neuroradiology, this is an unnecessary barrier to carrying out nerve imaging research. Therefore, adapting (semi)-automated algorithms from brain imaging research or creating custom

algorithms for nerve imaging should be a research priority over the coming years.

Finally, in terms of methods of analysis the greatest variability in the literature comes from T_2 -weighted MRI. Whilst it is possible to calculate absolute T_2 and proton density values (Pham et al., 2015; Wu et al., 2017; Vaeggemose et al., 2020), the required sequences are often more time consuming, but can give useful information about the source of T_2 -weighted signal intensity and shed light on the underlying pathophysiology. Another approach has been to take T_2 -weighted signal intensities and average them over an area of nerve to compare between groups (Pham et al., 2011), or to identify values above a cut of as “hyperintense lesions” (Pham et al., 2015). These approaches are problematic in light of subsequent data from Jende et al. (2018), demonstrating convincingly that there are areas of both hyper- and hypointense lesions, possibly reflecting different pathogenic mechanisms. Therefore, any assessment using T_2 -weighted MRI should assess both of these lesion types.

Future Directions

A number of priorities for future directions are apparent from the above review of available literature. The first relates to the fact there are no published studies on HIV neuropathy, despite 18 studies to date having developed MRI biomarkers of DPN. Broadening the scope of research to other forms of neuropathy, including HIV and chemotherapy-induced neuropathy, would allow us to answer questions on how specific these biomarkers are to DPN, or whether they represent nerve damage across a range of aetiologies. There is also significant debate about the pathological underpinnings of the changes apparent in diabetic neuropathy using MRI. Comparing and contrasting MRI signatures of neuropathies of different aetiologies, with different underlying pathological processes, may help to shed light on this issue.

Similarly, longitudinal imaging will also be of great value. By comparing the same patients at multiple timepoints we will be able to track the evolution of MRI changes and relate them to changes in other biomarkers and clinical assessments. This will also be a more powerful way to study if there are objective imaging changes which occur when transitioning from absence to presence of neuropathy, potentially allowing for the development of pre-symptomatic biomarkers which predict the risk of developing clinical neuropathy. Some researchers have already begun to investigate whether MRI can detect specific changes in the nerve that relate to the development of neuropathic pain (Jende et al., 2020b). Longitudinal imaging comparing patients before and after the development of neuropathic pain, or with increasing severities of neuropathic pain, would be a powerful tool in this regard. As discussed above, the single time point design used by previous studies led to difficulties in interpreting causal relationships between blood biomarkers and MRI signatures of neuropathy, for example whether high or low serum lipids confer increased risk of developing neuropathy (Jende et al., 2019). Tracking these relationships over time in cohort studies would help clarify.

In terms of technical aspects, ultra-high field MRI (e.g., 7 T) is becoming increasingly available and will allow even greater signal-to-noise, and therefore spatial resolution, than the current body of research discussed above. Felisaz et al. (2017) have pushed the resolution at 3 T to its extreme, achieving a resolution of $0.117 \times 0.147 \times 2 \text{ mm}^3$ using T_1 -weighted and Dixon imaging. At this level, the authors offer a tantalising glimpse at fascicular resolution nerve imaging with the ability to segment out structures within the nerve. Improving further on this resolution will allow more in-depth understanding of how individual nerve compartments change structurally over the course of DPN. The improved resolution available at 7 T will also be able to probe whether the increased proximal density of hyperintense and hypointense lesions shown in previous studies (e.g., Pham et al., 2015) is a true representation of the pathology in DPN, or is simply related to decreased sensitivity for picking up lesions at the smaller, distal extent of nerves when imaging at lower field strength. Finally, whilst there are methods for functional brain imaging to obtain indirect measures of activity of brain tissue, no such techniques exist yet for nerve imaging. There are numerous reasons for this, for example the clear neurovascular coupling which exists in the brain, with spatio-temporal relationships. Similar blood-flow measures are unlikely to be of value in nerve imaging. That is not, however, to say that measures will not be able to be developed which probe the ability of nerves to function, and we refer readers to the paper in this edition by Jende et al. (2021), exploring DTI as a surrogate measure of nerve function.

PROTOCOL AND REGISTRATION

The protocol used in this systematic review was published a priori on the University of York/National Institute of Health Research

(NIHR) international prospective register of systematic reviews (PROSPERO) at the following link https://www.crd.york.ac.uk/prospero/display_record.php?RecordID=167322.

In the original published protocol (Evans et al., 2020), we had aimed to search until Jan 16th 2020. However, preparation of this review was delayed by the coronavirus pandemic, and we therefore decided to extend the search to include the most up to date journal articles. Otherwise, the study was carried out as described in the original protocol.

DATA AVAILABILITY STATEMENT

The original contributions presented in the study are included in the article/supplementary material, further inquiries can be directed to the corresponding author/s.

AUTHOR CONTRIBUTIONS

ME, CW, AR, and DS were involved in overall structure and concept for review. Data collection/extraction and analysis by ME, CW, DH-S, AU, and KS. Manuscript writing by ME. All authors contributed to editing of manuscript.

FUNDING

ME was funded by a UK National Institute of Health Research (NIHR) academic clinical fellowship (ACF). ME and AR are funded by a grant by the UK Medical Research Council (MRC) and Versus Arthritis (PAINTORM - MR/W002388/1). PL was funded by a Wellcome Trust Fellowship. DS receives grants from the Dementia Research Institute (DRI), MRC and NIHR.

REFERENCES

- Behse, F., Buchthal, F., and Carlsen, F. (1977). Nerve biopsy and conduction studies in diabetic neuropathy. *J. Neurol. Neurosurg. Psychiatry* 40, 1072–1082. doi: 10.1136/jnnp.40.11.1072
- Breiner, A., Qrimli, M., Ebadi, H., Alabdali, M., Lovblom, L. E., Abraham, A., et al. (2017). Peripheral nerve high-resolution ultrasound in diabetes. *Muscle Nerve* 55, 171–178. doi: 10.1002/mus.25223
- Brownlee, M. (2001). Biochemistry and molecular cell biology of diabetic complications. *Nature* 414, 813–820. doi: 10.1038/414813a
- Calcutt, N. A. (2020). Diabetic neuropathy and neuropathic pain: a (con)fusion of pathogenic mechanisms? *Pain* 161, S65–S86. doi: 10.1097/j.pain.0000000000001922
- Calcutt, N. A., and Fernyhough, P. (2016). A brief introduction to the history and controversies of clinical trials in diabetic neuropathy. *Int. Rev. Neurobiol.* 127, 3–8.
- Cartwright, M. S., Passmore, L. V., Yoon, J. S., Brown, M. E., Caress, J. B., and Walker, F. O. (2008). Cross-sectional area reference values for nerve ultrasonography. *Muscle Nerve* 37, 566–571. doi: 10.1002/mus.21009
- Chalk, C., Benstead, T. J., and More, F. (2007). Aldose reductase inhibitors for the treatment of diabetic polyneuropathy. *Cochrane Database Syst. Rev.* 2010. doi: 10.1002/14651858.CD004572.pub2
- Cherry, C. L., Kamerman, P. R., Bennett, D. L., and Rice, A. S. (2012a). HIV-associated sensory neuropathy: Still a problem in the post-stavudine era? *Future Virol.* 7, 849–854. doi: 10.2217/fvl.12.77
- Cherry, C. L., Wadley, A. L., and Kamerman, P. R. (2012b). Painful HIV-associated sensory neuropathy. *Pain Manag.* 2, 543–552. doi: 10.2217/pmt.12.67
- Cherry, C. L., Wadley, A. L., and Kamerman, P. R. (2016). Diagnosing and treating HIV-associated sensory neuropathy: a global perspective. *Pain Manag.* 6, 191–199. doi: 10.2217/pmt.15.65
- Chung, S. S. M. (2003). Contribution of polyol pathway to diabetes-induced oxidative stress. *J. Am. Soc. Nephrol.* 14, 233S–236. doi: 10.1097/01.ASN.0000077408.15865.06
- Cudlip, S. A., Howe, F. A., Clifton, A., Schwartz, M. S., and Bell, B. A. (2002). Magnetic resonance neurography studies of the median nerve before and after carpal tunnel decompression. *J. Neurosurg.* 96, 1046–1051. doi: 10.3171/jns.2002.96.6.1046
- Dyck, P. J., Karnes, J. L., O'Brien, P., Okazaki, H., Lais, A., and Engelstad, J. (1986). The spatial distribution of fiber loss in diabetic polyneuropathy suggests ischemia. *Ann. Neurol.* 19, 440–449. doi: 10.1002/ana.410190504
- Eaton, R. P., Quails, C., Bicknell, J., Sibbitt, W. L., King, M. K., and Griffey, R. H. (1996). Structure-function relationships within peripheral nerves in diabetic neuropathy: the hydration hypothesis. *Diabetologia* 39, 439–446. doi: 10.1007/BF00400675
- Edward, R., Abdelalim, A. M., Ashour, A. S., Afifi, L., and Al-Athwari, A. (2020). A study of diffusion tensor imaging of median nerve in

- diabetic peripheral neuropathy. *Egypt. J. Neurol. Psychiatry Neurosurg.* 56:42. doi: 10.1186/s41983-020-00172-5
- Evans, M. C., Hohenschurz-Schmidt, D., Ugwudike, A., Shah, N., Bangertner, N., Rice, A. S. C., et al. (2020). A systematic review of magnetic resonance imaging (MRI) studies of diabetic and HIV peripheral neuropathy. *PROSPERO Int. Prospect. Regist. Syst. Rev.*
- Felisz, P. F., Maugeri, G., Busi, V., Vitale, R., Balducci, F., Gitto, S., et al. (2017). MR micro-neurography and a segmentation protocol applied to diabetic neuropathy. *Radiol. Res. Pract.* 2017:2761818. doi: 10.1155/2017/2761818
- Finnerup, N. B., Attal, N., Haroutounian, S., McNicol, E., Baron, R., Dworkin, R. H., et al. (2015). Pharmacotherapy for neuropathic pain in adults: a systematic review and meta-analysis. *Lancet. Neurol.* 14, 162–173. doi: 10.1016/S1474-4422(14)70251-0
- Freeman, O. J., Unwin, R. D., Dowsey, A. W., Begley, P., Ali, S., Hollywood, K. A., et al. (2016). Metabolic dysfunction is restricted to the sciatic nerve in experimental diabetic neuropathy. *Diabetes* 65, 228–238. doi: 10.2337/db15-0835
- Gaist, D., Jeppesen, U., Andersen, M., García Rodríguez, L. A., Hallas, J., and Sindrup, S. H. (2002). Statins and risk of polyneuropathy: a case-control study. *Neurology* 58, 1333–1337. doi: 10.1212/WNL.58.9.1333
- Gerevini, S., Agosta, F., Riva, N., Spinelli, E. G., Pagani, E., Caliendo, G., et al. (2016). Mr imaging of Brachial Plexus and limb-girdle muscles in patients with amyotrophic lateral sclerosis. *Radiology* 279, 553–561. doi: 10.1148/radiol.2015150559
- Griffey, R. H., Eaton, R. P., Sibbitt, R. R., Sibbitt, W. L., and Bicknell, J. M. (1988). Diabetic neuropathy: structural analysis of nerve hydration by magnetic resonance spectroscopy. *JAMA* 260, 2872–2878. doi: 10.1001/jama.1988.03410190120034
- Groener, J. B., Jende, J. M. E., Kurz, F. T., Kender, Z., Treede, R. D., Schuh-Hofer, S., et al. (2020). Understanding diabetic neuropathy—from subclinical nerve lesions to severe nerve fiber deficits: a cross-sectional study in patients with type 2 diabetes and healthy control subjects. *Diabetes* 69, 436–447. doi: 10.2337/db19-0197
- Hebert, P. R., Gaziano, J. M., Chan, K. S., and Hennekens, C. H. (1997). Cholesterol lowering with statin drugs, risk of stroke, and total mortality. An overview of randomized trials. *JAMA* 278, 313–321. doi: 10.1001/jama.1997.03550040069040
- International Diabetes Federation (2015). *IDF Diabetes Atlas*. Available online at: <http://www.diabetesatlas.org> (accessed June 6, 2021).
- Jende, J. M. E., Groener, J. B., Kender, Z., Hahn, A., Morgenstern, J., Heiland, S., et al. (2020a). Troponin T parallels structural nerve damage in type 2 diabetes: a cross-sectional study using magnetic resonance neurography. *Diabetes* 69, 713–723. doi: 10.2337/db19-1094
- Jende, J. M. E., Groener, J. B., Kender, Z., Rother, C., Hahn, A., Hilgenfeld, T., et al. (2020b). Structural nerve remodeling at 3-T MR neurography differs between painful and painless diabetic polyneuropathy in type 1 or 2 diabetes. *Radiology* 294, 405–414. doi: 10.1148/radiol.2019191347
- Jende, J. M. E., Groener, J. B., Oikonomou, D., Heiland, S., Kopf, S., Pham, M., et al. (2018). Diabetic neuropathy differs between type 1 and type 2 diabetes: insights from magnetic resonance neurography. *Ann. Neurol.* 83, 588–598. doi: 10.1002/ana.25182
- Jende, J. M. E., Groener, J. B., Rother, C., Kender, Z., Hahn, A., Hilgenfeld, T., et al. (2019). Association of serum cholesterol levels with peripheral nerve damage in patients with type 2 diabetes. *JAMA Netw. Open* 2:e194798. doi: 10.1001/jamanetworkopen.2019.4798
- Jende, J. M. E., Kender, Z., Mooshage, C., Groener, J. B., Alvarez-Ramos, L., Kollmer, J., et al. (2021). Diffusion tensor imaging of the sciatic nerve as a surrogate marker for nerve functionality of the upper and lower limb in patients with diabetes and prediabetes. *Front. Neurosci.* 15:642589. doi: 10.3389/fnins.2021.642589
- Jende, J. M. E., Kender, Z., Rother, C., Alvarez-Ramos, L., Groener, J. B., Pham, M., et al. (2020c). Diabetic polyneuropathy is associated with pathomorphological changes in human dorsal root ganglia: a study using 3T MR neurography. *Front. Neurosci.* 14:570744. doi: 10.3389/fnins.2020.570744
- Kammerman, P. R., Wadley, A. L., and Cherry, C. L. (2012). HIV-associated sensory neuropathy: risk factors and genetics. *Curr. Pain Headache Rep.* 16, 226–236. doi: 10.1007/s11916-012-0257-z
- Koehnner, D., Petropoulos, H., Eaton, R. P., Hart, B. L., and Brooks, W. M. (1995). Segmentation of small structures in MR images: semiautomated tissue hydration measurement. *J. Magn. Reson. Imaging* 5, 347–351. doi: 10.1002/jmri.1880050320
- Kollmer, J., Kästel, T., Jende, J. M. E., Bendszus, M., and Heiland, S. (2018). Magnetization transfer ratio in peripheral nerve tissue: does it depend on age or location? *Invest. Radiol.* 53, 397–402. doi: 10.1097/RLI.0000000000000455
- Kronlage, M., Bäumer, P., Pitarokoiili, K., Schwarz, D., Schwehr, V., Godel, T., et al. (2017). Large coverage MR neurography in CIDP: diagnostic accuracy and electrophysiological correlation. *J. Neurol.* 264, 1434–1443. doi: 10.1007/s00415-017-8543-7
- Kronlage, M., Schwehr, V., Schwarz, D., Godel, T., Heiland, S., Bendszus, M., et al. (2019). Magnetic resonance neurography: normal values and demographic determinants of nerve caliber and T2 relaxometry in 60 healthy individuals. *Clin. Neuroradiol.* 29, 19–26. doi: 10.1007/s00062-017-0633-5
- Kronlage, M., Schwehr, V., Schwarz, D., Godel, T., Uhlmann, L., Heiland, S., et al. (2018). Peripheral nerve diffusion tensor imaging (DTI): normal values and demographic determinants in a cohort of 60 healthy individuals. *Eur. Radiol.* 28, 1801–1808. doi: 10.1007/s00330-017-5134-z
- Lauria, G., Hsieh, S. T., Johansson, O., Kennedy, W. R., Leger, J. M., Mellgren, S. I., et al. (2010). European Federation of Neurological Societies/Peripheral Nerve Society guideline on the use of skin biopsy in the diagnosis of small fiber neuropathy. Report of a joint task force of the European Federation of Neurological Societies and the Peripheral. *Ner. J. Peripher. Nerv. Syst.* 17, 903–12, e44–e49. doi: 10.1111/j.1468-1331.2010.03023.x
- Lee, C., Liu, Q.-H., Tomkowicz, B., Yi, Y., Freedman, B. D., and Collman, R. G. (2003). Macrophage activation through CCR5- and CXCR4-mediated gp120-elicited signaling pathways. *J. Leukoc. Biol.* 74, 676–682. doi: 10.1189/jlb.0503206
- Lee, D., and Dauphinée, D. M. (2005). Morphological and functional changes in the diabetic peripheral nerve: using diagnostic ultrasound and neurosensory testing to select candidates for nerve decompression. *J. Am. Podiatr. Med. Assoc.* 95, 433–437. doi: 10.7547/0950433
- Leininger, G. M., Vincent, A. M., and Feldman, E. L. (2004). The role of growth factors in diabetic peripheral neuropathy. *J. Peripher. Nerv. Syst.* 9, 26–53. doi: 10.1111/j.1085-9489.2004.09105.x
- Moss, P. J., Huang, W., Dawes, J., Okuse, K., McMahon, S. B., and Rice, A. S. C. (2015). Macrophage–sensory neuronal interaction in HIV-1 gp120-induced neurotoxicity. *Br. J. Anaesth.* 114, 499–508. doi: 10.1093/bja/aeu311
- Novak, P., Pimentel, D. A., Sundar, B., Moonis, M., Qin, L., and Novak, V. (2015). Association of statins with sensory and autonomic ganglionopathy. *Front. Aging Neurosci.* 7:191. doi: 10.3389/fnagi.2015.00191
- Page, M. J., McKenzie, J. E., Bossuyt, P. M., Boutron, I., Hoffmann, T. C., Mulrow, C. D., et al. (2021). The PRISMA 2020 statement: an updated guideline for reporting systematic reviews. *BMJ* 372:n71. doi: 10.1136/bmj.n71
- Pham, M., Oikonomou, D., Baumer, P., Bierhaus, A., Heiland, S., Humpert, P. M., et al. (2011). Proximal neuropathic lesions in distal symmetric diabetic polyneuropathy findings of high-resolution magnetic resonance neurography. *Diabetes Care* 34, 721–723. doi: 10.2337/dc10-1491
- Pham, M., Oikonomou, D., Hornung, B., Weiler, M., Heiland, S., Bäumer, P., et al. (2015). Magnetic resonance neurography detects diabetic neuropathy early and with proximal predominance. *Ann. Neurol.* 78, 939–948. doi: 10.1002/ana.24524
- Riazi, S., Bril, V., Perkins, B. A., Abbas, S., Chan, V. W. S., Ngo, M., et al. (2012). Can ultrasound of the tibial nerve detect diabetic peripheral neuropathy?: a cross-sectional study. *Diabetes Care* 35, 2575–2579. doi: 10.2337/dc12-0739
- Schmid, A. B., Campbell, J., Hurley, S. A., Jbabdi, S., Andersson, J. L., Jenkinson, M., et al. (2018). Feasibility of diffusion tensor and morphologic imaging of peripheral nerves at ultra-high field strength. *Invest. Radiol.* 53, 705–713. doi: 10.1097/RLI.0000000000000492
- Scott, W. (2019). The psychosocial context of chronic pain in people living with HIV. *PAIN Rep.* 4:e721. doi: 10.1097/PR9.00000000000000721
- Scott, W., Arkuter, C., Kioskli, K., Kemp, H., McCracken, L. M., Rice, A. S. C., et al. (2018). Psychosocial factors associated with persistent pain in people with HIV: a systematic review with meta-analysis. *Pain* 159, 2461–2476. doi: 10.1097/j.pain.0000000000001369

- Seok, H. Y., Jang, J. H., Won, S. J., Yoon, J. S., Park, K. S., and Kim, B. J. (2014). Cross-sectional area reference values of nerves in the lower extremities using ultrasonography. *Muscle Nerve* 50, 564–570. doi: 10.1002/mus.24209
- Shibata, T., Suzuki, E., Yasuda, K., and Yasuda, K. (1998). Effects of aldose reductase inhibitor and prostaglandin I₂ analogue on diabetic neuropathy - Clinical study with magnetic resonance imaging. *J. Japan Diabetes Soc.* 41, 423–431. doi: 10.11213/tonyobyoy1958.41.423
- Smith, A. G., Howard, J. R., Kroll, R., Ramachandran, P., Hauer, P., Singleton, J. R., et al. (2005). The reliability of skin biopsy with measurement of intraepidermal nerve fiber density. *J. Neurol. Sci.* 228, 65–69. doi: 10.1016/j.jns.2004.09.032
- Tesfaye, S. (2011). Recent advances in the management of diabetic distal symmetrical polyneuropathy. *J. Diabetes Investig.* 2, 33–42. doi: 10.1111/j.2040-1124.2010.00083.x
- Tesfaye, S., Stevens, L. K., Stephenson, J. M., Fuller, J. H., Plater, M., Ionescu-Tirgoviste, C., et al. (1996). Prevalence of diabetic peripheral neuropathy and its relation to glycaemic control and potential risk factors: the EURODIAB IDDM complications study. *Diabetologia* 39, 1377–1384. doi: 10.1007/s001250050586
- Tievsky, A. L., Ptak, T., and Farkas, J. (1999). Investigation of apparent diffusion coefficient and diffusion tensor anisotropy in acute and chronic multiple sclerosis lesions. *AJNR. Am. J. Neuroradiol.* 20, 1491–1499.
- Vaeggemose, M., Haakma, W., Pham, M., Ringgaard, S., Tankisi, H., Ejksjaer, N., et al. (2020). Diffusion tensor imaging MR Neurography detects polyneuropathy in type 2 diabetes. *J. Diabetes Complications* 34:107439. doi: 10.1016/j.jdiacomp.2019.107439
- Vaeggemose, M., Pham, M., Ringgaard, S., Tankisi, H., Ejksjaer, N., Heiland, S., et al. (2017a). Diffusion tensor imaging MR neurography for the detection of polyneuropathy in type 1 diabetes. *J. Magn. Reson. Imaging* 45, 1125–1134. doi: 10.1002/jmri.25415
- Vaeggemose, M., Pham, M., Ringgaard, S., Tankisi, H., Ejksjaer, N., Heiland, S., et al. (2017b). Magnetic resonance neurography visualizes abnormalities in sciatic and tibial nerves in patients with type 1 diabetes and neuropathy. *Diabetes* 66, 1779–1788. doi: 10.2337/db16-1049
- Van Hecke, O., Austin, S. K., Khan, R. A., Smith, B. H., and Torrance, N. (2014). Neuropathic pain in the general population: a systematic review of epidemiological studies. *Pain* 155, 654–662. doi: 10.1016/j.pain.2013.11.013
- Wang, D., Wang, C., Duan, X., Yang, Z., Bai, Z., Hu, H., et al. (2018). MR T2 value of the tibial nerve can be used as a potential non-invasive and quantitative biomarker for the diagnosis of diabetic peripheral neuropathy. *Eur. Radiol.* 28, 1234–1241. doi: 10.1007/s00330-017-5043-1
- Wodarski, R., Bagdas, D., Paris, J. J., Pheby, T., Toma, W., Xu, R., et al. (2018). Reduced intraepidermal nerve fibre density, glial activation, and sensory changes in HIV type-1 Tat-expressing female mice. *PAIN Rep.* 3:e654. doi: 10.1097/PR9.0000000000000654
- Won, J. C., Kwon, H. S., Kim, C. H., Lee, J. H., Park, T. S., Ko, K. S., et al. (2012). Prevalence and clinical characteristics of diabetic peripheral neuropathy in hospital patients with Type2 diabetes in Korea. *Diabet. Med.* 29, e290–e296. doi: 10.1111/j.1464-5491.2012.03697.x
- Wu, C., Wang, G., Zhao, Y., Hao, W., Zhao, L., Zhang, X., et al. (2017). Assessment of tibial and common peroneal nerves in diabetic peripheral neuropathy by diffusion tensor imaging: a case control study. *Eur. Radiol.* 27, 3523–3531. doi: 10.1007/s00330-016-4698-3
- Xu, F., Zhao, L. H., Su, J., Bin, C., Chen, T., and Wang, X. Q., Chen, J. F., et al. (2014). The relationship between glycemic variability and diabetic peripheral neuropathy in type 2 diabetes with well-controlled HbA1c. *Diabetol. Metab. Syndr.* 6:139. doi: 10.1186/1758-5996-6-139

Conflict of Interest: AR undertakes consultancy and advisory board work for Imperial College Consultants- in the last 24 months this has included remunerated work for: Abide, Confo, Vertex, Pharmanovo, Lateral, Novartis, Mundipharma, Orion, Shanghai SIMR Biotech, Asahi Kasei, Toray & TheraNexis. AR was the owner of share options in Spinifex Pharmaceuticals from which personal benefit accrued upon the acquisition of Spinifex by Novartis in July 2015 and from which future milestone payments may occur. AR is also named as an inventor on patents: AR, Vandevoorde S., and Lambert D. M Methods using N-2-propenylhexadecanamide and related amides to relieve pain. WO 2005/079771. Okuse K. et al. Methods of treating pain by inhibition of vgf activity EP13702262.0/ WO2013 110945.

The remaining authors declare that the research was conducted in the absence of any commercial or financial relationships that could be construed as a potential conflict of interest.

Publisher's Note: All claims expressed in this article are solely those of the authors and do not necessarily represent those of their affiliated organizations, or those of the publisher, the editors and the reviewers. Any product that may be evaluated in this article, or claim that may be made by its manufacturer, is not guaranteed or endorsed by the publisher.

Copyright © 2021 Evans, Wade, Hohenschurz-Schmidt, Lally, UgwuDike, Shah, Bangerter, Sharp and Rice. This is an open-access article distributed under the terms of the Creative Commons Attribution License (CC BY). The use, distribution or reproduction in other forums is permitted, provided the original author(s) and the copyright owner(s) are credited and that the original publication in this journal is cited, in accordance with accepted academic practice. No use, distribution or reproduction is permitted which does not comply with these terms.



Fractional Anisotropy and Troponin T Parallel Structural Nerve Damage at the Upper Extremities in a Group of Patients With Prediabetes and Type 2 Diabetes – A Study Using 3T Magnetic Resonance Neurography

Johann M. E. Jende^{1†}, Zoltan Kender^{2†}, Jakob Morgenstern², Pascal Renn¹, Christoph Mooshage¹, Alexander Juerchott¹, Stefan Kopf^{2,3}, Peter P. Nawroth^{2,3,4}, Martin Bendszus¹ and Felix T. Kurz^{1,5*}

OPEN ACCESS

Edited by:

Peter Herman,
Yale University, United States

Reviewed by:

Helmar Lehmann,
University of Cologne, Germany
Claudia Cejas,
Fundación Para la Lucha Contra las
Enfermedades Neurológicas de la
Infancia (FLENI), Argentina

*Correspondence:

Felix T. Kurz
felix.kurz@med.uni-heidelberg.de

[†]These authors have contributed
equally to this work and share first
authorship

Specialty section:

This article was submitted to
Brain Imaging Methods,
a section of the journal
Frontiers in Neuroscience

Received: 14 July 2021

Accepted: 17 December 2021

Published: 24 January 2022

Citation:

Jende JME, Kender Z,
Morgenstern J, Renn P, Mooshage C,
Juerchott A, Kopf S, Nawroth PP,
Bendszus M and Kurz FT (2022)
Fractional Anisotropy and Troponin T
Parallel Structural Nerve Damage
at the Upper Extremities in a Group
of Patients With Prediabetes and Type
2 Diabetes – A Study Using 3T
Magnetic Resonance Neurography.
Front. Neurosci. 15:741494.
doi: 10.3389/fnins.2021.741494

¹ Department of Neuroradiology, Heidelberg University Hospital, Heidelberg, Germany, ² Department of Endocrinology, Diabetology and Clinical Chemistry, Heidelberg University Hospital, Heidelberg, Germany, ³ German Center of Diabetes Research, München, Germany, ⁴ Joint Institute for Diabetes and Cancer at Helmholtz-Zentrum Munich and Heidelberg University, Heidelberg, Germany, ⁵ German Cancer Research Center, Radiology E010, Heidelberg, Germany

Background: Recent studies have found that troponin T parallels the structural and functional decay of peripheral nerves at the level of the lower limbs in patients with type 2 diabetes (T2D). The aim of this study was to determine whether this finding can also be reproduced at the level of the upper limbs.

Methods: Ten patients with fasting glucose levels > 100 mg/dl (five with prediabetes and five with T2D) underwent magnetic resonance neurography of the right upper arm comprising T2-weighted and diffusion weighted sequences. The fractional anisotropy (FA), an indicator for the structural integrity of peripheral nerves, was calculated in an automated approach for the median, ulnar, and radial nerve. All participants underwent additional clinical, serological, and electrophysiological assessments.

Results: High sensitivity Troponin T (hsTNT) and HbA1c were negatively correlated with the average FA of the median, ulnar and radial nerve ($r = -0.84$; $p = 0.002$ and $r = -0.68$; $p = 0.032$). Both FA and hsTNT further showed correlations with items of the Michigan Hand Outcome Questionnaire ($r = -0.76$; $p = 0.010$ and $r = 0.87$; $p = 0.001$, respectively). A negative correlation was found for hsTNT and HbA1c with the total Purdue Pegboard Test Score ($r = -0.87$; $p = 0.001$ and $r = -0.68$; $p = 0.031$).

Conclusion: This study is the first to find that hsTNT and HbA1c are associated with functional and structural parameters of upper limb nerves in patients with impaired glucose tolerance and T2D. Our results support the hypothesis that hyperglycemia-related microangiopathy, represented by elevated hsTNT levels, is a contributor to nerve damage in diabetic polyneuropathy.

Keywords: diabetic polyneuropathy, magnetic resonance neurography (MRN), diffusion tensor imaging, microangiopathy, high-sensitivity Troponin T

INTRODUCTION

Diabetic neuropathy (DN) is one of the most prevalent and yet most poorly understood complications of diabetes mellitus resulting in a reduction of affected patients' quality of life and an enormous economic burden for the global healthcare system (Davies et al., 2006; Alleman et al., 2015). Although several pathophysiological pathways associated with DN have been identified and investigated in both preclinical and clinical studies, clinical studies on reliable markers that allow for both quantification and prediction of nerve damage in DN have come to controversial results (Callaghan et al., 2012; Spallone and Greco, 2013; Feldman et al., 2017).

In addition, it is well known that upper and lower limb nerves in DN behave differently regarding their functional properties and demands, which may result from the influence of length-dependent factors on neurological development, see e.g., Dyck et al. (1985). More recent works also indicate upper and lower limb specific nerve conduction velocities (NCVs) in contrast to their nerve cross-section area development (Nobue et al., 2020), and it has also been argued that a differential expression of slow hyperpolarization-activated cyclic nucleotide-gated channel isoforms between upper and lower limbs may contribute to earlier dysfunction of lower limbs in neuropathy (Marmoy et al., 2019). However, while DN is generally agreed to be a length dependent neuropathy, both histological studies (Dyck et al., 1986a) and recent imaging studies have found that structural nerve damage linked to demyelination in affected patients predominates at a proximal level of the affected extremities in patients with diabetes and prediabetes (Pham et al., 2015; Jende et al., 2018, 2021), indicating that the entire peripheral nervous system is affected throughout the entire course of DN and that, even in prediabetes, when blood glucose levels are at a lower level than in type 2 diabetes (T2D), structural nerve damage at a proximal level can already be detected (Jende et al., 2021).

One of the most challenging obstacles and potential confounder for clinical studies on DN of the upper extremities is that clinical examinations, such as clinical scores, and electrophysiological examinations are dependent on the patient's cooperation and individual perception of symptoms, as well as the rater's experience. In addition, electrophysiological examinations can be perceived as unpleasant or even painful. They also do not allow any conclusions on potential anatomical location, size, distribution, or composition of nerve lesions. Studies on non-invasive in vivo high resolution magnetic resonance neurography (MRN) have shown that diffusion tensor imaging (DTI) allows a very accurate and reproducible assessment of a nerve's structural integrity, thus providing a more objective tool for the assessment of nerve damage than clinical examinations alone, see e.g., Kronlage et al. (2018), or Jeon et al. (2018) and references therein. For instance, Lehmann et al. (2010) used DTI to reliably assess axonal regeneration in an animal model of crush neuropathy using high-field MRI at 11.7 Tesla. Specifically in the context of polyneuropathy, recent studies could show that DTI can be

used to visualize, detect, and quantify neuropathic changes in human type 1 and type 2 diabetes (T2D) in the lower leg (Vaeggemose et al., 2017, 2020; Edward et al., 2020; Xia et al., 2021).

In addition, a recent study on diffusion-weighted MRN found that elevated levels of Troponin T obtained from high sensitivity Troponin T (hsTNT) assays are associated with structural nerve damage at the level of the lower limbs in patients with T2D, supporting the hypothesis that hsTNT is a potential serological marker for microvascular disease and associated pathologies in T2D (Jende et al., 2020a). This is in line with previous studies that had shown hsTNT levels to be associated with the occurrence of microvascular complications in patients with T2D (Li et al., 2014). Also, it could be shown that the structural integrity of the sciatic nerve in patients with diabetes and prediabetes is related to the functionality of patient's arms and hands (Jende et al., 2020b, 2021).

The rationale for this study was therefore to examine nerve integrity in upper arm nerves in prediabetes and diabetes and its correlation to functional (clinical and electrophysiological) scores and specific serological markers of nerve ischemia and glucose control, to test, validate, and compare with earlier findings in lower limbs. Specifically, we investigated whether hsTNT parallels structural nerve damage and a decline in nerve function at the level of the upper limbs.

MATERIALS AND METHODS

Study Design and Participants

The local ethics committee (HEIST-DiC, local ethics number S-383/2016, clinicaltrials.gov identifier NCT03022721) approved this study and all participants gave written informed consent. Twelve patients with impaired glucose tolerance (six with prediabetes and six with T2D) took part in this prospective study between June 2018 and June 2019. Ten participants completed the study protocol (five with prediabetes and five with T2D; three female, seven male, mean age 59.30 years \pm 9.36; age range 42–75 years). Overall exclusion criteria were age <18, pregnancy, any contraindications for MR imaging, any history of cervical surgery or disc extrusion, any other risk factors for neuropathy such as alcoholism, malignant or infectious diseases, hypovitaminosis, monoclonal gammopathy, any previous or ongoing exposure to neurotoxic agents, and any chronic neurological diseases such as Parkinson's disease, restless leg syndrome, or multiple sclerosis. Additional exclusion criteria for controls were any signs of neuropathy in the participants medical history or in the clinical and electrophysiological examinations as shown below.

Clinical and Electrophysiological Examination

For every patient, a detailed medical history was documented and a physical examination including the neuropathy disability score (Young et al., 1993) was performed. Since no standardized

scoring system for the characterization of DN at the level of the upper extremities has been established to date, the overall presence of DN was determined using the well-known Gibbon's criteria according to which patients with an NDS ≥ 3 had DN, and no DN for NDS < 3 (Gibbons et al., 2010). The electrophysiological examination (Viasys Healthcare VikingQuest®, Viasys Healthcare GmbH, Höchberg) of the right arm included: distal motor latencies of the right median and ulnar nerve, motor and sensory amplitudes [compound muscle action potential (CMAPs) and sensory nerve action potential (SNAPs), respectively] of the median and ulnar nerve and both motor and sensory NCVs of the median and ulnar nerve. It was assured that skin temperature was at least 32°C throughout the examination. Since there is no established protocol for the evaluation of hand function in patients with diabetes and prediabetes, we chose the well-established Purdue-Pegboard score for the assessment of motor hand function in general (Tiffin and Asher, 1948) and items of daily life activity from the Michigan Hand Outcome Questionnaire (MHOQ; Shauver and Chung, 2013). Blood was drawn in fasting state and processed immediately under standardized conditions in the Central Laboratory of the University Hospital of Heidelberg. Albumin excretion in urine was detected in morning spot urine within all participants. Estimated glomerular filtration rate (GFR) was calculated with the CKD-EPI-formula (Levey et al., 2009). Prediabetes was defined as fasting glucose levels of 100–125 md/dL, and T2D was defined as fasting glucose levels of >125 md/dL. The serological parameter hsTNT was determined on Cobas E411 (Roche Diagnostics Ltd., Rotkreuz, Switzerland) using heparin plasma. As in previous works (Giannitsis et al., 2010), the limit of blank was 3 ng/L, and the limit of detection was 5 ng/L; both were found in compliance with guideline EP17-A of the Clinical and Laboratory Standards Institute. Further details on analytical characteristics and assay performance can be found in Giannitsis et al. (2010).

Magnetic Resonance Neurography Imaging Protocol

All participants underwent high-resolution MRN of the right upper arm in a 3.0 Tesla MR-scanner (Magnetom SKYRA, Siemens Healthineers, Erlangen, Germany). Participants were examined in prone position with the arm in elbow extension, and upper arm placement within the extremity coil was aligned with the longitudinal axis of the upper arm at an angle of 10° to the external magnetic induction field B_0 of the MR-scanner to avoid magic angle effects. A 15-channel transmit-receive extremity coil was employed and the following sequences were applied:

(1) Axial high-resolution T2-weighted turbo spin echo (TSE) 2D sequence with spectral fat saturation (mode: strong) without water suppression or magnetization preparation. Repetition time (TR) = 5970 ms, echo time (TE) = 55 ms, field of view (FOV) = 160 mm² × 160 mm², matrix size = 512 × 512, slice thickness = 4 mm, interslice gap = 0.8 mm, voxel size = 0.3 mm³ × 0.3 mm³ × 4.0 mm³, 24 slices, 24 acquired images, receiver bandwidth = 181 Hz/pixel, echo

spacing = 11.1 ms, turbo factor = 13, 15 echo trains per slice, parallel imaging factor = 2, averages = 3, acquisition time = 4:42 min.

(2) Axial diffusion-weighted two-dimensional echo-planar sequence images were recorded with spectral attenuated inversion recovery fat suppression (saturation mode: skewed): TR = 5100 ms; TE = 92.8 ms; $b = 0$ and 1000 s/mm²; directions = 20; FOV = 160 mm² × 160 mm²; matrix size = 128 × 128; slice thickness = 4 mm; voxel size = 1.3 mm × 1.3 mm × 4 mm; no interslice gap, 24 slices, 1512 acquired images, receiver bandwidth = 1,396 Hz/pixel, EPI factor = 128, parallel imaging factor = 3, averages = 3, acquisition time = 5:47 min.

In each participant, the sequence was centered to the middle of the upper arm.

Image Post-processing and Statistical Analysis

All images generated were pseudonymized. Images were analyzed in an automated approach using Nordic BRAINEX, a clinical software designed for automated calculation and reconstruction of fiber tracks in diffusion weighted imaging (O'Donnell et al., 2017). T2-weighted and diffusion-weighted sequences were coregistered automatically and the region of the median, ulnar and radial nerve was marked by a trained neuroradiologist with 6 years of experience in MRN imaging (Figures 1A–C). Based on the results of former studies on DTI in the sciatic nerve, the nerve's fiber tracks were automatically segmented with a threshold of >0.1 for the nerve's fractional anisotropy (FA), a dimensionless quantity for directed diffusion that has been shown to be correlated with axonal and myelin integrity (Kronlage et al., 2018; Jende et al., 2021). The average FA was calculated as the arithmetic mean of the radial, ulnar and median nerve's FA.

Statistical Analysis

Statistical data analysis was performed with GraphPad Prism 6. All data were tested for Gaussian normal distribution using the D'Agostino-Pearson omnibus normality test. Also, we applied the iterative Grubbs' test to identify and exclude potential outliers. If a Gaussian normal distribution was given, Pearson correlation coefficients were calculated for correlation analysis. If data were not Gaussian distributed, non-parametric Spearman correlation was applied for correlation analysis. For all tests, the level of significance was defined at $p < 0.05$. All results are presented as mean values \pm standard deviation (SD).

RESULTS

Demographic and Clinical Data

Ten participants completed the MRI scans. Of those, three had DN and seven had no DN. Grubbs test identified 3 electrophysiological values as outliers, which were removed for analysis. No outliers were identified for serological or MRN imaging data. A summary of all demographical, clinical, electrophysiological, serological, and MRN parameters acquired is provided in Table 1.

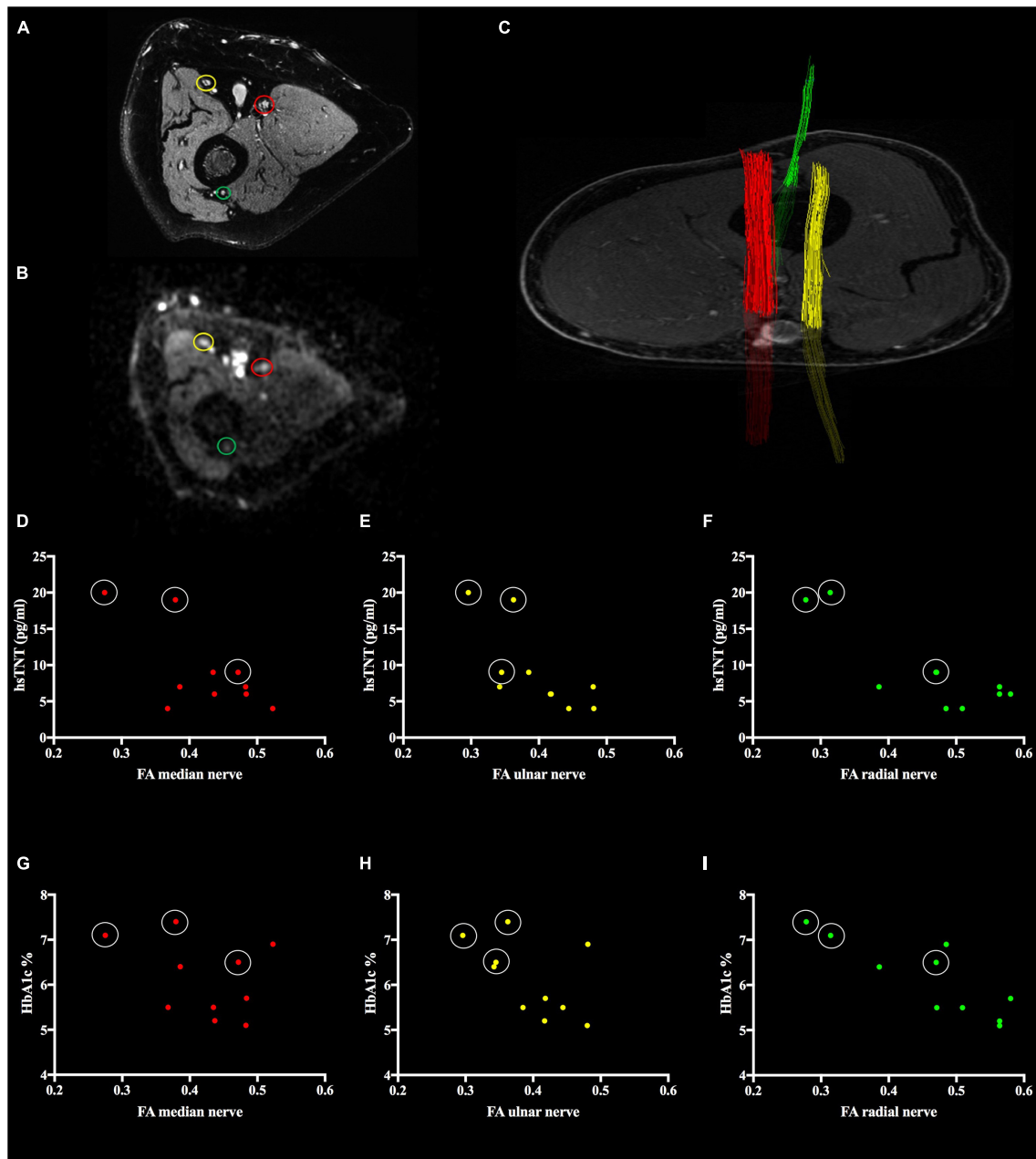


FIGURE 1 | Segmentation of nerve fiber tracts from diffusion tensor imaging and correlation of nerves' fractional anisotropy (FA) with high sensitivity Troponin T (hsTNT) assays. **(A)** T2-weighted sequence of the right upper arm. The median (red circle), ulnar (yellow circle), and radial (green circle) nerve are visible. **(B)** Diffusion-weighted image at $b = 1000 \text{ s/mm}^2$ of the same region as is **(A)**. **(C)** Three-dimensional reconstruction of the median (red), ulnar (yellow), and radial (green) nerve. **(D)** hsTNT vs median nerve's FA ($r = -0.67$; $p = 0.069$), **(E)** hsTNT vs ulnar nerve's FA ($r = -0.74$; $p = 0.035$), **(F)** hsTNT vs radial nerve's FA ($r = -0.86$; $p = 0.007$), **(G)** HbA1c vs median nerve's FA ($r = -0.34$; $p = 0.334$), **(H)** HbA1c vs ulnar nerve's FA ($r = -0.53$; $p = 0.113$), **(I)** HbA1c vs radial nerve's FA ($r = -0.84$; $p = 0.002$). In **(D–I)**, values of patients with diabetic neuropathy are encircled in white.

Correlation of Magnetic Resonance Neurography Data With Demographic, Clinical, and Serological Data

The average FA of the nerves at the upper right arm was negatively correlated with hsTNT and HbA1c ($r = -0.84$; $p = 0.002$ and $r = -0.68$; $p = 0.031$). In a controlled regression

analysis, the correlation between hsTNT and FA remained significant when controlled for HbA1c ($r = 0.71$; $p = 0.029$), whereas the correlation between FA and HbA1c levels did not remain significant when controlled for hsTNT ($r = -0.31$; $p = 0.417$). Individual correlations of the median, ulnar, and radial nerves are displayed in **Figures 1D–I**, in **Table 2**, and

in **Supplementary Table 1**. Further negative correlations of the average FA were found for skin auto-fluorescence ($r = -0.68$; $p = 0.031$) and the assessed items of the MHOQ ($r = -0.76$; $p = 0.010$). Positive correlations were found with the median nerve SNAP ($r = 0.80$; $p = 0.029$) and the ulnar nerve SNAP ($r = 0.89$; $p = 0.001$). No correlations were found with age, body-mass-index (BMI), or GFR.

Correlation of Troponin T and HbA1c With Clinical Data

Parameter hsTNT showed negative correlations with the total Pegboard score ($r = -0.87$; $p = 0.001$) and the ulnar nerve’s SNAP ($r = -0.87$; $p = 0.002$). Positive correlations were found with the assessed items of the MHOQ ($r = 0.87$; $p = 0.001$), skin auto-fluorescence ($r = 0.90$; $p < 0.001$), and HbA1c levels ($r = 0.66$; $p = 0.040$). HbA1c levels showed negative correlations with the total Pegboard score ($r = -0.68$; $p = 0.031$) and with skin auto-fluorescence ($r = 0.75$; $p = 0.012$). For both hsTNT and HbA1c, no correlations were found with age, BMI, or GFR. A detailed summary of all correlations of hsTNT, HbA1c, and FA values with clinical, serological, electrophysiological and demographic data is provided in **Table 2** and in **Supplementary Table 1**.

TABLE 1 | Demographic, clinical, serological, and MRN imaging data of all study participants.

Female	3
Male	7
Age (years)	59.30 ± 9.36
Body-mass-index (kg/m ²)	2934 ± 6.10
Median nerve fractional anisotropy	0.42 ± 0.07
Ulnar nerve fractional anisotropy	0.40 ± 0.06
Radial nerve fractional anisotropy	0.46 ± 0.10
Average fractional anisotropy	0.43 ± 0.07
Total Purdue Pegboard Test Score	63.0 ± 18.83
Daily life items of the Michigan Hand Outcome Questionnaire	3.90 ± 5.45
Median nerve motor conduction velocity (m/s)	50.89 ± 3.59
Median nerve CMAP (μV)	9.08 ± 3.19
Median nerve distal motor latency (ms)	3.60 ± 0.28
Median nerve sensory conduction velocity (m/s)	52.25 ± 7.38
Median nerve SNAP (μV)	12.49 ± 5.65
Ulnar nerve motor conduction velocity (m/s)	54.56 ± 4.39
Ulnar nerve CMAP (μV)	10.34 ± 2.43
Ulnar nerve distal motor latency (ms)	2.69 ± 0.31
Ulnar nerve sensory conduction velocity (m/s)	52.88 ± 7.38
Ulnar nerve SNAP (μV)	10.59 ± 5.26
Skin auto-fluorescence	2.32 ± 0.49
High sensitivity Troponin T (pg/mL)	9.10 ± 5.7
proBNP (pg/mL)	53.11 ± 26.67
HbA1c (%)	6.13 ± 0.83
Glomerular filtration rate (mL/min)	92.02 ± 13.74

All values are displayed as mean ± SD. proBNP: pro brain natriuretic peptide. m/s, meters per second; ms, milliseconds; μV, microvolts; pg/mL, picogram per milliliter; mL/min, milliliters per minute.

DISCUSSION

To our knowledge, this study is the first to assess peripheral nerve DTI at the level of the upper arm in patients with T2D and prediabetes. The results show that the average FA of the nerves at the upper arm is correlated with functional skills at the level of the hands and electrophysiological parameters at the level of the lower arms. This is in accordance with previous studies that found FA to be a reliable correlate for structural nerve integrity (Lehmann et al., 2010; Vaeggemose et al., 2017, 2020; Jende et al., 2021).

Average FA values for the upper arm nerves ranged between 0.40 and 0.46, whereby FA values were increasing from ulnar to median and radial nerves, see **Table 1**. Kronlage et al. reported FA values of upper limb nerves in a healthy cohort and found an age dependency [Figure 4 in Kronlage et al. (2018)]: mean FA values for ulnar, median, and radial nerve at age 59.4 years (the average age of participants in our study) were 0.51 ± 0.07 , 0.55 ± 0.08 , 0.57 ± 0.09 , respectively. These FA values are larger than the FA’s found for the prediabetes and diabetes patients in our cohort. This can be due to impaired structural nerve integrity, e.g., of the neuropathy patients; yet there were also differences in data acquisition such as a different MRI machine, extremity coil and DTI parameters. In addition, Kronlage et al. (2018) determined FA values for the central four slices, covering a distance of approximately 1.6 cm, while we determined averaged FA values over nerve distances larger than 9.6 cm (24 slices times 4 mm).

Another study by Breitenseher et al. found an average FA value of 0.44 ± 0.04 (range: 0.38–0.51) for averaged ulnar nerve FAs in different positions along the nerve covering 6.4 cm in a healthy collective (20 healthy participants, average age: 40 years), see Figure 3 in Breitenseher et al. (2015). Lowest FA values were found in the region of the cubital tunnel. Correcting for age (from 40 to 59.4 years) as suggested by Kronlage et al. (2018) with a correction factor of $-0.0026 \times [(age\ difference)/years]$ would yield an average FA value of 0.39 ± 0.04 for the Breitenseher cohort, which is in fact slightly lower than the FA value we found, also possibly due to differences in data acquisition.

This study further found that the median, ulnar, and radial nerve’s FA was associated with hsTNT levels. This is in line with previous studies which showed that hsTNT is well associated with microvascular damage and the severity of DN at the level of the lower limbs in patients with T2D (Li et al., 2014; Jende et al., 2020a). The results of this study now indicate that hsTNT also parallels structural nerve damage at the level of the upper limbs.

This study further found a positive correlation for hsTNT and HbA1c levels, and a negative correlation between HbA1c and the average FA of the upper arm nerves. This finding may suggest that hyperglycemia is the primary cause for nerve damage at the level of the upper limbs and that hsTNT is secondarily elevated as a consequence of hyperglycemia-induced microangiopathy. However, the impact of glucose control on the development and progression of DN in patients with T2D is controversially discussed since longitudinal clinical trials found no evidence for a positive impact of glucose control on the progression of DN in patients with T2D (Callaghan et al., 2012). Several studies have found that vascular factors appear to pose a more important risk

TABLE 2 | Correlation of HbA1c, high sensitivity Troponin T, and fractional anisotropy (FA) of the nerves of the upper limb with demographic, clinical, and serological data.

	HbA1c		hsTNT (pg/ml)		Average FA		Median nerve FA		Ulnar nerve FA		Radial nerve FA	
	r	p	r	p	r	p	r	p	r	p	r	p
Average FA	-0.68	0.031	-0.84	0.002			0.87	0.001	0.87	0.001	0.93	<0.001
Median nerve FA	-0.34	0.334	-0.68	0.032	0.87	0.001			0.69	0.026	0.69	0.027
Ulnar nerve FA	-0.53	0.113	-0.72	0.019	0.87	0.001	0.69	0.026			0.72	0.018
Radial nerve FA	-0.84	0.002	-0.83	0.003	0.93	<0.001	0.69	0.027	0.72	0.018		
Age (years)	0.44	0.200	0.39	0.271	-0.35	0.316	-0.12	0.732	-0.45	0.189	-0.37	0.289
BMI (kg/m ²)	0.17	0.635	-0.03	0.931	0.1	0.777	0.24	0.513	0.14	0.697	-0.04	0.921
Total Pegboard score	-0.68	0.031	-0.87	0.001	0.63	0.05	0.43	0.219	0.6	0.065	0.64	0.044
Daily life items of the MHOQ	0.59	0.075	0.87	0.001	-0.76	0.01	-0.73	0.018	-0.61	0.061	-0.70	0.024
Skin auto-fluorescence	0.75	0.012	0.9	<0.01	-0.68	0.031	-0.47	0.166	-0.5	0.142	-0.77	0.009
proBNP (pg/mL)	0.16	0.689	0.28	0.47	-0.23	0.552	0.06	0.869	-0.37	0.327	-0.33	0.392
GFR (mL/min)	0.39	0.265	0.15	0.689	<0.01	0.994	0.10	0.774	0.31	0.389	-0.26	0.47

factor for the development and progression of DN in T2D than glycemic control alone (Tesfaye et al., 2005). Taken together with the results of histological studies that found nerve ischemia to be a contributing factor to DN in T2D (Dyck et al., 1984, 1986a,b), our results and the results of imaging studies mentioned above, it seems well possible that even at early stages of DN or even before the occurrence of clinical symptoms the nerves of the proximal upper extremities show relatively low FA values even though HbA1c levels appear to be relatively normal.

The finding that both average FA and hsTNT were correlated with skin auto-fluorescence, a marker associated with hyperglycaemia, further supports this assumption. It is important to consider, however, that the correlation between FA and HbA1c did not remain significant in a partial correlation analysis controlled for hsTNT, whereas the correlation between hsTNT and FA remained stable after controlling for HbA1c. Therefore, the association between hsTNT and FA appears to be independent of HbA1c, indicating that microangiopathy leading to nerve damage is not solely related to hyperglycemia in the assessed cohort.

One may of course argue that skin auto-fluorescence, hsTNT, and FA are parameters that have been shown to be associated with age and that, therefore, the findings obtained from a small cohort of patients ranging from age 42 to 75 years may only represent the process of aging (Gerrits et al., 2008; Gore et al., 2014; Kronlage et al., 2018). While we cannot exclude an impact of the physiological process of aging on the results obtained, it should be considered that skin auto-fluorescence, FA, and hsTNT showed no correlation with age and that, therefore, patient age does not appear to be the main contributor to decreased FA or elevated hsTNT levels in the cohort examined. One may further argue that hsTNT tends to be elevated in patients with impaired renal function and that, as a consequence, the results only represent an impairment of renal function that has been shown to be associated with a worsening of symptoms in DPN (Wayand et al., 2000). One has to take into account, however, that we found no correlations between GFR and hsTNT. Also, no correlation was found between GFR and FA.

Our study has several limitations: first, the size of our cohort does not allow excluding all potential confounders or the assessment of gender differences. Also, we did not examine a control group to look for differences of FA or hsTNT levels. It should be considered, however, that the primary aim of this study was to investigate whether the FA of the proximal nerves at the upper limb is associated with clinical and serological parameters in patients with elevated blood glucose levels that are comparable to those found for the FA of the sciatic nerve.

Moreover, the small sample size of our study does not allow a meaningful statistical assessment of differences between patients with and without DN. While this is a limitation, it should be considered that the development of DN has been shown to be a continuous process during which subclinical nerve damage can already be visualized and quantified with MRN imaging prior to the occurrence of clinical symptoms (Groener et al., 2019; Morgenstern et al., 2021). In fact, the objective of this study was not to compare patients with and without DN, but to assess whether hsTNT is associated with a decrease in FA, that represents neurostructural deterioration mainly related to demyelination, and functional loss of proximal nerves at the upper limbs in patients with impaired glucose control. Our results indicate that an increase in hsTNT is associated with a decrease in FA, which, once the FA is low enough, causes an impairment of nerve function that ultimately results in neuropathic symptoms.

CONCLUSION

In summary, this study found correlations between hsTNT and the FA of the proximal nerves of the upper arm in a group of patients with prediabetes and T2D. This correlation was independent from HbA1c levels. Both hsTNT and FA were associated with functional and electrophysiological assessments of the arms and hands, indicating that microangiopathy contributes to structural nerve damage in prediabetes and T2D. Further longitudinal studies are warranted to assess the diagnostic and prognostic value of hsTNT and the nerves' FA at

the level of the upper arms with regard to the development and progression of diabetic polyneuropathy in prediabetes and T2D.

DATA AVAILABILITY STATEMENT

The datasets presented in this article are not readily available because they contain sensitive patient information. The data supporting the conclusions of this article will be made available upon reasonable request by any qualified researcher. Requests to access the datasets should be directed to FK, felix.kurz@med.uni-heidelberg.de.

ETHICS STATEMENT

The studies involving human participants were reviewed and approved by the Ethikkommission der Medizinischen Fakultät der Universität Heidelberg, Heidelberg, Germany. The patients/participants provided their written informed consent to participate in this study.

AUTHOR CONTRIBUTIONS

JJ, ZK, PN, MB, and FK designed and coordinated the study. JJ, ZK, JM, CM, AJ, and FK contributed to the organization of participants. JJ, AJ, PR, and FK collected MR data. JJ and FK developed image analysis tools, analyzed the data, and wrote the manuscript. ZK, JM, and SK collected the clinical, serological, and electrophysiological data. All authors contributed to the article and approved the submitted version.

REFERENCES

- Alleman, C. J. M., Westerhout, K. Y., Hensen, M., Chambers, C., Stoker, M., Long, S., et al. (2015). Humanistic and economic burden of painful diabetic peripheral neuropathy in Europe: a review of the literature. *Diabetes Res. Clin. Pract.* 109, 215–225. doi: 10.1016/j.diabres.2015.04.031
- Breitenseher, J. B., Kranz, G., Hold, A., Berzaczy, D., Nemeč, S. F., Sycha, T., et al. (2015). MR neurography of ulnar nerve entrapment at the cubital tunnel: a diffusion tensor imaging study. *Eur. Radiol.* 25, 1911–1918. doi: 10.1007/s00330-015-3613-7
- Callaghan, B. C., Cheng, H. T., Stables, C. L., Smith, A. L., and Feldman, E. L. (2012). Diabetic neuropathy: clinical manifestations and current treatments. *Lancet Neurol.* 11, 521–534. doi: 10.1016/S1474-4422(12)70065-0
- Davies, M., Brophy, S., Williams, R., and Taylor, A. (2006). The prevalence, severity, and impact of painful diabetic peripheral neuropathy in type 2 diabetes. *Diabetes Care* 29, 1518–1522. doi: 10.2337/dc05-2228
- Dyck, P. J., Karnes, J. L., Daube, J., O'Brien, P., and Service, F. J. (1985). Clinical and neuropathological criteria for the diagnosis and staging of diabetic polyneuropathy. *Brain* 108(Pt 4), 861–880. doi: 10.1093/brain/108.4.861
- Dyck, P. J., Karnes, J. L., O'Brien, P., Okazaki, H., Lais, A., and Engelstad, J. (1986a). The spatial distribution of fiber loss in diabetic polyneuropathy suggests ischemia. *Ann. Neurol.* 19, 440–449. doi: 10.1002/ana.410190504
- Dyck, P. J., Lais, A., Karnes, J. L., O'Brien, P., and Rizza, R. (1986b). Fiber Loss Is Primary and Multifocal in Surd Nerves in Diabetic Polyneuropathy. *Ann. Neurol.* 19, 425–439.
- Dyck, P. J., Karnes, J., O'Brien, P., Nukada, H., Lais, A., and Low, P. (1984). Spatial pattern of nerve fiber abnormality indicative of pathologic mechanism. *Am. J. Pathol.* 117, 225–238.

FUNDING

The German research council (DFG, SFB 1158) and the International Foundation for Research in paraplegia (IRP) provided financial support for personnel expenditure, MR imaging costs, and costs for the technical equipment required for electrophysiological and serological analysis. The DFG and the IRP had no influence on the study design, collection and analysis of data or on the writing of the article. JJ received grants from the German Research Foundation (SFB 1158) and from the International Foundation for Research in Paraplegia. ZK received grants from the Deutsches Zentrum für Diabetesforschung (DZD) e.V. PN received grants from the German research Council (DFG, SFB 1118 and 1158) the German Center of Diabetes Research (DZD), and from Novo Nordisk. MB received grants and personal fees from Codman, Guerbet, Bayer, and Novartis, personal fees from Roche, Teva, Springer, Boehringer, Grifols, Braun, and grants from the European Union, Siemens, the Dietmar Hopp foundation, Stryker and the German Research Council (DFG, SFB 1118 and 1158). FK was supported by the German Research Foundation (KU 3555/1-1), the Hoffmann-Klose foundation (Heidelberg University) and a research grant from Heidelberg University Hospital.

SUPPLEMENTARY MATERIAL

The Supplementary Material for this article can be found online at: <https://www.frontiersin.org/articles/10.3389/fnins.2021.741494/full#supplementary-material>

- Edward, R., Abdelalim, A. M., Ashour, A. S., Afifi, L., and Al-Athwari, A. (2020). A study of diffusion tensor imaging of median nerve in diabetic peripheral neuropathy. *Egypt. J. Neurol. Psychiatr. Neurosurg.* 56:42. doi: 10.1186/s41983-020-00172-5
- Feldman, E. L., Nave, K.-A., Jensen, T. S., and Bennett, D. L. H. (2017). New horizons in diabetic neuropathy: mechanisms, bioenergetics, and pain. *Neuron* 93, 1296–1313. doi: 10.1016/j.neuron.2017.02.005
- Gerrits, E. G., Lutgers, H. L., Kleefstra, N., Graaff, R., Groenier, K. H., Smit, A. J., et al. (2008). Skin autofluorescence. *Diabetes Care* 31, 517–521. doi: 10.2337/DC07-1755
- Giannitsis, E., Kurz, K., Hallermayer, K., Jarausch, J., Jaffe, A. S., and Katus, H. A. (2010). Analytical validation of a high-sensitivity cardiac troponin T assay. *Clin. Chem.* 56, 254–61. doi: 10.1373/clinchem.2009.132654
- Gibbons, C. H., Freeman, R., and Veves, A. (2010). Diabetic neuropathy. *Diabetes Care* 33, 2629–2634. doi: 10.2337/DC10-0763
- Gore, M. O., Seliger, S. L., deFilippi, C. R., Nambi, V., Christenson, R. H., Hashim, I. A., et al. (2014). Age- and sex-dependent upper reference limits for the high-sensitivity cardiac Troponin T assay. *J. Am. Coll. Cardiol.* 63, 1441–1448. doi: 10.1016/J.JACC.2013.12.032
- Groener, J. B., Jende, J. M. E., Kurz, F. T., Kender, Z., Treede, R.-D., Schuh-Hofer, S., et al. (2019). Understanding diabetic neuropathy: from subclinical nerve lesions to severe nerve fiber deficits. a cross-sectional study in patients with type 2 diabetes and healthy controls. *Diabetes* 69, 436–447. doi: 10.2337/db19-0197
- Jende, J. M. E., Groener, J. B., Kender, Z., Hahn, A., Morgenstern, J., Heiland, S., et al. (2020a). Troponin T parallels structural nerve damage in type 2 diabetes. A cross sectional study using magnetic resonance neurography. *Diabetes* 69, 713–723. doi: 10.2337/db19-1094

- Jende, J. M. E., Groener, J. B., Kender, Z., Rother, C., Hahn, A., Hilgenfeld, T., et al. (2020b). Structural nerve remodeling on 3-T MR Neurography differs between painful and painless diabetic polyneuropathy in either type 1 or type 2 diabetes. *Radiology* 294, 405–414. doi: 10.1148/radiol.2019191347
- Jende, J. M. E., Groener, J. B., Oikonomou, D., Heiland, S., Kopf, S., Pham, M., et al. (2018). Diabetic neuropathy differs between type 1 and type 2 diabetes: insights from magnetic resonance neurography. *Ann. Neurol.* 83, 588–598.
- Jende, J. M. E., Kender, Z., Mooshage, C., Groener, J. B., Alvarez-Ramos, L., Kollmer, J., et al. (2021). Diffusion tensor imaging of the sciatic nerve as a surrogate marker for nerve functionality of the upper and lower limb in patients with diabetes and prediabetes. *Front. Neurosci.* 15:190. doi: 10.3389/fnins.2021.642589
- Jeon, T., Fung, M. M., Koch, K. M., Tan, E. T., and Sneag, D. B. (2018). Peripheral nerve diffusion tensor imaging: overview, pitfalls, and future directions. *J. Magn. Reson. Imaging* 47, 1171–1189. doi: 10.1002/jmri.25876
- Kronlage, M., Schwehr, V., Schwarz, D., Godel, T., Uhlmann, L., Heiland, S., et al. (2018). Peripheral nerve diffusion tensor imaging (DTI): normal values and demographic determinants in a cohort of 60 healthy individuals. *Eur. Radiol.* 28, 1801–1808. doi: 10.1007/s00330-017-5134-z
- Lehmann, H. C., Zhang, J., Mori, S., and Sheikh, K. A. (2010). Diffusion tensor imaging to assess axonal regeneration in peripheral nerves. *Exp. Neurol.* 223, 238–244. doi: 10.1016/j.expneurol.2009.10.012
- Levey, A. S., Stevens, L. A., Schmid, C. H., Zhang, Y. L., Castro, A. F., Feldman, H. L., et al. (2009). A new equation to estimate glomerular filtration rate. *Ann. Int. Med.* 150, 604–612.
- Li, Q., Ryan, L., Sattar, N., Chalmers, J., Woodward, M., Poulter, N., et al. (2014). Do cardiac biomarkers NT-proBNP and hsTnT predict microvascular events in patients with type 2 diabetes? results from the ADVANCE trial. *Diabetes Care* 37, 2202–2210. doi: 10.2337/dc13-2625
- Marmoy, O. R., Furlong, P. L., and Moore, C. E. G. (2019). Upper and lower limb motor axons demonstrate differential excitability and accommodation to strong hyperpolarizing currents during induced hyperthermia. *J. Neurophysiol.* 121, 2061–2070. doi: 10.1152/jn.00464.2018
- Morgenstern, J., Groener, J. B., Jende, J. M. E., Kurz, F. T., Strom, A., Göpfert, J., et al. (2021). Neuron-specific biomarkers predict hypo- and hyperalgesia in individuals with diabetic peripheral neuropathy. *Diabetologia* 64, 2843–2855. doi: 10.1007/s00125-021-05557-6
- Nobue, A., Kunimasa, Y., Tsuneishi, H., Sano, K., Oda, H., and Ishikawa, M. (2020). Limb-Specific features and asymmetry of nerve conduction velocity and nerve trunk size in human. *Front. Physiol.* 11:1576. doi: 10.3389/fphys.2020.609006
- O'Donnell, L. J., Suter, Y., Rigolo, L., Kahali, P., Zhang, F., Norton, I., et al. (2017). Automated white matter fiber tract identification in patients with brain tumors. *Neuroimage Clin.* 13, 138–153. doi: 10.1016/j.nicl.2016.11.023
- Pham, M., Oikonomou, D., Hornung, M., Weiler, M., Heiland, S., Bäumer, P., et al. (2015). Magnetic resonance neurography detects diabetic neuropathy early and with proximal predominance. *Ann. Neurol.* 78, 939–948.
- Shauver, M. J., and Chung, K. C. (2013). The michigan hand outcomes questionnaire (MHQ) after 15 years of field trial. *Plast Reconstr. Surg.* 131, 779e–787e. doi: 10.1097/PRS.0b013e3182865d83
- Spallone, V., and Greco, C. (2013). Painful and painless diabetic neuropathy: one disease or two? *Curr. Diab. Rep.* 13, 533–549. doi: 10.1007/s11892-013-0387-7
- Tesfaye, S., Chaturvedi, N., Eaton, S. E. M., Ward, J. D., Manes, C., Ionescu-Tirgoviste, C., et al. (2005). Vascular risk factors and diabetic neuropathy. *N. Engl. J. Med.* 352, 341–350. doi: 10.1056/NEJMoa032782
- Tiffin, J., and Asher, E. J. (1948). The purdue pegboard: norms and studies of reliability and validity. *J. Appl. Psychol.* 32, 234–247. doi: 10.1037/h0061266
- Vaeggemose, M., Haakma, W., Pham, M., Ringgaard, S., Tankisi, H., Ejksjaer, N., et al. (2020). Diffusion tensor imaging MR neurography detects polyneuropathy in type 2 diabetes. *J. Diabetes Complications* 34:107439. doi: 10.1016/j.jdiacomp.2019.107439
- Vaeggemose, M., Pham, M., Ringgaard, S., Tankisi, H., Ejksjaer, N., Heiland, S., et al. (2017). Magnetic resonance neurography visualizes abnormalities in sciatic and tibial nerves in patients with type 1 diabetes and neuropathy. *Diabetes* 66, 1779–1788. doi: 10.2337/db16-1049
- Wayand, D., Baum, H., Schätzle, G., Schärf, J., Neumeier, D., Rodeheffer, R. J., et al. (2000). Cardiac troponin T and I in end-stage renal failure. *Clin. Chem.* 46, 1345–1350. doi: 10.1373/clinchem.2009.130740
- Xia, X., Dai, L., Zhou, H., Chen, P., Liu, S., Yang, W., et al. (2021). Assessment of peripheral neuropathy in type 2 diabetes by diffusion tensor imaging: a case-control study. *Eur. J. Radiol.* 145:110007. doi: 10.1016/j.ejrad.2021.110007
- Young, M. J., Boulton, A. J. M., Macleod, A. F., Williams, D. R. R., and Onksen, P. H. S. (1993). A multicentre study of the prevalence of diabetic peripheral neuropathy in the United Kingdom hospital clinic population. *Diabetologia* 36, 150–154.

Conflict of Interest: The authors declare that the research was conducted in the absence of any commercial or financial relationships that could be construed as a potential conflict of interest.

Publisher's Note: All claims expressed in this article are solely those of the authors and do not necessarily represent those of their affiliated organizations, or those of the publisher, the editors and the reviewers. Any product that may be evaluated in this article, or claim that may be made by its manufacturer, is not guaranteed or endorsed by the publisher.

Copyright © 2022 Jende, Kender, Morgenstern, Renn, Mooshage, Juerchott, Kopf, Nawroth, Bendszus and Kurz. This is an open-access article distributed under the terms of the Creative Commons Attribution License (CC BY). The use, distribution or reproduction in other forums is permitted, provided the original author(s) and the copyright owner(s) are credited and that the original publication in this journal is cited, in accordance with accepted academic practice. No use, distribution or reproduction is permitted which does not comply with these terms.



High-Resolution Ultrasound and Magnetic Resonance Imaging of Abnormal Ligaments in Thoracic Outlet Syndrome in a Series of 16 Cases

Suren Jengojan¹, Maria Bernathova^{1*}, Thomas Moritz², Gerd Bodner³, Philipp Sorgo^{1,4} and Gregor Kasprian¹

¹ Department of Biomedical Imaging and Image-guided Therapy, Medical University of Vienna, Vienna, Austria, ² Radiology Department, Christchurch Hospital, Christchurch, New Zealand, ³ Neuromuscular Imaging Center Döbling, Vienna, Austria, ⁴ Karl Landsteiner Private University, Krems, Austria

OPEN ACCESS

Edited by:

Felix Tobias Kurz,
Heidelberg University Hospital,
Germany

Reviewed by:

Heather Smith,
Midwestern University, United States
Stephen Annest,
Vascular Institute of the Rockies,
United States

*Correspondence:

Maria Bernathova
maria.bernathova@medunivien.ac.at

Specialty section:

This article was submitted to
Brain Imaging Methods,
a section of the journal
Frontiers in Neuroscience

Received: 17 November 2021

Accepted: 22 December 2021

Published: 02 February 2022

Citation:

Jengojan S, Bernathova M,
Moritz T, Bodner G, Sorgo P and
Kasprian G (2022) High-Resolution
Ultrasound and Magnetic Resonance
Imaging of Abnormal Ligaments in
Thoracic Outlet Syndrome in a Series
of 16 Cases.

Front. Neurosci. 15:817337.
doi: 10.3389/fnins.2021.817337

Introduction: Neurogenic thoracic outlet syndrome (NTOS) is a complex entity that comprises various clinical presentations, which are all believed to result from mechanical stress to the brachial plexus. Causes for the stress can include fibrous bands, spanning from the transverse processes, stump, or cervical ribs to the pleural cupula. The aim of this case series is to document how the combined potential of high-resolution neurography, including high-resolution ultrasound (HRUS), and magnetic resonance imaging (MRI) can be used to identify, anatomical compression sites, such as stump ribs and their NTOS associated ligamentous bands.

Materials and Methods: Retrospective chart and image reviews identified patients, who underwent HRUS between 2011 and 2021 and the diagnosis of NTOS caused by accessory ligaments was subsequently confirmed by radiological imaging (MRI) and/or surgical exploration.

Results: Sixteen patients were included in this study. In all cases, a ligament extending from the tip of a stump rib to the pleural cupula could be depicted. In all cases, these structures led to compression of the lower trunk of the brachial plexus. All surgically explored cases confirmed the radiological findings.

Conclusion: This case-series demonstrates that HRUS and MRI can directly and reliably visualize accessory costocupular ligaments and a stump rib in patients with symptoms of NTOS. HRUS may be used as the first imaging modality to diagnose suspected NTOS.

Keywords: thoracic outlet syndrome, cervical ribs, fibrous ligaments, high-resolution ultrasound, magnetic resonance imaging, fiber tracking

INTRODUCTION

The thoracic outlet syndrome (TOS) is a complex syndrome that comprises various clinical neurovascular entities, which are all believed to result from mechanical stress in the region that is clinically referred to as the thoracic outlet region (Ferrante, 2012). The anatomical complexity of this region has been described as long ago as the end of the 19th century and still poses a considerable challenge to clinicians and radiologists (Zuckerkindl, 1876; Martinoli et al., 2010).

Pathologic processes or predispositions leading to a TOS can be divided into anatomical or functional causes (e.g., postural and respiratory alterations) (Vanti et al., 2007). Depending on the structures affected, TOS is divided into an arterial type (A-TOS), a venous form (V-TOS), and into the most common, neurogenic TOS (NTOS), which represents approximately 90% of TOS. NTOS is further divided into the so-called “true”-NTOS, where there are objective anatomical and/or electrodiagnostic findings and the so-called “disputed”-NTOS where such findings cannot be established. The percentage of disputed NTOS has been reported at a rate of as much as 85% in the literature (Vanti et al., 2007). A potential cause of NTOS is compression of the brachial plexus trunks within the scalene musculature (Leonhard et al., 2016).

The clinical presentation of TOS varies substantially and, in addition to vascular symptoms, most commonly involves wasting of the thenar and hypothenar eminence, of the ulnar intrinsic muscles, and the medial forearm muscles (Baumer et al., 2014). The diagnosis of TOS is frequently established by clinical examination, with false-positive rates of typical clinical tests ranging from 9 to 77% (Nord et al., 2008). Previously, the task of imaging in clinically suspected TOS was mainly limited to detecting osseous anomalies and angiographic or color Doppler flow changes in the subclavian vessels during postural changes (Braun, 2010).

Compression and hemodynamically relevant stenosis of the subclavian artery occurs due to cervical ribs, scalenus anticus muscle, costoclavicular narrowing.

In up to 85 % of the A-TOS cases cervical ribs are present resulting in A-TOS with vascular and neurological symptoms.

Compression of the subclavian artery leads to upper limb ischemia and cooling, pain, fatigability, claudication, pallor, and decrease or absence of distal pulsations, while neurological symptoms are only secondary to the vascular anomalies in A-TOS (Ferrante and Ferrante, 2017).

However, while only 5–10% of osseous anomalies are considered causative of TOS, up to 66% of NTOS patients show soft tissue variants at surgical exploration, such as muscle or ligament variants that affect the neurovascular bundle (Makhoul and Machleder, 1992; Roos, 1999; **Figure 1**).

Among the soft tissue variants, the ligaments in the thoracic outlet region have been a particular focus of attention in patients with NTOS. Juvonen et al. (1995) have reported variable fibrous cervical bands in the thoracic outlet region in more than 50% of the general population and in more than 90% of patients treated surgically for NTOS (Urschel and Grewal, 1995). Roos et al. have described several different variants of such fibrous bands. Two distinct types (Roos Types I and II) run from the tip of a cervical

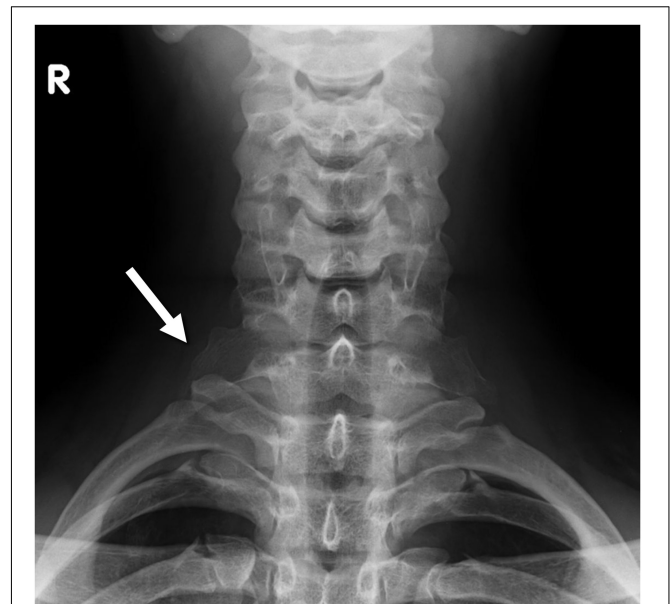


FIGURE 1 | Radiograph of the cervical spine shows a stump rib on both sides (white arrow).

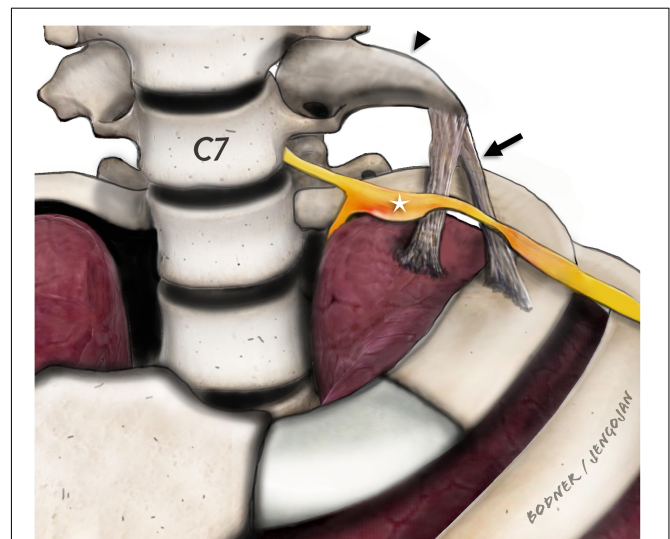


FIGURE 2 | Para-sagittal/para-coronal illustration of the stump rib (black arrowhead) and the fibrous ligaments (black arrow). Adjacent to the tip of the stump rib (C7), the fibrous ligaments are drawn which extend either to the first rib or to the pleural cupula as described by Emil Zuckerkindl. The inferior brachial plexus (C8 and T1) components (white star) are displaced and enlarged with obvious constriction at the direct level of the crossing fibrous ligaments. In our study, we only detected ligaments extending to the pleural cupula.

rib or hypertrophic transverse process to the upper aspect of the first rib and partly to the pleural cupula. The course of these ligaments typically crosses the C7 and/or C8 cervical root and the inferior trunk of the brachial plexus and may be a cause of entrapment of these structures (Roos, 1976; **Figure 2**).

According to the literature there is, no well-defined or precise naming of rudimentary/incomplete cervical ribs, we therefore defined a pointed, elongated C7 transverse process or incomplete cervical rib with a fibrous ligament arising at its tip as stump rib throughout this manuscript.

Until today these ligaments have been hardly approached by imaging. The emergence of more sophisticated magnetic resonance imaging (MRI) and high-resolution ultrasound (HRUS) has changed the technical capabilities and the possibilities to visualize these small structures in an anatomical region, which is generally difficult to be accessed. As yet, there are only very few studies that have focused on the imaging of such ligaments and only one case report involving HRUS has been published (Simon et al., 2013; Baumer et al., 2014).

The use of clinical high field (3 tesla) MR has led to improvements in spatial resolution and better signal-to-noise ratios in visualizing small structures such as peripheral nerves, including the difficult system of the brachial plexus (Mallouhi et al., 2012). Diffusion tensor imaging (DTI) has shown promising results in the assessment of the brachial plexus in peripheral nerve entrapment syndromes (Makhoul and Machleder, 1992; Roos, 1999; Braun, 2010; Vargas et al., 2010; Tagliafico et al., 2011; Ferrante, 2012). Entrapment of the brachial plexus produced by structures, such as cervical ribs and fibrous bands, has been reported in seven of thirty patients with clinical signs of TOS using 3 Tesla MR-Neurography with a positive predictive value of 100% (Baumer et al., 2014). To our knowledge, the combined use of HRUS and MRI with and without the use of peripheral nerve tractography has not been systematically evaluated in a series of patients with anatomical compression of the brachial plexus.

The aim of this retrospective multimodal imaging study is to: (a) demonstrate the reliable possibility of visualization of ligaments in the thoracic outlet region by means of HRUS; (b) review the HRUS features of the ligaments and compression; and (c) correlate these features to the clinical, surgical, and MRI findings. Furthermore, we seek to evaluate whether the deterministic DTI based tractography of the brachial plexus can provide additional imaging aspects in anatomical conditions that lead to NTOS.

MATERIALS AND METHODS

The study was conducted according to the Declaration of Helsinki and was approved by the local Institutional Ethics Review Board (IRB) of the Medical University of Vienna.

A retrospective analysis was conducted of the HRUS images of all patients who presented with a final diagnosis of NTOS caused by abnormal ligaments who had been treated surgically or who had had a 3 Tesla MRI examination. Ultrasound examinations were performed using HRUS equipment (GE Logiq e9, ML6-15-D, and L8-18i-D). Findings were documented in the para-axial, para-coronal, and para-sagittal planes using both still images and dynamic video sequences in both the resting position and in dynamic arm movement and forced inspiration and expiration.

High-Resolution Ultrasound Image Evaluation

The HRUS examinations were reviewed in consensus by two radiologists with more than 5 years of experience in peripheral nerve imaging. Images were assessed for an increase in nerve diameter defined as a focal or regional increase of the cross-sectional area (CSA) by more than 25% or signs of fascicular swelling, as well as a significant course deviation, defined as a sudden pointed kink of the whole nerve with a sustained change in the course by more than 30 degrees (minimal value in all imaged planes). Furthermore, the images were evaluated with regard to hyperechoic linear structures that resembled ligaments, their respective courses, and possible subclavian artery narrowing.

Magnetic Resonance Imaging and Diffusion Tensor Imaging Evaluation

Existing MRI examinations of those who matched the inclusion criteria and were retrospectively assessed.

The MRI examinations [coil: 16-channel neurovascular coil; imaging sequences: sagittal and transversal T2-weighted (T2w) turbo spin echo (TSE), parasagittal short term inversion recovery (STIR), paracoronal T1w TSE, parasagittal T2W volume isotropic turbo spin-echo acquisition (VISTA), axial DTI] were reviewed in consensus by two radiologists with more than 5 years' experience in peripheral nerve MR imaging. Nerve diameter enlargement, increased T2W signal, as well as significant nerve fiber course deviation was assessed. In addition, the images were evaluated with regard to the fibrous bands described on HRUS, which affected the brachial plexus or subclavian vessels.

The DTI source data (axial, echo-planar, single-shot DTI sequence, *b*-values of 0 and 700 s/mm², 16 diffusion encoding directions, slice thickness 3 mm, acquisition time 6 min 10 s) was post-processed using the Philips Intellispace Workstation (Philips Medical Systems, Best, Netherlands). The transaxial DTI data was used to identify the nerves and myelon. Deterministic tractography of the brachial plexus was performed one experienced examiner by placing regions of interest (ROIs) along the course of the respective nerves, using standard fiber reconstruction thresholds (*FA* = 0.15, angle change = 27°) and a FACT (fiber assignment by continuous tracking) algorithm. The post-processing procedure took around 20–30 min per plexus.

Clinical Record Review

The patient history was accessed in the local RIS by searching for documents relevant for the study of the central clinical problem (NTOS). Radiological reports, reports of functional tests (e.g., nerve conduction studies), surgical reports, and discharge letters were analyzed for information relevant to the study. Surgical image documentation was also accessed, if applicable.

RESULTS

There were 158 patients evaluated using HRUS for suspected NTOS during the study period. Of those, 16 patients were

TABLE 1 | Detailed chart review of all patients included in this study. In the top column the symptoms, results, therapies and examinations considered in this study are listed.

Case number/ Age/Sex	Neurologic symptoms	Muscular/Sensory (M, S) symptoms	Affected side	Symptom duration	Previous surgery	Sonography	MR (3 Tesla)	Treatment
1/29y/F	Median nerve atrophy intrinsic muscles	M, S	bilateral	15 years	Unilateral (left) first rib and subsequent cervical rib resection	Stump rib C7, accessory ligament from tip to pleural dome, diversion and constriction C8; C7 riding on cervical rib tip, marked swelling C8	Yes	Surgical resection
2/35y/M	Ulnar distribution	M, S	right	2 years	Carpal tunnel syndrome on the right side and "trigger finger"	Stump rib C7, accessory ligament from tip to pleural dome, diversion and constriction C8, Th1; C7 riding on cervical rib tip, swelling C7, C8, Th1	Yes	Surgical resection
3/75y/M	Ulnar distribution	M, S	left	10 years	none	Stump rib C7, accessory ligament from the tip to the pleural dome, displacement and constriction of C8, riding of C7 on the rib	Yes	Conservative
4/26y/F	Median distribution	M, S	right	3 years	none	Stump rib C7, C6 root riding on edge tip, during head turn. Accessory ligament from the tip to the pleural dome	Yes	Conservative
5/33y/F	Median nerve territory, clinical diagnosis of carpal tunnel syndrome and ulnar neuropathy at the elbow	S	right	unknown	none	Stump rib on the right side with an accessory ligament to the pleural dome, compression, and displacement of C8, C7 riding on tip of the rib	Yes	Surgical resection
6/53y/F	Weakness of the left forearm, clumsiness of the hand, nuchal pain, paraesthesia in both hands, all fingers	M, S	left	10 years	none	Stump rib C7 with pseudarthrosis on the left, accessory ligament from tip to pleural dome, diversion and constriction C8	Yes	Surgical resection
7/56y/F	Diffuse pain radiating from the shoulder down the hand, territory not compatible with radicular or peripheral pattern	S	left	15 years	none	Stump rib on the left with riding and constriction of C8. Accessory ligament to the pleural dome.	Yes	Conservative
8/50y/F	Ulnar distribution, clinically suspected Loge de Guyon syndrome	M, S	bilateral	10 years	none	Stump rib C7 on both sides, only right side symptomatic, accessory ligament to the pleural dome, compression, and displacement of C8	Yes	Surgical resection
9/55y/F	Clinically atypical carpal tunnel syndrome on the right side	M, S	right	8 years	none	Stump rib C7 on the right side, accessory ligament to the pleural dome	Yes	Surgical resection
10/45y/F	Unclear dysesthesia of the hand, nuchal pain	M,S	right	3 years	none	Stump rib C7 on both sides. No direct contact to the nerves	Yes	Conservative
11/45y/M	Diffuse pain in the right hand	M	right	unknown	none	Stump rib C7 on the right side, accessory ligament to the pleural dome	Yes	Conservative
12/74y/F	C8 muscle weakness	M	right	unknown	none	Stump rib C7, accessory ligament from tip to pleural dome following medial border of scalenus medius muscle, indentation C8/Th1	No	Surgical resection
13/43y/F	Adductor pollicis brevis atrophy, dysesthesia C8/Th1	M,S	right	2 years	none	Stump rib C7, accessory ligament from tip to pleural dome following medial border of scalenus medius muscle, thickened inferior trunk C8/Th1	No	Surgical resection
14/54y/F	Atrophy of intrinsic hand muscles and abductor pollicis brevis muscle, pain C8/Th1, Raynaud syndrome	M,S	right	unknown	none	Stump rib C7, accessory ligament from tip to pleural dome following medial border of scalenus medius muscle, thickened inferior trunk C8/Th1	No	Surgical resection
15/25/F	Acute scapula alata with atrophy of the serratus anterior muscle. Hypesthesia of the thumb and forefinger.	M, S	right	one week	none	Stump rib C7 on both sides, accessory ligament from tip to pleural dome thickening and displacement C7/C8	Yes	Surgical resection
16/49y/F	Atrophy of intrinsic hand muscles and abductor pollicis brevis muscle, arm pain	M,S	right	15 y	none	Stump rib C7, accessory ligament from tip to pleural dome following medial border of scalenus medius muscle, thickened inferior trunk C8/Th1	No	Surgical resection

diagnosed with NTOS, and were, therefore, eligible for the study [mean age 47 years (SD, 15 years), 13 females, 3 males]. All of them reported spontaneous development of clinical symptoms that showed a broad spectrum from diffuse pain radiating from the shoulder down the upper extremity, to distinct atrophy of the C8 muscles (for details, see **Table 1**). The mean time to final diagnosis was 8 years (SD, 5 years) based on the responses of 11 patients. In five patients, the duration of symptoms could not be reliably determined.

Sonographically, a common pattern of a slightly hyperechoic, anisotropic, linear structure that extended from the tip of a stump rib ($n = 16$) to the pleural cupula could be depicted (**Figures 3, 4**).

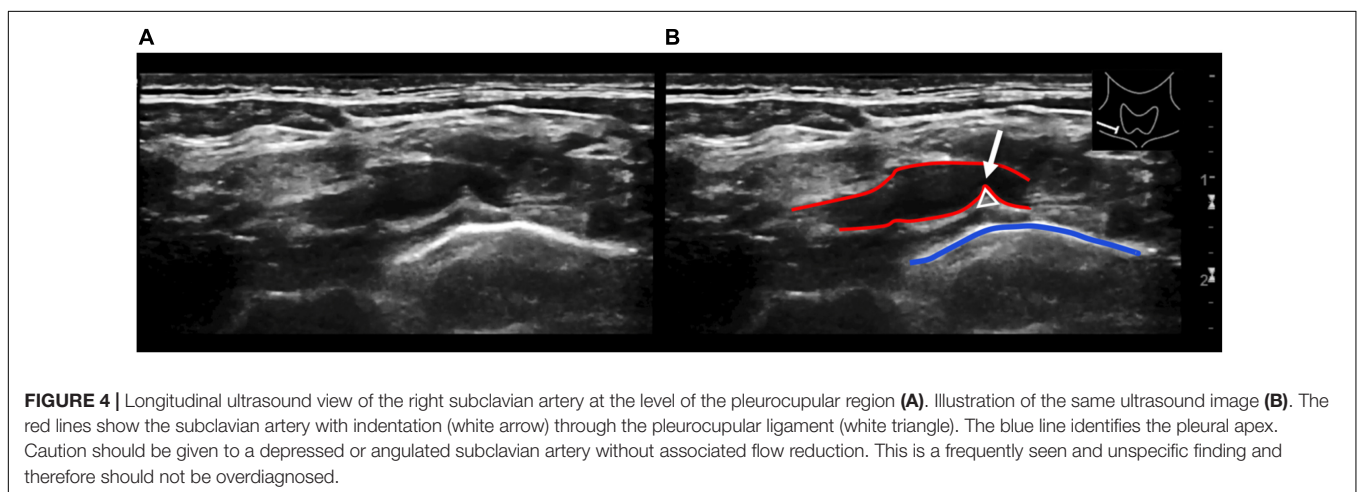
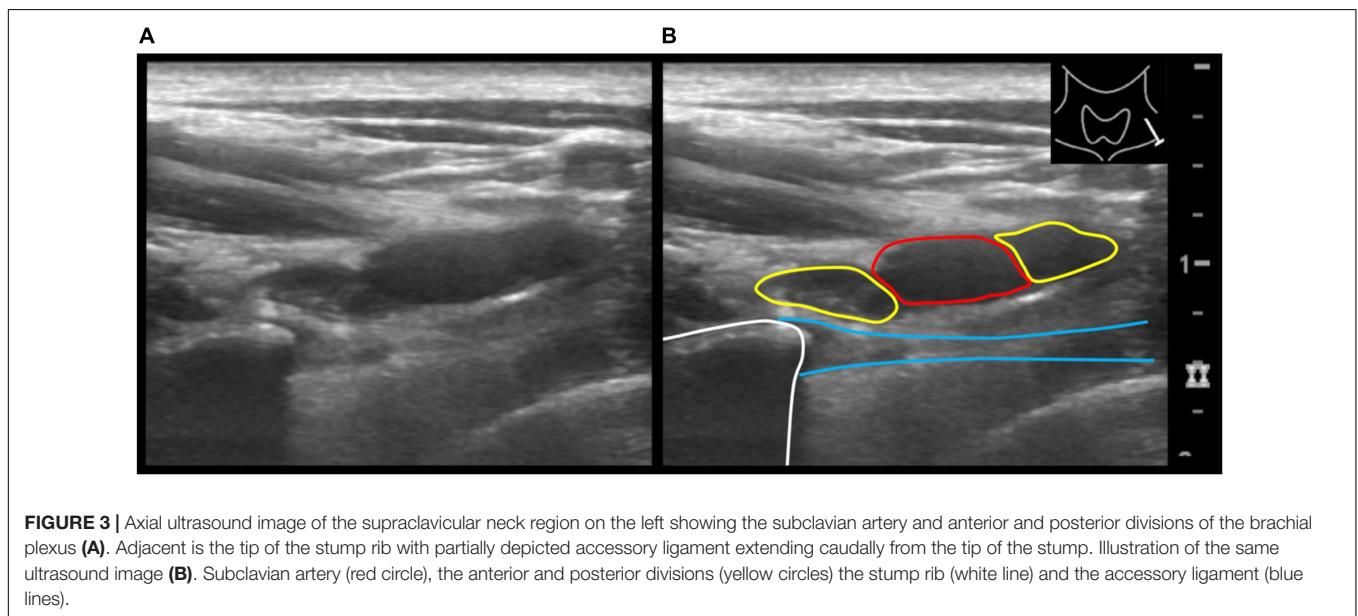
High-resolution ultrasound was able to assess the direct effect of the anatomical variants on the roots of the brachial plexus. In all cases, the ligament crossed the path of the subclavian artery, leading to a visible indentation of the artery and the C7 or C8 anterior ramus, which resulted in a significant course deviation of cervical roots even in the resting position. Five

patients also showed an impression on the nerve fibers C8 and T1, accompanied by a focal thickening, compared to both the contralateral side and the neighboring nerve fibers.

Of all the eligible patients, two had already received surgical treatment for NTOS symptoms at the affected extremity without clinical benefit. A summary of clinical, neurological, and HRUS findings is given in **Table 1**. Eleven eligible patients subsequently received surgical treatment, where the HRUS finding of a costo- or transverso-cupular ligament was confirmed in all cases (**Figure 5**).

Twelve patients were examined with 3 Tesla MRI (Philips Achieva, Best, Netherlands). MRI showed (best seen in the parasagittal STIR sequence) a thin, T2w-hypointense, band-like structure, extending caudally from the tip of the stump rib toward the pleural dome.

A clear T2w/STIR signal increase, a significant course alteration or a compression has been demonstrated in the inferior plexus portions (C7, C8, or T1 spinal nerves, inferior trunk,



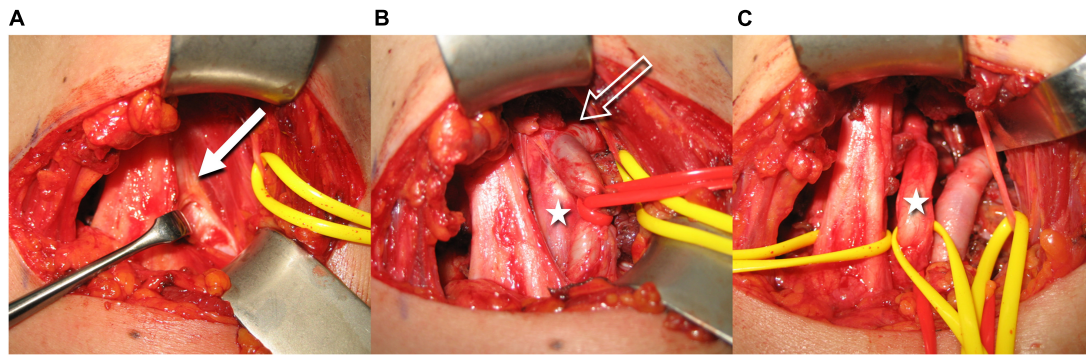


FIGURE 5 | Intraoperative images illustrate the resection steps of the accessory ligament (the left side of the images is dorsal, top is cranial, right is ventral, and bottom is caudal). The white arrow shows the fibrous ligament above the neurovascular bundle **(A)**. After partial excision, a section of the brachial plexus is visible (white star). The constriction of the subclavian artery becomes evident (void white arrow) **(B)**. After complete removal of the fibrous band, the neurovascular bundle is now fully mobilized **(C)** (Courtesy of Prof. O. Aszmann).

or medial cord). In all patients, MRI confirmed the findings of HRUS, the deviation, impingement, or swelling of the affected nerve roots, including the stump rib and the fibrous ligament.

Diffusion tensor imaging-based fiber tractography of the brachial plexus and myelon was performed in ten patients. One data set could not be evaluated due to severe patient motion. In the remaining data sets, fibers of the upper brachial plexus nerve roots were visualized. Visualization of the inferior brachial plexus was limited due to breathing artifacts in 5/7 cases and did not reveal any abnormalities without knowledge of the structural MR findings. In 3/10 cases (**Figure 6**) a deviation of portions of the brachial plexus could be visualized in 3D by tractography.

DISCUSSION

This case series highlights the novel diagnostic feasibility of HRUS in patients with NTOS. We assessed 16 patients with NTOS where the HRUS diagnosis of accessory cervical ligaments that exert mechanical pressure on the brachial plexus were confirmed surgically or with MR tomography.

Accessory ligaments were first described by Emil Zuckerkandl at the end of the 19th century and have long been recognized in the anatomical and surgical literature as having a significant clinical relevance with regard to TOS and the thoracic outlet region (Roos, 1976, 1999; Redenbach and Nelems, 1998). Their occurrence is related to a hypertrophic transverse process, a cervical rib or stump rib, from which they strain toward the pleural cupula or the first rib—which corresponds to our findings in HRUS. In our series, HRUS was not only able to visualize the accessory cervical ligament, but also the cervical stump rib.

Although Doppler sonography is a well-established modality in the diagnosis of arterial TOS, the use of HRUS for the diagnosis of NTOS is still in its infancy. The patients in our sample showed indentation of the subclavian artery at a resting position and a moderate increase in the flow velocity during arm elevation; however, only one of the patients demonstrated a vessel stenosis considered to be hemodynamically relevant. The changing indentation of the vessel wall certainly represents

significant chronic mechanical stress to the vessel and might well be a predisposing factor for future vessel damage. Nevertheless, as it has been described previously indented or angulated subclavian artery without any hemodynamically relevant stenosis is non-specific and is seen also in patients with other conditions and should not be misinterpreted or overdiagnosed (Ferrante and Ferrante, 2017). The other typical imaging findings in patients our sample with NTOS generally did not vary from the HRUS findings in other compression neuropathies throughout the body and included thickening, indentation, or compression of nerve structures, as well as changes in echotexture with a loss of fascicular structure and increased hypoechogenicity, as well as course deviation. In our cohort, all of these imaging features were found to various degrees.

In addition to changes in neural structures and vessels, the results of our study indicate that HRUS may also be able to scan for bone and muscle variants or anomalies. All stump ribs, cervical ribs, or hypertrophied transverse processes were clearly depicted using HRUS. However, this needs to be targeted in future research.

We are aware of one study dealing with feasibility of high-field MRI in TOS (Baumer et al., 2014) who used a dedicated, customized surface coil and confirmed the possibility of visualization of fibrous bands compressing the brachial plexus (Baumer et al., 2014), findings that are also fully consistent with our MRI results. However, compared to MRI, HRUS brings several potential advantages: first, substantially higher spatial resolution using commercially available high-end equipment. Second, direct patient contact with the examiner, with the possibility of direct history taking and so-called “sonopalpation” (Boon et al., 2012), i.e., targeted application of pressure with the HRUS probe or the finger of the examiner and direct clinical correlation by a positive Tinel’s sign. Third, the possibility of a dynamic examination technique without the limitation of motion artifacts (breathing, pulsation of the vessels) (Vargas et al., 2009). This translates to several advantages, as TOS often shows a dynamic etiology and causes may be found both in detail or during arm or breathing motion.

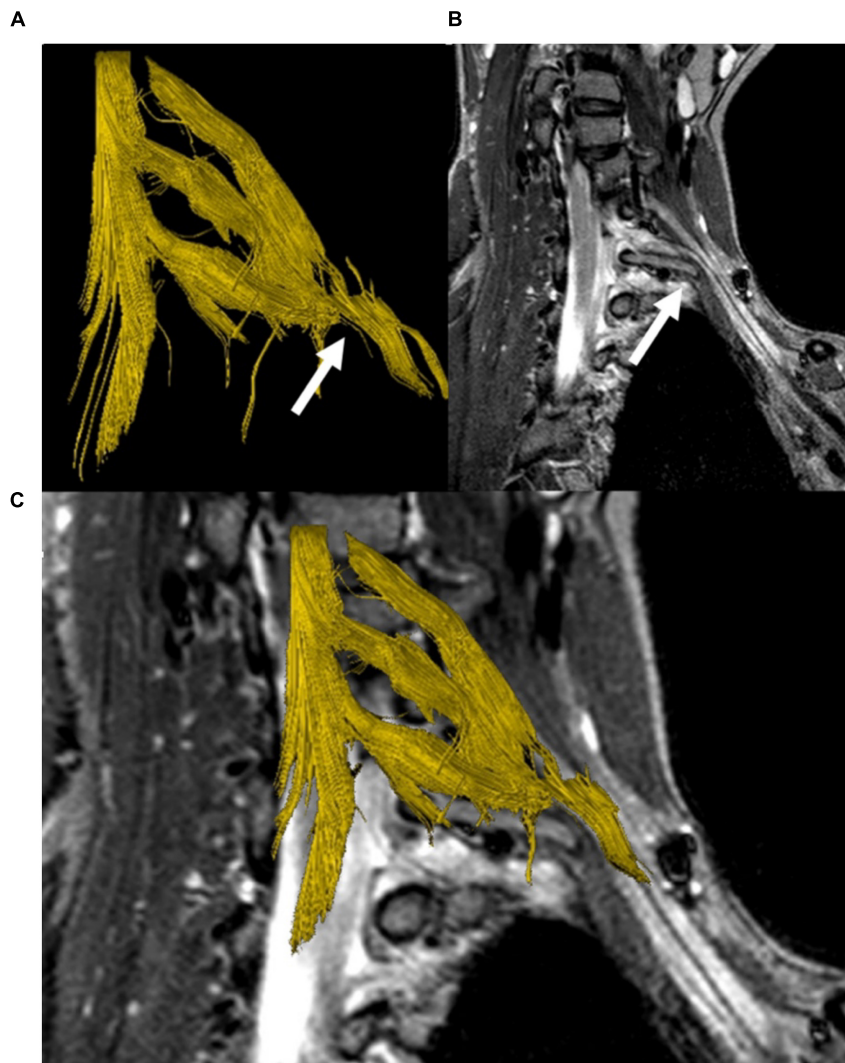


FIGURE 6 | DTI-based fiber tractography of the left brachial plexus in a patient with a cervical stump rib (C7). 3D fiber tract reconstruction of neuronal fibers generated from DTI data **(A)**, parasagittal STIR-MRI sequence demonstrating the peak apex of the stump rib with clear elevation and a shift of the lower brachial plexus segments (white arrow) **(B)**. Merging of the fiber track and anatomical series **(C)** demonstrates the cervical rib's impact on the course of neuronal fibers, causing a plausible, visible correlation between the MRI and DTI/FT data sets.

Generally, we consider the approach of using HRUS as clinically oriented screening instrument and MRI as a complementary and confirmatory modality to be most appropriate for the assessment of patients with TOS. As both modalities need a certain level of experience, the examiner must be trained in peripheral nerve imaging. However, by combining both modalities patients would benefit from the high sensitivity of ultrasound and high specificity of MRI in assessing peripheral nerve compression by ligaments.

More advanced techniques such as DTI, are technically challenging, potentially limited by breathing motions in the plexus region in proximity of the lung apex. However, in some cases DTI based tractography allowed a 3D visualization of the nerve course deviation. This plastic and easily comprehensible visualization may be

specifically useful for surgeons in the preparation of the decompressive surgery.

Due to the manual segmentation of DTI datasets currently required, deterministic tractography of the brachial plexus is still relatively time-consuming (20–30 min per plexus) and requires further technical improvements to become more applicable in clinical routine. In the future examiner independent probabilistic tractography approaches and optimized motion insensitive DTI sequence acquisition schemes will lead to more robust results.

All the above-mentioned factors may contribute to a quick and precise diagnosis in patients with NTOS. This is urgently needed, as these patients usually experience a long time until their diagnosis (a mean of 9 years in our sample) and the detection and often unspecific clinical presentation may lead to unnecessary surgery (Roos, 1999).

There are limitations to this study that arise from the retrospective case series design. A retrospective evaluation may be subject to a selection or measurement bias. The lack of a control group for the patients in this case series is another limitation. However, as patient outcomes or treatment success was not the subject of this study and the examinations were performed in a standardized fashion, all of these limitations can be considered less serious. This, together with the fact that the study sample is the largest sample that has been observed through imaging methods, makes this case series a valuable piece of information that is meant to be an entry point into further research on this topic.

In conclusion, this case series demonstrates that HRUS can directly visualize accessory costocupular ligaments in their anatomical context in patients with symptoms of NTOS. Combining HRUS with MR-Neurography is a highly sensitive and optimal imaging approach in these conditions and may, therefore, be able to significantly improve patient care for TOS patients.

DATA AVAILABILITY STATEMENT

Requests for access to the datasets used for this study can be directed to SJ, suren.jengojan@meduniwien.ac.at and MB, maria.bernathova@meduniwien.ac.at.

REFERENCES

- Baumer, P., Kele, H., Kretschmer, T., Koenig, R., Pedro, M., Bendszus, M., et al. (2014). Thoracic outlet syndrome in 3T MR neurography-fibrous bands causing discernible lesions of the lower brachial plexus. *Eur. Radiol.* 24, 756–761. doi: 10.1007/s00330-013-3060-2
- Boon, A. J., Smith, J., and Harper, C. M. (2012). Ultrasound applications in electrodiagnosis. *PM R* 4, 37–49. doi: 10.1016/j.pmrj.2011.07.004
- Braun, R. M. (2010). Thoracic outlet syndrome: a primer on objective methods of diagnosis. *J. Hand Surg. Am.* 35, 1539–1541. doi: 10.1016/j.jhsa.2010.03.018
- Ferrante, M. A. (2012). The thoracic outlet syndromes. *Muscle Nerve* 45, 780–795.
- Ferrante, M. A., and Ferrante, N. D. (2017). The thoracic outlet syndromes: part 2. The arterial, venous, neurovascular, and disputed thoracic outlet syndromes. *Muscle Nerve* 56, 663–673. doi: 10.1002/mus.25535
- Juvonen, T., Satta, J., Laitala, P., Luukkonen, K., and Nissinen, J. (1995). Anomalies at the thoracic outlet are frequent in the general population. *Am. J. Surg.* 170, 33–37. doi: 10.1016/s0002-9610(99)80248-7
- Leonhard, V., Smith, R., Caldwell, G., and Smith, H. F. (2016). Anatomical variations in the brachial plexus roots: implications for diagnosis of neurogenic thoracic outlet syndrome. *Ann. Anat.* 206, 21–26. doi: 10.1016/j.aanat.2016.03.011
- Makhoul, R. G., and Machleder, H. I. (1992). Developmental anomalies at the thoracic outlet: an analysis of 200 consecutive cases. *J. Vasc. Surg.* 16, 534–42; discussion 542–5.
- Mallouhi, A., Marik, W., Prayer, D., Kainberger, F., Bodner, G., and Kasprian, G. (2012). 3T MR tomography of the brachial plexus: structural and microstructural evaluation. *Eur. J. Radiol.* 81, 2231–2245. doi: 10.1016/j.ejrad.2011.05.021
- Martinoli, C., Gandolfo, N., Perez, M. M., Klauser, A., Palmieri, F., Padua, L., et al. (2010). Brachial plexus and nerves about the shoulder. *Semin. Musculoskelet. Radiol.* 14, 523–546.

ETHICS STATEMENT

The studies involving human participants were reviewed and approved by the Ethics Committee of the Medical University of Vienna. Written informed consent for participation was not required for this study in accordance with the national legislation and the institutional requirements.

AUTHOR CONTRIBUTIONS

GB, SJ, GK, MB, and TM contributed to conception and design of the study. MB and PS organized the database. PS performed the statistical analysis. MB and TM wrote the first draft of the manuscript. GB, SJ, and GK wrote sections of the manuscript. SJ wrote the submitted version. All authors contributed to manuscript revision, read, and approved the submitted version.

FUNDING

This study was supported by Division of Neuroradiology and Musculoskeletal Radiology, Medical University of Vienna.

- Nord, K. M., Kapoor, P., Fisher, J., Thomas, G., Sundaram, A., Scott, K., et al. (2008). False positive rate of thoracic outlet syndrome diagnostic maneuvers. *Electromyogr. Clin. Neurophysiol.* 48, 67–74.
- Redenbach, D. M., and Nelems, B. (1998). A comparative study of structures comprising the thoracic outlet in 250 human cadavers and 72 surgical cases of thoracic outlet syndrome. *Eur. J. Cardiothorac. Surg.* 13, 353–360. doi: 10.1016/s1010-7940(98)00037-2
- Roos, D. B. (1976). Congenital anomalies associated with thoracic outlet syndrome. Anatomy, symptoms, diagnosis, and treatment. *Am. J. Surg.* 132, 771–778. doi: 10.1016/0002-9610(76)90456-6
- Roos, D. B. (1999). Thoracic outlet syndrome is underdiagnosed. *Muscle Nerve* 22, 126–9; discussion 137–8. doi: 10.1002/(sici)1097-4598(199901)22:1<126::aid-mus21>3.0.co;2-s
- Simon, N. G., Ralph, J. W., Chin, C., and Kliot, M. (2013). Sonographic diagnosis of true neurogenic thoracic outlet syndrome. *Neurology* 81, 1965–1965. doi: 10.1212/01.wnl.0000436621.33155.ed
- Tagliafico, A., Calabrese, M., Puntoni, M., Pace, D., Baio, G., Neumaier, C. E., et al. (2011). Brachial plexus MR imaging: accuracy and reproducibility of DTI-derived measurements and fibre tractography at 3.0-T. *Eur. Radiol.* 21, 1764–1771. doi: 10.1007/s00330-011-2100-z
- Urschel, J. D., and Grewal, R. P. (1995). Congenital cervical bands in thoracic outlet syndrome. *Am. J. Surg.* 170:524. doi: 10.1016/s0002-9610(99)80345-6
- Vanti, C., Natalini, L., Romeo, A., Tosarelli, D., and Pillastrini, P. (2007). Conservative treatment of thoracic outlet syndrome. A review of the literature. *Eura. Medicophys.* 43, 55–70.
- Vargas, M. I., Delavelle, J., Kohler, R., Becker, C. D., and Lovblad, K. (2009). Brain and spine MRI artifacts at 3Tesla. *J. Neuroradiol.* 36, 74–81. doi: 10.1016/j.neurad.2008.08.001
- Vargas, M. I., Viallon, M., Nguyen, D., Delavelle, J., and Becker, M. (2010). Diffusion tensor imaging (DTI) and tractography of the brachial plexus: feasibility and initial experience in neoplastic conditions. *Neuroradiology* 52, 237–245. doi: 10.1007/s00234-009-0643-3

Zuckerkindl, E. (1876). Beitrag zur deskriptiven und topographischen Anatomie des unteren Halsdreiecks. *Z. Anat.* 2, 54–69.

Conflict of Interest: The authors declare that the research was conducted in the absence of any commercial or financial relationships that could be construed as a potential conflict of interest.

Publisher's Note: All claims expressed in this article are solely those of the authors and do not necessarily represent those of their affiliated organizations, or those of the publisher, the editors and the reviewers. Any product that may be evaluated in

this article, or claim that may be made by its manufacturer, is not guaranteed or endorsed by the publisher.

Copyright © 2022 Jengojan, Bernathova, Moritz, Bodner, Sorgo and Kasprian. This is an open-access article distributed under the terms of the Creative Commons Attribution License (CC BY). The use, distribution or reproduction in other forums is permitted, provided the original author(s) and the copyright owner(s) are credited and that the original publication in this journal is cited, in accordance with accepted academic practice. No use, distribution or reproduction is permitted which does not comply with these terms.



Magnetic Resonance Neurography Reveals Smoking-Associated Decrease in Sciatic Nerve Structural Integrity in Type 2 Diabetes

Johann M. E. Jende^{1†}, Christoph Mooshage^{1†}, Zoltan Kender², Stefan Kopf^{2,3}, Jan B. Groener^{2,3}, Sabine Heiland^{1,4}, Alexander Juerchott¹, Peter Nawroth^{2,3,5}, Martin Bendszus¹ and Felix T. Kurz^{1,6*}

¹ Department of Neuroradiology, Heidelberg University Hospital, Heidelberg, Germany, ² Department of Endocrinology, Diabetology and Clinical Chemistry, Heidelberg University Hospital, Heidelberg, Germany, ³ German Center of Diabetes Research, München-Neuherberg, Germany, ⁴ Division of Experimental Radiology, Department of Neuroradiology, Heidelberg, Germany, ⁵ Joint Institute for Diabetes and Cancer at Helmholtz-Zentrum Munich and Heidelberg University, Heidelberg, Germany, ⁶ Department of Radiology (E010), German Cancer Research Center, Heidelberg, Germany

OPEN ACCESS

Edited by:

Roberto Esposito,
ASUR Marche, Italy

Reviewed by:

Su Xiaoyun,
Huazhong University of Science
and Technology, China
Aleksandra Araszkiwicz,
Poznan University of Medical
Sciences, Poland

*Correspondence:

Felix T. Kurz
felix.kurz@med.uni-heidelberg.de

†These authors share first authorship

Specialty section:

This article was submitted to
Brain Imaging Methods,
a section of the journal
Frontiers in Neuroscience

Received: 08 November 2021

Accepted: 17 December 2021

Published: 15 February 2022

Citation:

Jende JME, Mooshage C,
Kender Z, Kopf S, Groener JB,
Heiland S, Juerchott A, Nawroth P,
Bendszus M and Kurz FT (2022)
Magnetic Resonance Neurography
Reveals Smoking-Associated
Decrease in Sciatic Nerve Structural
Integrity in Type 2 Diabetes.
Front. Neurosci. 15:811085.
doi: 10.3389/fnins.2021.811085

Objective: It is controversially discussed in how far smoking contributes to diabetic polyneuropathy (DPN) in type 2 diabetes (T2D). Diffusion-weighted magnetic resonance neurography (MRN) at 3 Tesla has been shown to provide objective values for structural nerve integrity in patients with T2D. The aim of this study was to investigate the contribution of cigarette smoking on structural nerve integrity in T2D.

Methods: This cross-sectional prospective cohort study investigated the structural integrity of the sciatic nerve in 10 smokers, 40 never-smokers, and 20 ex-smokers with T2D and 10 healthy control subjects, using diffusion tensor imaging MRN at 3 Tesla and semi-automated nerve fiber tracking. Results were correlated with clinical, electrophysiological, and serological data.

Results: The sciatic nerve's fractional anisotropy (FA), a parameter for structural nerve integrity, was significantly lower in smokers with T2D when compared to controls ($p = 0.002$) and never-smokers ($p = 0.015$), and lower in ex-smokers when compared to controls ($p = 0.015$). In addition, sciatic nerve radial diffusivity, a marker of myelin damage, was increased in smokers versus controls and never-smokers ($p = 0.048$, $p = 0.049$, respectively). Furthermore, FA in T2D patients was negatively correlated with clinical and electrophysiological markers of DPN. FA also showed negative correlations with the pulse wave velocity, a marker of arterial stiffness and associated microangiopathy, in controls ($r = -0.70$; $p = 0.037$), never-smokers ($r = -0.45$; $p = 0.004$), ex-smokers ($r = -0.55$; $p = 0.009$), and a similar trend in smokers ($r = -0.63$; $p = 0.076$). Negative correlations were found between FA and skin auto-fluorescence, a marker of tissue advanced glycation end product accumulation and therefore long-term glycemic stress in T2D, in never-smokers ($r = -0.39$; $p = 0.020$) and smokers ($r = -0.84$; $p = 0.004$), but not in ex-smokers ($r = -0.07$; $p = 0.765$).

Conclusion: The findings indicate that smoking contributes to sciatic nerve damage in T2D, potentially worsening DPN due to glycemic stress and less microangiopathy-associated myelin damage in active smokers, while angiopathic effects predominate in ex-smokers. To stop smoking may therefore pose a promising preventive measure to slow the progression of DPN in T2D.

Keywords: smoking, diabetic polyneuropathy, magnetic resonance neurography (MRN), type 2 diabetes, diffusion tensor imaging

INTRODUCTION

Distal symmetric diabetic polyneuropathy (DPN) is one of the most disabling complications of diabetes with increasing prevalence affecting about 200 million patients worldwide causing high morbidity and extensive healthcare costs (Alleman et al., 2015). The poor effect of adjusting serum glucose on the course of DPN in type 2 diabetes (T2D) indicates that pathophysiological mechanisms other than the effects of hyperglycemia play an important role in the development of DPN (Tesfaye et al., 2005; Toth et al., 2012). Although several additional clinical and serological risk factors for developing DPN such as obesity, hypertension, hyperglycemia, dyslipidemia, and a decrease in renal function have been identified in clinical studies, the exact pathophysiological mechanisms underlying DPN remain poorly understood. As a result, there still is a lack of sufficient therapeutic strategies and preventive measures for this disorder (Gaede et al., 1999; Tesfaye et al., 2005; Elliott et al., 2009).

A broadly accepted hypothesis assumes that, in addition to glycation of surface molecules of axons and Schwann cells induced by hyperglycemia, nerve ischemia as a consequence of microangiopathy is another major contributor to nerve damage and the occurrence of painful symptoms in DPN, especially in T2D (Shillo et al., 2019). In this context, it has been discussed controversially whether cigarette smoking as a potential cause for microangiopathy contributes to damage of peripheral nerves in DPN (Benbow et al., 1997; Clair et al., 2015). Although several clinical studies concluded that smoking increases the risk for DPN, and it was found recently that smoking is associated with structural changes in dorsal root ganglia (Jende et al., 2020c), it has not yet been possible to quantify the amount and extent of structural nerve damage caused by smoking *in vivo*. Also, it remains to be determined whether the main contributing factor to nerve damage caused by smoking in T2D is either microangiopathy as a consequence of oxidative stress to the endothelium or oscillations of blood glucose induced by smoking (Csordas and Bernhard, 2013; Christensen et al., 2020).

It is further unknown whether damage to peripheral nerves caused by smoking is reversible once a patient stops smoking (Clair et al., 2015). Recent studies on high resolution magnetic resonance neurography (MRN) at three Tesla (3T) found that, in spite of the progression of clinical symptoms from distal to proximally, the maximum of visible nerve lesions occurs in the sciatic nerve at thigh level (Jende et al., 2020b). It

has further been demonstrated that parameters obtained from diffusion tensor imaging (DTI) can serve as reliable parameters for the assessment of structural nerve integrity in T2D (Heckel et al., 2015). In particular, previous studies found that the DTI fractional anisotropy (FA) of peripheral nerves was positively correlated with electrophysiological parameters of both axonal and myelin sheath integrity, whereas axial diffusivity showed positive correlations with parameters of axonal integrity and radial diffusivity showed negative correlations with parameters of myelin sheath integrity (Jende et al., 2020a).

The aim of this study was to investigate the impact of smoking on the sciatic nerve's structural integrity in patients with T2D by combining diffusion-weighted 3T MRN of the sciatic nerve with detailed clinical, serological and electrophysiological parameters obtained from smokers, ex-smokers and never-smokers with T2D as well as healthy controls.

MATERIALS AND METHODS

Study Design and Participants

This study was approved by the local ethics committee (clinicaltrials.gov identifier NCT03022721) and all participants gave written informed consent. Participants were screened and recruited at the outpatient clinic of the Department of Endocrinology at Heidelberg University Hospital, where all clinical, serological, and electrophysiological examinations took place. Thereafter, patients underwent MRN at the Department of Neuroradiology at Heidelberg University Hospital, where image processing was performed. All patient data were pseudonymized and participating researchers at the Department of Neuroradiology were completely blinded to all patient data. In total, 70 patients with T2D (10 active smokers, 20 ex-smokers, 40 never-smokers; female: 31; male: 39) and 10 age-matched controls (7 women, 3 men) took part in this single-center study between September 2016 and June 2020. Patients with T2D were divided into three groups (smokers, ex-smokers, and never-smokers). Smokers were identified first, and, thereafter, never-smokers and ex-smokers were matched for age, sex, body-mass index (BMI), hemoglobin A1c (HbA1c) levels, cholesterol levels, parameters of renal function, medication, and disease duration, in order to minimize confounding factors that might influence structural nerve integrity. Matching was accepted as adequate when no significant difference was found for each pair-wise group comparison. Recruitment proved to be time-consuming due to difficulties in enrolling smokers with T2D to undergo the extensive study protocol, the subsequent detailed matching process of ex-smokers,

Abbreviations: DPN, diabetic polyneuropathy; T2D, type 2 diabetes; FA, fractional anisotropy; MRN, magnetic resonance neurography; NDS, Neuropathy Disability Score; NSS, Neuropathy Symptom Score.

never-smokers, and healthy participants, as well as the COVID-19 pandemic.

The control group was matched to the three groups for age, BMI, lipid profile, and parameters of renal function. Detailed information on patient recruitment is given in **Figure 1**.

For all participants, exclusion criteria were age <18, pregnancy, any contraindications for MR imaging, any history of lumbar surgery or disk protrusion, any other risk factors for neuropathy such as alcoholism, malignant or infectious diseases, hypovitaminosis, monoclonal gammopathy, any previous or ongoing exposure to neurotoxic agents, and any chronic neurological diseases such as Parkinson's disease, restless leg syndrome, or multiple sclerosis. To exclude severe renal insufficiency as potential confounders, only patients with an estimated glomerular filtration rate (eGFR) > 60 ml/min were included in this study.

Clinical and Electrophysiological Examination

For every patient, a detailed medical history was documented. Patients with T2D who had never smoked were assigned to the group of never-smokers, patients who had stopped smoking >1 year ago were assigned to the group of ex-smokers and patients who were actively smoking were assigned to the group of smokers. Control subjects who had never smoked were assigned to the control group.

An examination of neuropathic symptoms was performed according to the guidelines issued by the German Society for Diabetology, including evaluation of the neuropathy disability score (NDS) and the neuropathy symptom score (NSS) (Young et al., 1993).

The electrophysiological examination (Viasys Healthcare VikingQuest®, Viasys Healthcare GmbH, Höchberg) of the right leg included: distal motor latencies (DML) of the right tibial and peroneal nerve, motor and sensory amplitudes [compound muscle action potentials (CMAPs), and sensory nerve action potentials (SNAPs), respectively] of the tibial, peroneal, and sural nerves, and nerve conduction velocities (NCVs) of the tibial, peroneal, and sural nerves. All examinations were performed in accordance with international standards for electrophysiological examinations and with specifications as issued by the manufacturer of the testing device, see also Stålberg et al. (2019) and Natus Medical Incorporated (2020) for further details. It was assured that skin temperature was at least 32°C throughout the examination.

The intima media thickness (IMT) was assessed with duplex ultrasonographic examination of both carotid arteries (SonoAce X8; Samsung Group). The pulse wave velocity was calculated using non-invasive blood pressure measurements of the arms and ankles (ABI System 1000; Boso d.o.o.).

Dermal accumulation of advanced glycation end products (AGE) was assessed non-invasively measuring skin auto fluorescence (SAF) with an AGE reader (AGE Reader SU, DiagnOptics BV, Netherlands). A skin surface of about 4 cm² was assessed at the volar surface of the forearm (Fernando et al., 2019). For the calculation of SAF, the average emitted light intensity per nm was divided by the average extinction

light intensity per nm and multiplied by 100. SAF is expressed in arbitrary units (AU) (Corine van de Zande et al., 2020). Blood was drawn in fasting state and processed immediately under standardized conditions in the central laboratory of Heidelberg University Hospital. Albumin excretion in urine was detected in morning spot urine within all participants. Estimated glomerular filtration rate was calculated with the CKD-EPI-formula (Levey et al., 2009).

Magnetic Resonance Neurography Imaging Protocol

All participants underwent high-resolution MRN of the right leg in a 3.0 Tesla MR-scanner (Magnetom TIM-TRIO, Siemens, Erlangen, Germany). A 15-channel transmit-receive extremity coil was used, and the following sequence protocol was applied:

(1) an axial high resolution T2-weighted turbo spin echo 2D sequence with spectral fat saturation of the right mid-thigh and the following parameters: repetition time (TR) 5970 ms, echo time (TE) 55 ms, field of view (FOV) 160 × 160 mm², matrix size 512 × 512, slice thickness 4 mm, interslice gap = 0.35 mm, voxel size 0.3 × 0.3 × 4.0 mm³, 3 averages, 24 images.

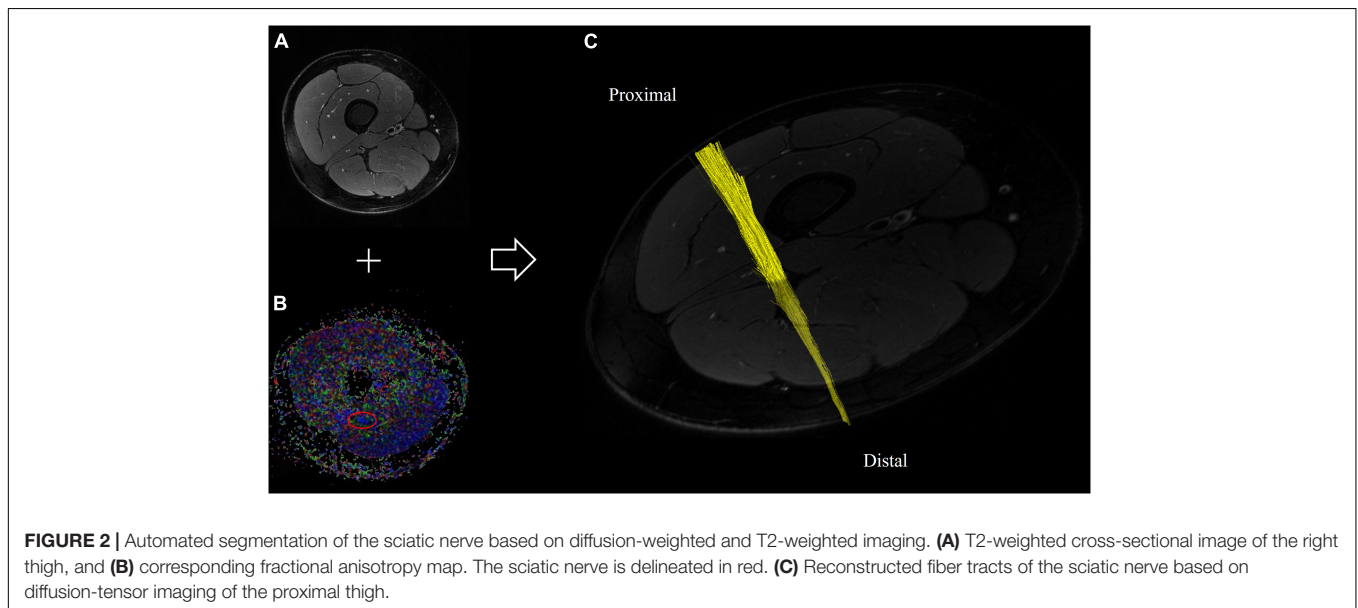
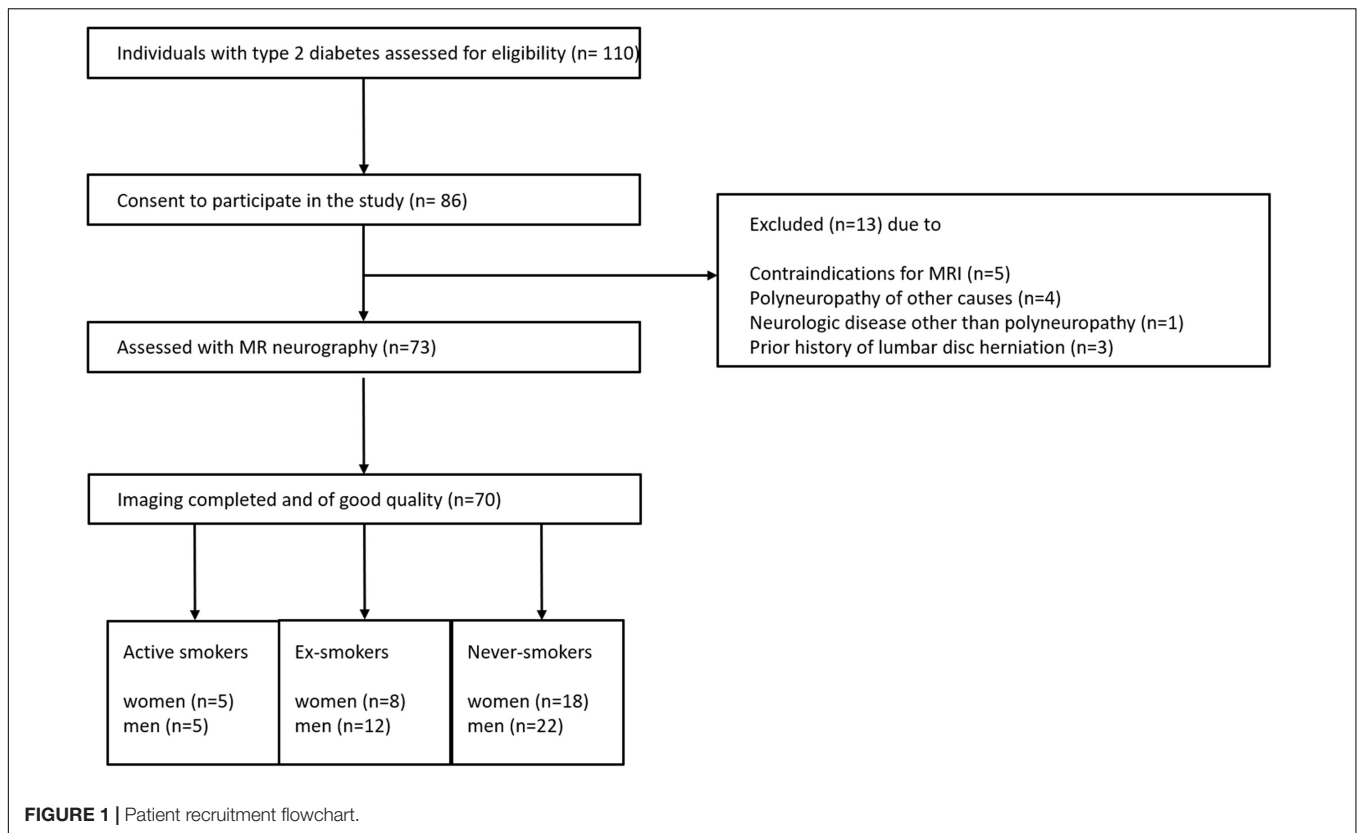
(2) DTI with an axial fat-suppressed, diffusion-weighted two-dimensional echo-planar sequence with the following parameters: TR = 5100 ms; TE = 92.8 ms; b = 0 and 1000 s/mm²; directions = 20; FOV = 160 × 160 mm²; matrix size = 128 × 128; slice thickness = 4 mm; voxel size = 1.3 × 1.3 × 4 mm³; no interslice gap, 3 averages, 24 slices, 1512 images.

Image Post-processing

All images were pseudonymized and subsequently analyzed in an automated approach using Nordic BRAINEX (NordicNeuroLab AS, 2019), a United States Food and Drug Administration–approved processing software designed for automated calculation and reconstruction of fiber tracts in diffusion-weighted imaging (Christidi et al., 2016). A total of 84 × 1536 = 129,024 images were analyzed accordingly. T2-weighted and diffusion-weighted sequences were co-registered, and the region of the sciatic nerve was marked by two trained neuroradiologists with 6 and 2 years of experience in MRN imaging, respectively. The nerve was automatically segmented with a threshold of >0.1 for the nerve's FA, a dimensionless quantity that measures directed diffusion, with values between 0 (isotropic diffusion) and 1 (diffusion in only one direction). A tract turning angle of 41.4 degrees, a minimum fiber length of 20 mm, and one seed per voxel were chosen, as done in previous studies (Jende et al., 2021). After nerve fibers were tracked, the nerve tensor eigenvalues λ₁, λ₂, and λ₃ and the average FA were automatically determined by Nordic BRAINEX. Axial diffusivity (AD), radial diffusivity (RD), and mean diffusivity (MD) were subsequently calculated based on the obtained tensor eigenvalues as AD = λ₁, RD = (λ₂ + λ₃)/2, and MD = (λ₁ + λ₂ + λ₃)/3. An illustration of the process of automated nerve segmentation is given in **Figure 2**.

Statistical Analysis

Statistical data analysis was performed with GraphPad Prism 6. All data were tested for Gaussian normal distribution using



the D’Agostino-Pearson omnibus normality test. If a Gaussian normal distribution was given, *t*-tests were used for comparisons of two groups, one-way ANOVAs with Tukey correction for multiple comparisons were applied for comparisons of more than two groups and Bonferroni-corrected Pearson correlation coefficients were calculated for correlation analysis. If data were

not Gaussian distributed, the Mann–Whitney test was used for comparisons of two groups, the Kruskal–Wallis test with Dunn correction for multiple comparisons was used for multiple comparisons of more than three groups and non-parametric Spearman correlations were applied for correlation analysis. For all tests, the level of significance was defined at $p < 0.05$.

RESULTS

Clinical and Epidemiological Data

Ten active smokers (5 women, 5 men, 15.79 pack years \pm 14.19; range: 1–57, mean age 53.20 ± 12.85 years, BMI 30.48 ± 3.60 kg/m², disease duration 10.60 ± 12.30 years) with T2D, 20 ex-smokers (8 women, 12 men; 20.09 ± 12.05 years after smoking, mean age 59.42 ± 6.87 years, BMI 28.42 ± 5.52 kg/m², disease duration 11.79 ± 10.54 years) with T2D, 40 never-smokers (18 women, 22 men, mean age 57.44 ± 14.01 years, BMI 28.45 ± 5.02 kg/m², disease duration 12.93 ± 11.21 years) with T2D, and 10 age matched controls (7 women, 3 men, mean age 49.80 ± 12.89 years, BMI 28.05 ± 5.69 kg/m²) took part in this study. For all groups, ANOVA showed no differences for age ($p = 0.186$), sex ($p = 0.151$), BMI ($p = 0.678$) or NDS scores ($p = 0.103$).

For T2D patient groups, no significant difference in disease duration was found ($p = 0.744$). Oral antidiabetic medication (metformin) was used by 4 smokers, 8 ex-smokers, and 13 never-smokers. Insulin was used by 4 smokers, 5 ex-smokers, and 11 never smokers. A total of 42 participants with T2D suffered from hypertension. Anti-hypertensive medication (beta blockers, renin-angiotensin-aldosterone inhibitors, calcium antagonists) were used by 8 smokers, 12 ex-smokers, and 22 never-smokers. Diuretics (thiazides, loop diuretics) were taken by 5 smokers, 4 ex-smokers, and 6 never-smokers. 100 mg aspirin daily was taken by 2 active smokers, 7 ex-smokers, and 7 never-smokers. Statins were taken by 5 active smokers, 10 ex-smokers, and 16 never-smokers.

Compared to controls, NSS scores were higher in ex-smokers ($p = 0.026$) and never-smokers ($p = 0.036$), but not in smokers ($p = 0.233$). There was no difference between the NSS scores of T2D patient groups. The pulse wave velocity (PWV), a marker of arterial stiffness and associated microangiopathy (Kim and Kim, 2019), was higher in ex-smokers compared to controls ($p = 0.036$).

Serological Data

HbA1c levels were higher in never-smokers and ex-smokers when compared to controls ($p = 0.003$ and $p = 0.005$, respectively). There was no significant difference between HbA1c levels of T2D patient groups. High sensitivity Troponin T (hsTNT), a marker of cardiovascular disease, was higher in ex-smokers when compared to controls ($p = 0.038$). High-density lipoprotein (HDL) cholesterol was higher in smokers in comparison to ex-smokers ($p = 0.016$). No significant differences were found for cystatin c, glomerular filtration rate (GFR), N-terminal pro-brain natriuretic peptide (proBNP), total serum cholesterol, low-density lipoprotein (LDL) cholesterol, or triglycerides.

Electrophysiological Data

Tibial NCV was higher in controls compared to ex-smokers and smokers ($p = 0.047$ and $p = 0.018$, respectively). Peroneal NCV was higher in controls compared to ex-smokers ($p = 0.012$) and to smokers ($p = 0.033$). No significant differences were found for sural NCV and amplitudes, tibial and peroneal CMAP, or tibial

and peroneal DML. A detailed summary of all group comparisons on epidemiological, electrophysiological, and serological data is provided in **Table 1**.

Magnetic Resonance Neurography Imaging Data

Comparison of Groups and Correlation With Clinical Scores and Demographic Data

FA as the main imaging parameter for structural nerve integrity, was higher in controls when compared to ex-smokers ($p = 0.015$) and smokers ($p = 0.002$) but not when compared to never-smokers ($p = 0.361$; **Figure 3A**). FA was also higher in never-smokers when compared to smokers ($p = 0.015$). A summary of all group comparisons for imaging data is provided in **Table 1**. In controls, FA showed negative correlations with age ($r = -0.75$; $p = 0.013$), likewise in never smokers ($r = -0.50$; $p = 0.001$). This finding could not be reproduced for ex-smokers and smokers. In smokers with T2D, FA showed negative correlations with BMI ($r = -0.75$; $p = 0.013$). In never-smokers, ex-smokers and smokers with T2D, FA was negatively correlated with the NDS score ($r = -0.49$; $p = 0.001$, $r = -0.52$; $p = 0.031$, and $r = -0.70$; $p = 0.024$, respectively). In smokers, FA also showed a negative correlation with the NSS score ($r = -0.69$, $p = 0.028$). No correlations were found with pack years or the average number of cigarettes per day in smokers. A detailed survey of correlations between FA and all other parameters acquired is provided in **Table 2**.

For RD, a parameter indicative for the damage to myelin, ANOVA showed higher values in smokers compared to controls ($p = 0.048$) and never-smokers ($p = 0.049$; **Figure 3B**).

In never-smokers, RD was correlated with age ($r = 0.44$; $p = 0.005$). In smokers, RD was correlated with the BMI ($r = 0.68$; $p = 0.042$). RD was positively correlated with the NDS score in never-smokers ($r = 0.39$; $p = 0.017$) and smokers ($r = 0.68$; $p = 0.046$), but not in ex-smokers ($r = 0.275$; $p = 0.286$). No correlations were found with the NSS score. A detailed survey of correlations between RD and all other parameters is provided in **Table 3**.

For all groups, no significant differences were found for AD, a parameter supposed to represent axonal integrity (**Figure 3C**). In smokers, AD was correlated with the BMI ($r = 0.76$; $p = 0.011$). No other correlations were found for AD with any of the acquired clinical scores or demographic data. A detailed survey of correlations of AD and with all other parameters is provided in **Table 4**.

Correlation With Electrophysiological Data

FA showed positive correlations with tibial and peroneal NCV in never-smokers ($r = 0.34$; $p = 0.042$ and $r = 0.41$; $p = 0.014$, respectively), ex-smokers ($r = 0.60$; $p = 0.007$, and $r = 0.70$; $p < 0.001$, respectively), and smokers ($r = 0.67$; $p = 0.034$ and $r = 0.85$; $p = 0.003$, respectively) with T2D. Further positive correlations were found between FA and tibial and peroneal CMAP in never-smokers ($r = 0.45$; $p = 0.006$ and $r = 0.58$; $p < 0.001$, respectively) and ex-smokers ($r = 0.55$; $p = 0.014$ and $r = 0.64$; $p = 0.003$, respectively), while a similar trend was found in smokers ($r = 0.51$ $p = 0.136$ and $r = 0.64$; $p = 0.066$, respectively).

TABLE 1 | Comparison of imaging, clinical, electrophysiological, apparatus-bound, and serologic parameters between controls, type 2 diabetes (T2D) never-smokers, ex-smokers, and smokers.

Parameter	Controls	T2D never-smokers	T2D ex-smokers	T2D smokers	P-Value	P-Value controls vs. never-smokers	P-Value controls vs. ex-smokers	P-Value controls vs. smokers	P-Value never-smokers vs. ex-smokers	P-Value never-smokers vs. smokers	P-Value ex-smokers vs. smokers
Fractional anisotropy	0.52 ± 0.04	0.48 ± 0.06	0.43 ± 0.09	0.40 ± 0.08	<0.001	0.361	0.015	0.002	0.126	0.015	0.601
Radial diffusivity [10 ⁻⁵ mm ² /s]	73.78 ± 11.94	77.71 ± 10.42	88.33 ± 24.44	93.53 ± 18.82	0.008	0.904	0.105	0.048	0.091	0.049	0.856
Axial diffusivity [10 ⁻⁵ mm ² /s]	182.80 ± 23.58	171.80 ± 19.41	172.80 ± 30.86	174.40 ± 14.05	0.592	0.523	0.676	0.843	0.999	0.988	0.998
Women/Men	7w3m	18w22m	8w12m	5w5m	0.151	0.170	0.124	0.531	0.961	0.983	0.904
Age (years)	49.80 ± 12.89	57.44 ± 14.01	59.42 ± 6.87	53.20 ± 12.85	0.186	0.309	0.200	0.927	0.939	0.768	0.573
Body-mass index (kg/m ²)	28.05 ± 5.69	28.45 ± 5.02	28.42 ± 5.52	30.48 ± 3.6	0.508	0.996	0.997	0.712	>0.999	0.677	0.730
NDS	0.30 ± 0.67	2.28 ± 2.85	2.94 ± 3.27	2.70 ± 2.67	0.103	0.22	0.097	0.22	0.777	0.892	0.892
NSS	0 ± 0	3.31 ± 3.21	3.78 ± 3.70	3.10 ± 3.41	0.027	0.036	0.026	0.232	>0.999	>0.999	>0.999
Tibial NCV (m/s)	47.10 ± 7.75	42.65 ± 5.07	40.76 ± 5.31	38.90 ± 8.01	0.017	0.151	0.047	0.018	0.488	0.227	0.489
Tibial CMAP (μV)	15.56 ± 8.18	12.91 ± 9.43	1212 ± 6.68	9.45 ± 5.91	0.427	0.808	0.728	0.361	0.988	0.648	0.851
Tibial DML (ms)	5.39 ± 3.18	7.46 ± 4.89	5.51 ± 3.63	6.53 ± 5.72	0.398	0.583	>0.999	0.944	0.465	0.940	0.943
Peroneal NCV (m/s)	46.00 ± 3.30	42.14 ± 6.17	39.24 ± 5.12	39.11 ± 6.60	0.008	0.247	0.012	0.033	0.525	0.852	>0.999
Peroneal CMAP (μV)	7.81 ± 2.08	5.83 ± 3.40	4.99 ± 2.79	4.54 ± 4.49	0.069	0.519	0.214	0.076	>0.999	0.900	>0.999
Peroneal DML (ms)	4.45 ± 1.81	6.43 ± 3.84	5.49 ± 2.87	6.67 ± 4.55	0.401	0.433	0.901	0.550	0.800	0.998	0.849
Sural NCV (m/s)	48.78 ± 7.24	46.17 ± 6.00	45.92 ± 5.58	45.05 ± 9.94	0.693	>0.999	>0.999	>0.999	>0.999	>0.999	>0.999
Sural SNAP (μV)	9.78 ± 6.82	7.44 ± 4.49	5.16 ± 3.21	4.95 ± 3.48	0.054	0.515	0.077	0.134	0.348	0.501	>0.999
SAF (AU)	1.81 ± 0.37	2.15 ± 0.54	2.28 ± 0.48	2.32 ± 0.53	0.072	0.344	0.091	0.162	>0.999	>0.999	>0.999
Pulse wave velocity (m/s)	7.30 ± 1.56	8.26 ± 1.65	9.32 ± 1.78	8.75 ± 1.92	0.036	0.355	0.036	0.249	0.187	0.654	0.654
Intima-media thickness (ratio)	0.97 ± 0.21	0.92 ± 0.25	0.96 ± 0.23	0.75 ± 0.23	0.114	0.915	0.999	0.172	0.914	0.194	0.116
HbA1c (%)	5.45 ± 0.17	7.28 ± 1.90	7.05 ± 1.02	6.33 ± 1.29	0.002	0.003	0.005	0.467	>0.999	0.852	0.802
Cystatin C (mg/l)	0.73 ± 0.11	0.82 ± 0.17	0.9 ± 0.21	0.91 ± 0.26	0.185	0.568	0.173	0.177	0.551	0.543	0.996
Glomerular filtration rate (ml/min)	92.64 ± 8.97	88.39 ± 16.75	89.59 ± 17.90	79.36 ± 20.93	0.386	0.922	0.974	0.381	0.996	0.505	0.468
Total serum cholesterol (mg/dl)	204.80 ± 48.38	196.20 ± 41.63	189.60 ± 46.23	195.20 ± 45.71	0.865	0.958	0.854	0.968	0.956	>0.999	0.989
HDL cholesterol (mg/dl)	54.63 ± 12.06	55.15 ± 16.55	45.59 ± 10.64	67.80 ± 22.29	0.077	>0.999	0.614	>0.999	0.190	0.632	0.016
LDL cholesterol (mg/dl)	131.00 ± 39.60	110.90 ± 35.44	110.30 ± 39.37	107.60 ± 41.03	0.475	0.861	>0.999	0.879	>0.999	>0.999	>0.999
Triglycerides (mg/dl)	78.25 ± 15.35	79.95 ± 28.37	68.12 ± 14.69	77.90 ± 32.58	0.462	0.999	0.789	>0.999	0.412	0.998	0.770
Troponin T (pg/dl)	8.24 ± 8.69	7.93 ± 3.29	12.81 ± 7.62	10.90 ± 6.76	0.009	>0.999	0.038	0.530	0.066	>0.999	>0.999
proBNP (pg/dl)	24.13 ± 9.48	25.05 ± 9.08	27.00 ± 9.16	21.90 ± 8.48	0.554	0.994	0.881	0.955	0.882	0.762	0.496

All values are displayed as mean ± standard deviation.

NDS, Neuropathy Disability Score; NSS, Neuropathy Symptom Score; NCV, Nerve Conduction Velocity; CMAP, compound muscle action potential; DML, Peroneal Distal Motor Latencies; SNAP, Sensory Nerve Action Potential; SAF, Skin Auto Fluorescence; HbA1c, hemoglobin A1c; HDL, High-Density Lipoprotein; LDL, Low-Density Lipoprotein; proBNP, pro-Brain Natriuretic Peptide; m/s, meters per second; mm, millimeter, μV, microvolt; ms, milliseconds; AU, arbitrary units; mg/dl, milligram per deciliter; mg/l, milligram per liter; ml/min, milliliters per minute; pg/dl, picogram per deciliter.

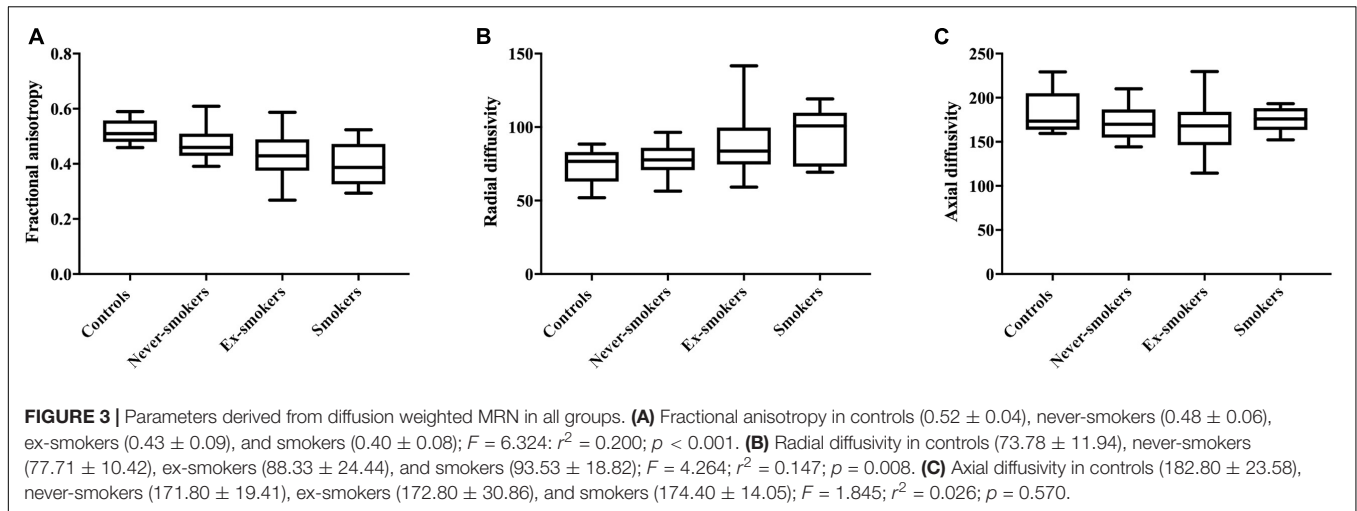


TABLE 2 | Correlation of the sciatic nerve’s fractional anisotropy (FA) with demographic, clinical, apparatus-bound, and serological parameters.

	FA controls		FA T2D never-smokers		FA T2D ex-smokers		FA T2D smokers	
	<i>r</i>	<i>p</i>	<i>r</i>	<i>p</i>	<i>r</i>	<i>p</i>	<i>r</i>	<i>p</i>
Radial diffusivity	-0.26	0.469	-0.67	<0.001	-0.89	<0.001	-0.80	0.010
Axial diffusivity	0.36	0.305	0.29	0.071	-0.35	0.144	-0.65	0.044
Sex	0.01	0.974	0.16	0.328	0.22	0.347	0.29	0.410
Age (years)	-0.75	0.013	-0.50	0.001	-0.21	0.372	-0.47	0.173
Body-mass index (kg/m ²)	0.17	0.635	-0.29	0.074	-0.003	0.990	-0.75	0.013
NDS	-0.02	0.955	-0.50	0.001	-0.523	0.031	-0.70	0.024
NSS	<i>n.a.</i>	<i>n.a.</i>	-0.12	0.479	-0.06	0.812	-0.69	0.028
Tibial NCV (m/s)	0.41	0.236	0.34	0.042	0.60	0.007	0.67	0.034
Tibial CMAP (μV)	0.09	0.806	0.45	0.006	0.55	0.014	0.51	0.136
Tibial DML (ms)	-0.21	0.553	0.06	0.710	-0.32	0.180	-0.59	0.074
Peroneal NCV (m/s)	0.53	0.117	0.41	0.014	0.70	0.001	0.85	0.003
Peroneal CMAP (μV)	0.15	0.675	0.58	<0.001	0.64	0.003	0.64	0.066
Peroneal DML (ms)	-0.12	0.733	0.01	0.938	-0.42	0.075	-0.58	0.099
Sural NCV (m/s)	-0.06	0.877	-0.03	0.887	-0.15	0.597	-0.05	0.927
Sural SNAP (μV)	0.38	0.279	0.32	0.069	0.34	0.167	0.26	0.540
SAF (AU)	-0.41	0.241	-0.39	0.020	-0.07	0.765	-0.84	0.004
PWV (m/s)	-0.70	0.037	-0.45	0.004	-0.51	0.027	-0.59	0.094
IMT	-0.61	0.061	-0.09	0.599	-0.26	0.289	-0.69	0.039
HbA1c (%)	-0.47	0.242	0.13	0.422	0.05	0.859	-0.35	0.329
Cystatin C (mg/l)	0.41	0.317	-0.37	0.038	0.07	0.800	0.31	0.420
Glomerular filtration rate (ml/min)	-0.37	0.369	0.45	0.012	-0.17	0.512	-0.26	0.506
Total serum cholesterol (mg/dl)	-0.12	0.770	0.26	0.109	-0.20	0.423	-0.30	0.397
HDL cholesterol (mg/dl)	-0.29	0.489	0.08	0.622	-0.30	0.229	-0.34	0.343
LDL cholesterol (mg/dl)	-0.03	0.937	0.24	0.149	-0.11	0.687	-0.24	0.502
Triglycerides (mg/dl)	-0.13	0.759	0.27	0.093	-0.08	0.745	0.46	0.178
Troponin T (pg/dl)	-0.43	0.292	-0.26	0.153	0.20	0.432	-0.36	0.341
proBNP (pg/dl)	-0.15	0.716	-0.25	0.169	0.23	0.368	0.38	0.309
Years since smoke stop	<i>n.a.</i>	<i>n.a.</i>	<i>n.a.</i>	<i>n.a.</i>	-0.11	0.672	<i>n.a.</i>	<i>n.a.</i>
Cigarettes/day	<i>n.a.</i>	<i>n.a.</i>	<i>n.a.</i>	<i>n.a.</i>	<i>n.a.</i>	<i>n.a.</i>	-0.23	0.520
Years smoking	<i>n.a.</i>	<i>n.a.</i>	<i>n.a.</i>	<i>n.a.</i>	<i>n.a.</i>	<i>n.a.</i>	-0.37	0.365
Pack years	<i>n.a.</i>	<i>n.a.</i>	<i>n.a.</i>	<i>n.a.</i>	<i>n.a.</i>	<i>n.a.</i>	-0.32	0.445

NDS, Neuropathy Disability Score; NSS, Neuropathy Symptom Score; NCV, Nerve Conduction Velocity; CMAP, compound muscle action potential; DML, Peroneal Distal Motor Latencies; SNAP, Sensory Nerve Action Potential; SAF, Skin Auto Fluorescence; PWV, Pulse Wave Velocity; IMT, Intima Media Thickness; HbA1c, hemoglobin A1c; HDL, High-Density Lipoprotein; LDL, Low-Density Lipoprotein; proBNP, pro-Brain Natriuretic Peptide; m/s, meters per second; μV, microvolt; ms, milliseconds; AU, arbitrary units; mg/dl, milligram per deciliter; mg/l, milligram per liter; ml/min, milliliters per minute; pg/dl, picogram per deciliter.

TABLE 3 | Correlation of the sciatic nerve's radial diffusivity (RD; in 10^{-5} mm²/s) with demographic, clinical, apparatus-bound, and serological parameters.

	RD controls		RD T2D never-smokers		RD T2D ex-smokers		RD T2D smokers	
	<i>r</i>	<i>p</i>	<i>r</i>	<i>p</i>	<i>r</i>	<i>p</i>	<i>r</i>	<i>p</i>
Fractional anisotropy	-0.26	0.469	-0.67	<0.001	-0.89	<0.001	-0.80	0.010
Axial diffusivity	0.70	0.023	0.47	0.003	0.72	0.001	0.86	0.003
Sex	0.11	0.760	-0.07	0.655	-0.24	0.307	-0.17	0.655
Age (years)	-0.04	0.916	0.44	0.005	0.17	0.467	0.22	0.571
Body-mass index (kg/m ²)	-0.27	0.456	0.06	0.732	-0.09	0.696	0.68	0.042
NDS	-0.43	0.221	0.39	0.017	0.28	0.286	0.67	0.046
NSS			0.26	0.114	-0.22	0.403	0.44	0.242
Tibial NCV (m/s)	-0.33	0.358	-0.26	0.125	-0.50	0.028	-0.48	0.186
Tibial CMAP (μV)	<0.01	0.989	-0.37	0.031	-0.59	0.008	-0.78	0.013
Tibial DML (ms)	0.12	0.749	-0.21	0.233	0.42	0.076	0.72	0.028
Peroneal NCV (m/s)	0.14	0.696	-0.34	0.046	-0.49	0.034	-0.86	0.006
Peroneal CMAP (μV)	0.27	0.456	-0.51	0.002	-0.56	0.012	-0.83	0.012
Peroneal DML (ms)	0.38	0.282	-0.09	0.625	0.38	0.112	0.76	0.029
Sural NCV (m/s)	0.35	0.322	0.10	0.612	0.31	0.266	-0.26	0.670
Sural SNAP (μV)	0.04	0.908	-0.26	0.153	-0.07	0.770	0.57	0.182
SAF (AU)	-0.19	0.591	0.44	0.009	0.07	0.765	0.59	0.112
PWV (m/s)	-0.15	0.701	0.19	0.269	0.33	0.171	0.56	0.152
IMT (ratio)	0.02	0.957	0.28	0.084	0.25	0.317	0.74	0.035
HbA1c (%)	-0.36	0.383	-0.30	0.060	-0.09	0.720	0.68	0.046
Cystatin C (mg/l)	0.04	0.920	0.11	0.566	-0.15	0.571	0.04	0.932
Glomerular filtration rate (ml/min)	<0.01	0.994	-0.13	0.499	0.21	0.428	-0.01	0.988
Total serum cholesterol (mg/dl)	0.36	0.384	-0.29	0.073	-0.06	0.802	0.63	0.068
HDL cholesterol (mg/dl)	-0.11	0.792	-0.05	0.757	0.14	0.593	0.43	0.243
LDL cholesterol (mg/dl)	0.42	0.295	-0.21	0.216	-0.11	0.666	0.44	0.234
Triglycerides (mg/dl)	0.18	0.670	-0.33	0.043	-0.01	0.964	0.20	0.608
Troponin T (pg/dl)	-0.55	0.155	0.30	0.108	-0.29	0.241	0.71	0.040
proBNP (pg/dl)	0.06	0.879	0.26	0.166	-0.27	0.276	-0.46	0.257
Years since smoke stop	<i>n.a.</i>	<i>n.a.</i>	<i>n.a.</i>	<i>n.a.</i>	0.03	0.902	<i>n.a.</i>	<i>n.a.</i>
Cigarettes/day	<i>n.a.</i>	<i>n.a.</i>	<i>n.a.</i>	<i>n.a.</i>	<i>n.a.</i>	<i>n.a.</i>	0.31	0.422
Years smoking	<i>n.a.</i>	<i>n.a.</i>	<i>n.a.</i>	<i>n.a.</i>	<i>n.a.</i>	<i>n.a.</i>	-0.21	0.651
Pack years	<i>n.a.</i>	<i>n.a.</i>	<i>n.a.</i>	<i>n.a.</i>	<i>n.a.</i>	<i>n.a.</i>	0.03	0.946

NDS, Neuropathy Disability Score; NSS, Neuropathy Symptom Score; NCV, Nerve Conduction Velocity; CMAP, compound muscle action potential; DML, Peroneal Distal Motor Latencies; SNAP, Sensory Nerve Action Potential; SAF, Skin Auto Fluorescence; PWV, Pulse Wave Velocity; IMT, Intima Media Thickness; HbA1c, hemoglobin A1c; HDL, High-Density Lipoprotein; LDL, Low-Density Lipoprotein; proBNP, pro-Brain Natriuretic Peptide; m/s, meters per second; μV, microvolt; mm, millimeter; ms, milliseconds; AU, arbitrary units; mg/dl, milligram per deciliter; mg/l, milligram per liter; ml/min, milliliters per minute; pg/dl, picogram per deciliter.

RD showed correlations with peroneal NCV and CMAP in never-smokers ($r = -0.34$; $p = 0.046$ and $r = -0.51$; $p = 0.002$), ex-smokers ($r = -0.49$; $p = 0.034$ and $r = -0.56$; $p = 0.012$) and smokers ($r = -0.86$; $p = 0.033$ and $r = -0.83$; $p = 0.012$) as well as correlations with tibial CMAP in never smokers ($r = -0.37$; $p = 0.031$), ex-smokers ($r = -0.59$; $p = 0.008$) and smokers ($r = -0.78$; $p = 0.013$) with T2D.

AD was correlated with tibial DML in ex-smokers and smokers ($r = 0.51$; $p = 0.032$ and $r = 0.64$; $p = 0.046$, respectively) with T2D. In smokers with T2D, AD was further correlated with peroneal NCV ($r = -0.73$; $p = 0.027$) and peroneal CMAP ($r = -0.85$; $p = 0.004$).

Correlation With Additional Paraclinical Data

FA showed negative correlations with the pulse wave velocity in controls ($r = -0.70$; $p = 0.037$), never-smokers ($r = -0.45$;

$p = 0.004$), ex-smokers ($r = -0.51$; $p = 0.027$), and a similar trend in smokers ($r = -0.59$; $p = 0.094$) with T2D. In smokers with T2D, IMT as a surrogate marker of cardiovascular disease in diabetes (Sibal et al., 2011) was negatively correlated with FA ($r = -0.69$; $p = 0.039$). Negative correlations were found between FA and SAF, a measure of the tissue deposition of advanced glycation end product and therefore of the degree of glycemic stress in diabetes, in never-smokers ($r = -0.39$; $p = 0.020$) and smokers ($r = -0.84$; $p = 0.004$), but not in ex-smokers with T2D ($r = -0.07$; $p = 0.765$).

RD was positively correlated with the IMT in smokers ($r = 0.74$; $p = 0.035$). No correlations were found between RD and PWV. RD was positively correlated with skin auto-fluorescence in never-smokers ($r = 0.44$; $p = 0.009$) and a similar trend was seen in smokers ($r = 0.59$; $p = 0.122$) but not in ex-smokers ($r = 0.07$; $p = 0.765$).

TABLE 4 | Correlation of the sciatic nerve's axial diffusivity (AD; in 10^{-5} mm²/s) with demographic, clinical, apparatus-bound, and serological parameters.

	AD controls		AD T2D never-smokers		AD T2D ex-smokers		AD T2D smokers	
	r	p	r	p	r	p	r	p
Fractional anisotropy	0.36	0.305	0.29	0.071	-0.35	0.144	-0.65	0.044
Radial diffusivity	0.70	0.023	0.47	0.003	0.72	0.001	0.86	0.003
Sex	0.36	0.306	0.02	0.918	-0.07	0.767	0.13	0.727
Age (years)	-0.48	0.166	-0.01	0.936	-0.01	0.965	0.13	0.721
Body-mass index (kg/m ²)	-0.45	0.193	-0.32	0.048	-0.23	0.342	0.76	0.011
NDS	-0.42	0.225	-0.05	0.779	-0.18	0.493	0.44	0.207
NSS			0.26	0.106	-0.48	0.049	0.44	0.199
Tibial NCV (m/s)	-0.09	0.806	0.02	0.906	-0.17	0.511	-0.26	0.466
Tibial CMAP (μV)	0.04	0.916	0.09	0.595	-0.41	0.088	-0.61	0.062
Tibial DML (ms)	0.11	0.760	-0.18	0.305	0.51	0.032	0.64	0.046
Peroneal NCV (m/s)	0.36	0.313	0.04	0.808	0.08	0.753	-0.73	0.027
Peroneal CMAP (μV)	0.42	0.225	0.06	0.736	-0.07	0.776	-0.85	0.004
Peroneal DML (ms)	0.32	0.366	-0.10	0.573	0.08	0.763	0.66	0.053
Sural NCV (m/s)	0.54	0.110	0.02	0.939	0.29	0.311	0.17	0.750
Sural SNAP (μV)	0.56	0.090	0.08	0.676	0.39	0.120	0.09	0.834
SAF (AU)	-0.55	0.101	0.22	0.205	-0.07	0.786	0.57	0.109
PWV (m/s)	-0.45	0.225	-0.19	0.264	<0.01	0.985	0.30	0.438
IMT	-0.22	0.548	0.21	0.201	-0.04	0.882	0.62	0.077
HbA1c (%)	-0.22	0.605	-0.28	0.076	-0.13	0.630	0.69	0.027
Cystatin C (mg/l)	0.44	0.271	-0.31	0.086	-0.19	0.485	-0.05	0.900
Glomerular filtration rate (ml/min)	-0.38	0.355	0.38	0.040	0.20	0.466	0.21	0.594
Total serum cholesterol (mg/dl)	0.38	0.355	-0.02	0.920	-0.30	0.246	0.48	0.157
HDL cholesterol (mg/dl)	0.03	0.938	-0.03	0.872	-0.06	0.830	0.10	0.789
LDL cholesterol (mg/dl)	0.38	0.359	0.14	0.417	-0.28	0.289	0.44	0.201
Triglycerides (mg/dl)	0.30	0.468	-0.11	0.518	-0.12	0.658	0.24	0.512
Troponin T (pg/dl)	-0.44	0.271	0.06	0.769	-0.34	0.180	0.42	0.255
proBNP (pg/dl)	-0.01	0.976	0.01	0.974	-0.30	0.248	-0.58	0.105
Years since smoke stop	n.a.	n.a.	n.a.	n.a.	-0.14	0.590	n.a.	n.a.
Cigarettes/day	n.a.	n.a.	n.a.	n.a.	n.a.	n.a.	0.41	0.245
Years smoking	n.a.	n.a.	n.a.	n.a.	n.a.	n.a.	-0.22	0.600
Pack years	n.a.	n.a.	n.a.	n.a.	n.a.	n.a.	-0.05	0.914

NDS, Neuropathy Disability Score; NSS, Neuropathy Symptom Score; NCV, Nerve Conduction Velocity; CMAP, compound muscle action potential; DML, Peroneal Distal Motor Latencies; SNAP, Sensory Nerve Action Potential; SAF, Skin Auto Fluorescence; PWV, Pulse Wave Velocity; IMT, Intima Media Thickness; HbA1c, hemoglobin A1c; HDL, High-Density Lipoprotein; LDL, Low-Density Lipoprotein; proBNP, pro-Brain Natriuretic Peptide; m/s, meters per second; μV, microvolt; mm, millimeter; ms, milliseconds; AU, arbitrary units; mg/l, milligram per liter; ml/min, milliliters per minute; mg/dl, milligram per deciliter; pg/dl, picogram per deciliter.

Correlation With Serologic Data

In never-smokers, FA showed negative correlations with cystatin c and positive correlations with GFR ($r = -0.37$; $p = 0.038$ and $r = 0.45$; $p = 0.012$). No correlations were found between FA and HbA1c levels, cholesterol levels or triglycerides.

In smokers, RD was correlated with HbA1c levels ($r = 0.68$; $p = 0.046$) and hsTNT ($r = 0.71$; $p = 0.048$). No further correlations of AD with serologic parameters were found in any of the groups. A detailed summary of all correlations of imaging parameters is given in **Tables 2–4**.

DISCUSSION

The key findings of this study were that (i) the sciatic nerve's FA is lower in smokers and ex-smokers with T2D compared to age-matched controls, and that the FA in smokers with T2D is lower than in never-smokers with T2D; (ii) in all T2D patient groups, FA was negatively correlated with the NDS, tibial and peroneal

NCV and CMAP, and PWV; (iii) in never-smokers and smokers, FA was negatively correlated with SAF, whereas in ex-smokers no such correlation could be found; and (iv) in smokers, RD was positively correlated with hsTNT, SAF, BMI, and HbA1c levels.

The finding that the sciatic nerve's FA was lower in smokers compared to controls and never-smokers suggests that cigarette smoking contributes to nerve damage in patients with T2D, and that, therefore, to quit smoking may pose a useful preventive measure to slow the progression of DPN, as suggested by previous studies (Kar et al., 2016). The finding of a lower FA in ex-smokers compared to controls suggests that the negative effect of smoking on structural nerve integrity in T2D is not completely reversible once a patient quits smoking, supporting previous studies that found smoking prevention in adolescents with diabetes to be of importance with regards to the development and progression of DPN (Jaiswal et al., 2017; Christensen et al., 2020). The finding that RD, but not AD was higher in smokers with T2D when compared to controls and never-smokers with T2D, suggests that smoking primarily causes damage to the myelin sheath in T2D,

since RD has previously been shown to be a marker for myelin integrity (Heckel et al., 2015; Vaeggemose et al., 2017; Kurz et al., 2018). The correlations of FA and RD with electrophysiological parameters and clinical scores indicate that both parameters pose reliable parameters for structural nerve integrity in T2D as suggested by recent studies (Jende et al., 2021).

The finding that FA was negatively correlated with SAF in smokers, but not in ex-smokers, suggests that the deposition of advanced glycation end products in or around peripheral nerves and subsequent myelin damage may be more relevant in active smokers than in ex-smokers. In contrast, the absence of a correlation between FA and SAF in ex-smokers and the findings that both hsTNT and PWV, markers of microangiopathy in T2D (Jende et al., 2020a), are higher in ex-smokers versus controls, while PWV was not significantly associated with FA decrease in smokers, may suggest that microvascular impairment associated nerve damage predominates over effects of hyperglycemia in T2D ex-smokers.

The correlation of RD with IMT, hsTNT and HbA1c levels in smokers further supports the hypothesis that hyperglycemia, macroangiopathy, and microangiopathy induced by smoking contribute to myelin damage in T2D in the sense of a “triple hit” (Nilsson et al., 2004; Christensen et al., 2020). The finding that the sciatic nerve’s RD was positively correlated with the BMI in smokers further supports the hypothesis that the impact of smoking on nerve integrity is worse in obese patients with T2D (Jaiswal et al., 2017).

The results of this study are of importance with regard to the effect of glucose control on the progression of DPN in T2D: since former studies have found that normalization of blood glucose levels in T2D is not beneficial for slowing the progression of DPN, it might be of interest to future studies to assess whether the effect of glucose control in T2D differs between smokers, ex-smokers and never-smokers.

This explorative study is limited by the fact that only cross-sectional data were analyzed, which does not allow for causative conclusions on the effects of smoking on myelin damage in T2D. Another limitation is the fact that our sample size, in particular the number of active smokers, is too small for multivariate analysis of all potential confounders. One must consider, however, that all patient groups were matched for gender, age, BMI, HbA1c levels, parameters of renal function, and total serum cholesterol. It is therefore unlikely that the effects found in our cohort are caused by other effects than those induced by cigarette smoking.

One may of course argue that we did not separate DPN patients from patients without DPN. However, it should be noted that all patient groups were matched for NDS and that previous MRN imaging studies have found that DPN is a continuous process during which nerve lesions accumulate in asymptomatic patients who start to experience symptoms once a certain amount of structural nerve damage is reached (Groener et al., 2019). Therefore, assessing the sciatic nerve’s structural integrity with MRN imaging parameters allows for more accurate correlations and group comparisons than dividing patients into two groups based on clinical scores (Vaeggemose et al., 2017; Jende et al., 2020a).

In summary, this study is the first to find that structural nerve integrity assessed by MR neurography is lower in smokers with T2D compared to ex-smokers with T2D and age-matched controls, which is most likely due to damage to the affected nerves’ myelin sheath. Our findings suggest that in smokers with T2D, hyperglycemia, obesity, micro- and macroangiopathy contribute to myelin damage, whereas in ex-smokers microangiopathy appears to be the main contributing factor. Our results indicate that cigarette smoking is harmful to peripheral nerves in T2D and that, therefore, interventions to stop smoking may be promising preventive measures to slow down the progression of DPN. Further longitudinal studies are required to verify this hypothesis.

DATA AVAILABILITY STATEMENT

The datasets presented in this article are not readily available because they contain sensitive patient information. The data supporting the conclusions of this article will be made available upon reasonable request by any qualified researcher. Requests to access the datasets should be directed to FK, felix.kurz@med.uni-heidelberg.de.

ETHICS STATEMENT

The studies involving human participants were reviewed and approved by Ethikkommission der medizinischen Fakultät der Universität Heidelberg, Alte Glockengießerei 11/1, 69115 Heidelberg, Germany. The patients/participants provided their written informed consent to participate in this study.

AUTHOR CONTRIBUTIONS

JJ, MB, SH, PN, and FK designed and coordinated the study. JJ, CM, JG, AJ, and FK contributed to the organization of participants. JJ, AJ, and FK collected MR data. FK developed image analysis tools. ZK, JG, and SK collected clinical, serological, and electrophysiological data. JJ and FK analyzed the data and wrote the manuscript with input from all coauthors. All authors contributed to the article and approved the submitted version.

FUNDING

This study was supported by the German Research Foundation (SFB 1158, 1118) and the International Foundation for Research in Paraplegia (IRP). Both DFG and IRP had no influence on the study design, collection, and analysis of data or on the writing of the article.

ACKNOWLEDGMENTS

We thank Dorothea Willich (Department of Neuroradiology, Heidelberg University Hospital) for her ongoing support and excellent technical performance of all MRN examinations.

REFERENCES

- Alleman, C. J. M., Westerhout, K. Y., Hensen, M., Chambers, C., Stoker, M., Long, S., et al. (2015). Humanistic and economic burden of painful diabetic peripheral neuropathy in Europe: a review of the literature. *Diabet. Res. Clin. Pract.* 109, 215–225. doi: 10.1016/j.diabres.2015.04.031
- Benbow, S. J., Williams, G., and MacFarlane, I. A. (1997). Smoking habits and painful diabetic neuropathy. *J. Diabet. Complications* 11, 334–337.
- Christensen, D. H., Knudsen, S. T., Gylfadottir, S. S., Christensen, L. B., Nielsen, J. S., Beck-Nielsen, H., et al. (2020). Metabolic factors, lifestyle habits, and possible polyneuropathy in early type 2 diabetes: a nationwide study of 5,249 patients in the danish centre for strategic research in type 2 diabetes (DD2) cohort. *Diabet. Care* 43, 1266–1275. doi: 10.2337/dc19-2277
- Christidi, F., Karavasilis, E., Samiotis, K., Bisdas, S., and Papanikolaou, N. (2016). Fiber tracking: a qualitative and quantitative comparison between four different software tools on the reconstruction of major white matter tracts. *Eur. J. Radiol. Open* 3, 153–161. doi: 10.1016/j.ejro.2016.06.002
- Clair, C., Cohen, M. J., Eichler, F., Selby, K. J., and Rigotti, N. A. (2015). The effect of cigarette smoking on diabetic peripheral neuropathy: a systematic review and meta-analysis. *J. Gen. Intern. Med.* 30, 1193–1203. doi: 10.1007/s11606-015-3354-y
- Corine van de Zande, S., de Vries, J. K., Akker-Scheek, I., van den Zwerver, J., and Smit, A. J. (2020). A physically active lifestyle is related to a lower level of skin autofluorescence in a large population with chronic-disease (LifeLines cohort). *J. Sport Health Sci.* S2095-2546(20)30123-X. doi: 10.1016/J.JSHS.2020.09.007
- Csordas, A., and Bernhard, D. (2013). The biology behind the atherothrombotic effects of cigarette smoke. *Nat. Publ. Group* 10, 219–230. doi: 10.1038/nrcardio.2013.8
- Elliott, J., Tesfaye, S., Chaturvedi, N., Gandhi, R. A., Stevens, L. K., Emery, C., et al. (2009). Large-fiber dysfunction in diabetic peripheral neuropathy is predicted by cardiovascular risk factors. *Diabet. Care* 32, 1896–1900. doi: 10.2337/dc09-0554
- Fernando, M. E., Crowther, R. G., Lazzarini, P. A., Sangla, K. S., Wearing, S., Buttner, P., et al. (2019). Within- and between-body-site agreement of skin autofluorescence measurements in people with and without diabetes-related foot disease. *J. Diabet. Sci. Technol.* 13, 836–846. doi: 10.1177/1932296819853555
- Gaede, P., Vedel, P., Parving, H.-H. H., Pedersen, O., Aagaenaes, O., and Parving, H.-H. H. (1999). Intensified multifactorial intervention in patients with type 2 diabetes mellitus and microalbuminuria: the Steno type 2 randomised study. *Lancet* 353, 617–622. doi: 10.1016/S0140-6736(98)07368-1
- Groener, J. B., Jende, J. M. E., Kurz, F. T., Kender, Z., Treede, R.-D., Schuh-Hofer, S., et al. (2019). Understanding diabetic neuropathy: from subclinical nerve lesions to severe nerve fiber deficits. A cross-sectional study in patients with type 2 diabetes and healthy controls. *Diabetes* 69, 436–447. doi: 10.2337/db19-0197
- Heckel, A., Weiler, M., Xia, A., Ruetters, M., Pham, M., Bendszus, M., et al. (2015). Peripheral nerve diffusion tensor imaging: assessment of axon and myelin sheath integrity. *PLoS One* 10:e0130833. doi: 10.1371/journal.pone.0130833
- Jaiswal, M., Divers, J., Dabelea, D., Isom, S., Bell, R. A., Martin, C. L., et al. (2017). Prevalence of and risk factors for diabetic peripheral neuropathy in youth with type 1 and type 2 diabetes: search for diabetes in youth study. *Diabet. Care* 40, 1226–1232. doi: 10.2337/dc17-0179
- Jende, J. M. E., Kender, Z., Rother, C., Alvarez-Ramos, L., Groener, J. B., Pham, M., et al. (2020c). Diabetic polyneuropathy is associated with pathomorphological changes in human dorsal root ganglia: a study using 3T MR neurography. *Front. Neurosci.* 14:570744. doi: 10.3389/fnins.2020.570744
- Jende, J. M. E., Groener, J. B., Kender, Z., Rother, C., Hahn, A., Hilgenfeld, T., et al. (2020b). Structural nerve remodeling at 3-T MR neurography differs between painful and painless diabetic polyneuropathy in type 1 or 2 diabetes. *Radiology* 294, 405–414. doi: 10.1148/radiol.2019191347
- Jende, J. M. E., Groener, J. B., Kender, Z., Hahn, A., Morgenstern, J., Heiland, S., et al. (2020a). Troponin T parallels structural nerve damage in type 2 diabetes: a cross-sectional study using magnetic resonance neurography. *Diabetes* 69, 713–723. doi: 10.2337/db19-1094
- Jende, J. M. E., Kender, Z., Mooshage, C., Groener, J. B., Alvarez-Ramos, L., Kollmer, J., et al. (2021). Diffusion tensor imaging of the sciatic nerve as a surrogate marker for nerve functionality of the upper and lower limb in patients with diabetes and prediabetes. *Front. Neurosci.* 15:642589. doi: 10.3389/fnins.2021.642589
- Kar, D., Gillies, C., Zaccardi, F., Webb, D., Seidu, S., Tesfaye, S., et al. (2016). Relationship of cardiometabolic parameters in non-smokers, current smokers, and quitters in diabetes: a systematic review and meta-analysis. *Cardiovasc. Diabetol.* 15, 158–158. doi: 10.1186/s12933-016-0475-5
- Kim, H.-L., and Kim, S.-H. (2019). Pulse wave velocity in atherosclerosis. *Front. Cardiovasc. Med.* 6:41. doi: 10.3389/fcvm.2019.00041
- Kurz, F. T., Buschle, L. R., Hahn, A., Jende, J. M. E., Bendszus, M., Heiland, S., et al. (2018). Diffusion effects in myelin sheath free induction decay. *J. Magn. Reson.* 297, 61–75.
- Levey, A. S., Stevens, L. A., Schmid, C. H., Zhang, Y. L., Castro, A. F., Feldman, H. I., et al. (2009). A new equation to estimate glomerular filtration rate. *Ann. Intern. Med.* 150, 604–612.
- Natus Medical Incorporated (2020). *Nicolet VikingQuest User Guide Version 21.1*. Pleasanton, CA: Natus Medical Incorporated.
- Nilsson, P. M., Gudbjörnsdóttir, S., Eliasson, B., Cederholm, J., and Steering Committee of the Swedish National Diabetes Register. (2004). Smoking is associated with increased HbA1c values and microalbuminuria in patients with diabetes—data from the national diabetes register in Sweden. *Diabet. Metab.* 30, 261–268.
- Shillo, P., Sloan, G., Greig, M., Hunt, L., Selvarajah, D., Elliott, J., et al. (2019). Painful and painless diabetic neuropathies: what is the difference? *Curr. Diabet. Rep.* 19:32. doi: 10.1007/s11892-019-1150-5
- Sibal, L., Agarwal, S. C., and Home, P. D. (2011). Carotid intima-media thickness as a surrogate marker of cardiovascular disease in diabetes. *Diabet. Metab. Syndr. Obes.* 4, 23–34. doi: 10.2147/DMSO.S8540
- Stålbjerg, E., van Dijk, H., Falck, B., Kimura, J., Neuwirth, C., Pitt, M., et al. (2019). Standards for quantification of EMG and neurography. *Clin. Neurophysiol.* 130, 1688–1729. doi: 10.1016/j.clinph.2019.05.008
- Tesfaye, S., Chaturvedi, N., Eaton, S. E. M., Ward, J. D., Manes, C., Ionescu-Tirgoviste, C., et al. (2005). Vascular risk factors and diabetic neuropathy. *N. Engl. J. Med.* 352, 341–350. doi: 10.1056/NEJMoa032782
- Toth, P. P., Simko, R. J., Palli, S. R., Koselleck, D., Quimbo, R. A., and Cziraky, M. J. (2012). The impact of serum lipids on risk for microangiopathy in patients with type 2 diabetes mellitus. *Cardiovasc. Diabetol.* 11:109. doi: 10.1186/1475-2840-11-109
- Vaeggemose, M., Pham, M., Ringgaard, S., Tankisi, H., Ejksjaer, N., Heiland, S., et al. (2017). Diffusion tensor imaging MR neurography for the detection of polyneuropathy in type 1 diabetes. *J. Magn. Reson. Imaging* 45, 1125–1134. doi: 10.1002/jmri.25415
- Young, M. J., Boulton, A. J., MacLeod, A. F., Williams, D. R., and Sonksen, P. H. (1993). A multicentre study of the prevalence of diabetic peripheral neuropathy in the United Kingdom hospital clinic population. *Diabetologia* 36, 150–154. doi: 10.1007/BF00400697

Conflict of Interest: The authors declare that the research was conducted in the absence of any commercial or financial relationships that could be construed as a potential conflict of interest.

Publisher's Note: All claims expressed in this article are solely those of the authors and do not necessarily represent those of their affiliated organizations, or those of the publisher, the editors and the reviewers. Any product that may be evaluated in this article, or claim that may be made by its manufacturer, is not guaranteed or endorsed by the publisher.

Copyright © 2022 Jende, Mooshage, Kender, Kopf, Groener, Heiland, Juerchott, Nawroth, Bendszus and Kurz. This is an open-access article distributed under the terms of the Creative Commons Attribution License (CC BY). The use, distribution or reproduction in other forums is permitted, provided the original author(s) and the copyright owner(s) are credited and that the original publication in this journal is cited, in accordance with accepted academic practice. No use, distribution or reproduction is permitted which does not comply with these terms.



Quantitative MR-Neurography at 3.0T: Inter-Scanner Reproducibility

Fabian Preisner¹, Rouven Behnisch², Véronique Schwehr¹, Tim Godel¹, Daniel Schwarz¹, Olivia Foesleitner¹, Philipp Bäumer³, Sabine Heiland¹, Martin Bendszus¹ and Moritz Kronlage^{1*}

¹ Department of Neuroradiology, Heidelberg University Hospital, Heidelberg, Germany, ² Institute of Medical Biometry and Informatics, Heidelberg University, Heidelberg, Germany, ³ Center for Radiology dia.log, Altötting, Germany

Background: Quantitative MR-neurography (MRN) is increasingly applied, however, the impact of the MR-scanner on the derived parameters is unknown. Here, we used different 3.0T MR scanners and applied comparable MR-sequences in order to quantify the inter-scanner reproducibility of various MRN parameters of the sciatic nerve.

Methods: Ten healthy volunteers were prospectively examined at three different 3.0T MR scanners and underwent MRN of their sciatic nerve using comparable imaging protocols including diffusion tensor imaging (DTI) and T2 relaxometry. Subsequently, inter-scanner agreement was assessed for seven different parameters by calculating the intraclass correlation coefficients (ICCs) and the standard error of measurement (SEM).

Results: Assessment of inter-scanner reliability revealed good to excellent agreement for T2 (ICC: 0.846) and the quantitative DTI parameters, such as fractional anisotropy (FA) (ICC: 0.876), whereas moderate agreement was observed for proton spin density (PD) (ICC: 0.51). Analysis of variance identified significant inter-scanner differences for several parameters, such as FA ($p < 0.001$; $p = 0.02$), T2 ($p < 0.01$) and PD ($p = 0.02$; $p < 0.01$; $p = 0.02$). Calculated SEM values were mostly within the range of one standard deviation of the absolute mean values, for example 0.033 for FA, 4.12 ms for T2 and 27.8 for PD.

Conclusion: This study quantifies the measurement imprecision for peripheral nerve DTI and T2 relaxometry, which is associated with the use of different MR scanners. The here presented values may serve as an orientation of the possible scanner-associated fluctuations of MRN biomarkers, which can occur under similar conditions.

Keywords: magnetic resonance imaging, peripheral nervous system, magnetic resonance neurography, biomarkers, reproducibility of results

OPEN ACCESS

Edited by:

Matthew Craig Evans,
Imperial College London,
United Kingdom

Reviewed by:

Jingyun Chen,
NYU Grossman School of Medicine,
United States
Arvin Arani,
Mayo Clinic, United States

*Correspondence:

Moritz Kronlage
Moritz.Kronlage@med.uni-
heidelberg.de

Specialty section:

This article was submitted to
Brain Imaging Methods,
a section of the journal
Frontiers in Neuroscience

Received: 17 November 2021

Accepted: 25 January 2022

Published: 16 February 2022

Citation:

Preisner F, Behnisch R,
Schwehr V, Godel T, Schwarz D,
Foesleitner O, Bäumer P, Heiland S,
Bendszus M and Kronlage M (2022)
Quantitative MR-Neurography at 3.0T:
Inter-Scanner Reproducibility.
Front. Neurosci. 16:817316.
doi: 10.3389/fnins.2022.817316

INTRODUCTION

Magnetic resonance neurography (MRN) has become a valuable technique for evaluation of the peripheral nervous system (PNS) (Filler et al., 1996; Thawait et al., 2011; Chhabra et al., 2018). Morphological nerve imaging, which usually includes high-resolution, T2-weighted (T2w) sequences, has already been established in clinical routine and enables detection of tissue damage on a fascicular level (Pham et al., 2014; Baumer et al., 2016). The diagnostic value of morphological

MRN, however, may seem limited since various neuropathies present with the common feature of an elevated T2w-signal, with or without an increase in fascicle caliber (Bäumer et al., 2011; Kronlage et al., 2017a). Quantitative imaging techniques, such as diffusion tensor imaging (DTI) (Baumer et al., 2014; Breckwoldt et al., 2015; Breitenseher et al., 2015) and T2 relaxometry (Kollmer et al., 2015; Vaeggemose et al., 2017a; Kronlage et al., 2019b) might improve the diagnostic performance of MRN by providing additional contrasts and thus potentially pave the way for a formulation of standardized diagnostic criteria.

Diffusion tensor imaging, which has been evaluated in peripheral neuropathies of various etiologies, allows to assess microstructural organization of anisotropic tissues, such as peripheral nerves, and offers four major biomarkers (Hagmann et al., 2006; Mori and Zhang, 2006). The fractional anisotropy (FA) serves as a marker of nervous tissue integrity and technically describes the degree of anisotropy of diffusion being a scalar value between zero (isotropic diffusion) and one (all diffusion in one direction) (Kronlage et al., 2017b; Godel et al., 2019; Kim et al., 2019). While mean diffusivity (MD) characterizes the overall diffusion independent of the direction, axial diffusivity (AD) provides a measure of water diffusion parallel to axonal fiber tracts. Radial diffusivity (RD), on the other hand, quantifies diffusion perpendicular to the principal nerve axis and is considered a biomarker of demyelination (Heckel et al., 2015; Kronlage et al., 2017b).

T2 relaxometry is a quantitative imaging technique that provides an estimate of the transverse relaxation time (T2), and also yields the parameter proton spin density (PD). In contrast to T2, PD is regarded as a semi-quantitative parameter since it is directly dependent on the MR signal and related parameters. T2 relaxometry is commonly based on a multi-echo spin echo (MSE) sequence and fitting of an exponential function (Tofts and du Boulay, 1990; Boulby, 2003). While T2 relaxometry has been extensively studied in the central nervous system, only a few studies have applied it to peripheral nerves with promising results (Kollmer et al., 2015, 2018; Vaeggemose et al., 2017b; Fortanier et al., 2020). In particular, it may allow for a better understanding of pathological mechanisms on a macromolecular level, since T2 reflects free-water protons and PD accounts for total water content including protons bound to macromolecules (Tofts and du Boulay, 1990; MacKay et al., 1994; Tofts, 2003).

Quantitative imaging techniques are increasingly studied in the PNS. While many of them have been proposed to produce valuable MR-biomarkers, they still have not been implemented in clinical routine yet, since it is essential to prove their reliability and reproducibility upon application. Preferably, the measurement error that is expected in different situations should be quantified in order to obtain orientation values regarding the precision of quantitative MRN techniques since the use of different hardware, software and/or readers are known to influence quantitative parameters (Guggenberger et al., 2012, 2013; Preisner et al., 2019, 2021). Furthermore, normative data is dependent on imaging parameters, demographic variables and post-processing algorithms (Chen et al., 2019; Hofstadler et al., 2019; Kronlage et al., 2019b). Recent studies have shown that DTI and T2 relaxometry of peripheral nerves provide reliable results

when considering different readers or repetitive scans (Andreisek et al., 2010; Tagliafico et al., 2011; Ho et al., 2017; Preisner et al., 2019, 2021). However, those studies were conducted on identical MR scanners. In a real-world setting a change of the MR scanner is not unlikely, especially in a follow-up of a systemic neuropathy over several years. Moreover, a potential use of quantitative biomarkers as objective criteria for specific neuropathies is only conceivable if the influence of the scanner hardware is only minor. Also, when defining threshold values as diagnostic criteria for certain diseases, it is crucial to know the range of fluctuation, which must be considered, when different scanners are used. While one study reported promising first results for FA and MD measurements using different scanners (Guggenberger et al., 2013), a systematic assessment of inter-scanner reliability of peripheral nerve MRN biomarkers is still lacking.

The purpose of this study was therefore to assess the inter-scanner reliability of sciatic nerve DTI and T2 relaxometry by providing intraclass correlation coefficient (ICC-) and standard error of measurement (SEM-) values, respectively. We prospectively examined a cohort of ten healthy volunteers who each underwent MRN on three different MR scanners.

MATERIALS AND METHODS

This study was approved by the institutional ethics committee. Written informed consent was obtained from all participants. The study design is summarized in **Figure 1**.

Study Subjects

Ten healthy adults (>18 years, 5 men, 5 women) were prospectively enrolled for this study. Mean age was 25.4 ± 1.1 years (range: 24 – 28 years), mean height was 1.73 ± 0.11 m, mean weight was 69.6 ± 19.2 kg and mean BMI was 23 ± 3.9 (range: 18.4 – 29.9). Exclusion criteria were any known or history of peripheral nerve disease as well as general contradictions for MRI.

MR Imaging

All participants received three different MR scans of their sciatic nerve using three different MR scanners: (1) Magnetom Prisma-FIT (bore size 60 cm) (Siemens Healthineers, Erlangen, Germany), (2) Magnetom Skyra (bore size 70 cm) (Siemens Healthineers), and (3) Magnetom TIM-TRIO (bore size 60 cm) (Siemens Healthineers). Every scan was performed in supine position with legs extended using a 15-channel transmit-receive knee coil (Siemens Healthineers), which was placed at mid to distal thigh level. The coil was positioned such that its distal end aligned to the distal patella in order to ensure high reproducibility. Additional pads were used to immobilize the thigh and to avoid motion artifacts. Then, MRN protocols were carried out including high-resolution T2-weighted imaging, DTI and T2 relaxometry. Care was taken that parameters determining contrast and geometry were comparable with respect to the different hardware. Detailed sequence parameters are listed in **Table 1**. Representative MRN images are shown in **Figure 2**.

TABLE 1 | MR imaging parameters.

	T2w (turbo spin echo sequence)			Diffusion tensor imaging (single-shot echo planar imaging sequence)			T2 relaxometry (12-echo multi-echo spin echo sequence)		
	Prisma	Skyra	Trio	Prisma	Skyra	Trio	Prisma	Skyra	Trio
Repetition time (TR) [ms]	8,150	8,150	7,000	4,000	4,000	4,000	2,400	2,400	2,400
Echo time (TE) [ms]	54	54	55	83	93	92.8	10, 20...120	10, 20...120	10, 20...120
Field of view (FOV) [mm ²]	160 × 160	160 × 160	160 × 160	160 × 160	170 × 170	160 × 160	159 × 159	159 × 159	159 × 159
Matrix size	512 × 333	512 × 333	512 × 333	128 × 128	128 × 128	128 × 128	192 × 169	192 × 169	192 × 169
Slice thickness [mm]	3.5	3.5	3.5	4	4	4	3.5	3.5	3.5
Interslice gap [mm]	3.85	3.85	3.85	5.2	5.2	5.2	3.5	3.5	3.5
Number of slices	41	41	41	18	18	18	11	11	11
Fat suppression	Yes	Yes	Yes	Yes	Yes	Yes	Yes	Yes	Yes
Number of averages	2	2	2	3	3	3	1	1	1
Echo train length	13	13	13	59	59	59	12	12	12
Refocusing flip angle [°]	150	150	150	180	180	180	180	180	180
b-value 1 [s/mm ²]	n.a.	n.a.	n.a.	0	0	0	n.a.	n.a.	n.a.
b-value 2 [s/mm ²]	n.a.	n.a.	n.a.	1,000	1,000	1,000	n.a.	n.a.	n.a.
Diffusion encoding directions	n.a.	n.a.	n.a.	21	21	21	n.a.	n.a.	n.a.
Bandwidth (Hz/Pixel)	180	180	181	1,220	1,220	1,395	190	190	190
Acquisition time	3 min 56 s	3 min 56 s	3 min 23 s	4 min 32 s	4 min 32 s	4 min 48 s	6 min 43 s	6 min 43 s	6 min 44 s

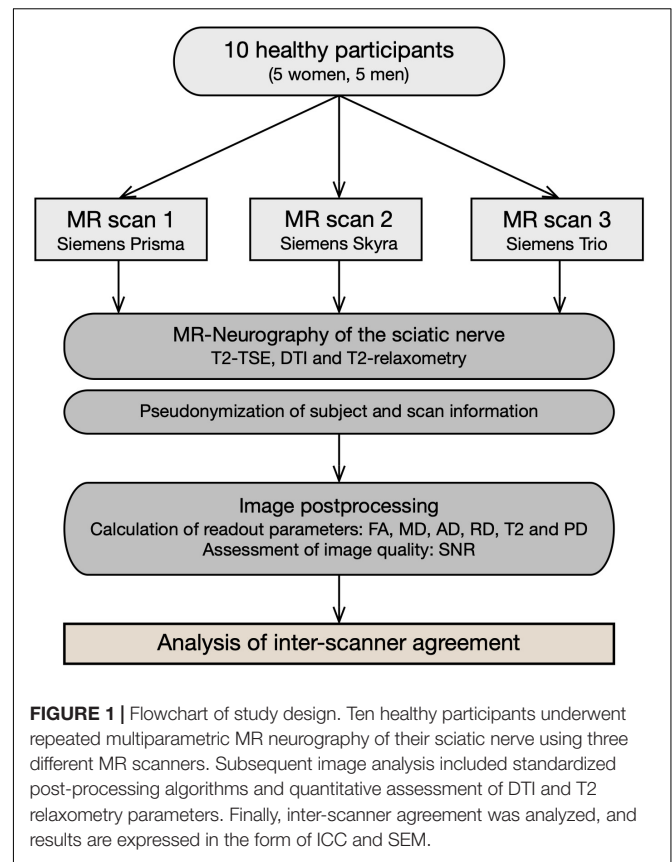


FIGURE 1 | Flowchart of study design. Ten healthy participants underwent repeated multiparametric MR neurography of their sciatic nerve using three different MR scanners. Subsequent image analysis included standardized post-processing algorithms and quantitative assessment of DTI and T2 relaxometry parameters. Finally, inter-scanner agreement was analyzed, and results are expressed in the form of ICC and SEM.

Analysis of Quantitative Magnetic Resonance Neurography

Images were analyzed using the DICOM-viewer OsiriX (Pixmeo Sarl, Switzerland). Initially, image quality was rated as sufficient or insufficient by F.P. (with more than 5 years of experience in neuromuscular imaging) for further analysis. Subsequently, region-of-interest (ROI) based manual nerve segmentation was performed for seven centrally located slices of the image slab using the high-resolution T2-weighted images in which the borders of the nerve were clearly identifiable. Similar approaches have been used in various studies of systemic neuropathies (Kronlage et al., 2017b; Simon et al., 2017; Lichtenstein et al., 2018) and healthy volunteers (Preisner et al., 2019, 2021). To avoid the inclusion of perineurial fat, nerve segmentation was restricted to the tibial portion of the sciatic nerve. All obtained ROIs were then copied to the corresponding b0-image ($b = 0$ s/mm²) for DTI analysis and to the corresponding multi-echo spin echo (MSE) slice (TE_{20ms}) for assessment of T2 relaxometry using the software's in-built image co-registration tool and, if necessary, manually corrected for distortion artifacts, as described previously (Preisner et al., 2021).

Subsequently, the DTI-derived parameters FA, MD, AD and RD were obtained for each slice separately using the OsiriX plug-in DTI map with a preset for noise threshold of 14 (referring to the voxel signal value in the b0-image [arbitrary units]). T2 relaxometry was conducted using a 12-echo MSE sequence

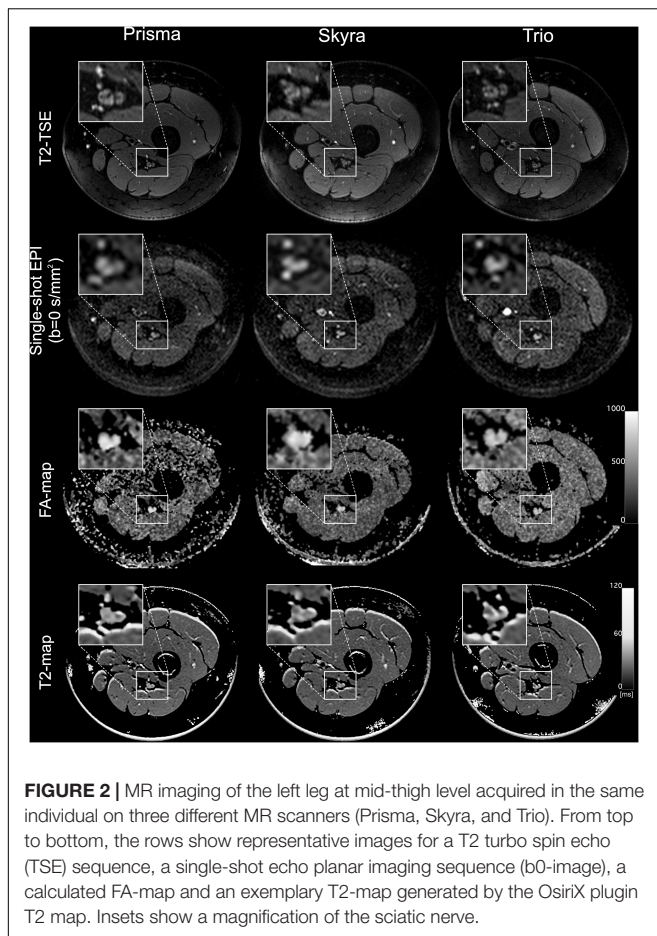


FIGURE 2 | MR imaging of the left leg at mid-thigh level acquired in the same individual on three different MR scanners (Prisma, Skyra, and Trio). From top to bottom, the rows show representative images for a T2 turbo spin echo (TSE) sequence, a single-shot echo planar imaging sequence (b0-image), a calculated FA-map and an exemplary T2-map generated by the OsiriX plugin T2 map. Insets show a magnification of the sciatic nerve.

($TE_{10-120\text{ ms}}, \Delta = 10\text{ ms}$), of which only the six even echoes ($TE_{20,40,60,80,120\text{ ms}}$) were used for further quantitative analysis. This included a slice-wise determination of the ROI signal intensity using the OsiriX plug-in ROI-enhancement and fitting to a mono-exponential function:

$$S(TE) = PD \times e^{-\frac{TE}{T2}} + \text{offset},$$

as described in previous works (Milford et al., 2015; Kronlage et al., 2017a), where $S(TE)$ equals the signal intensity at a given echo time TE , $T2$ is the transverse relaxation time and PD is a value proportional to proton density per voxel. Moreover, a normalized PD was calculated (further referred to as PD_{Ratio}) by dividing the PD of the sciatic nerve by a PD of skeletal muscle, the latter of which was assessed by ROI-based measurements in the adjacent musculature (M. semimembranosus or M. adductor magnus). After slice-wise calculation of DTI parameters, $T2$ and PD , all parameters were averaged over all seven slices for further analysis.

Quantitative Assessment of Image Quality

The signal-to-noise ratio (SNR) is commonly reported to describe image quality. To determine SNR_{DTI} , we used a “five-region approach” in the b0-image. Therefore, a total number of four

ROIs with identical size (4 cm^2) were positioned in the corners of the background and the standard deviations of the background signals were averaged over all four ROIs to calculate “noise.” Nerve signal intensity was subsequently divided by noise to calculate SNR_{DTI} (Supplementary Figure 1). This was performed on all seven slices, which were used for further DTI-analysis, and SNR values then were averaged over all slices. SNR of T2 relaxometry was assessed similarly using the MSE sequence (TE_{10ms}).

Statistical Analysis

Statistical testing was performed using SPSS (Version 24; SPSS Inc.) and R (Version 4.0.3; R Foundation for Statistical Computing). Graphs were created using GraphPad Prism (Version 9.0.2; GraphPad Software Inc.).

Descriptive statistics include mean values, standard deviation, interquartile range, and minimum to maximum values for every quantitative MRN parameter. One-way analysis of variance with pairwise comparisons was conducted to test for differences between scanners and Bonferroni correction was applied to correct for multiplicity. To assess inter-scanner agreement, a two-way mixed effects model, ICC (3,1) according to Shrout and Fleiss, was applied and ICCs with 95% confidence intervals (CIs) were calculated (Shrout and Fleiss, 1979). According to Koo and Li, ICC values between 0.5 and 0.75, between 0.75 and 0.9, and greater 0.9 were regarded as indicative for moderate, good and excellent agreement (Koo and Li, 2016). Additionally, mean absolute percentage errors between MR scanners were calculated for each parameter and participant and subsequently averaged over all participants, respectively. In this context, the mean value between the three scans served as the accepted true value for each parameter. Furthermore, Bland-Altman analyses for FA, T2, PD and PD_{Ratio} were calculated and measurement bias with 95% CIs as well as upper and lower limits of agreements are reported. Measurement distribution within the limits of agreement is visualized in Bland-Altman plots. P -values ≤ 0.05 were regarded as statistically significant.

RESULTS

Descriptive Statistics

Detailed descriptive statistics for all parameters and MR scans are shown in Figure 3 and Supplementary Table 1. The overall mean value and standard deviation averaged over all MR scanners was 0.61 ± 0.05 for FA, $1152.8 \pm 98.9 \times 10^{-6}\text{ mm}^2/\text{s}$ for MD, $2076.2 \pm 161.7 \times 10^{-6}\text{ mm}^2/\text{s}$ for AD, $690.6 \pm 96 \times 10^{-6}\text{ mm}^2/\text{s}$ for RD, $66.8 \pm 5.9\text{ ms}$ for T2, 213 ± 30.1 for PD and 0.66 ± 0.03 for PD_{Ratio} .

Comparison of mean values of the different MR scanners by ANOVA showed predominantly small but statistically significant differences for FA (Prisma vs. Skyra: 0.601 vs. 0.632, $p < 0.001$; Skyra vs. Trio: 0.632 vs. 0.597, $p = 0.022$), for MD (Skyra vs. Trio: 1,189 vs. $1,121 \times 10^{-6}\text{ mm}^2/\text{s}$, $p < 0.01$), for AD (Prisma vs. Skyra: 2,054 vs. $2,182 \times 10^{-6}\text{ mm}^2/\text{s}$, $p = 0.016$; Skyra vs. Trio: 2,182 vs. $1,993 \times 10^{-6}\text{ mm}^2/\text{s}$, $p < 0.01$), for T2 (Prisma vs. Skyra:

66.2 vs. 68.3 ms, $p < 0.01$) and for PD (Prisma vs. Skyra: 235 vs. 217, $p = 0.022$; Prisma vs. Trio: 235 vs. 187, $p < 0.001$; Skyra vs. Trio: 217 vs. 187, $p = 0.016$). No significant differences could be detected for RD and PD_{Ratio}.

Inter-Scanner Agreement

Assessment of inter-scanner reliability showed good agreement for FA, MD and T2 with ICCs ranging from 0.83 for MD to 0.88 for FA (all ICC values in **Table 2**). Excellent agreement was observed for RD with an ICC of 0.92. Inter-scanner reliability was moderate regarding AD, PD and PD_{Ratio} with ICC values ranging from 0.51 for PD to 0.7 for AD.

Calculated SEM values were mostly within the observed standard deviation of the overall mean values, for example SEM was 0.033 for FA, 4.12 ms for T2 and 27.8 for PD. SEM values for all parameters as well as mean absolute percentage errors are listed in **Table 2**.

Bland-Altman analysis is shown in **Table 3** and **Supplementary Figure 2**. Maximal measurement bias between two MR scanners was 0.035 for FA, 67.9×10^{-6} mm²/s for MD, 188.8×10^{-6} mm²/s for AD, 11.7×10^{-6} mm²/s for RD, 2.4 ms for T2, 48.44 for PD and 0.003 for PD_{Ratio}.

Signal-to-Noise Ratio

Mean SNR values were calculated for DTI (SNR_{DTI}) and the T2 relaxometry sequence (SNR_{T2}) for all three MR scanners, respectively. Analyses of variance showed that SNR_{DTI} was significantly higher for Prisma and Skyra compared to Trio (Prisma vs. Trio, $p = 0.03$; Skyra vs. Trio, $p = 0.002$). SNR_{T2} was significantly higher for Prisma compared to Skyra and Trio (Prisma vs. Skyra, $p = 0.001$; Prisma vs. Trio, $p = 0.027$) (**Figure 3** and **Table 4**).

DISCUSSION

This study evaluated the reproducibility of peripheral nerve DTI and T2 relaxometry in different MR scanners at the same field strength. We examined a healthy cohort using three different MR scanners (all 3.0T) and quantified measurement accuracy by reporting ICC- and SEM values for seven different parameters. As a principal finding, differences of some DTI and T2 relaxometry

parameters were statistically significant between scanners. In order to provide a measure that allows to estimate the inaccuracy attributed to a change of the MR scanner in an individual patient follow-up, we report the standard error of measurement (SEM) for each parameter.

The authors are aware of only one study by Guggenberger et al. (2013) that has systematically assessed the agreement of FA and apparent diffusion coefficient (ADC) values of the median nerve using three different MR scanners. Similar to that study, we observed that quantitative parameters, such as FA, can differ significantly between different MR scanners. This may in part result from differences in SNR (**Figure 3**) and the fact that noise plays a role as a systematic source of error when calculating quantitative parameters. Also, factors that are not transparent to the user, such as correction or interpolation processes during image acquisition, may lead to systematic differences in quantitative MRN values. PD was the parameter with the highest inter-scanner variation, as we expected due to the parameter's dependency on technical properties, such as RF coil, and signal attenuation. Thus, absolute PD values should always be interpreted carefully. Normalizing PD to adjacent muscle tissue has shown to be a more robust parameter and can be used to improve comparability between different scanners, yet accompanying muscular changes should always be considered when observing systemic neuropathies (Kronlage et al., 2019a).

Like in many reliability studies, Guggenberger et al. expressed their results by reporting the ICC, which is a commonly used parameter to describe the reliability of measurements and ranges between 0 and 1. Although the ICC is a useful statistical measure, it should be interpreted with care since different forms of ICC exist and results may vary depending on the selected form, even if applied to the same data (Koo and Li, 2016). Additionally, ICC values can be affected by several factors, such as data range, which means that a higher ICC value does not necessarily indicate less variability (Stratford and Goldsmith, 1997; Lee et al., 2012). In light of these limitations, we here provide the standard error of measurement (SEM) for every parameter in addition to ICC values. The SEM estimates measurement precision independently of the sample variance and is expressed in the same physical unit as the measured quantity, thereby providing a more

TABLE 2 | Intraclass correlation coefficients (ICCs) and the standard error of measurement (SEM).

Variables	ICC (3,1)	95% CI	SEM	Mean absolute percentage error [%]
FA	0.876	[0.687, 0.964]	0.033	4.37
MD	0.828	[0.588, 0.949]	70.46 [10^{-6} mm ² /s]	4.47
AD	0.697	[0.361, 0.904]	138.8 [10^{-6} mm ² /s]	5.85
RD	0.915	[0.776, 0.976]	50.06 [10^{-6} mm ² /s]	4.35
T2	0.846	[0.624, 0.955]	4.12 [ms]	3.48
PD	0.51	[0.119, 0.826]	27.8 [†]	11.12
PD ratio	0.635	[0.272, 0.88]	0.03	2.39

Intraclass correlation coefficients (ICC) with 95% confidence intervals (CI) were calculated according to Shrout and Fleiss. Calculation of SEM values is based on Popovic and Thomas (2017). FA, fractional anisotropy; MD, mean diffusivity; AD, axial diffusivity; RD, radial diffusivity; T2, transverse relaxation time; PD, proton spin density; [†]proportional to proton density per voxel.

useful framework for decision making in clinical practice (Popovic and Thomas, 2017).

The expected measurement error, which is associated with different readers (interreader) and repeated scans (test-retest)

without switching between different MR scanners, has been estimated in recent studies and corresponding SEM values have been calculated for various quantitative MRN parameters (Preisner et al., 2019, 2021). The SEM values observed in our

TABLE 3 | Bland-Altman analyses for inter-scanner agreement.

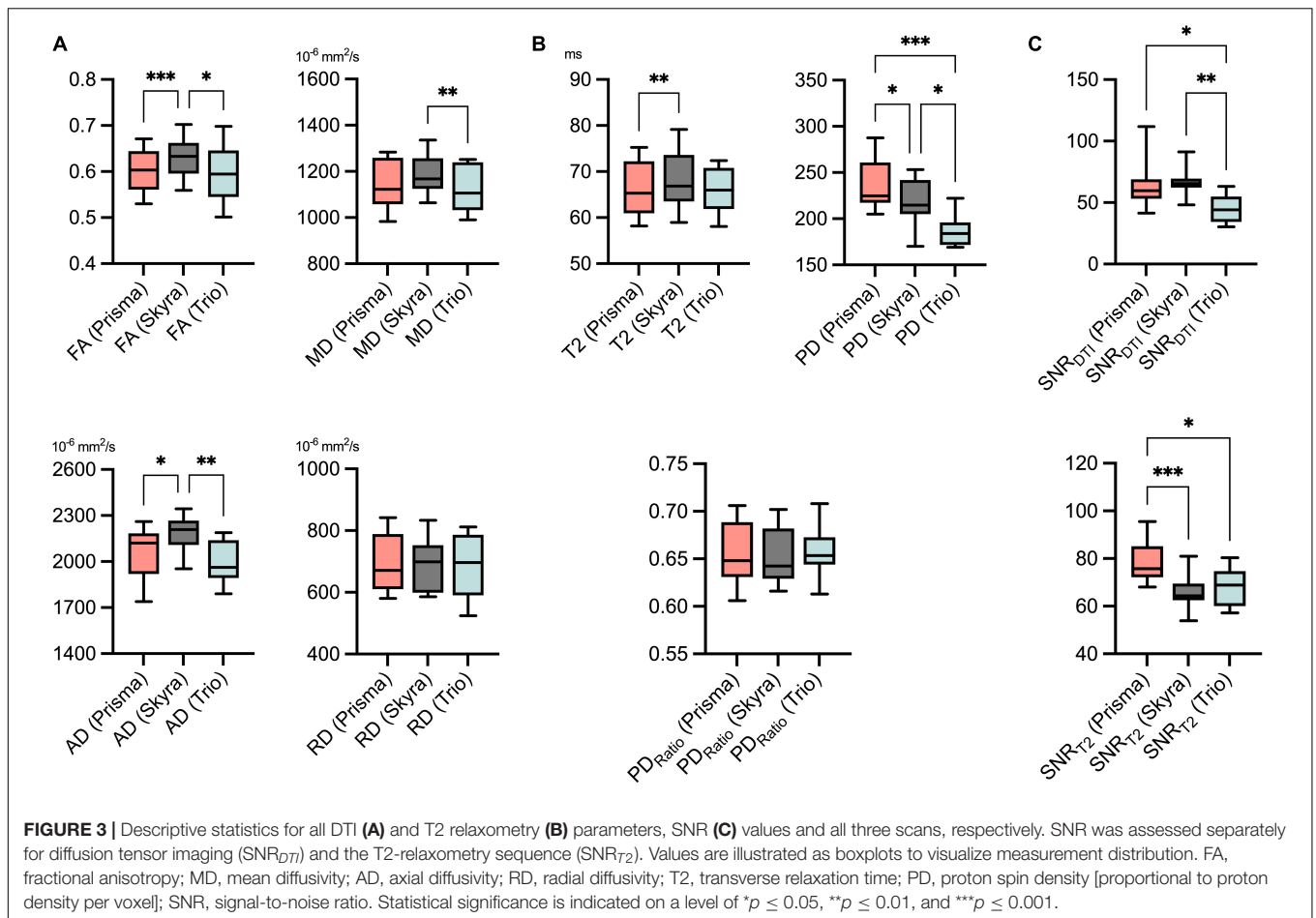
Variables	Prisma vs. Skyra	Skyra vs. Trio	Prisma vs. Trio
FA			
bias	-0.031	0.035	0.004
sd of bias	0.015	0.032	0.029
lloa of 95% CI	-0.061	-0.028	-0.053
uloa of 95% CI	-0.001	0.098	0.061
MD [10^{-6} mm²/s]			
bias	-41	67.9	26.93
sd of bias	64	48.68	58.83
lloa of 95% CI	-166	-27.51	-88.39
uloa of 95% CI	84.5	163.3	142.2
AD [10^{-6} mm²/s]			
bias	-127.7	188.8	61.04
sd of bias	11.07	121.8	107.1
lloa of 95% CI	-344.6	-49.95	-148.8
uloa of 95% CI	89.15	427.5	270.9
RD [10^{-6} mm²/s]			
bias	4.47	7.2	11.67
sd of bias	39.77	38.43	47.75
lloa of 95% CI	-73.48	-68.12	-81.92
uloa of 95% CI	-82.42	82.52	105.3
T2 [ms]			
bias	-2.11	2.42	0.31
sd of bias	1.5	4.29	3.65
lloa of 95% CI	-5.05	-5.99	-6.84
uloa of 95% CI	0.82	10.83	7.46
PD			
bias	17.92	30.52	48.44
sd of bias	16.41	26.35	24.13
lloa of 95% CI	-14.25	-21.13	1.15
uloa of 95% CI	50.09	82.17	95.73
PD ratio			
bias	0.001	-0.003	-0.002
sd of bias	0.018	0.028	0.032
lloa of 95% CI	-0.034	-0.057	-0.063
uloa of 95% CI	0.036	0.051	0.06

FA, fractional anisotropy; MD, mean diffusivity; AD, axial diffusivity; RD, radial diffusivity; T2, transverse relaxation time; PD, proton spin density; sd, standard deviation; lloa, lower limit of agreement; uloa, upper limit of agreement; CI, confidence intervals.

TABLE 4 | Quantitative signal-to-noise ratio (SNR) analysis for the diffusion tensor imaging (DTI) and T2 relaxometry sequence.

Variables	Prisma (N = 10)	Skyra (N = 10)	Trio (N = 10)	Prisma vs. Skyra	Skyra vs. Trio	Prisma vs. Trio
SNR (DTI)						
mean	64	66.5	45.2	$p = 0.99$	$p = 0.002$	$p = 0.03$
standard deviation	20.7	10.9	11.1			
SNR (T2)						
mean	78.5	65.9	68.11	$p = 0.001$	$p = 0.99$	$p = 0.027$
standard deviation	8.6	7.4	7.9			

Calculated p values are displayed as results from analysis of variance with pairwise comparisons and Bonferroni correction.



study, which accounts for the use of different MR scanners, demonstrate a slightly higher measurement error compared to interreader and test-retest observations with one particular MR scanner. For example, we report an SEM for FA considering examinations on different MR scanners of 0.033. In contrast, a repeated MR examination on the same scanner or a change of the reader have been described by SEM values of 0.02, respectively (Preisner et al., 2019). Furthermore, we calculate a measurement error for T2 of SEM = 4.1 ms when using different MR scanners. This value may be compared to a previously reported SEM of 2.7 ms for repeated measurements on the exact same MR scanner (Preisner et al., 2021).

This observation becomes even more relevant when calculating the minimum detectable difference (MDD, equals $2.8 \times \text{SEM}$), which can help to decide whether an observed difference may likely be attributed measurement error, or whether it really indicates a change in the true value (Popovic and Thomas, 2017). If a measured difference is larger than the MDD, there is high certainty that it is due to a change in the true value, e.g., reflecting a substantial change in tissue physiology. As the MDD increases along with SEM and thus a change of the MR scanner, it becomes evident that a greater difference in values will be required to confidently distinguish healthy from diseased nerves when using different MR scanners.

For example, the MDD for FA associated with a change of MR scanner is $2.8 \times 0.033 = 0.092$. Differences in sciatic nerve FA values between patients and healthy participants have been previously reported and ranged between 0.06 and 0.25 (Mathys et al., 2013; Bernabeu et al., 2016; Markvardsen et al., 2016; Vaeggemose et al., 2017a; Kim et al., 2019). While these differences were statistically significant on a group level, some of these differences, in a theoretical setting and on an individual patient level, would be lower than the calculated MDD and thus not reliably distinguishable from variations due to measurement error.

On a group level, however, these differences may have a lesser impact. The systematic difference between two scanners is reflected by the measurement bias observed in our study. For example, maximal measurement bias for FA was 0.035, which is smaller compared to previously reported differences in patients and healthy participants (see above) and within the standard range of the overall mean values. Similar observations can be made for other DTI parameters as well as T2 relaxometry. However, this systematic bias should be considered, especially when participants of particular study groups are examined at different MR scanners, since this bias alone may lead to statistically significant results.

Taken together, our results concerning the use of different MR scanners produced a higher measurement error compared to recently published measurement errors for repeated scans on the same scanner or a change of reader (Preisner et al., 2019, 2021). This becomes relevant regarding the use of quantitative MRN techniques as biomarkers, since their potential would be limited for individual follow-up examinations, especially when expected differences are subtle, e.g., in cases of peripheral nerve trauma or longitudinal observation of diffusion parameters, where minor changes may reflect fiber organization or myelin sheath integrity (Mathys et al., 2013). Using different MR scanners for larger group studies, however, may in certain situations be justifiable since overall differences – despite in part statistically significant – are not expected to substantially impact the differentiation between healthy and diseased nerves. In this context, however, it is also important to note that statistical significance does not necessarily imply clinical relevance, since small and non-significant differences can be clinically relevant and vice versa. Also, statistical significance is dependent of the power of the test. Due to our study design, we chose an ANOVA with pairwise comparisons, which has a higher power compared to a non-paired test. Therefore, we would like to focus not only on statistical significance but would like to emphasize the absolute amount of this systematic bias, which we quantified in this study, and which may aid as an orientation in future situations when a change of scanner hardware occurs.

There are limitations to this study. First, ten healthy volunteers were included. A larger cohort as well as the inclusion of patients with peripheral nerve disease would allow for optimal variability assessment of quantitative MRN and improve interpretation of measurement fluctuations in relation to inter-scanner differences. The fact that we only used MR scanners from one vendor can be regarded as another limitation. MR scanners from different vendors might introduce a greater variability in hardware and sequence parameters are expected to vary more substantially between different vendors, e.g., regarding RF pulse shape and gradient ramping. Thus, using MR scanners from more than one vendor may have led to higher measurement variability. Minor differences in DTI sequence parameters regarding field of view, echo time and pixel bandwidth may also contribute to the here reported discrepancies in SNR and affect the determined measurement error of DTI parameters, which must be regarded as another relevant limitation of this study. Especially minor variations regarding the field of view with identical matrix size led to different voxel sizes between MR scanners. Taken this into account, we would expect an advantage in SNR_{DTI} for Skyra of approximately 13%, but only a 4% higher SNR_{DTI} was observed. This, in turn, may be a consequence of hardware differences between the two MR scanners, since Prisma has a smaller bore size and allowed for lower TE values due to a stronger gradient system. Furthermore, SNR calculations were conducted using ROI-based measurements in separate signal and noise regions, although it is known that the use of multi-channel coils and reconstruction filters can lead to over- or underestimation of SNR when using such methods (Dietrich et al., 2007). Like in many *in vivo* studies, an approach based on repeated acquisition to calculate the SNR was not considered

feasible with respect to the acquisition time and potential motion artifacts. As a compromise, we used a “five-region approach,” calculated the standard deviation of background noise instead of mean values, and averaged over multiple slices to compensate for inhomogeneous spatial distribution of noise. However, a certain bias is to be expected with this method, which should be considered another limitation. Moreover, we used one vendor-independent post-processing method for analysis of all scans. This allowed to minimize systematic differences resulting during post-processing and helped to attribute the observed differences to the acquisition and processing stages. Furthermore, we focused on the sciatic nerve since it is still the most commonly examined nerve in MRN and most suitable due to its straight course and great caliber. An inclusion of small caliber nerves, for example at the upper extremity, may have led to a higher measurement variability. However, a recent study suggests that DTI- and in particular FA-values of the sciatic nerve can be considered as an objective parameter for the structural integrity of the entire PNS in diabetic neuropathy (Jende et al., 2021). Thus, quantitative MRN of the sciatic nerve seems conceivable in follow-up of systemic neuropathies, although this concept still must be evaluated for other forms of systemic neuropathies in future studies. Lastly, we chose a manual nerve segmentation approach, since it is regarded a well-established method in MRN and proven to result in reliable and reproducible values, both between different readers and scans (Preisner et al., 2019, 2021). In the future, automatic segmentation methods may also become implemented into clinical practice (Balsiger et al., 2018).

In summary, this study quantifies the measurement imprecision for peripheral nerve DTI and T2 relaxometry, which is associated with the use of different MR scanners. The here presented values may serve as an orientation of the possible scanner-associated fluctuations of MRN biomarkers, which can occur under similar conditions.

DATA AVAILABILITY STATEMENT

The raw data supporting the conclusions of this article will be made available by the authors, without undue reservation.

ETHICS STATEMENT

The studies involving human participants were reviewed and approved by the Ethics Committee of the Medical Faculty of the University of Heidelberg. The patients/participants provided their written informed consent to participate in this study.

AUTHOR CONTRIBUTIONS

MK, PB, FP, and MB designed and coordinated the study. VS organized the participants. VS and MK collected the MR data. FP, MK, TG, OF, DS, and SH performed image post-processing and analysed the data. RB performed the main statistical analysis. FP and MK wrote the manuscript with input from all co-authors.

FUNDING

SH (SFB 1118), DS (SFB 1118), and MB (SFB 1158) were supported by the German Research Foundation. FP and DS were supported by a Physician-Scientist Fellowship of the Medical Faculty of the University of Heidelberg. OF receives a research grant from the Rahel Goitein-Straus Support Program of the Medical Faculty of the University of Heidelberg. TG was supported by a Memorial Fellowship from the Else

Kröner-Fresenius-Foundation and received research grants from Amicus Therapeutics.

SUPPLEMENTARY MATERIAL

The Supplementary Material for this article can be found online at: <https://www.frontiersin.org/articles/10.3389/fnins.2022.817316/full#supplementary-material>

REFERENCES

- Andreisek, G., White, L. M., Kassner, A., and Sussman, M. S. (2010). Evaluation of diffusion tensor imaging and fiber tractography of the median nerve: preliminary results on intrasubject variability and precision of measurements. *AJR Am. J. Roentgenol.* 194, W65–W72. doi: 10.2214/ajr.09.2517
- Balsiger, F., Steindel, C., Arn, M., Wagner, B., Grunder, L., El-Koussy, M., et al. (2018). Segmentation of peripheral nerves from magnetic resonance neurography: a fully-automatic, deep learning-based approach. *Front. Neurol.* 9:777. doi: 10.3389/fneur.2018.00777
- Bäumer, P., Dombert, T., Staub, F., Kaestel, T., Bartsch, A. J., Heiland, S., et al. (2011). Ulnar neuropathy at the elbow: MR neurography–nerve T2 signal increase and caliber. *Radiology* 260, 199–206. doi: 10.1148/radiol.11102357
- Baumer, P., Kele, H., Xia, A., Weiler, M., Schwarz, D., Bendszus, M., et al. (2016). Posterior interosseous neuropathy: supinator syndrome vs fascicular radial neuropathy. *Neurology* 87, 1884–1891. doi: 10.1212/wnl.0000000000003287
- Baumer, P., Pham, M., Ruetters, M., Heiland, S., Heckel, A., Radbruch, A., et al. (2014). Peripheral neuropathy: detection with diffusion-tensor imaging. *Radiology* 273, 185–193. doi: 10.1148/radiol.14132837
- Bernabeu, A., Lopez-Celada, S., Alfaro, A., Mas, J. J., and Sanchez-Gonzalez, J. (2016). Is diffusion tensor imaging useful in the assessment of the sciatic nerve and its pathologies? Our clinical experience. *Br. J. Radiol.* 89:20150728. doi: 10.1259/bjr.20150728
- Boulby, P. A. (2003). “T2: the transverse relaxation time,” in *Quantitative MRI of the Brain: Measuring Changes Caused by Disease*, ed. P. S. Tofts (Hoboken, NJ: Wiley and Sons Ltd), 143–201.
- Breckwoldt, M. O., Stock, C., Xia, A., Heckel, A., Bendszus, M., Pham, M., et al. (2015). Diffusion tensor imaging adds diagnostic accuracy in magnetic resonance neurography. *Invest. Radiol.* 50, 498–504. doi: 10.1097/rli.0000000000000156
- Breitenseher, J. B., Kranz, G., Hold, A., Berzaczky, D., Nemes, S. F., Sycha, T., et al. (2015). MR neurography of ulnar nerve entrapment at the cubital tunnel: a diffusion tensor imaging study. *Eur. Radiol.* 25, 1911–1918. doi: 10.1007/s00330-015-3613-7
- Chen, Y., Haacke, E. M., and Li, J. (2019). Peripheral nerve magnetic resonance imaging [version 1; peer review: 2 approved]. *F1000Res.* 8:1803. doi: 10.12688/f1000research.19695.1
- Chhabra, A., Madhuranthakam, A. J., and Andreisek, G. (2018). Magnetic resonance neurography: current perspectives and literature review. *Eur. Radiol.* 28, 698–707. doi: 10.1007/s00330-017-4976-8
- Dietrich, O., Raya, J. G., Reeder, S. B., Reiser, M. F., and Schoenberg, S. O. (2007). Measurement of signal-to-noise ratios in MR images: influence of multichannel coils, parallel imaging, and reconstruction filters. *J. Magn. Reson. Imaging* 26, 375–385. doi: 10.1002/jmri.20969
- Filler, A. G., Kliot, M., Howe, F. A., Hayes, C. E., Saunders, D. E., Goodkin, R., et al. (1996). Application of magnetic resonance neurography in the evaluation of patients with peripheral nerve pathology. *J. Neurosurg.* 85, 299–309. doi: 10.3171/jns.1996.85.2.0299
- Fortanier, E., Ogier, A. C., Delmont, E., Lefebvre, M. N., Viout, P., Guye, M., et al. (2020). Quantitative assessment of sciatic nerve changes in Charcot-Marie-Tooth type 1A patients using magnetic resonance neurography. *Eur. J. Neurol.* 27, 1382–1389. doi: 10.1111/ene.14303
- Godel, T., Pham, M., Kele, H., Kronlage, M., Schwarz, D., Brune, M., et al. (2019). Diffusion tensor imaging in anterior interosseous nerve syndrome – functional MR Neurography on a fascicular level. *Neuroimage Clin.* 21:101659. doi: 10.1016/j.nicl.2019.101659
- Guggenberger, R., Nanz, D., Bussmann, L., Chhabra, A., Fischer, M. A., Hodler, J., et al. (2013). Diffusion tensor imaging of the median nerve at 3.0 T using different MR scanners: agreement of FA and ADC measurements. *Eur. J. Radiol.* 82, e590–e596. doi: 10.1016/j.ejrad.2013.05.011
- Guggenberger, R., Nanz, D., Puippe, G., Ruffbach, K., White, L. M., Sussman, M. S., et al. (2012). Diffusion tensor imaging of the median nerve: intra-, inter-reader agreement, and agreement between two software packages. *Skeletal Radiol.* 41, 971–980. doi: 10.1007/s00256-011-1310-4
- Hagmann, P., Jonasson, L., Maeder, P., Thiran, J. P., Wedeen, V. J., and Meuli, R. (2006). Understanding diffusion MR imaging techniques: from scalar diffusion-weighted imaging to diffusion tensor imaging and beyond. *Radiographics* 26 (Suppl. 1), S205–S223. doi: 10.1148/rg.26si065510
- Heckel, A., Weiler, M., Xia, A., Ruetters, M., Pham, M., Bendszus, M., et al. (2015). Peripheral nerve diffusion tensor imaging: assessment of axon and myelin sheath integrity. *PLoS One* 10:e0130833. doi: 10.1371/journal.pone.0130833
- Ho, M. J., Manoliu, A., Kuhn, F. P., Stieltjes, B., Klarhofer, M., Feiweier, T., et al. (2017). Evaluation of reproducibility of diffusion tensor imaging in the brachial plexus at 3.0 T. *Invest. Radiol.* 52, 482–487. doi: 10.1097/rli.0000000000000363
- Hofstadler, B., Bäumer, P., Schwarz, D., Kronlage, M., Heiland, S., Bendszus, M., et al. (2019). MR neurography: normative values in correlation to demographic determinants in children and adolescents. *Clin. Neuroradiol.* 30, 671–677. doi: 10.1007/s00062-019-00834-9
- Jende, J. M. E., Kender, Z., Mooshage, C., Groener, J. B., Alvarez-Ramos, L., Kollmer, J., et al. (2021). Diffusion tensor imaging of the sciatic nerve as a surrogate marker for nerve functionality of the upper and lower limb in patients with diabetes and prediabetes. *Front. Neurosci.* 15:642589. doi: 10.3389/fnins.2021.642589
- Kim, H. S., Yoon, Y. C., Choi, B. O., Jin, W., Cha, J. G., and Kim, J. H. (2019). Diffusion tensor imaging of the sciatic nerve in Charcot-Marie-Tooth disease type I patients: a prospective case-control study. *Eur. Radiol.* 29, 3241–3252. doi: 10.1007/s00330-018-5958-1
- Kollmer, J., Hund, E., Hornung, B., Hegenbart, U., Schonland, S. O., Kimmich, C., et al. (2015). In vivo detection of nerve injury in familial amyloid polyneuropathy by magnetic resonance neurography. *Brain* 138(Pt 3), 549–562. doi: 10.1093/brain/awu344
- Kollmer, J., Weiler, M., Purrucker, J., Heiland, S., Schonland, S. O., Hund, E., et al. (2018). MR neurography biomarkers to characterize peripheral neuropathy in AL amyloidosis. *Neurology* 91, e625–e634. doi: 10.1212/wnl.0000000000006002
- Koo, T. K., and Li, M. Y. (2016). A guideline of selecting and reporting intraclass correlation coefficients for reliability research. *J. Chiropr. Med.* 15, 155–163. doi: 10.1016/j.jcm.2016.02.012
- Kronlage, M., Baumer, P., Pitarokouli, K., Schwarz, D., Schwehr, V., Godel, T., et al. (2017a). Large coverage MR neurography in CIDP: diagnostic accuracy and electrophysiological correlation. *J. Neurol.* 264, 1434–1443. doi: 10.1007/s00415-017-8543-7
- Kronlage, M., Pitarokouli, K., Schwarz, D., Godel, T., Heiland, S., Yoon, M. S., et al. (2017b). Diffusion tensor imaging in chronic inflammatory demyelinating polyneuropathy: diagnostic accuracy and correlation with electrophysiology. *Invest. Radiol.* 52, 701–707. doi: 10.1097/rli.0000000000000394
- Kronlage, M., Schwehr, V., Schwarz, D., Godel, T., Heiland, S., Bendszus, M., et al. (2019b). Magnetic resonance neurography: normal values and demographic determinants of nerve caliber and T2 relaxometry in 60 healthy individuals. *Clin. Neuroradiol.* 29, 19–26. doi: 10.1007/s00062-017-0633-5

- Kronlage, M., Knop, K. C., Schwarz, D., Godel, T., Heiland, S., Bendszus, M., et al. (2019a). Amyotrophic lateral sclerosis versus multifocal motor neuropathy: utility of mr neurography. *Radiology* 292, 149–156. doi: 10.1148/radiol.2019182538
- Lee, K. M., Lee, J., Chung, C. Y., Ahn, S., Sung, K. H., Kim, T. W., et al. (2012). Pitfalls and important issues in testing reliability using intraclass correlation coefficients in orthopaedic research. *Clin. Orthop. Surg.* 4, 149–155. doi: 10.4055/cios.2012.4.2.149
- Lichtenstein, T., Sprenger, A., Weiss, K., Slebocki, K., Cervantes, B., Karampinos, D., et al. (2018). MRI biomarkers of proximal nerve injury in CIDP. *Ann. Clin. Transl. Neurol.* 5, 19–28. doi: 10.1002/acn3.502
- MacKay, A., Whittall, K., Adler, J., Li, D., Paty, D., and Graeb, D. (1994). In vivo visualization of myelin water in brain by magnetic resonance. *Magn. Reson. Med.* 31, 673–677. doi: 10.1002/mrm.1910310614
- Markvardsen, L. H., Vaeggemose, M., Ringgaard, S., and Andersen, H. (2016). Diffusion tensor imaging can be used to detect lesions in peripheral nerves in patients with chronic inflammatory demyelinating polyneuropathy treated with subcutaneous immunoglobulin. *Neuroradiology* 58, 745–752. doi: 10.1007/s00234-016-1692-z
- Mathys, C., Aissa, J., Meyer Zu Horste, G., Reichelt, D. C., Antoch, G., Turowski, B., et al. (2013). Peripheral neuropathy: assessment of proximal nerve integrity by diffusion tensor imaging. *Muscle Nerve* 48, 889–896. doi: 10.1002/mus.23855
- Milford, D., Rosbach, N., Bendszus, M., and Heiland, S. (2015). Mono-exponential fitting in T2-relaxometry: relevance of offset and first echo. *PLoS One* 10:e0145255. doi: 10.1371/journal.pone.0145255
- Mori, S., and Zhang, J. (2006). Principles of diffusion tensor imaging and its applications to basic neuroscience research. *Neuron* 51, 527–539. doi: 10.1016/j.neuron.2006.08.012
- Pham, M., Bäumer, P., Meinck, H. M., Schiefer, J., Weiler, M., Bendszus, M., et al. (2014). Anterior interosseous nerve syndrome: fascicular motor lesions of median nerve trunk. *Neurology* 82, 598–606. doi: 10.1212/wnl.000000000000128
- Popovic, Z. B., and Thomas, J. D. (2017). Assessing observer variability: a user's guide. *Cardiovasc. Diagn. Ther.* 7, 317–324. doi: 10.21037/cdt.2017.03.12
- Preisner, F., Bäumer, P., Wehrstein, M., Friedmann-Bette, B., Hackbusch, M., Heiland, S., et al. (2019). Peripheral nerve diffusion tensor imaging: interreader and test-retest reliability as quantified by the standard error of measurement. *Clin. Neuroradiol.* 30, 679–689. doi: 10.1007/s00062-019-00859-0
- Preisner, F., Behnisch, R., Foesleitner, O., Schwarz, D., Wehrstein, M., Meredig, H., et al. (2021). Reliability and reproducibility of sciatic nerve magnetization transfer imaging and T2 relaxometry. *Eur. Radiol.* 31, 9120–9130. doi: 10.1007/s00330-021-08072-9
- Shrout, P. E., and Fleiss, J. L. (1979). Intraclass correlations: uses in assessing rater reliability. *Psychol. Bull.* 86, 420–428. doi: 10.1037//0033-2909.86.2.420
- Simon, N. G., Lagopoulos, J., Paling, S., Pfluger, C., Park, S. B., Howells, J., et al. (2017). Peripheral nerve diffusion tensor imaging as a measure of disease progression in ALS. *J. Neurol.* 264, 882–890. doi: 10.1007/s00415-017-8443-x
- Stratford, P. W., and Goldsmith, C. H. (1997). Use of the standard error as a reliability index of interest: an applied example using elbow flexor strength data. *Phys. Ther.* 77, 745–750. doi: 10.1093/ptj/77.7.745
- Tagliafico, A., Calabrese, M., Puntoni, M., Pace, D., Baio, G., Neumaier, C. E., et al. (2011). Brachial plexus MR imaging: accuracy and reproducibility of DTI-derived measurements and fibre tractography at 3.0-T. *Eur. Radiol.* 21, 1764–1771. doi: 10.1007/s00330-011-2100-z
- Thawait, S. K., Chaudhry, V., Thawait, G. K., Wang, K. C., Belzberg, A., Carrino, J. A., et al. (2011). High-resolution MR neurography of diffuse peripheral nerve lesions. *AJNR Am. J. Neuroradiol.* 32, 1365–1372. doi: 10.3174/ajnr.A2257
- Tofts, P. S. (2003). “Proton density of tissue water,” in *Quantitative MRI of the Brain: Measuring Changes Caused by Disease*, ed. P. S. Tofts (Hoboken, NJ: Wiley and Sons Ltd), 83–108.
- Tofts, P. S., and du Boulay, E. P. (1990). Towards quantitative measurements of relaxation times and other parameters in the brain. *Neuroradiology* 32, 407–415. doi: 10.1007/bf00588474
- Vaeggemose, M., Pham, M., Ringgaard, S., Tankisi, H., Ejskjaer, N., Heiland, S., et al. (2017a). Magnetic resonance neurography visualizes abnormalities in sciatic and tibial nerves in patients with type 1 diabetes and neuropathy. *Diabetes* 66, 1779–1788. doi: 10.2337/db16-1049
- Vaeggemose, M., Vaeth, S., Pham, M., Ringgaard, S., Jensen, U. B., Tankisi, H., et al. (2017b). Magnetic resonance neurography and diffusion tensor imaging of the peripheral nerves in patients with Charcot-Marie-Tooth Type 1A. *Muscle Nerve* 56, E78–E84. doi: 10.1002/mus.25691

Conflict of Interest: The authors declare that the research was conducted in the absence of any commercial or financial relationships that could be construed as a potential conflict of interest.

Publisher's Note: All claims expressed in this article are solely those of the authors and do not necessarily represent those of their affiliated organizations, or those of the publisher, the editors and the reviewers. Any product that may be evaluated in this article, or claim that may be made by its manufacturer, is not guaranteed or endorsed by the publisher.

Copyright © 2022 Preisner, Behnisch, Schwehr, Godel, Schwarz, Foesleitner, Bäumer, Heiland, Bendszus and Kronlage. This is an open-access article distributed under the terms of the Creative Commons Attribution License (CC BY). The use, distribution or reproduction in other forums is permitted, provided the original author(s) and the copyright owner(s) are credited and that the original publication in this journal is cited, in accordance with accepted academic practice. No use, distribution or reproduction is permitted which does not comply with these terms.



Performance of Single-Shot Echo-Planar Imaging in Diffusion Tensor Imaging in Rat Sciatic Nerve Compared With Readout-Segmented Echo-Planar Imaging

OPEN ACCESS

Edited by:

Felix Tobias Kurz,
Heidelberg University Hospital,
Germany

Reviewed by:

Han Lv,
Capital Medical University, China
Chengde Liao,
Yunnan Cancer Hospital, China
Johann M. E. Jende,
Heidelberg University Hospital,
Germany

*Correspondence:

Hanqing Lyu
13510269808@139.com
Xiaofeng Lin
linxf22@mail.sysu.edu.cn

†These authors have contributed
equally to this work and share first
authorship

Specialty section:

This article was submitted to
Brain Imaging Methods,
a section of the journal
Frontiers in Neuroscience

Received: 28 December 2021

Accepted: 29 March 2022

Published: 12 May 2022

Citation:

Chen Y, Pan Z, Meng F, Li Z, Hu Y,
Yu X, Gao J, Guo Y, Lyu H and Lin X
(2022) Performance of Single-Shot
Echo-Planar Imaging in Diffusion
Tensor Imaging in Rat Sciatic Nerve
Compared With Readout-Segmented
Echo-Planar Imaging.
Front. Neurosci. 16:844408.
doi: 10.3389/fnins.2022.844408

Yueyao Chen^{1†}, Zhongxian Pan^{1†}, Fanqi Meng¹, Zhujing Li¹, Yuanming Hu¹, Xuewen Yu²,
Jinyun Gao¹, Yihao Guo³, Hanqing Lyu^{1*} and Xiaofeng Lin^{4*}

¹ Department of Radiology, Shenzhen Traditional Chinese Medicine Hospital, The Fourth Clinical Medical College of Guangzhou University of Chinese Medicine, Shenzhen, China, ² Department of Pathology, Shenzhen Traditional Chinese Medicine Hospital, The Fourth Clinical Medical College of Guangzhou University of Chinese Medicine, Shenzhen, China, ³ Magnetic Resonance Collaboration, Siemens Healthcare, Guangzhou, China, ⁴ Department of Nuclear Medicine, The Seventh Affiliated Hospital, Sun Yat-sen University, Shenzhen, China

Objectives: To compare the performances of single-shot echo-planar imaging (SS-EPI) and readout-segmented echo-planar imaging (RS-EPI) for diffusion tensor imaging (DTI) of the rat sciatic nerve.

Methods: Eight healthy adult male Sprague-Dawley rats were anesthetized and scanned with a 3T MRI scanner using SS-EPI and RS-EPI DTI sequences. The image quality in terms of the morphology of the nerve, distortions of the nearby femur, muscles, and homogeneity of neuromuscular were evaluated and scored. The correlations between the DTI parameters including fractional anisotropy (FA), axial diffusivity (AD), radial diffusivity (RD), apparent diffusion coefficient (ADC), and histopathological parameters were calculated by using the Pearson correlation coefficient and compared by the modified Fisher Z-transform, respectively.

Results: The quality scores were higher for the images from the SS-EPI sequence compared with the RS-EPI sequence for characteristics such as sharpness of the sciatic nerve margin ($P = 0.008$), artifacts of the sciatic nerve ($P = 0.008$), and homogeneity of the neuromuscular region ($P = 0.007$), as well as the contrast-to-noise ratio (CNR) of DW images ($P < 0.001$). The correlation coefficients were higher for the FA and RD values from the SS-EPI sequence compared with those from the RS-EPI sequence. Furthermore, the correlation coefficients between FA and myelin thickness ($P = 0.027$), FA and diameter of the myelinated fiber ($P = 0.036$), as well as RD and myelin thickness ($P = 0.05$) were statistically higher for the SS-EPI sequence compared with those for the RS-EPI sequence.

Conclusion: Diffusion tensor imaging analysis of the rat sciatic nerve showed that the image quality from the SS–EPI sequence was significantly higher compared with that from the RS–EPI sequence. Furthermore, the FA and RD derived from the SS–EPI sequence are promising and sensitive biomarkers to detect the histopathological changes in the rat sciatic nerve.

Keywords: magnetic resonance imaging, diffusion tensor imaging, single-shot echo-planar imaging, readout-segmented echo-planar imaging, peripheral nerve

INTRODUCTION

Diffusion tensor imaging (DTI) is a functional non-invasive MRI sequence that is widely used to evaluate cerebral white matter fiber tracts in the brain. DTI is also routinely used to assess the integrity of the peripheral nerves, especially in experimental animal studies of nerve injury. Several preclinical and animal studies have shown that DTI parameters such as fractional anisotropy (FA) and radial diffusivity (RD) are associated with axon density and myelin abnormalities (Chen et al., 2017; Farinas et al., 2020; Zheng et al., 2021). Therefore, DTI parameters such as FA and RD are highly sensitive biomarkers for the early detection of peripheral nerve dysfunction and monitoring the progression of peripheral nerve degeneration and regeneration (Chen et al., 2017; Farinas et al., 2020; Zheng et al., 2021).

Deep and prolonged anesthesia significantly increases the risk of animal death during *in-vivo* MRI studies. Furthermore, the risk of death from anesthesia is higher while performing continuous MRI to monitor peripheral nerve repair because the same animal is anesthetized and revived several times during the examination. Hence, to minimize the risk of death from anesthesia, DTI needs to be carried out in a shorter duration while ensuring sufficient quality. Furthermore, higher resolution is required for optimal analysis of the sciatic nerves in small experimental animals. Therefore, scan time, nerve display, and parameter accuracy are critically important while using DTI for peripheral nerve MRI studies in experimental animals.

Single-shot echo-planar imaging (SS–EPI) and readout-segmented echo-planar imaging (RS–EPI) are the two main types of DTI sequences. The conventional SS–EPI is more prone to susceptibility artifacts such as geometric distortions, image blurring, and ghosting artifacts (Drake-Pérez et al., 2018). Therefore, readout-segmented echo-planar imaging (RS–EPI) was developed to reduce distortion artifacts and increase image resolution (Porter and Heidemann, 2009). Better performance of the RS–EPI sequence in terms of image quality and lesion detection has improved the diagnostic performance of DTI in the brain (Kida et al., 2016), skull base and orbit (Yeom et al., 2013; Chen et al., 2020), breast (Bogner et al., 2012), kidney (Friedli et al., 2017), pelvis (Thian et al., 2014), and the sacroiliac joint (Zhang et al., 2021). However, RS–EPI significantly increases the scan time and is sensitive to movement artifacts. These two characteristics are the main obstacles in animal MRI studies.

In our preliminary study, the image quality from the SS–EPI sequence was significantly higher compared with the RS–EPI sequence for the diffusion tensor imaging of sciatic nerve repair in rats. In the liver and pediatric brains, SS–EPI sequences

showed better image quality with reduced susceptibility and motion artifacts compared with the RS–EPI sequence (Yeom et al., 2013; Xie et al., 2021). However, the performances of SS–EPI DTI and RS–EPI DTI have not been compared with assessing peripheral nerves in small animals. Therefore, in this study, we compared the image quality of the sciatic nerve between the SS–EPI and RS–EPI sequences. We also analyzed the correlation between DTI parameters from the SS–EPI and RS–EPI sequences and the histological parameters of the rat sciatic nerve to identify morphological and histological changes in the rat sciatic nerve.

MATERIALS AND METHODS

Subjects

All interventions and animal care procedures were performed in accordance with the Guidelines and Policies and were approved by the Institutional Animal Use and Care Committee. All animals were obtained from the Animal Experiment Center of Guangdong province. The animals were housed in a standard animal facility with 12-h on/off light conditions and allowed free access to standard food and water. Eight male adult healthy Sprague-Dawley rats weighing 250 ± 20 g were used in this study.

Magnetic Resonance Imaging

In total, eight healthy adult male Sprague-Dawley rats were anesthetized to deep sleep (7% chloralhydrate, 5 ml/kg, intraperitoneal injection) and scanned at 3T (MAGNETOM Prisma, Siemens Healthcare, Erlangen, Germany). After anesthesia, each rat was placed prone in a rat coil (6-cm diameter, 8 channel, Suzhou Medcoil Healthcare Co., Ltd.) with their limbs fixed with medical adhesive tape to further prevent movement. Both hind limbs were positioned symmetrically.

Two Axial DTI sequences (SS–EPI and RS–EPI) were performed according to the parameters as follows (see **Table 1** for detailed parameters): SS–EPI DWI (TE/TR 72/3,500 ms, slice thickness 1.5 mm, the field of view 70×70 , matrix size 100×100 , voxel size $0.7 \text{ mm} \times 0.7 \text{ mm}$, *b*-values 0 and 800 s/mm^2 , readout segments 1); RS–EPI DWI (TE/TR 58/4,000 ms, slice thickness 1.5 mm, the field-of-view 70×70 , matrix size 100×100 , voxel size $0.7 \text{ mm} \times 0.7 \text{ mm}$, *b*-values 0 and 800 s/mm^2 , readout segment 7). The axial plane was perpendicular to the long axis of the sciatic nerve. A coronal fat-suppressed T2-weighted image was obtained to display the morphology of bilateral sciatic nerves and to ensure the correct position of the region of interest (ROI) for DTI parameters measurement in the sciatic nerve (see **Figure 1**).

TABLE 1 | Sequence parameters for single-shot and readout-segmented echo-planar imaging.

Sequence parameter	Single-shot echo-planar imaging (SS-EPI)	Readout-segmented echo-planar imaging (RS-EPI)
Diffusion mode	MDDW	MDDW
Diffusion directions	20	20
Diffusion schema	Monopolar	Monopolar
<i>b</i> -value (s/mm ²)	0, 800	0, 800
Fat suppression	fat saturation	fat saturation
Repetition time (ms)	3,500	4,000
Echo time (ms)	72	58
Field of view (mm ²)	70 × 70	70 × 70
Voxel size (mm ²)	0.7 × 0.7	0.7 × 0.7
Slice thickness (mm)	1.5	1.5
Matrix	100 × 100	100 × 100
No. of sections	20	20
Section thickness (mm)	1.5	1.5
Intersection gap (%)	0	0
Phase-encoding direction	Anteroposterior	Anteroposterior
Echo spacing (ms)	1.13	0.54
No. of readout segments	1	7
Acquisition time (min:s)	4:06	14:12

Image Analysis

Image analysis was performed by two independent readers (Reader 1, a radiologist with 10 years of experience in DTI of the nerve; Reader 2, with 3 years of experience in DTI of the nerve). Both readers were blinded to the histopathologic results. Data of the two DTI sequences were transferred to the workstation (*Syngo Via 2*, Siemens) and post-processed for image quality evaluation and DTI parameters measurement. DTI images including *b* = 0, 800 images, FA, AD, RD, and ADC maps were generated simultaneously in Neuro 3D modules. The image quality was assessed qualitatively on DWI *b* = 800 image based on the following factors: sharpness of nerve margin, artifacts of nerve, artifacts of the femur, artifacts of ventral muscles, artifacts of dorsal muscles, homogeneity of neuromuscular. All images were rated according to a scale: 1, unacceptable image quality severely deteriorated by artifacts; 2, acceptable image quality with mild artifacts; 3, artifact-free image without distortions and with great anatomic detail (Thian et al., 2014). Contrast-to-noise ratio (CNR) was defined as the difference between the mean signal intensity of the nerve (S nerve) and that of the muscle surrounding on DW images (S muscle) divided by the SD on the lesion ROI (σ nerve) and normal tissue ROI (σ muscle) of the subtraction dataset as follows (Bogner et al., 2012)

$$CNR = \frac{S_{nerve} - S_{muscle}}{\sqrt{\sigma_{nerve}^2 - \sigma_{muscle}^2}}$$

The diffusion tensor parameters (FA, AD, RD, and ADC) were measured and calculated on the corresponding map generated on a workstation (*Syngo Via 2*, Siemens). ROIs of approximately 4 mm² were manually drawn on the adjacent 3 slices of the sciatic nerve. The three measurements were averaged for data analysis.

Special attention was paid to positioning the ROIs as precisely as possible to minimize the partial volume effect. Transverse DTI images were linked with coronal T2-weighted images to ensure the correct and consistent position of ROIs in the sciatic nerve. Tractography was obtained on the same workstation. A multiple ROI method was used to reconstruct diffusion tensor tractography (DTT). The threshold of FA was set to be 0.15, the maximum fiber angle was 35° and the minimum fiber length was 15 mm (Chen et al., 2017).

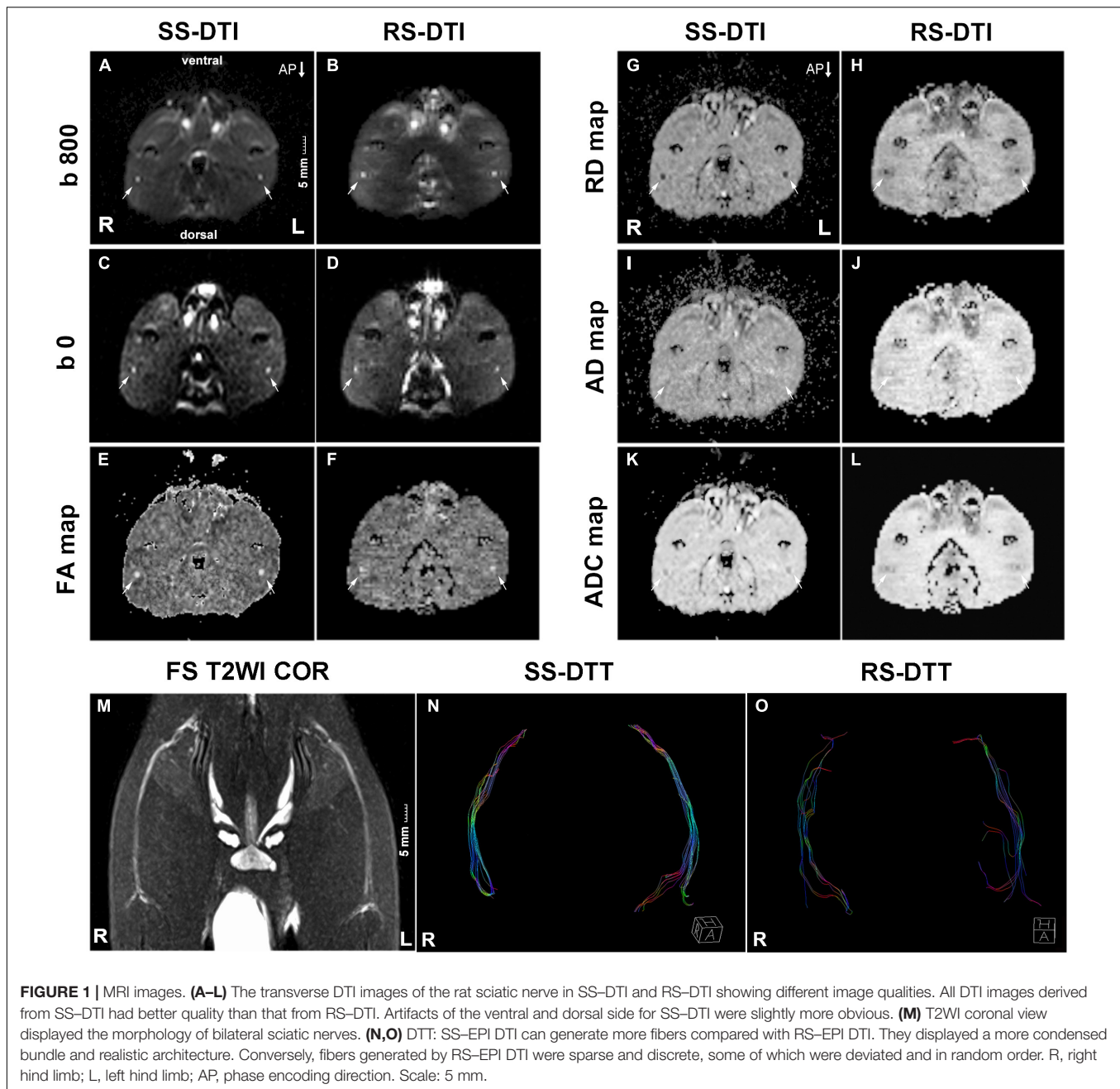
Histopathologic Assessment

Animals were executed after MRI by transcardial perfusion with PBS followed by 4% paraformaldehyde in 0.1 M PBS (pH 7.4). The middle stumps of the sciatic nerves were harvested and postfixed in 4% glutaraldehyde. As shown in **Figures 5A,B**, transverse semi-thin sections (1 μ m thickness) were prepared and stained with toluidine blue to detect nerve myelin. For the quantification of toluidine blue staining, sections of the middle stumps were analyzed morphometrically. In brief, an objective magnification of $\times 1,000$ was used to take digital images of the entire cross-sectional area of the nerve (60 \times 40 μ m, 13.7 pixels/ μ m) on a microscope (Olympus BX60, Japan) for detailed histological quantification. Of these images, five randomly selected measured images (per image area, 240 μ m²; total area, 1,200 μ m² of different regions per nerve segment and animal were analyzed, as described previously. ImageJ software¹ was used to perform analysis to determine the percentage of axon area (POAA), percentage of myelin area (POMA), thickness of myelin (TOM), and diameter of myelinated fibers (DOMF). The final value used for statistical analysis represents the mean of five measuring images per nerve segment and animal.

Statistical Analysis

The image quality scores between SS-EPI and RS-EPI were compared using the Wilcoxon rank-sum test on several aspects (sharpness of nerve margin, artifacts of nerve, artifacts of femur, artifacts of ventral muscles, artifacts of dorsal muscles, and homogeneity of neuromuscular). The inter-observer variability between the two radiologists for the scores was evaluated using a linear-weighted inter-rater agreement (Kappa) test with a calculation of 95% CI. The values of Kappa over 0.75, from 0.40 to 0.75, and below 0.4 were regarded as excellent, fair to good, and poor, respectively. The Shapiro-Wilk test showed that all DTI parameters were normally distributed (*P* > 0.05 for all parameters). Differences in these parameters (FA, AD, RD, and ADC) between SS-EPI and RS-EPI were compared using the paired *t*-test. The degree of association between DTI parameters and histopathological parameters was calculated by using the Pearson correlation coefficient. These coefficients of SS-EPI and RS-EPI were then compared by using the modified Fisher Z-transform (Meng et al., 2014; Friedli et al., 2017). A two-sided *P*-value of 0.05 or less indicated a significant result. Statistical analysis was performed by using SPSS (version 23, IBM SPSS, Chicago) and MedCalc (version 19.1.2, MedCalc Software bv,

¹<https://imagej.net>



Ostend, Belgium). Plots were created by using GraphPad Prism (Version 7.0) and RStudio (Version 1.4.1717).

RESULTS

Morphology of Rat Sciatic Nerve

The bilateral sciatic nerve was best displayed on the coronal view of T2WI STIR. They split above the knee joint into tibial and peroneal nerves, and 2–3 sub-branches can be shown downward (**Figure 1M**). In our study, the thickness of the normal rat sciatic nerve trunk ranged from 1 mm to 2 mm.

Comparison of Image Quality

The image quality scores of the two DTI images for the sharpness of nerve margin, artifacts of nerve, artifacts of the femur, artifacts of ventral muscles, artifacts of dorsal muscles, and homogeneity of neuromuscular are shown in **Table 2** and **Figures 1A–L, 2**. The interobserver agreement between the two independent radiologists was excellent ($\text{Kappa} = 0.837\text{--}0.937$). **Figure 2** showed the image quality scores rated by reader 1 (the more senior radiologist). The image quality scores of SS–EPI were significantly higher than those of RS–EPI in terms of blurring of nerve margin ($P = 0.008$), artifacts of the nerve ($P = 0.008$), and homogeneity of neuromuscular ($P = 0.007$). RS–EPI scored

TABLE 2 | Comparisons of image quality scores and inter-observer agreements between SS-EPI and RS-EPI.

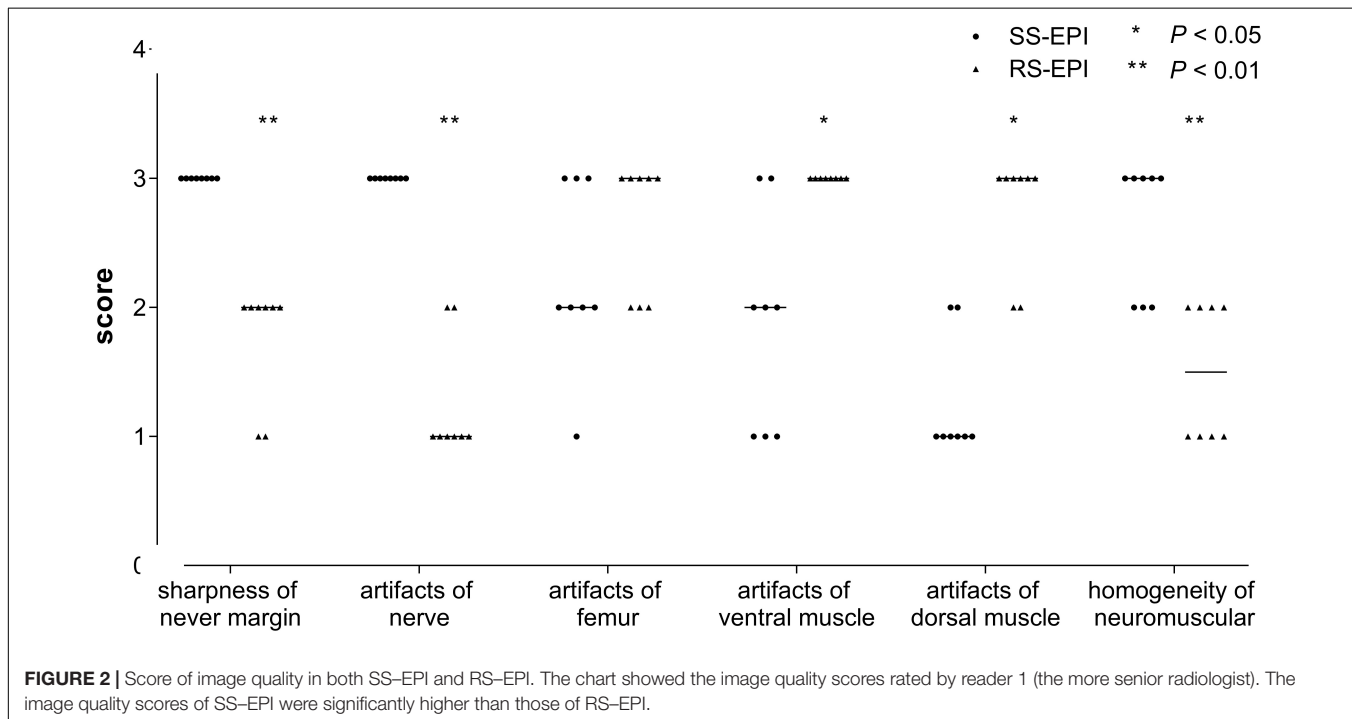
Image quality evaluation	Reader 1		Reader 2		Kappa (95%CI)
	SS-EPI/RS-EPI Median (range)	P-value	SS-EPI/RS-EPI Median (range)	P-value	
Sharpness of the nerve margin	3 (3–3)/2 (1–2)	0.008*	3 (2–3)/2 (1–2)	0.008*	0.837 (0.626–1.000)
Artifacts of the nerve	3 (3–3)/1 (1–2)	0.008*	3 (3–3)/1 (1–2)	0.007*	0.937 (0.817–1.000)
Artifacts of the femur	2 (1–3)/3 (2–3)	0.257	2 (1–3)/2.5 (2–3)	0.414	0.899 (0.703–1.000)
Artifacts of the ventral muscles	2 (1–3)/3 (3–3)	0.024*	2 (1–3)/3 (2–3)	0.023*	0.921 (0.766–1.000)
Artifacts of the dorsal muscles	1 (1–2)/3 (2–3)	0.010*	1 (1–2)/2.5 (2–3)	0.015*	0.862 (0.684–1.000)
Homogeneity of the neuromuscular region	3 (2–3)/1.5 (1–2)	0.007*	2.5 (2–3)/1.5 (1–2)	0.011*	0.920 (0.766–1.000)

Data are listed for both readers as reader1/reader 2.

Two independent readers rated the parameters on a scale from 1 (low) to 3 (high).

SS-EPI, single-shot echo-planar imaging; RS-EPI, readout-segmented echo-planar imaging; CI, confidence interval.

* $P \leq 0.05$.



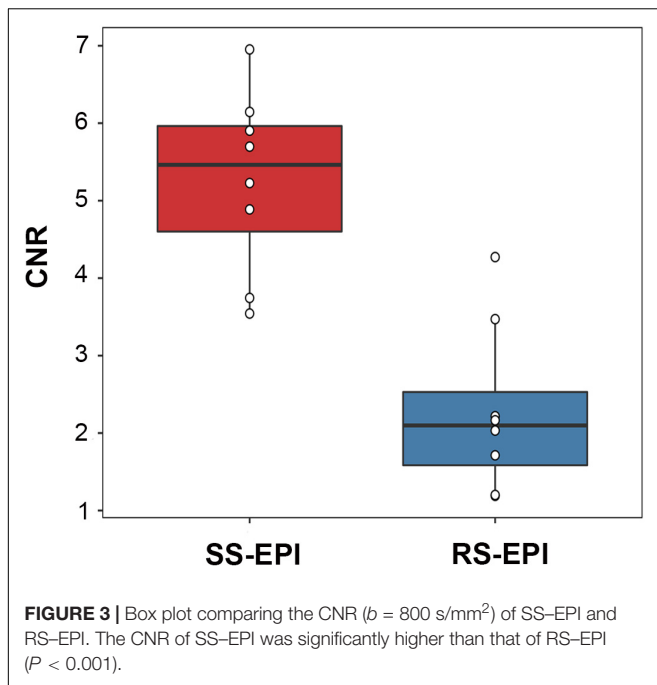
higher than SS-EPI with regard to artifacts of ventral muscles ($P = 0.024$) and artifacts of dorsal muscles ($P = 0.010$). As shown in **Figure 3**, the CNR of SS-EPI was significantly higher than that of RS-EPI (5.26 ± 1.17 vs. 2.28 ± 1.07 , $P < 0.001$).

Comparison of Diffusion Tensor Imaging Parameters and Diffusion Tensor Tractography

Figure 4 shows the comparison of DTI parameters between SS-EPI and RS-EPI. The FA of SS-EPI was significantly

higher than that of RS-EPI (0.661 ± 0.010 vs. 0.607 ± 0.009 , $P < 0.001$), and the RD of SS-EPI was significantly lower than that of RS-EPI ($0.593 \mu\text{m}^2/\text{ms} \pm 0.020$ vs. $0.693 \mu\text{m}^2/\text{ms} \pm 0.018$, $P < 0.001$). There were not significantly different between SS-EPI and RS-EPI for ADC ($1.134 \mu\text{m}^2/\text{ms} \pm 0.040$ vs. $1.179 \mu\text{m}^2/\text{ms} \pm 0.048$, $P = 0.061$) and AD ($2.128 \mu\text{m}^2/\text{ms} \pm 0.068$ vs. $2.060 \mu\text{m}^2/\text{ms} \pm 0.127$, $P = 0.280$).

DTT: SS-EPI DTI can generate more fibers compared with RS-EPI DTI. They displayed a more condensed bundle and realistic architecture. Conversely, fibers generated by RS-EPI



DTI were sparse and discrete, some of which were deviated and in random order.

Correlation Between Diffusion Tensor Imaging Parameters and Histopathological Parameters

Table 3 shows the correlation coefficients between DTI parameters and histopathological parameters for both SS-EPI and RS-EPI. For both sequences, FA was correlated with all of the histopathological parameters ($r = 0.913\text{--}0.963$ for SS-EPI, and $r = 0.741\text{--}0.897$ for RS-EPI, $P \leq 0.001\text{--}0.036$), except the diameter of myelinated fibers for RS-EPI ($r = 0.623$, $P = 0.099$); and RD was correlated with all of the histopathological parameters ($r = -0.886$ to -0.948 for SS-EPI, and $r = -0.709$ to -0.812 for RS-EPI, $P \leq 0.001\text{--}0.049$), except the percentage of axon area for RS-EPI ($r = -0.691$, $P = 0.058$). ADC derived from the SS-EPI sequence was related to all of the histopathological parameters ($r = -0.738$ to -0.769 , $P \leq 0.026\text{--}0.037$), except the diameter of myelinated fibers ($r = -0.686$, $P = 0.060$); While ADC from the RS-EPI sequence was not correlated with any of the histopathological parameters (all $P > 0.05$). No statistical correlation was found between AD for either sequence and any of the histopathological parameters (all $P > 0.05$).

The difference between two correlation coefficients obtained from SS-EPI and RS-EPI was assessed and the results are shown in Table 3 and Figure 5. The overall correlation coefficients of FA and RD obtained with SS-EPI were numerically higher than that with RS-EPI, and the coefficients between FA and myelin thickness ($P = 0.027$), FA and myelinated fiber diameter ($P = 0.036$), and RD and myelin thickness ($P = 0.05$) for SS-EPI were statistically higher than that for RS-EPI.

DISCUSSION

In this study, the single-shot echo-planar imaging (SS-EPI) sequence showed better image quality of the rat sciatic nerve DTI compared with the readout-segmented echo-planar imaging (RS-EPI) sequence. Furthermore, the SS-EPI-derived DTI parameters were superior and showed stronger linear correlations with the histopathological parameters of the rat sciatic nerve compared with the RS-EPI-derived DTI parameters.

In this study, the image quality scores of the SS-EPI sequence were significantly higher than those of the RS-EPI sequence regarding the clarity of the sciatic nerve margins, sciatic nerve artifacts, and neuromuscular junction homogeneities. The differences between SS-EPI and RS-EPI results in this study can be explained by three plausible reasons. Firstly, RS-EPI is extremely sensitive to motion artifacts compared with SS-EPI. The invisible trembling after anesthesia can lead to motion artifacts, especially in small structures such as the sciatic nerve. Furthermore, the acquisition time is longer for RS-EPI compared with SS-EPI because multiple shots with shorter echo train lengths are captured along the readout direction for the k -space in RS-EPI (Friedli et al., 2017). This may account for the blurred margins and more obvious artifacts of the sciatic nerve in the RS-EPI images in this study. Moreover, the scanning time for SS-EPI in our study was significantly shorter compared with the scanning time for RS-EPI (4:06 min vs. 14:12 min). Shorter scanning times reduce the risk of motion artifacts. In our study, seven readout segments (14:12 min) were chosen as the upper limit to complete other functional sequences during the anesthesia time. The small size of the peripheral nerves in small experimental animals poses a challenge for MRI scanning analysis. MRI with smaller voxels enhanced the spatial resolution of the images but also introduced motion artifacts (Van der Pol et al., 2018). Furthermore, stronger signals from the smaller coils increased the motion artifacts (Gruber et al., 2018; Vergara Gomez et al., 2019).

Second, the main advantage of RS-EPI compared with SS-EPI is the significant reduction of geometric distortion caused by susceptibility artifacts (Bogner et al., 2012; Yeom et al., 2013). The performances of RS-EPI and SS-EPI are comparable when the susceptibility artifacts are less severe. Yeom et al. (2013) demonstrated that the overall image quality of RS-EPI was significantly higher than that of SS-EPI for anatomical regions prone to distortion, such as the orbit, skull base, and posterior fossa. These areas are adjacent to the paranasal sinus gas and bone tissues, which are easily prone to magnetic susceptibility artifacts. The sciatic nerve is located deep inside the muscle mass. Furthermore, differences in the magnetization rate are small between the sciatic nerve and the adjacent tissues. Therefore, magnetic sensitivity artifacts are not commonly observed in this region. Hence, SS-EPI shows better image quality. The image scores for the femur and muscles (adjacent to the air) are superior for RS-EPI compared with the SS-EPI sequence in this study for the same reasons mentioned above.

Thirdly, in this study, SS-EPI showed superior nerve tissue contrast. The CNR for SS-DWI was higher compared with the RS-DWI. This is because the nerve signal intensity for SS-DWI is higher compared with RS-DWI, while the signal intensities of the

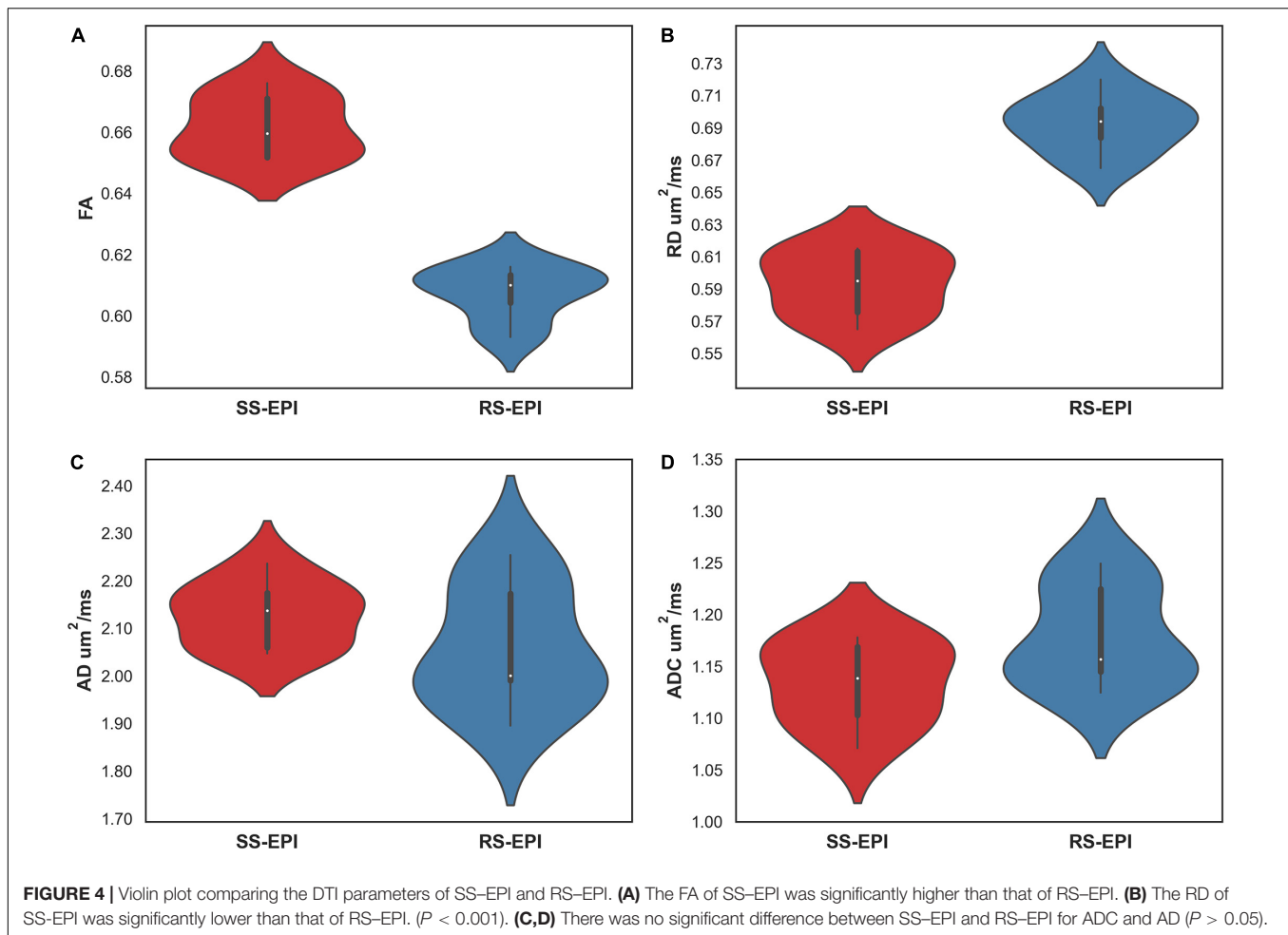


TABLE 3 | Correlation coefficients between DTI parameters and histopathological parameters.

	FA		P-value	RD		P-value	AD		P-value	ADC		P-value
	SS-EPI	RS-EPI		SS-EPI	RS-EPI		SS-EPI	RS-EPI		SS-EPI	RS-EPI	
POAA	0.913 ($P = 0.002^*$)	0.897 (0.003 *)	0.853	-0.898 (0.002 *)	-0.691 (0.058)	0.158	-0.298 (0.474)	-0.226 (0.591)	0.916	-0.769 (0.026 *)	-0.232 (0.581)	0.214
POMA	0.952 ($<0.001^*$)	0.769 (0.026 *)	0.077	-0.948 ($<0.001^*$)	-0.812 (0.014 *)	0.160	-0.415 (0.307)	-0.082 (0.847)	0.631	-0.753 (0.031 *)	-0.193 (0.647)	0.208
TOM	0.963 ($<0.001^*$)	0.741 (0.036 *)	0.027 *	-0.944 ($<0.001^*$)	-0.709 (0.049 *)	0.050 *	-0.377 (0.357)	-0.089 (0.834)	0.681	-0.738 (0.037 *)	-0.144 (0.734)	0.196
DOMF	0.923 (0.001 *)	0.623 (0.099)	0.036 *	-0.886 (0.003 *)	-0.716 (0.046 *)	0.245	-0.400 (0.326)	0.005 (0.990)	0.566	-0.686 (0.060)	-0.073 (0.863)	0.209

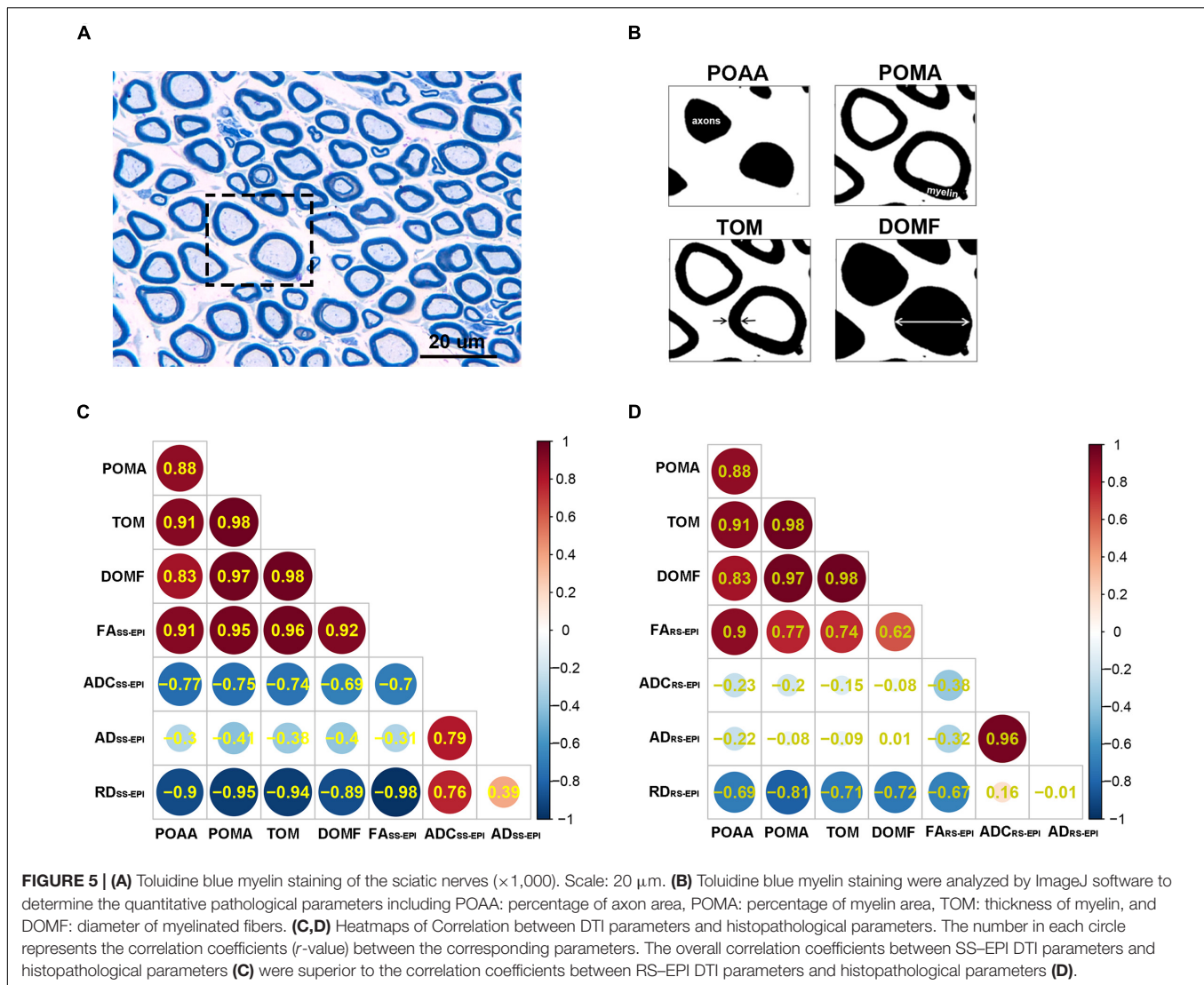
The independent P-value is the result of comparison of correlated correlations. The P-value in parentheses is the result of correlation.

DTI, Diffusion tensor imaging; FA, fractional anisotropy; RD, radial diffusivity; AD, axial diffusivity; ADC, apparent diffusion coefficient; SS-EPI, single-shot echo-planar imaging; RS-EPI, readout-segmented echo-planar imaging; POAA, percentage of axon area; POMA, percentage of myelin area; TOM, thickness of myelin; DOMF, diameter of myelinated fiber.

* $P \leq 0.05$.

muscles for the two DWIs were close. Besides, the additional T2 contrast in SS-EPI DWI resulted in the T2 shine-through effect. T2 shine-through effect is advantageous in evaluating lesions with high T2 intensity that occur within the brain parenchyma or are found immediately adjacent to the brain parenchyma (Yeom et al., 2013). However, RS-EPI with shorter TE reduced the T2

contrast in the DTI images (Chen et al., 2020). In addition, the k-space coverage of SS-EPI is more efficient (Bogner et al., 2012). This might explain the better tissue contrast of rat sciatic nerve (T2 high intensity) on SS-EPI DWI compared with RS-EPI in our study. Thus, the sharper nerve edge, fewer artifacts, and better tissue contrast of SS-DWI made the ROI for sciatic



nerve measurements easier to draw and more accurate. This explains why SS-EPI DTI can generate richer fibers with a more condensed bundle compared with RS-EPI DTI as well.

In our study, the ADC values for SS-EPI and RS-EPI were not significantly different and were comparable to previously published values (Bogner et al., 2012; Friedli et al., 2017). The FA and RD values for SS-EPI were significantly different from those for RS-EPI, which corroborates with the significantly higher motion artifacts and lower SNRs and T2 contrast in the rat sciatic nerve DTI with the RS-EPI sequence. These factors could affect the accuracy of the measured values and interfere with the precision of the ROI.

DTI is a useful technique for accurately assessing peripheral nerve pathology because it provides quantitative information regarding the orientation and structural features. FA quantifies the packing density of axons within a voxel and represents the degree of directed water diffusion; RD quantifies the diffusion perpendicular to the axonal orientation; AD quantifies the diffusion along the axons in parallel with the predominant fiber

orientation and represents the average diffusivity in all spatial directions (Jeon et al., 2018). FA and RD values are the most stable and sensitive biomarkers among the DTI metrics to evaluate peripheral nerve regeneration (Naraghi et al., 2015; Chen et al., 2017). Previous studies on peripheral nerve repair have shown that the density and integrity of myelin increase during the process of nerve fiber regeneration, thereby resulting in higher FA and lower RD values (Chen et al., 2017; Farinas et al., 2020; Zheng et al., 2021). Conversely, nerve anisotropy (FA) values decrease, and RD values increase during peripheral nerve degeneration in healthy older individuals or individuals with peripheral nerve disease because of decreased number of myelinated fibers (Jeon et al., 2018; Lichtenstein et al., 2021). Therefore, FA and RD values are sensitive biomarkers to detect minor changes in the myelination of the peripheral nerves. In our study, the FA and RD values for both SS-EPI and RS-EPI significantly correlated with several myelin-related pathological parameters of the rat sciatic nerve. However, the overall correlation coefficients of FA and RD from the SS-EPI sequence were higher than

those from the RS–EPI sequence. Furthermore, the correlation coefficients between FA and myelin thickness, FA and myelinated fiber diameter, and RD and myelin thickness for SS–EPI were statistically higher than the corresponding correlation coefficients for RS–EPI. This explains the better image quality of SS–EPI, as shown in **Figure 1**. These data demonstrate that SS–EPI provides better image quality of the rat sciatic nerve. Moreover, SS–EPI provided more sensitive and accurate histological information regarding the rat sciatic nerve compared with the RS–EPI.

There are several reasons for not choosing coronal planes for EPI of the rat sciatic nerve. First, a rat sciatic nerve is very small, with diameters that can range between 1 and 2.5 mm; diameters can also be 1 mm when atrophied. Accurately displaying the sciatic nerve in a single plane because of its curvature and the ROI in the coronal view can also be challenging. Partial volume effects also diminish the accuracy of the measured values. Second, the upper and lower edges of the image in the coronal view are closer to both ends of the coil. The loss of signal encountered at the coil edge can significantly affect DTI quality and evaluation. However, the cross-sectional scan is performed at the center of the coil, thereby avoiding the above-mentioned problems.

This study has a few limitations. First, since healthy adult rats were used in this study, the differences in the DTI parameters for the pathological changes in the sciatic nerve were small. In future studies, RS–EPI and SS–EPI parameters should be compared in studies examining rats with sciatic nerve injury. Second, we could not prevent the voluntary movement of live animals during MRI scanning; therefore, we performed deep anesthesia and secured the limbs with tape to prevent movement. However, this did not prevent motion artifacts in the RS–EPI sequence. In future MRI experiments, it is advised that an embedded device should be used for better immobilization of rats with reduced voluntary movements. Third, RS-EPI with various readout segments was not performed in this study. It is plausible that reducing readout segments with short acquisition times may lower the motion artifacts and improve the performance of RS–EPI in detecting rat sciatic nerve pathology. Last, the image quality scoring and ROI drawing in quantitative measurement of DTI metrics in our study were subjective to some extent. The objective assessment method should be used in the future (Jende et al., 2021, 2022).

CONCLUSION

For the rat sciatic nerve DTI imaging, the SS–EPI sequence has significantly higher image quality compared with the RS–EPI sequence. The FA and RD derived from the SS–EPI sequence

might be more sensitive and quantitative biomarkers to detect the histopathological change of the rat sciatic nerve.

DATA AVAILABILITY STATEMENT

The raw data supporting the conclusions of this article will be made available by the authors, without undue reservation.

ETHICS STATEMENT

The animal study was reviewed and approved by the Institutional Animal Care and Use Committee, Jennio Biotech Co., Ltd.

AUTHOR CONTRIBUTIONS

YC: data collection and analysis, experiment design, and writing of the manuscript. FM and ZL: rat MRI scan and sequence optimization. YG: technical assistance. YH: sequence optimization guidance, editing, and discussion and revision of the manuscript. ZP: statistical analysis of data and creation of statistical charts. XY: pathological staining and analysis. XL and HL: full access to all the data in the study and take responsibility for the integrity of the data and the accuracy of the data analysis. All authors contributed to the article and approved the submitted version.

FUNDING

This research was supported by the National Natural Science Foundation of China (Grant Code: 81903960) and the Natural Science Foundation of Guangdong Province (Grant Code: 2020A1515010732).

ACKNOWLEDGMENTS

We thank the national application master Gui Jin Li from Siemens Healthcare for his contribution to technical support and sequence optimization on Prisma 3T MR. We thank the SYNGO application support of Asia Pacific Soon Fee Boon from Siemens Healthcare for her excellent assistance in DTI post-processing and analysis. We thank Suzhou Medcoil Healthcare Co., Ltd. for the MRI animal coil supplied for our study.

REFERENCES

- Bogner, W., Pinker-Domenig, K., Bickel, H., Chmelik, M., Weber, M., Helbich, T. H., et al. (2012). Readout-segmented echo-planar imaging improves the diagnostic performance of diffusion-weighted MR breast examinations at 3.0 T. *Radiology* 263, 64–76. doi: 10.1148/radiol.12111494
- Chen, H. H., Hu, H., Chen, W., Cui, D., Xu, X. Q., Wu, F. Y., et al. (2020). Thyroid-associated orbitopathy: evaluating microstructural changes of extraocular muscles and optic nerves using readout-segmented echo-planar imaging-based diffusion tensor imaging. *Korean J. Radiol.* 21, 332–340. doi: 10.3348/kjr.2019.0053
- Chen, Y. Y., Zhang, X., Lin, X. F., Zhang, F., Duan, X. H., Zheng, C. S., et al. (2017). DTI metrics can be used as biomarkers to determine the therapeutic effect of stem cells in acute peripheral nerve injury. *J. Magn. Reson. Imaging* 45, 855–862. doi: 10.1002/jmri.25395
- Drake-Pérez, M., Boto, J., Fitsiori, A., Lovblad, K., and Vargas, M. I. (2018). Clinical applications of diffusion weighted imaging in neuroradiology. *Insights Imaging* 9, 535–547. doi: 10.1007/s13244-018-0624-3

- Farinas, A. F., Manzanera Esteve, I. V., Pollins, A. C., Cardwell, N. L., Kaoutzanis, C., Nussenbaum, M. E., et al. (2020). Diffusion magnetic resonance imaging predicts peripheral nerve recovery in a rat sciatic nerve injury model. *Plast. Reconstr. Surg.* 145, 949–956. doi: 10.1097/PRS.0000000000006638
- Friedli, I., Crowe, L. A., de Perrot, T., Berchtold, L., Martin, P. Y., de Seigneux, S., et al. (2017). Comparison of readout-segmented and conventional single-shot for echo-planar diffusion-weighted imaging in the assessment of kidney interstitial fibrosis. *J. Magn. Reson. Imaging* 46, 1631–1640. doi: 10.1002/jmri.25687
- Gruber, B., Froeling, M., Leiner, T., and Klomp, D. (2018). RF coils: a practical guide for nonphysicists. *Journal of magnetic resonance imaging. JMRI* 48, 590–604. doi: 10.1002/jmri.26187
- Jende, J. M. E., Kender, Z., Mooshage, C., Groener, J. B., Alvarez-Ramos, L., Kollmer, J., et al. (2021). Diffusion tensor imaging of the sciatic nerve as a surrogate marker for nerve functionality of the upper and lower limb in patients with diabetes and prediabetes. *Front. Neurosci.* 3:642589. doi: 10.3389/fnins.2021.642589
- Jende, J. M. E., Mooshage, C., Kender, Z., Kopf, S., Groener, J. B., Heiland, S., et al. (2022). Magnetic resonance neurography reveals smoking-associated decrease in sciatic nerve structural integrity in type 2 diabetes. *Front. Neurosci.* 15:811085. doi: 10.3389/fnins.2021.811085
- Jeon, T., Fung, M. M., Koch, K. M., Tan, E. T., and Sneag, D. B. (2018). Peripheral nerve diffusion tensor imaging: overview, pitfalls, and future directions. *J. Magn. Reson. Imaging* 47, 1171–1189. doi: 10.1002/jmri.25876
- Kida, I., Ueguchi, T., Matsuoka, Y., Zhou, K., Stemmer, A., and Porter, D. (2016). Comparison of diffusion-weighted imaging in the human brain using readout-segmented EPI and PROPELLER Turbo Spin echo with single-shot EPI at 7 T MRI. *Invest. Radiol.* 51, 435–439. doi: 10.1097/RLI.0000000000000248
- Lichtenstein, T., Sprenger, A., Weiss, K., Große Hokamp, N., Maintz, D., Schlamann, M., et al. (2021). MRI DTI and PDFD as biomarkers for lower motor neuron degeneration in ALS. *Front. Neurosci.* 15:682126. doi: 10.3389/fnins.2021.682126
- Meng, X. L., Rosenthal, R., and Rubin, D. B. (2014). Comparing correlated correlation coefficients. *Psychol. Bull.* 111, 172–175. doi: 10.1037/0033-2909.111.1.172
- Naraghi, A. M., Awdeh, H., Wadhwa, V., Andreisek, G., and Chhabra, A. (2015). Diffusion tensor imaging of peripheral nerves. *Semin. Musculoskelet. Radiol.* 19, 191–200. doi: 10.1055/s-0035-1546824
- Porter, D. A., and Heidemann, R. M. (2009). High resolution diffusion-weighted imaging using readout-segmented echo-planar imaging, parallel imaging and a two-dimensional navigator-based reacquisition. *Magn. Reson. Med.* 62, 468–475. doi: 10.1002/mrm.22024
- Thian, Y. L., Xie, W., Porter, D. A., and Weileng Ang, B. (2014). Readout-segmented echo-planar imaging for diffusion-weighted imaging in the pelvis at 3T-A feasibility study. *Acad. Radiol.* 21, 531–537. doi: 10.1016/j.acra.2014.01.005
- Van der Pol, C. B., Chung, A., Lim, C., Gandhi, N., Tu, W., McInnes, M., et al. (2018). Update on multiparametric MRI of urinary bladder cancer. *J. Magn. Reson. Imaging* 48, 882–896. doi: 10.1002/jmri.26294
- Vergara Gomez, T. S., Dubois, M., Glybovski, S., Larrat, B., de Rosny, J., Rockstuhl, C., et al. (2019). Wireless coils based on resonant and nonresonant coupled-wire structure for small animal multinuclear imaging. *NMR Biomed.* 32:e4079. doi: 10.1002/nbm.4079
- Xie, S., Masokano, I. B., Liu, W., Long, X., Li, G., Pei, Y., et al. (2021). Comparing the clinical utility of single-shot echo-planar imaging and readout-segmented echo-planar imaging in diffusion-weighted imaging of the liver at 3 tesla. *Eur. J. Radiol.* 135:109472. doi: 10.1016/j.ejrad.2020.109472
- Yeom, K. W., Holdsworth, S. J., Van, A. T., Iv, M., Skare, S., Lober, R. M., et al. (2013). Comparison of readout-segmented echo-planar imaging (EPI) and single-shot EPI in clinical application of diffusion-weighted imaging of the pediatric brain. *AJR Am. J. Roentgenol.* 200, W437–W443. doi: 10.2214/AJR.12.9854
- Zhang, H., Huang, H., Zhang, Y., Tu, Z., Xiao, Z., Chen, J., et al. (2021). Diffusion-weighted MRI to assess sacroiliitis: improved image quality and diagnostic performance of readout-segmented echo-planar imaging (EPI) over conventional single-shot EPI. *AJR Am. J. Roentgenol.* 217, 450–459. doi: 10.2214/AJR.20.23953
- Zheng, C., Yang, Z., Chen, S., Zhang, F., Rao, Z., Zhao, C., et al. (2021). Nanofibrous nerve guidance conduits decorated with decellularized matrix hydrogel facilitate peripheral nerve injury repair. *Theranostics* 11, 2917–2931. doi: 10.7150/thno.50825

Conflict of Interest: YG was employed by the company Siemens Healthineers, Guangzhou, China.

The remaining authors declare that the research was conducted in the absence of any commercial or financial relationships that could be construed as a potential conflict of interest.

Publisher's Note: All claims expressed in this article are solely those of the authors and do not necessarily represent those of their affiliated organizations, or those of the publisher, the editors and the reviewers. Any product that may be evaluated in this article, or claim that may be made by its manufacturer, is not guaranteed or endorsed by the publisher.

Copyright © 2022 Chen, Pan, Meng, Li, Hu, Yu, Gao, Guo, Lyu and Lin. This is an open-access article distributed under the terms of the Creative Commons Attribution License (CC BY). The use, distribution or reproduction in other forums is permitted, provided the original author(s) and the copyright owner(s) are credited and that the original publication in this journal is cited, in accordance with accepted academic practice. No use, distribution or reproduction is permitted which does not comply with these terms.

Advantages of publishing in Frontiers



OPEN ACCESS

Articles are free to read for greatest visibility and readership



FAST PUBLICATION

Around 90 days from submission to decision



HIGH QUALITY PEER-REVIEW

Rigorous, collaborative, and constructive peer-review



TRANSPARENT PEER-REVIEW

Editors and reviewers acknowledged by name on published articles

Frontiers

Avenue du Tribunal-Fédéral 34
1005 Lausanne | Switzerland

Visit us: www.frontiersin.org

Contact us: frontiersin.org/about/contact



REPRODUCIBILITY OF RESEARCH

Support open data and methods to enhance research reproducibility



DIGITAL PUBLISHING

Articles designed for optimal readership across devices



FOLLOW US

@frontiersin



IMPACT METRICS

Advanced article metrics track visibility across digital media



EXTENSIVE PROMOTION

Marketing and promotion of impactful research



LOOP RESEARCH NETWORK

Our network increases your article's readership